THE UNIVERSITY *of* EDINBURGH

Investigation of Host Factors in Influenza A Virus Infection

Susana Keane

College of Medicine and Veterinary Medicine

The Royal (Dick) School of Veterinary Studies

The Roslin Institute

Dissertation submitted for the degree of Doctor of Philosophy

The University of Edinburgh

2022

Declaration of authenticity

I declare that this thesis was composed by myself, that the work contained herein is my own except where explicitly stated otherwise in the text, and that this work has not been submitted for any other degree or professional qualification.

Susana Keane

Acknowledgements

This thesis is the product of a PhD conducted in the face of many challenges, both personal and global. There are many people who have supported me in a plethora of ways, without whom this would not have been possible and to whom I am immensely grateful.

Firstly, I would like to thank my supervisor Professor Paul Digard, who kindly adopted me into his group when I found myself supervisor-less. His continuous support, encouragement and guidance has been invaluable, not to mention his knowledge and insight. I would also like to thank my secondary supervisor, Dr Christine Tait-Burkard, for her encouragement, advice, and her vital role in creating the sense of community in the virology groups of Roslin. Additionally, thank you to Dr Sara Clohisey who acted as my external advisor and kindly supported me while I briefly tried my hand at animal work.

I would also like to thank the BBSRC EastBIO doctoral training partnership for funding this PhD, additional training and my professional internship.

I am endlessly grateful for the support of past and current members of the Digard group, particularly Dr Nikki Smith who acted as my in-lab supervisor for my first year and gave me an important foundation of knowledge, skills and confidence. I am also grateful to Drs Lita Murphey, Seema Jasim, Liliane Chung, Rute Pinto, Carina Conceição, Elly Gaunt, Hui-Min Lee, Spring Tan and Nisha Kriplani for their guidance and friendship. Additionally, I would like specifically to thank Dr Nisha Kriplani for her efforts cloning impossible plasmids for me, and Dr Hui-Min Lee for finishing off some western blotting for me when I ran out of time. These wonderful women have offered me so much support and I am inspired by all of them.

I have had the privilege to work with so many brilliant people whose friendship has seen me through the hardest times. In particular, Rosemary Blake has been an incredible support as we laughed and cried our way through our final year together. I could not have asked for a better colleague, flatmate or friend. Thank you also to Agata Wawszczyk, Izzy Hoskins and Emily Lowndes and who have helped make the pandemic survivable with their joyous company. The wider virology community at the Roslin Institute including Elle Mcluskey, Alex Brown, Ola Diebold, Colin Sharp, Pleon Pankew and Federico De Angelis have all contributed to a fun and supportive work environment for which I am thankful.

Finally, I would like to thank my family. My parents, James and Sandra Keane have been unwavering in their support of me throughout this PhD (both emotionally and financially!). I am forever grateful for the opportunities they have provided for me to get to this point and for their belief and confidence in me and my skills. Thank you to my sister and best friend, Georgy Keane, who always lets me rant and ramble about science, and brings me joy and laughter constantly.

Table of Contents

Lay summary

Influenza A virus (IAV) is a pathogen that causes a highly contagious respiratory disease, “flu”, which can be fatal in certain at risk populations, including the immunosuppressed, the very old, and the very young. The virus infects millions of people worldwide every year in seasonal epidemics and has been responsible for larger pandemics. There are antiviral drugs available that target IAV, however the virus is able to mutate and become resistant to these treatments.

IAV has a genome that encodes a small number of essential proteins for its lifecycle, and relies heavily on host proteins for efficient replication. Proteins encoded by the host genome that the virus needs to replicate are called “host factors”. Host factors include cell surface receptors, proteins that are required for the replication of the viral genome, and factors involved in the detection of and immunity against the virus. These host factors are attractive targets for the treatment of IAV because, when the virus is not targeted directly, it cannot mutate to develop resistance as easily. Such drug targets can be identified in many different ways, for example through prior knowledge of a host protein and its functions, or through large scale screens which aim to identify factors required for viral replication.

In this study, we investigated three human proteins that had been previously linked to IAV infection in order to dissect their role in the virus lifecycle and to evaluate their suitability as drug targets.

First, JMJD6, a protein that has many roles in immunity and has been linked to the lifecycles of other viruses. Previous work, in which JMJD6 was depleted in cells, suggested that IAV could not replicate efficiently in the absence of the protein. The data collected in this study suggested that this finding was actually an artefact of the

tools used to deplete JMJD6, and that the protein was not required for IAV to replicate normally.

Another potential host factor that had been identified in a genome-wide CRISPR-Cas9 screen, CMTR1, was also investigated. The data presented in this study suggested that targeting CMTR1 alone is unlikely to be effective for the treatment of IAV infection. However, preliminary data showed that further investigation should be made into the targeting of CMTR1 in combination with other antiviral treatments.

Finally, IGF2BP1 was examined. This protein had been identified in the meta-analysis of genome-wide host factor screens for IAV. IGF2BP1 was chosen for analysis in this study due to its function in binding an RNA modification that is known to be present in the IAV genome. We found that depletion or chemical inhibition of this protein did not affect IAV replication.

The work presented in this study rules out these three proteins as individual targets for drug treatment of IAV and therefore informs the direction of future study.

Abstract

Influenza A virus (IAV) causes a contagious respiratory disease which can be fatal in at risk populations. Seasonal epidemics of IAV infection are responsible for as many as 650,000 human deaths annually. Antiviral drugs currently available for the treatment of IAV infection target viral polypeptides. However, as an RNA virus, IAV is able to mutate and rapidly develop resistance to these drugs. For this reason, new approaches which focus on targeting the host are being explored. IAV interacts with many host proteins which are necessary for efficient completion of the viral lifecycle; these host factors potentially make attractive drug targets for the treatment of IAV, as development of resistance to host-targeted treatments is predicted to be slower.

Host factors required for IAV replication have been identified through a number of routes including targeted research based on previous knowledge of the virus and the host, and large scale screens. The work presented in this thesis aimed to investigate three cellular proteins that had been previously proposed as pro-viral host factors for IAV. Using RNA interference (RNAi) and chemical inhibitors, I sought to dissect the role of these proteins in the viral lifecycle and to assess their suitability as drug targets in the treatment of IAV infection.

The arginine demethylase JMJD6 had been suggested to have a proviral role in IAV replication. In the process of refining previously developed RNAi procedures for depleting JMJD6, I found that a published siRNA used to study JMJD6 induced an interferon (IFN) response in cells. Here, I showed that IAV was able to replicate normally in cells in which JMJD6 was depleted by alternative RNAi methods that did not induce an IFN response and in *JMJD6*$^{-/-}$ cells, strongly suggesting that the previous finding was likely an artefact of the approach used to deplete JMJD6. Thus JMJD6 was determined not to be a host factor of IAV or a suitable target for the treatment of IAV infection.

Next, a host factor that had been identified in a genome-wide CRISPR screen was investigated. The cap 2'-O-methyltransferase, CMTR1, had been proposed to be required for preventing detection of viral mRNA via the IFN signalling pathway. In my hands, knockdown of CMTR1 using RNAi did not lead to enhanced IFN response to infection, nor did it inhibit the replication of IAV in cell culture. This did not support CMTR1 alone as an effective target for IAV treatment. However, preliminary results investigating CMTR1 knockdown in combination with the viral cap-dependent endonuclease inhibitor Baloxavir, suggested that future work should examine CMTR1 as a target to enhance other antiviral treatment.

Finally, the N^6-methyladenosine (m^6A) reader protein IGF2BP1 was examined. IAV RNAs, both genomic and messenger, are known to contain the m^6A modification, which is required for optimal replication efficiency. IGF2BP1, which binds to m^6A modified mRNA to enhance stability, has been linked to IAV replication in host interaction screens. However, using RNAi and chemical inhibition, I did not find that IGF2BP1 was required for IAV replication or spread. Furthermore, overexpression of IGF2BP1 showed no effect on IAV replication. Together these findings rule out IGF2BP1 as an IAV host factor and drug target.

Overall, the work presented in this study did not support the three host proteins investigated as being suitable drug targets for the treatment of IAV, although CMTR1 could still be investigated as a target for combination therapy. The ruling out of JMJD6 and IGF2BP1 can help to focus future work investigating host targets for IAV treatment.

Abbreviations

ALKBH5	α-ketoglutarate-dependent dioxygenase AlkB homologue 5
ANOVA	Analysis of variance
BMDM	Bone marrow derived macrophages
CARD	Caspase activation and recruitment domains
CBC	Cap binding complex
CMTR1	Cap1 2'O-ribose methyltransferase 1
COPI	Coat protein I
CRM1	Chromosome maintenance 1
CTD	C-terminal domain
DAMP	Damage associated molecular pattern
DC	Dendritic cells
DMSO	Dimethyl sulphoxide
dsRNA	double stranded RNA
eIF	Eukaryotic translation Initiation Factor
ER	Endoplasmic reticulum
FACS	Fluorescence-activated cell sorting
FMDV	Foot and mouth disease virus
FTO	Fat mass and obesity-associated protein
HA	Haemagglutinin
HAT	Human airway trypsin-like protease
HBV	Hepatitis B virus
HCV	Hepatitis C virus
HEK	Human Embryonic Kidney
HIV	Human immunodeficiency virus
hnRNP	Heterogeneous nuclear ribonucleoprotein
hpi	Hours post infection
HPIDB	Host pathogen interaction database
HuR	Hu antigen R
IAV	Influenza A virus
IFIT	Interferon-induced protein with tetratricopeptide repeats
IFITM	Interferon-induced transmembrane protein
IFN	Interferon
IFNAR	Type 1 IFN-α/β receptor

IGF2BP	Insulin-like growth factor 2 mRNA binding protein
IL	Interleukin
IRF	Interferon response factor
ISG	Interferon stimulated gene
JMJD6	Jumonji domain containing protein 6
KH	hnRNP-K homology
M1	Matrix protein 1
M2	Matrix protein 2
MAVS	Mitochondrial antiviral-signalling protein
MDA5	Melanoma differentiation-associated protein 5
MeRIP-seq	Methylated RNA immunoprecipitation sequencing
METTL	Methyltransferase-like
MOI	Multiplicity of infection
mRNA	Messenger RNA
MTOC	Microtubule organising centre
MW	Molecular weight
NAI	Neuraminidase inhibitor
NK	Natural killer
NLS	Nuclear localisation signal
NP	Nucleoprotein
ns	Not significant
NS1	Non-structural protein 1
NXF1	Nuclear export factor 1
ORF	Open reading frame
P0	Passage zero
P1	Passage 1
PA	Polymerase acidic protein
PA-m6A-seq	Photo-crosslinking-assisted m6A sequencing
PAMP	Pathogen-associated molecular pattern
PAR-CLIP	Photoactivatable-Ribonucleoside-Enhanced Crosslinking and Immunoprecipitation
PB1	Polymerase basic protein 1
PB2	Polymerase basic protein 2
pfu	Plaque forming units
PIAS	Protein Inhibitor of Activated STAT

Poly I:C	Polyinosinic:polycytidylic acid
PR8	Influenza A/Puerto Rico/8/1934
PRMT1	Protein arginine methyltransferase 1
PRR	Pattern recognition receptors
qPCR	Quantitative polymerase chain reaction
RHA	RNA helicase A
RIG-I	Retinoic acid-inducible gene I
RNA pol II	RNA polymerase II
RNAi	RNA interference
RNF5	Ring finger protein 5
RNP	Ribonucleoprotein
RRM	RNA recognition motifs
SAM	S-adenosylmethionine
SDS-PAGE	Sodium dodecyl sulphate - polyacrylamide gel electrophoresis
SEAP	Secreted embryonic alkaline phosphatase
SeV	Sendai virus
SG	Stress granules
sgRNA	Single guide RNA
shRNA	Short hairpin RNA
siRNA	Small interfering RNA
ssRNA	single stranded RNA
STAT	Signal transducer and activator of transcription
TLR	Toll-like receptor
TMPRSS2	Transmembrane protease serine S1 member 2
TNF	Tumour necrosis factor
TRAF6	Tumour necrosis factor receptor-associated factor 6
TREX	Transcription export
TRIM	Tripartite motif containing protein
UBR4	N-recognising domain-containing E3 ligase 4
UTR	Untranslated region
VACV	Vaccinia virus
VLP	Virus-like particle
VSV	Vesicular stomatitis virus
ZBP1	Z-DNA-binding protein

List of figures and tables

Chapter 6

Chapter 1: Introduction to influenza A virus

1.1. General introduction to influenza

The term “influenza” describes a viral respiratory infection with characteristic symptoms that include fever, cough, headache, muscle and joint pain, malaise, sore throat, and rhinitis (Macias et al., 2021). Influenza viruses spread from host to host via aerosol, droplets and contact transmission (Killingley & Nguyen-Van-Tam, 2013), and primarily infect the airway and alveolar epithelial cells in humans (Flerlage *et al.*, 2021; Kalil & Thomas, 2019) leading to the respiratory and systemic symptoms. Most cases are described as mild, where symptoms last for approximately two weeks and no medical intervention is required. However, influenza can lead to severe disease and can be fatal in certain at risk populations, including immunosuppressed individuals, pregnant people, the very old, and the very young (Macias *et al.*, 2021; World Health Organization, 2018). Annually, there are up to 50 million symptomatic cases recorded in the European Union/European Economic Area (European Centre for Disease Prevention and Control, 2022) and up to 5 million severe cases globally (World Health Organization, 2018). This leads to significant economic burden and contributes to substantial loss of health-related quality of life (Fragaszy *et al.*, 2018). Furthermore, every year influenza is associated with the deaths of 15,000-70,000 European citizens (European Centre for Disease Prevention and Control, 2022), and the World Health Organisation estimates that influenza causes up to 650,000 human deaths globally each year (World Health Organization, 2018).

There are four types of influenza viruses, A to D, which belong to the family *Orthomyxoviridae*. Influenza in humans can be caused by A, B, or C viruses, although the C viruses are rarely diagnosed and usually only cause mild symptoms (Sederdahl & Williams, 2020). The type A and B viruses are the predominant types that cause

disease, and a mix of A and B strains circulate within human populations at any given time, causing seasonal epidemics of varying severity. Seasonal epidemics occur in the winter in temperate climates, generally between November and April in the Northern hemisphere and June to October in the Southern (European Centre for Disease Prevention and Control, 2022). In tropical regions, influenza outbreaks may occur throughout the year (World Health Organization, 2018). Surveillance of the circulating influenza strains is carried out worldwide (World Health Organization, 2018), as well as in individual countries (UK Health Security Agency, 2022), which informs vaccine design and allows monitoring of drug resistance (discussed in section 1.4).

Influenza A viruses (IAVs), which are more genetically diverse than the type B viruses, have a broader host range with established animal reservoirs, which B viruses lack (Koutsakos *et al.*, 2016). Circulation of IAV in both humans and animals allows for genetic mixing and reassortment of viral genomes. This can lead to the emergence of zoonotic strains with greater transmissibility and virulence that are antigenically different form the current circulating strains, meaning that humans have little to no resistance (Krammer *et al.*, 2018; Nypaver *et al.*, 2021). These new strains cause global pandemics which occur every 10 to 50 years. The effects that IAV has on human populations, both in seasonal epidemics and sporadic pandemics, mean that study of the virus, its lifecycle and potential routes of treatment is of great importance.

1.2. Influenza A virus and lifecycle

1.2.1. IAV virion structure and composition

IAV particles are pleomorphic, so can be found as spheres, filaments, or as intermediate bacilliform structures (Chu *et al.*, 1949; Mosley & Wyckoff, 1946; Vijayakrishnan *et al.*, 2013). Spherical virions, which are approximately 100 nm in diameter on average, are common in laboratory-adapted IAV strains such as

influenza A/Puerto Rico/8/1934 (H1N1) (PR8) (Mosley & Wyckoff, 1946), as the filamentous and bacilliform structures are selected against during passage in eggs or MDCK cells (Kilbourne & Murphy, 1960; Seladi-Schulman *et al.*, 2013). Mammalian clinical isolate strains of IAV, including those associated with pandemics, commonly also produce filamentous, elongated virions that can measure up to 30 μm in length (Basu *et al.*, 2011; Bruce *et al.*, 2010; Roberts *et al.*, 1998). Shorter filaments, virions under 250 nm long, are termed bacilliform virions, which represent an intermediate category (Dadonaite *et al.*, 2016; Vijayakrishnan *et al.*, 2013). Filamentous structures may be selected for *in vivo*, as Seladi-Schulman *et al*. reported that serial passage of the spherical IAV strain, PR8, in guinea pigs yielded filamentous variants (Seladi-Schulman *et al.*, 2013). Additionally, filamentous virions are thought to enhance transmissibility of the virus in guinea pigs and in ferrets (Campbell *et al.*, 2014; Lakdawala *et al.*, 2011) and to be associated with increased susceptibility to secondary infections in mice (Speshock *et al.*, 2007). One theory as to the mechanism of this, is that the filamentous morphology allows for the virion to interact with a greater area of the host cell surface, and thus enhances cell entry (Li *et al.*, 2021).

Regardless of morphology, all IAV virions are enclosed by a lipid bilayer envelope, acquired from the host cell plasma membrane upon viral egress from the cell, with incorporated viral transmembrane glycoproteins, hemagglutinin (HA) and neuraminidase (NA) (**Figure 1.1A**) (Compans *et al.*, 1970; Harris *et al.*, 2006; Schulze, 1970). The most abundant, HA, forms homotrimers on the surface of the virion which outnumber NA homotetramers 4:1 (Webster & Pereira, 1968). The antigenic and sequence structure of both of these glycoproteins are used as the basis of IAV classification: 16 subtypes of HA and nine of NA have been identified so far in avian hosts (Fouchier *et al.*, 2005), and two more of each have been found exclusively in bats (Tong *et al.*, 2013). The tetrameric M2 proton channel is also embedded into

the viral envelope but at much lower levels (Pinto *et al.*, 1992). Additionally, host proteins have been detected in the viral envelope (Hutchinson *et al.*, 2014; Shaw *et al.*, 2008). The envelope is supported by a matrix of oligomerised M1 protein (Harris *et al.*, 2001; Sha & Luo, 1997), which interacts with the envelope to determine the morphology of the virion (Bourmakina & García-Sastre, 2003; Roberts *et al.*, 1998).

Under this matrix layer, within the virion, eight individual viral ribonucleoprotein (vRNP) complexes contain the segments of the viral genome in complex with a single copy of the viral RNA-dependent RNA polymerase (RdRp) and multiple nucleoprotein (NP) molecules (**Figure 1.1B**) (Baudin *et al.*, 1994). Each NP monomer binds to approximately 24 nucleotides via the phosphate backbone (Ortega *et al.*, 2000; Scholtissek & Becht, 1971), and interactions between these NP monomers lead to a helical organisation (Ruigrok & Baudin, 1995; Yamanaka *et al.*, 1990). The resulting antiparallel, double helix structure folds back on itself so that the conserved, semi-complementary 5' and 3' ends of each segment can form a partially double stranded structure (Compans *et al.*, 1972; Hsu *et al.*, 1987). This approximately 15 base pair panhandle structure is bound by the RdRp which consists of three subunits: polymerase acidic protein (PA), polymerase basic 1 protein (PB1) and polymerase basic 2 protein (PB2) (Coloma *et al.*, 2009; Hsu *et al.*, 1987). Additional components of the IAV virion include non-structural protein 1 (NS1) and nuclear export protein (NEP), which are incorporated in low quantities (Hutchinson *et al.*, 2014; Richardson & Akkina, 1991).

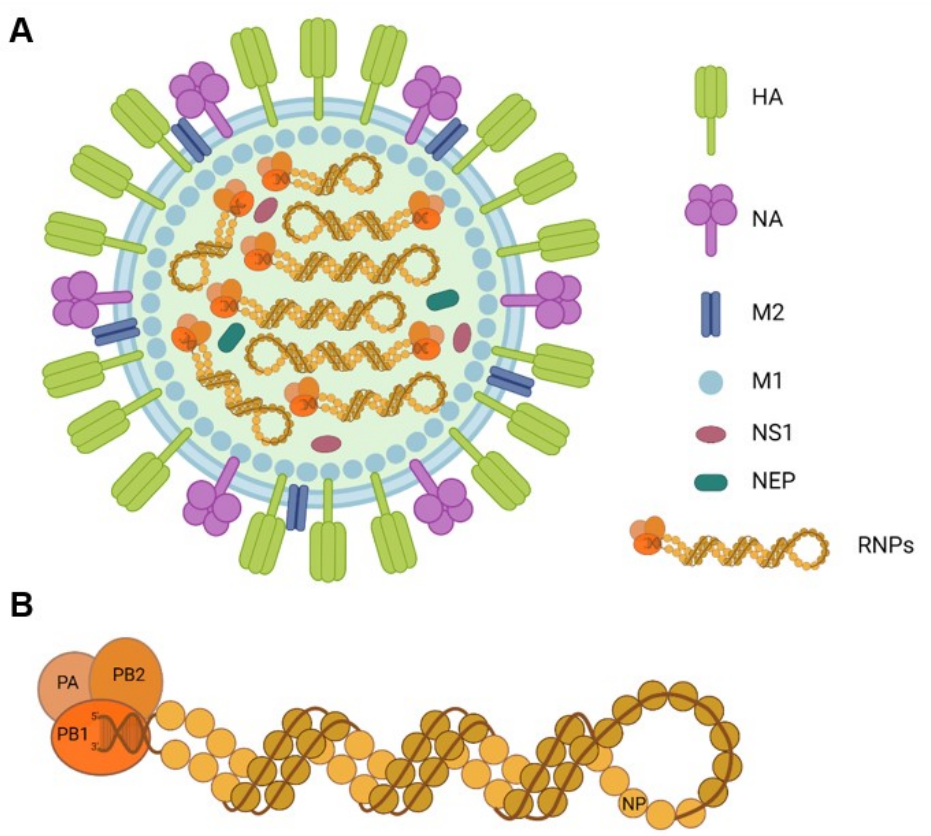

Figure 1.1 IAV virion and RNP structure. A: *Virion and core viral proteins* ***B:*** *vRNP structure. Created using Biorender.com, adapted from Prof Paul Digard and Dr Rute Pinto.*

1.2.2. Viral genome

The IAV genome is comprised of eight single-stranded, negative sense RNA segments of varying size that add up to a total of approximately 13.5 kb (McGeoch *et al.*, 1976; Palese & Schulman, 1976). Each segment of vRNA contains at least one major open reading frame (ORF) which, once transcribed into mRNA, is faithfully translated to encode a protein product. IAV also employs mRNA splicing, ribosomal frame-shifting and alternative translation initiation mechanisms in order to expand its coding capacity. As a result, each genome encodes 10 core proteins, essential for the viral lifecycle, and multiple accessory proteins, some of which are listed in

Table 1.1 (Chen *et al.*, 2018; Pinto *et al.*, 2021; Vasin *et al.*, 2014).

Table 1.1 IAV gene products. *Segment and protein sizes based on PR8*

Genome Segment	Gene product(s)	Protein size (amino acids)	Mechanism of expression	Reported function(s)
1	PB2	759	Main ORF	Subunit of the viral RdRp; binds the 5' cap of host mRNA for cap-snatching (Blaas *et al.*, 1982; Ulmanen *et al.*, 1981); can inhibit RIG-I signalling via MAVS (Graef *et al.*, 2010)
	PB2-S1	508	Spliced mRNA	Inhibits RIG-I signalling via MAVS (Yamayoshi *et al.*, 2016)
2	PB1	757	Main ORF	Subunit of the viral RdRp; catalyses nucleotide addition during mRNA elongation (Braam *et al.*, 1983)
	PB1-F2	87	Alternative ORF	Pro-apoptotic and pro-inflammatory effects; inhibits RIG-I signalling (Chen *et al.*, 2001; Cheung *et al.*, 2020; Dudek *et al.*, 2011)
	PB1-N40	718	Alternative ORF	Interacts with RdRp with unknown effect (Wise *et al.*, 2009)
3	PA	716	Main ORF	Subunit of the viral RdRp; cap-dependent endonuclease, cleaves host pre-mRNA for cap-snatching (Dias *et al.*, 2009)
	PA-X	152	Ribosomal frameshift	Modifies the host immune response and contributes to host cell shut-off (Jagger *et al.*, 2012)
	PA-N155	562	Alternative ORF	Currently unknown (Muramoto *et al.*, 2013)
	PA-N182	535	Alternative ORF	Currently unknown (Muramoto *et al.*, 2013)
4	HA	565	Main ORF	Surface glycoprotein; mediates receptor binding, viral entry and budding (Ohuchi *et al.*, 1997)
5	NP	498	Main ORF	Encapsidates viral genome; acts as a cofactor for the RdRp; required for nuclear import of the vRNP (Scholtissek & Becht, 1971; Wang *et al.*, 1997)
	eNP	504	Alternative ORF	Currently unknown (Wise *et al.*, 2019)
6	NA	454	Main ORF	Surface glycoprotein; facilitates viral attachment; possesses sialidase activity which mediates release of viral progeny from the host cell surface (Griffin *et al.*, 1983; Palese *et al.*, 1974)
7	M1	252	Main ORF	Structural protein; involved in viral budding, assembly and morphology (Sha & Luo, 1997)
	M2	97	Spliced mRNA	Proton ion channel (Yoshimura & Ohnishi, 1984)
	M42	99	Spliced mRNA	Functional alternative to M2 (Wise *et al.*, 2012)
8	NS1	230	Main ORF	Antagonises IFN through multiple mechanisms (García-Sastre *et al.*, 1998; Ji *et al.*, 2021)
	NS2/NEP	121	Spliced mRNA	Mediates nuclear export of vRNPs (O'Neill *et al.*, 1998)
	NS3	187	Spliced mRNA	Associated with switching from avian to mammalian hosts (Selman *et al.*, 2012)
	tNS1	216	Alternative ORF	Inhibits IRF3 activation (Kuo *et al.*, 2016)

1.2.3. IAV Lifecycle

1.2.3.1. Viral entry and nuclear import of vRNPs

In infection, the IAV HA proteins bind to sialic acid residues of glycoproteins on the surface of epithelial cells in the respiratory (and digestive in birds) tracts (Ohuchi *et al.*, 1997; Weis *et al.*, 1988). HA subtypes from avian IAVs are thought to preferentially bind to sialic acids that are linked to the rest of the oligosaccharide by an α-2,3 linkage, whereas human HA subtypes have a higher specificity for sialic acids with a α-2,6 linkage. Single amino acid changes in HA can alter its specificity for sialic acid and therefore host tropism of the virus (Matrosovich *et al.*, 2000; Yamada *et al.*, 2006), as has been seen in human outbreaks of so called “bird flu” (Shinya *et al.*, 2005). This tropism also determines where in the host a virus can infect, depending on the distribution of each type of sialic acid linkage (Costa *et al.*, 2012). For example, Shinya *et al*. reported that α-2,3-linked sialic acid residues are more prevalent in the lower respiratory tract of humans than in the upper airways, which could explain why some avian strains replicate efficiently in human lungs, although they are not easily transmitted to and between humans (Shinya *et al.*, 2006).

At the cell surface, the HA precursor protein (HA0) is cleaved by host cell proteases into functional subunits, HA1 and HA2. In humans this cleavage is mediated by human airway trypsin-like protease (HAT) and transmembrane protease serine S1 member 2 (TMPRSS2) which are expressed on the surface of airway epithelial cells (Böttcher *et al.*, 2006; Limburg *et al.*, 2019). Other proteases that have been reported to cleave the HA of human-adapted viruses include matriptase (Beaulieu *et al.*, 2013) and TMPRSS4 (Chaipan *et al.*, 2009). HA cleavage can also occur during the generation of progeny virions, so that the particles released are infectious and this cell surface processing is not necessary for entry into the new cell (described below).

HA-receptor binding triggers virion internalisation via a number of routes, including clathrin-mediated endocytosis and macropinocytosis (de Vries *et al.*, 2011; Lakadamyali *et al.*, 2006). Inside the cell, the virus is trafficked to the endosome, where low pH, between 5.5 and 5.0, induces a conformational change of HA which exposes a highly conserved fusion peptide in the N-terminus of the HA2 subunit, which inserts into the endosomal membrane (Bullough *et al.*, 1994; Maeda *et al.*, 1981; White *et al.*, 1982). Once inserted, multiple HA trimers cluster into "fusogenic units" which function to bring the opposing membranes of the virus and the endosome together for fusion (Hamilton *et al.*, 2012). The low pH of the endosome also activates the M2 proton channels, which open to acidify the viral core, leading to the release of the vRNPs into the cytoplasm (Yoshimura & Ohnishi, 1984).

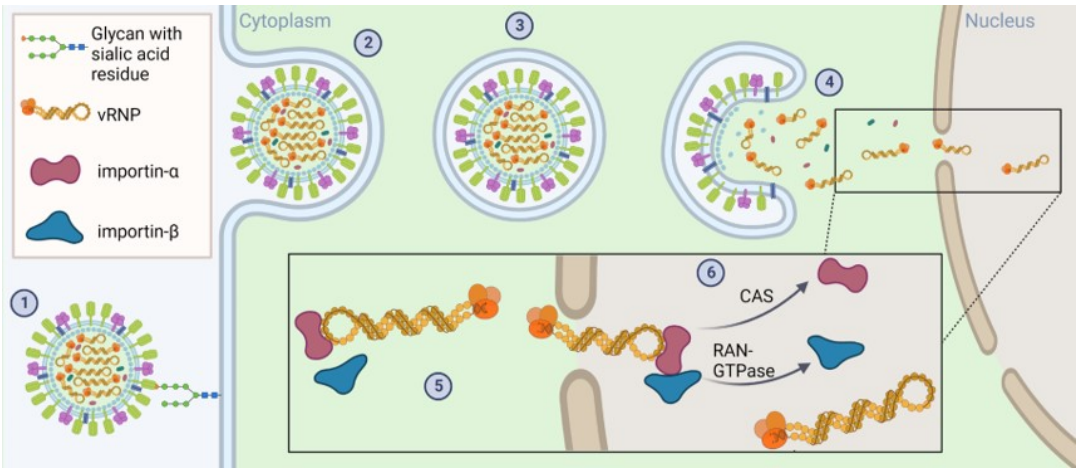

Figure 1.2 IAV entry and nuclear import of vRNPs. ***(1)*** *HA attaches to sialic acid on cell surface glycoproteins.* ***(2)*** *The virion is internalised by receptor-mediated endocytosis or micropinocytosis.* ***(3)*** *As the pH in the endosome drops, M2 proton channels open to acidify the viral core.* ***(4)*** *The viral envelope fuses with the endosomal membrane and the contents of the virion are released into the cytoplasm.* ***(5)*** *vRNPs are transported into the nucleus by importin-α and importin-β.* ***(6)*** *Importin-α and importin-β are dissociated from the vRNP by CAS and RAN-GTPase, respectively. Created using Biorender.com.*

Trafficking of the vRNPs from the cytoplasm to the nucleus is mediated by host machinery and pathways. Importin-α is recruited to a non-canonical nuclear

localisation signal (NLS) at the NP N-terminus; this adaptor protein is recognised by the importin-β transport receptor which mediates transport of the vRNPs to the nucleus (Cros *et al.*, 2005; Martin & Helenius, 1991b; O'Neill *et al.*, 1995; Wang *et al.*, 1997). The importin-α-importin-β-vRNP complex passes through the nuclear pore complex into the nucleus, where the CAS protein and RAN-GTPase mediate dissociation of importin-α and importin-β, respectively, releasing the vRNP into the nucleus (**Figure 1.2**) (Kutay *et al.*, 1997; O'Neill *et al.*, 1995).

1.2.3.2. Transcription and genome replication

In the nucleus, the viral genome segments are transcribed into mRNA (Herz *et al.*, 1981). This is primed by a process called cap snatching, where PB2 binds to the 5' cap of nascent host transcripts, and PA cleaves the mRNA 10-15 nucleotides downstream (Krug *et al.*, 1980a; Krug *et al.*, 1979; Ulmanen *et al.*, 1981; Yuan *et al.*, 2009). This process is enhanced by the interaction of the RdRp with the cellular RNA polymerase II (RNA pol II), which synthesises the capped transcripts (Engelhardt *et al.*, 2005). The PA RdRp subunit binds a phosphorylated serine residue in the C-terminal domain (CTD) of the largest RNA pol II subunit, RBP1 (Engelhardt *et al.*, 2005; Lukarska *et al.*, 2017). However cap-snatching from synthetic mRNA has been observed *in vitro* in the absence of RNA pol II (Bouloy *et al.*, 1978; Krug *et al.*, 1980b) so this interaction is not strictly required. Following cleavage, the cap-binding domain of PB2 rotates to move the capped primer into the active site of the PB1 subunit, which catalyses mRNA synthesis using the viral genome (vRNA) as a template (**Figure 1.3**) in the 3' to 5' direction (Braam *et al.*, 1983; Reich *et al.*, 2014). A conserved polyuridine (U) stretch at the 5' end of each vRNA molecule acts as a signal for the mRNA to be polyadenylated by reiterative copying of the poly(U) motif (Poon *et al.*, 1999; Robertson *et al.*, 1981).

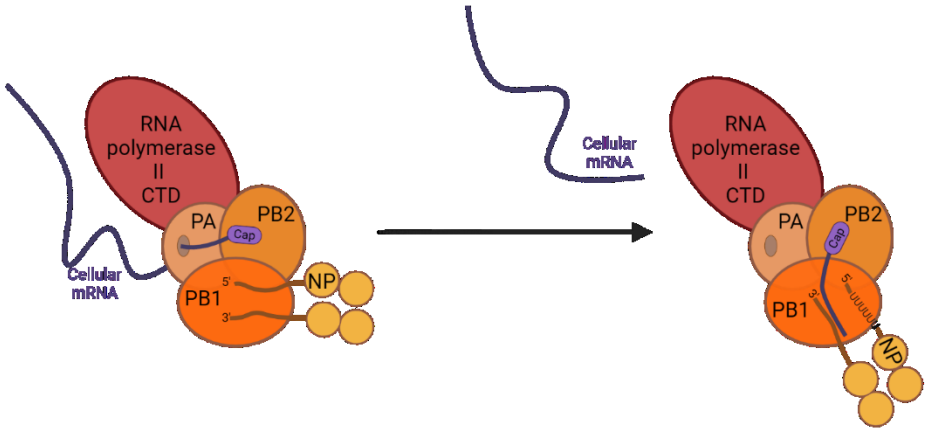

Figure 1.3 Influenza A virus cap snatching. *PA interacts with the C-terminal domain (CTD) of the largest subunit of cellular RNA polymerase II, PB2 binds the 5'-cap of nascent host transcripts. PA cleaves the host transcript 10-15 nucleotides downstream of the cap to generate a primer for transcription of the IAV genome. The primer is moved into the PB1 active site and viral transcription is initiated. Created using Biorender.com*

These viral mRNA molecules therefore resemble cellular mRNAs, with a 5' cap and 3' poly(A) tail, so are processed, exported and translated by host machinery. The cap and tail structures recruit host proteins involved in RNA processing, including spliceosome components and the transcription export (TREX) complex. TREX subsequently recruits nuclear export factor 1 (NXF1) which is the major export factor for host mRNA (York & Fodor, 2013). NXF1 can also be recruited to poly(A) tail binding factors such as CPSF6 (York & Fodor, 2013). NFX1 has been shown to interact with viral mRNAs in infected cells (Wang *et al.*, 2008b), and depletion of this host protein by RNA interference (RNAi) was shown to decrease the nuclear export of viral mRNAs (Read & Digard, 2010). Interestingly, NFX1 knockdown had a greater effect on the export of transcripts encoding genes expressed later in infection, particularly HA, M1 and M2 (Read & Digard, 2010). Transcripts encoding the polymerase proteins and NP, which are expressed earlier in infection, showed very weak dependence on NFX1 for nuclear export (Read & Digard, 2010), indicating that these viral transcripts rely on other host factors for nuclear export, although the

specific host factors involved are yet to be reported. The transcription of host mRNA by RNA pol II has also been shown to be required for the nuclear export of viral transcripts, as chemical inhibition of the host polymerase was shown to cause nuclear retention of certain viral transcripts (Amorim *et al.*, 2007).

Once exported, viral mRNAs are thought initially to be translated in a canonical manner in which translation initiation factors are recruited to the 5' cap and the 3' poly(A) tail, which subsequently recruit ribosomal subunits (Dou *et al.*, 2018). Later in infection, some strains of IAV shut off the synthesis of host proteins (Katze *et al.*, 1986). Here, translation of viral transcripts can continue via non-canonical, cap-independent routes of initiation that are mediated by sequences in the 5' untranslated region (UTR) of viral RNAs (de Rozières *et al.*, 2022; Garfinkel & Katze, 1993). Following translation, the same importin-α-importin-β pathway used for vRNP import is also used to traffic newly synthesised NP through the nuclear pore complex (Huet *et al.*, 2010). Import of newly synthesised PB2 is mediated by importin-α5 which it binds via a classical NLS in its C-terminal domain (Tarendeau *et al.*, 2007). Newly translated PB1 and PA form a dimer which is trafficked into the nucleus by Ran binding protein 5 (RanBP5), a member of the importin-β family, which binds to the PB1 N-terminal domain (Deng *et al.*, 2006a; Fodor & Smith, 2004; Hutchinson *et al.*, 2011). The newly synthesised vRNP components assist in transcription of viral mRNAs and facilitate replication of the viral genome.

Replication of the IAV genome is a primer-independent process which produces uncapped, positive sense complementary RNA (cRNA) with no poly(A) tail (Hay *et al.*, 1982; York *et al.*, 2013). This process involves *de novo* initiation of RNA synthesis on the 3' terminus of the RNP-associated vRNA segment (Deng *et al.*, 2006b). The cRNA is incorporated into a complex with newly synthesised NP and RdRp subunits to make complementary RNPs (cRNPs) (Vreede *et al.*, 2004; York *et al.*, 2013). Recent

evidence suggests that the host protein acidic nuclear phosphoprotein 32 A (ANP32A) interacts with the vRNP-associated parental RdRp to facilitate recruitment of the newly synthesised viral proteins to the cRNA (Carrique *et al.*, 2020; Long *et al.*, 2016). The cRNP is then used as a template for vRNA synthesis. This process is also primer-independent, and requires a second newly synthesised RdRp (Fan *et al.*, 2019; Jorba *et al.*, 2009). The vRNA is then incorporated into new, progeny vRNPs.

1.2.3.3. Nuclear export of vRNPs

Export of the new vRNPs to the cytoplasm require two viral proteins, M1 and NEP (Bui *et al.*, 1996; Martin & Helenius, 1991a; O'Neill *et al.*, 1998). NEP, also known as NS2 as it is the product of the alternative spicing of the NS transcript, interacts with M1 after they have both been imported into the nucleus concurrently with the RNP components (Akarsu *et al.*, 2003; Shimizu *et al.*, 2011). M1 binds to the new vRNPs with high affinity (Baudin *et al.*, 2001), acting as an adaptor protein for NEP, which interacts with the host nuclear export factor CRM1 (chromosome maintenance 1, also known as exportin 1) via two nuclear export signals (NES) in the N-terminal domain of the viral protein (Huang *et al.*, 2013; Iwatsuki-Horimoto *et al.*, 2004). Mutation of either of these NES sites results in delayed nuclear export of vRNPs (Iwatsuki-Horimoto *et al.*, 2004; Neumann *et al.*, 2000). An NES has also been identified in the N-terminal domain of M1, which was shown to be required for efficient nuclear export of vRNPs (Cao *et al.*, 2012). Furthermore, interaction of NP with NFX1 has been shown to induce CRM1-mediated export of NP (Chutiwitoonchai & Aida, 2016; Elton *et al.*, 2001). Elton *et al*. found that NP bound CRM1 *in vitro*, and that overexpression of the host protein resulted in cytoplasmic accumulation of NP, independent of M1 and NEP (Elton *et al.*, 2001). More recently, Chutiwitoonchai & Aida reported that depletion of NXF1 resulted in accumulation of NP and M1 protein and vRNA in the nucleus, which the authors propose could suggest an NEP-independent mechanism

of vRNP nuclear export (Chutiwitoonchai & Aida, 2016), although this was not directly shown.

1.2.3.4. Virion assembly

Once in the cytoplasm, vRNPs accumulate near the microtubule organising centre (MTOC) and the PB2 subunits of the vRNPs bind to Rab11a, a host GTPase associated with recycling endosomes (Amorim *et al.*, 2011; Momose *et al.*, 2007; Veler *et al.*, 2022). Rab11a then facilitates trafficking of the vRNPs to the plasma membrane via the microtubule network (Amorim *et al.*, 2011). Currently accepted models suggest that in this process, the vRNPs are docked to recycling endosomes to be carried to the plasma membrane (Amorim *et al.*, 2011; Bhagwat *et al.*, 2020; Chou *et al.*, 2013; Lakdawala *et al.*, 2014; Momose *et al.*, 2011). An alternative model has been proposed, in which the endoplasmic reticulum (ER) is remodelled around the MTOC in infected cells, leading to the formation of irregularly coated vesicles which contain Rab11 and traffic vRNPs to the plasma membrane (**Figure 1.4**) (de Castro Martin *et al.*, 2017). For both of these models, it is not yet known how the vRNPs are transferred to the plasma membrane.

Structural components of the virion envelope, HA, NA and M2, are synthesised and folded in rough ER before being transported through the Golgi apparatus, to the plasma membrane (Doms *et al.*, 1993). During transport through the ER and Golgi, HA and NA are glycosylated which enhances folding and oligomerisation by recruiting host chaperone proteins (Daniels *et al.*, 2003). In some cells, TMPRSS2 expressed in the Golgi cleaves newly synthesised HA0 during its trafficking to the plasma membrane so that the progeny virions do not require cleavage to enter new cells (Böttcher-Friebertshäuser *et al.*, 2010; Böttcher-Friebertshäuser *et al.*, 2013).

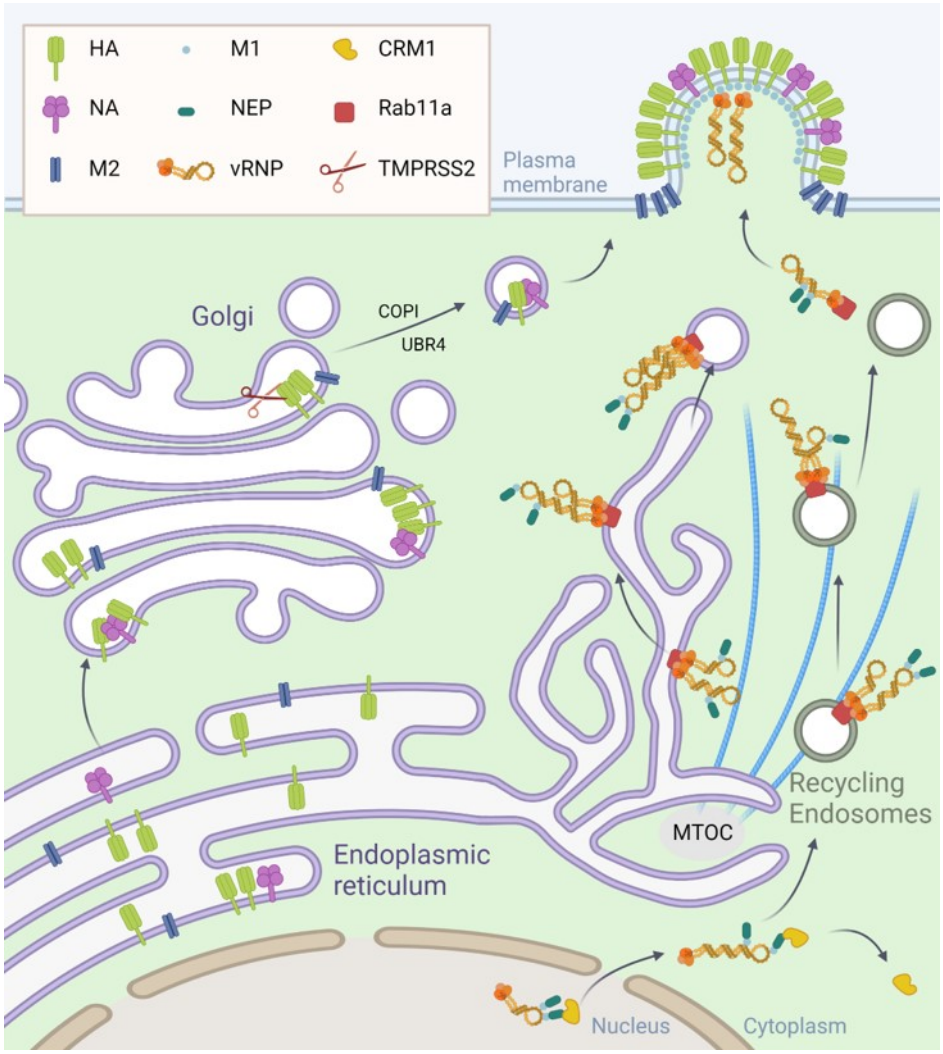

Figure 1.4 Apical transport of nuclear components. *Following CRM1-mediated nuclear export, vRNPs, with piggybacking M1 and NEP, are trafficked to the plasma membrane either on Rab11a-positive recycling endosomes, or via the ER that has remodelled around the microtubule organising centre (MTOC). Viral envelope proteins, HA, NA and M2 are synthesised in the endoplasmic reticulum and transported through the Golgi. In the Golgi, HA may be cleaved by TMPRSS2. The envelope proteins are then trafficked to the plasma membrane, which is mediated by host factors such as COPI and UBR4. At the plasma membrane, the viral components are accumulated and progeny viruses begin to bud.*

During exocytic transport, and at the apical membrane, both HA and NA have been shown to associate with sphingolipid and cholesterol-rich membrane patches (lipid raft microdomains) via their transmembrane domains (Barman & Nayak, 2000; Scheiffele *et al.*, 1997). M2 accumulates at the boundaries of these lipid rafts,

clustering with HA (Hughey *et al.*, 1992; Leser & Lamb, 2005; Rossman *et al.*, 2010). Several host proteins and systems have been associated with the apical targeting of the envelope proteins, for example, the coat protein I (COPI) complex, which mediates vesicle transport between the ER and the Golgi, and endosomal trafficking (Sun *et al.*, 2013). Inhibition of COPI subunit recruitment was associated with reduced surface expression of the viral membrane proteins and defective viral assembly (Sun *et al.*, 2013). The host protein ubiquitin N-recognising domain-containing E3 ligase 4 (UBR4) has been found to interact with M2 and to influence the apical targeting of M2 and the glycoproteins (Tripathi *et al.*, 2015). Loss of UBR4 expression in cells was seen to reduce expression of M2 protein, both overall and at the surface, suggesting that UBR4 may protect M2 from degradation as well as facilitate its translocation to the membrane (Tripathi *et al.*, 2015). Furthermore, Rab11a has also been associated with transport of M2 to the cell surface (Rossman *et al.*, 2010).

The route by which M1 reaches the plasma membrane has only recently begun to be revealed. M1 does not contain an apical localisation signal, like those in the transmembrane domains of HA and NA (Barman & Nayak, 2000; Scheiffele *et al.*, 1997), so was hypothesised to “piggyback” via its interactions with the glycoproteins, M2 and vRNPs (Ali *et al.*, 2000; Pohl *et al.*, 2016). In a recent study, Petrich *et al*. used advanced microscopy techniques in cells expressing fluorescently tagged IAV proteins to analyse the interactions of M1 with the viral envelope proteins. They determined that M1 was recruited to the plasma membrane by M2 (Petrich *et al.*, 2021) via a direct interaction between M1 and M2 that was already known to be important for virion assembly (Chen *et al.*, 2008). They also observed that interactions of M1 with the cytoplasmic tails of HA and NA, which had also been reported previously (Ali *et al.*, 2000), occurred subsequently, but were not strong enough to recruit the matrix protein to the membrane (Petrich *et al.*, 2021). The authors only

reported this M1-M2 interaction near to the plasma membrane, not during trafficking of M2, and hypothesised that M1 diffuses freely through the cytoplasm to reach the membrane (Petrich *et al.*, 2021). However, the system used in this study did not include components of the vRNPs (Petrich *et al.*, 2021), so cannot rule out that, in infection, M1 is trafficked through the cytoplasm by piggybacking on vRNPs prior to binding with M2. It is also unknown how NEP is trafficked to the apical membrane for virion assembly, but association with M1 may mean that these nuclear export proteins are co-transported together (Yasuda *et al.*, 1993).

1.2.3.5. Budding and release

The sites where the structural proteins are accumulated at lipid rafts in the apical membrane are known as budding sites, or budzones. While the exact trigger for budding initiation is not known, studies have shown that exogenous expression of individual IAV proteins, namely NA, HA and M1, lead to the budding of virus like particles (VLPs) (Chen *et al.*, 2007; Gómez-Puertas *et al.*, 2000; Lai *et al.*, 2010). Another study reported that the minimum requirement for VLP formation was expression of one of the glycoproteins with both M1 and M2 (Chlanda *et al.*, 2015). However it is important to note that these VLPs are not completely analogous to virions, and these overexpression systems do not accurately represent expression levels of the individual proteins so could result in activity and interactions that are not seen in infection (Nayak *et al.*, 2009). Furthermore, these VLPs do not contain vRNPs so cannot provide insight into how these structures influence viral budding.

The vRNPs are delivered to the budzones and organised so that the eight genome segments are bundled together. The segments are assembled in a “7+1” configuration where a central vRNP is surrounded by the 7 others (Noda *et al.*, 2018). This bundling is facilitated by packaging signals at various regions of the vRNPs that mediate RNA-RNA interactions between the genome segments (Dadonaite *et al.*, 2019). The

cytoplasmic tails of both glycoproteins and of M2 have been shown to be required for accumulation of vRNPs at the bud zone and for efficient packaging of vRNPs into virions (Iwatsuki-Horimoto *et al.*, 2006; McCown & Pekosz, 2005; Takizawa *et al.*, 2016; Zhang *et al.*, 2000). However, direct interactions between the envelope proteins and vRNPs have not been reported, so they likely require M1, which interacts with all of these viral components (Ali *et al.*, 2000; Baudin *et al.*, 2001; McCown & Pekosz, 2005), as an adaptor.

A lot of evidence points to the importance of M1 in the budding process. Firstly, M1 is able to interact with all of the viral components, as described above. The matrix protein also interacts with the plasma membrane which leads to M1 oligomerisation (Hilsch *et al.*, 2014). This oligomerisation is required for the formation of the matrix layer below the viral envelope that provides structure and stability (Calder *et al.*, 2010; Harris *et al.*, 2001; Sha & Luo, 1997), and has been hypothesised to lead to elongation of the budding virion (Rossman & Lamb, 2011). Furthermore, infection of cells with recombinant baculoviruses or vaccinia viruses encoding IAV M1 produces single-protein filamentous VLPs (Gómez-Puertas *et al.*, 2000; Latham & Galarza, 2001), although in transfection based VLP studies, the IAV glycoproteins and M2 are also required (Chen *et al.*, 2007; Chlanda *et al.*, 2015).

Next, M2, which is primarily localised at the outer periphery of the lipid rafts making up the budzones, alters the curvature of the membrane in order to “pinch off” the budding virions from the plasma membrane (Rossman *et al.*, 2010; Schmidt *et al.*, 2013). Following this membrane scission, the budding particles remain attached via binding of HA to sialic acid on cell surface glycoproteins which must be cleaved by NA in order for the progeny virions to be released (Griffin *et al.*, 1983; Palese *et al.*, 1974). NA has also been suggested to cleave sialylated glycoproteins in the mucous produced by the respiratory epithelium, which would facilitate spread of the virions to

new cells, as well as aiding entry to cells by removing “decoy” receptors (Cohen *et al.*, 2013).

The entire lifecycle of IAV is relatively quick; *in vitro* infection experiments at high multiplicity of infection (MOI) have observed the shedding of infectious virus particles from infected MDCK cells in as little as five hours (Abdoli *et al.*, 2013). At lower MOIs, shedding can be detected between eight and 24 hours post infection (Abdoli *et al.*, 2013). This timing, however, differs between cell lines (Gaush & Smith, 1968) and virus strains (Parvin *et al.*, 2015), and also depends on culture conditions and the host immune response. The development of new tools and techniques, including bioluminescent strains of IAV, will allow real-time tracking of the viral lifecycle, both *in vitro* and *in vivo*, that may further elucidate the mechanisms behind infection dynamics (Kim *et al.*, 2022).

1.3. The immune response to IAV in humans

1.3.1. Innate immune response to IAV infection

The innate immune response is the host’s first line of defence against pathogens. A successful innate immune response against IAV rapidly detects the virus and prevents its replication and spread. Additionally, the innate immune response activates and informs the adaptive immune response, which clears the virus and infected cells, and generates memory cells for protection against future infections. However, in addition to clearing the pathogen, a robust immune response can also cause damage to and compromise the function of host tissue. In fact much of the pathology and many of the symptoms associated with IAV infection are caused by the immune response (Fukuyama & Kawaoka, 2011; George *et al.*, 2021; Kaiser *et al.*, 2001; Wu & Metcalf, 2020). The initial innate immune response to IAV infection in the human respiratory tract, as well as viral tactics of immune evasion are discussed below.

1.3.1.1. Cells involved in innate immunity against IAV

1.3.1.1.1. Respiratory epithelial cells

Epithelial cells of the respiratory tract are the primary target of human strains of IAV. The types and relative abundance of epithelial cells differs throughout the tract. Conducting airways, which includes the trachea, the bronchi and the bronchioles, are rich in ciliated and mucin-producing secretory cells (Mifsud *et al.*, 2021; Whitsett & Alenghat, 2015). Together, these work to form and clear a mucosal barrier that prevents pathogens from accessing the cells. Pathogens, including IAV are non-specifically trapped in the mucous layer above the cells, and beating of the cilia move them out of the respiratory tract (Whitsett & Alenghat, 2015). The importance of mucins in defence against IAV was first noted in the 1940s (Anderson *et al.*, 1948). Mucin proteins, which in humans include MUC1 and MUC5AC are heavily glycosylated and contain sialic acid residues. As mentioned above, the sialylated mucins impair and delay the movement of IAV by binding to HA, before being cleaved by NA (Cohen *et al.*, 2013). Although IAV is able to overcome this mucosal blocking via NA activity, mucins remain an important barrier in infection. *Muc1*$^{-/-}$ mice have been reported to show increased severity of IAV infection (McAuley *et al.*, 2017). Conversely, overexpression of MUC5AC in mice limited infection and excessive inflammatory responses (Ehre *et al.*, 2012).

Deeper in the lungs, the epithelium of the alveoli is made up of squamous type I alveolar cells (or pneumocytes), that interact closely with the endothelial cells of pulmonary capillaries and facilitate gas exchange, and cuboidal type II pneumocytes, which secrete surfactant (Mifsud *et al.*, 2021; Whitsett & Alenghat, 2015). Surfactant lipids and proteins are required for the normal structure and function of the alveoli, as they reduce surface tension to prevent lung collapse (Whitsett & Alenghat, 2015). They also have antiviral properties; for example, surfactant protein D binds to glycans

on HA, near the sialic acid binding cite, to neutralise virions and prevent infection of epithelial cells (Hartshorn *et al.*, 2008; LeVine *et al.*, 2001).

1.3.1.1.2. Innate effector cells

Resident alveolar macrophages are long lived cells that reside in the lumen of the alveoli. They function as scavenger cells and become activated when they detect pathogen-associated molecular patterns (PAMPs) via intracellular pattern recognition receptors (PRRs) following phagocytosis of the virus or infected cells, or when they are infected themselves (Chen *et al.*, 2018; Roberts, 2020). Activated alveolar macrophages phagocytose infected epithelial cells, limiting the spread of the virus and produce pro-inflammatory cytokines to attract and activate other immune cells (Chen *et al.*, 2018; Tumpey *et al.*, 2005). They can also be infected by some strains of IAV, potentially using receptors other than sialic acid (Londrigan *et al.*, 2012; Rodgers & Mims, 1982).

Pro-inflammatory cytokines secreted by infected epithelial cells and activated alveolar macrophages promote the infiltration of other innate effector cells into the lungs (Chen *et al.*, 2018; Mifsud *et al.*, 2021). These cells include monocytes, natural killer (NK) cells, neutrophils and dendritic cells (DCs). Briefly, monocytes act as phagocytic antigen presenting cells and can differentiate into macrophages or DCs (Roberts, 2020). NK cells are cytotoxic lymphocytes that recognise cells expressing reduced major histocompatibility complex (MHC) class I, which is downregulated on the surface of infected cells and induce lysis or apoptosis (Ljunggren & Kärre, 1990), NK cells can also recognise IAV-infected cells by binding to viral HA, expressed on the cell surface, via sialic acid residues on their NKp46 receptor (Arnon *et al.*, 2004; Arnon *et al.*, 2001; Mandelboim *et al.*, 2001). Neutrophils are granulocytes that, in addition to their role in phagocytic clearance of virus particles and infected cells, release cytotoxic granules to create an inhospitable environment for pathogens and induce

the death of infected cells (George *et al.*, 2021). They also secrete chemokines to recruit both innate and adaptive immune cells to the inflammatory environment (George *et al.*, 2021). DCs are professional antigen presenting cells which initiate and direct the adaptive immune response. Following either infection or phagocytic uptake of the virus, DCs migrate to the lymph nodes to present antigens derived from IAV to T lymphocytes (Fonteneau *et al.*, 2003; GeurtsvanKessel *et al.*, 2008).

1.3.1.2. Immune sensing

Innate immunity against IAV requires the rapid detection of viral PAMPs in infected cells, and later in phagocytic cells. Host PRRs bind to these viral PAMPs, and initiate the production and secretion of interferons (IFNs), pro-inflammatory cytokines and the expression of a variety genes encoding antiviral factors. A variety of PRRs have been found to be involved in the immune sensing of IAV, including Retinoic acid-inducible gene I (RIG-I), Toll-like Receptors (TLRs), and the Z-DNA binding protein 1 (ZBP1).

1.3.1.2.1. Retinoic acid-inducible gene I (RIG-I)

RIG-I is one of three members of the RIG-I-like receptor family of RNA helicase proteins encoded by the human genome, which also includes melanoma differentiation-associated protein 5 (MDA5), and laboratory of genetics and physiology 2 (LGP2) (Kang *et al.*, 2002; Yoneyama *et al.*, 2005; Yoneyama *et al.*, 2004). RIG-I, the primary PRR for the detection of IAV, is ubiquitously expressed in the cytoplasm of all human cells, and has recently been shown to also localise to the nucleus in IAV-infected A549 cells (a human alveolar epithelial cell line) (Liu *et al.*, 2018). This PRR is activated by the binding of its CTD to short, blunt ended double stranded RNA (dsRNA) or single stranded RNA (ssRNA) containing an exposed 5'-triphosphate (Cui *et al.*, 2008; Hornung *et al.*, 2006; Schmidt *et al.*, 2009). Ligand binding stimulates an ATP-dependent conformational change that liberates the N-terminal caspase activation and recruitment domains (CARDs) of RIG-I, which

mediate the downstream signalling (Gee *et al.*, 2008; Kowalinski *et al.*, 2011). Once released, the CARDs are lysine 63-linked poly-ubiquitinated by various ubiquitin ligases, including tripartite motif containing protein 25 (TRIM25), Riplet or TRIM4 (Oshiumi *et al.*, 2013; Yan *et al.*, 2014), although the relative contribution of these factors is debated (Choudhury *et al.*, 2022; Hayman *et al.*, 2019). The ubiquitin chains on the CARDs facilitate the assembly of RIG-I homo-oligomers along the RNA ligand, and thus the recruitment of the adapter molecule mitochondrial antiviral-signalling protein (MAVS) (Patel *et al.*, 2013; Peisley *et al.*, 2014). MAVS is a transmembrane protein expressed on the surface of mitochondria, with a cytoplasmic N-terminal CARD (Seth *et al.*, 2005) that interacts with the RIG-I CARDs to trigger MAVS oligomerisation (Hou *et al.*, 2011). MAVS oligomerisation also requires lysine 63-linked poly-ubiquitination, which, in this case, is mediated by TRIM31 (Liu *et al.*, 2017a). The RIG-I-MAVS aggregates subsequently recruit various downstream signalling molecules, leading to the activation and nuclear translocation of the transcription factors IFN-regulatory factor 3 (IRF3), and NF-κB, which mediate the expression of IFNs and pro-inflammatory cytokines (**Figure 1.5**) (Seth *et al.*, 2005).

RIG-I has been shown to bind to and be activated by the double stranded panhandle structure of the intact viral genome (Liu *et al.*, 2015a; Rehwinkel *et al.*, 2010). IAV infection also produces a variety of other RIG-I agonists including mini viral RNAs (mvRNAs) which are formed during dysregulated vRNA replication (Te Velthuis *et al.*, 2018). RIG-I is very important for the immune sensing of IAV in mammalian infection, and *RIG-I*$^{-/-}$ cells show attenuated expression of a large range of immune-related genes, particularly IFNα/β genes (Loo *et al.*, 2008; Opitz *et al.*, 2007). Furthermore, *RIG-I*$^{-/-}$ mice show defective IFN production and delayed IAV clearance, as well as impaired adaptive immune responses and immune memory (Kandasamy *et al.*, 2016).

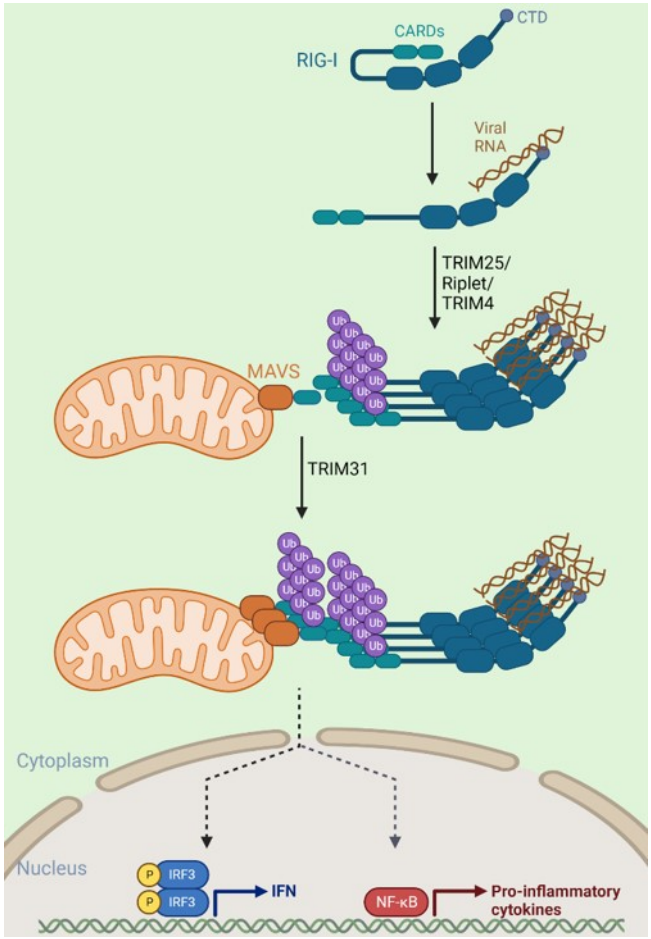

Figure 1.5 RIG-I signalling in response to viral RNA. *The CTD of RIG-I binds to viral RNA (either single stranded or double stranded RNA containing exposed 5'-triphosphate or short, blunt molecules of dsRNA), inducing a conformational change that liberates the N-terminal caspase activation and recruitment domains (CARDs). These CARDs in RIG-I are then lysine 63-linked poly-ubiquitinated by cellular enzymes such as TRIM25, Riplet and TRIM4. The ubiquitin chains facilitate the oligomerisation of activated RIG-I and the recruitment of mitochondrial antiviral-signalling protein (MAVS). MAVS is lysine 63-linked poly-ubiquitinated by TRIM31 and oligomerises with RIG-I. Aggregates of RIG-I and MAVS recruit signalling factors that lead to the activation of IFN-regulatory factor 3 (IRF3) and NF-κB, which mediate transcription of IFNs and pro-inflammatory cytokines. Created with Biorender.com.*

Further demonstrating the importance of RIG-I in IAV immune sensing, the virus has developed many strategies to suppress the RIG-I signalling pathway (Opitz *et al.*, 2007). NS1 has been shown to interact directly with multiple components of the RIG-I signalling pathway, and with RIG-I itself. For example, the RNA-binding domain of NS1 from influenza A/Brevig Mission/1918 (H1N1) was shown to interact with the

second CARD domain of RIG-I (Jureka *et al.*, 2015), and the NS1 of PR8 has been co-precipitated with RIG-I in overexpression experiments (Mibayashi *et al.*, 2007; Pichlmair *et al.*, 2006). Furthermore, the PR8 NS1 has recently been shown to inhibit expression of RIG-I by binding to a repressor of the *RIG-I* gene (Kumari *et al.*, 2020). Another mechanism of RIG-I inhibition that has been attributed to NS1 is the binding of TRIM25 or Riplet, which inhibits the ubiquitination of RIG-I required for its oligomerisation (Gack *et al.*, 2009; Rajsbaum *et al.*, 2012). This was found to be the case for multiple strains of virus, although the NS1 proteins from avian-adapted strains could not interact with human Riplet and bound preferentially to the galline orthologue of TRIM25, indicating species specificity and host adaptation of this immune antagonism (Rajsbaum *et al.*, 2012). Of note, the chicken genome does not contain genes encoding RIG-I or Riplet (Barber *et al.*, 2010; Magor *et al.*, 2013), which would explain why avian-adapted IAV strains would not be able to suppress its signalling.

Additionally, the PB2 proteins of some strains of IAV have been found to contain mitochondrial targeting signals at their N-termini (Carr *et al.*, 2006; Woodfin & Kazim, 1993), which allows the co-localisation and interaction of this normally nuclear polymerase subunit with MAVS (Graef *et al.*, 2010). This interaction inhibits IFN expression in MAVS overexpressing cells (Graef *et al.*, 2010). Graef *et al*. also reported that PB2 mitochondrial localisation was seen in the seasonal strains of human IAV tested, but not in avian strains; and that mutant strains, with the mitochondrial targeting signal removed, induced greater expression of IFN (Graef *et al.*, 2010). PB2-S1, an accessory protein transcribed from spliced mRNA of the PB2 segment, has also been shown to have mitochondrial localisation and inhibit RIG-I signalling (Yamayoshi *et al.*, 2016), presumably also via inhibition of MAVS. Furthermore, the protein expressed from the +1 ORF of the PB1 gene, PB1-F2, has

been seen to inhibit RIG-I signalling at the level of MAVS (Dudek *et al.*, 2011; Varga *et al.*, 2011). Moreover, Cheung *et al*. recently reported that the PB1-F2 of influenza A/Zhejiang/DTID-ZJU01/2013 (H7N9), but not of A/Wilson-Smith Neurotropic/1933 (WSN; H1N1), inhibited the interaction of TRIM31 with MAVS and thus MAVS oligomerisation (Cheung *et al.*, 2020).

Although RIG-I is the primary PRR for the detection of IAV in humans, MDA5, which signals in a similar way but binds to longer dsRNA ligands, has been found to be involved in the detection of highly pathogenic avian strains of IAV (H5N1) in both chicken and duck cells (Liniger *et al.*, 2012; Wei *et al.*, 2014). In chicken cells, MDA5 is able to partially compensate for the lack of RIG-I and facilitate an IFN response following IAV detection (Liniger *et al.*, 2012). MDA5 was also implicated in the sensing of IAV in an *in vivo* RNAi screen in mice (Benitez *et al.*, 2015). In this study, mice were infected with a library of mutant viruses that lacked NS1 but encoded various small interfering (si) RNAs targeting host genes, and the dominant strains were determined 96 hours post infection. IAV encoding MDA5-targeting siRNA emerged as a dominant strain in wild type mice but not in MDA5 deficient (*Ifih1*$^{-/-}$) mice (Benitez *et al.*, 2015). However, upon further investigation *in vitro*, MDA5 knockout was shown to only moderately decrease the IFN response to IAV, and an MDA5-mediated IFN response to IAV could not be detected in RIG-I deficient cells (Benitez *et al.*, 2015). This suggested that MDA5 may not recognise IAV-related PAMPs directly, but perhaps contributes to the amplification of IFN-associated gene expression in a RIG-I-dependent manner (Benitez *et al.*, 2015; Li *et al.*, 2022a).

1.3.1.2.2. Toll-like Receptors (TLRs)

Three human TLRs, 3, 7 and 8 are known to recognise viral RNA in order to induce antiviral gene expression (Malik & Zhou, 2020). All three, as well as TLR4 and 10 have been reported to be involved in the detection of IAV in cells of the innate immune

system (Malik & Zhou, 2020). Binding of TLRs to their ligands induce their dimerization and recruitment of adaptor proteins, myeloid differentiation primary response protein 88 (MyD88) or TIR-domain-containing adapter-inducing interferon-β (TRIF). This activates signalling cascades which result in the activation and nuclear localisation of transcription factors including IRF3, IRF7, and NF-κB. These mediate the expression of IFNs and pro-inflammatory cytokines (Malik & Zhou, 2020; Mifsud *et al.*, 2021).

TLR3 is expressed in the endosomal compartment of epithelial cells, fibroblasts, macrophages, and of DCs (Ioannidis *et al.*, 2013; Jelinek *et al.*, 2011). Binding of TLR3 to dsRNA in the endosome initiates the recruitment of TRIF and the induction of signalling that activates both IFN and pro-inflammatory cytokine expression (Yamamoto *et al.*, 2003). Other than the genome panhandle, which has not been reported to bind to TLR3, the normal IAV lifecycle does not generate dsRNA due to the recruitment of the cellular RNA helicase UAP56 to NP in the nucleus (Wisskirchen *et al.*, 2011),so the exact IAV PAMP that TLR3 binds in as yet unknown (Mifsud *et al.*, 2021). Pre-treatment of mice with a TLR3 agonist protected mice against lethal challenges with three strains of IAV (Wong *et al.*, 2009). However, this does not necessarily prove the direct sensing of IAV by TLR3. The authors of this study also found that pre-treatment with an agonist of TLR9, which binds DNA, provided protection against PR8 infection in mice (Wong *et al.*, 2009). IAV does not possess or produce DNA, so TLR9 is not detecting the virus directly. A subsequent study also reported that pre-activation of TLR9, as well as lipoprotein-binding TLRs, provides protection against IAV in mice (Tuvim *et al.*, 2012). This was likely due to non-specific stimulation of a pro-inflammatory response that inhibited IAV infection rather than an IAV-specific effect, which could also be the mechanism by which TLR3 stimulation provided protection.

Supporting the role of TLR3 in the direct innate immune sensing of IAV in infected cells, Le Goffic *et al*. reported that bronchial epithelial cells (BEAS-2B) in which TLR3 was inhibited by the overexpression of a non-functional dominant-negative form of the gene, showed greatly reduced NF-κB activity in response to infection with an H3N2 influenza (A/Scotland/20/1974) (Le Goffic et al., 2007). The same group also found that the lungs of *TLR3*$^{-/-}$ mice infected with IAV showed reduced production of pro-inflammatory cytokines and increased production of virus compared to wild type mice (Le Goffic et al., 2006). Interestingly, with this reduced inflammatory response, the *TLR3*$^{-/-}$ mice had a survival advantage, despite greater viral titres, demonstrating the immunopathological effects of inflammatory responses to IAV (Le Goffic et al., 2006).

TLR7 and 8 are endosomal ssRNA sensors (Heil *et al.*, 2004). Both are expressed in monocytes and DCs (Gorden *et al.*, 2005), TLR7 expression has also been observed on the apical surface of human airway epithelium (Ioannidis *et al.*, 2013), and TLR8 is highly expressed in neutrophils (Hayashi *et al.*, 2003). When activated by ligand binding, these receptors recruit MyD88 and activate a signalling cascade that results in IRF3 and NF-κB activation (Malik & Zhou, 2020). TLR7 was first reported to be activated by IAV in murine DCs, where cells generated from *TLR7*$^{-/-}$ mice showed reduced pro-inflammatory cytokine and IFN production in response to IAV infection or transfection with viral RNA (Diebold *et al.*, 2004). Soon after, a reduced immune response to IAV was also observed in human DCs treated with a TLR7 antagonist (Wang *et al.*, 2006). Similarly, neutrophils generated from *TLR7*$^{-/-}$ mice were also reported to have impaired anti-IAV immunity (Wang *et al.*, 2008a). TLR8 activation by the transfection of viral RNA was shown in 293T cells stably expressing the PRR (Wang *et al.*, 2008a). A more recent study observed that specifically blocking either TLR7 or TLR8 in human monocytes prior to IAV infection resulted in reduced expression of different sets of cytokines (de Marcken *et al.*, 2019). For example,

inhibition of TLR7 but not of TLR8 led to reduced production of interleukin (IL)-1β and IL-6, whereas blockade of TLR8 but not TLR7 resulted in decreased tumour necrosis factor (TNF) α (de Marcken *et al.*, 2019). Of note, TLR7 activation by IAV has not been reported in airway epithelial cells, only the expression of the receptor and its activation in these cells by a synthetic agonist (Ioannidis *et al.*, 2013).

The cell surface receptor TLR4 does not recognise viral molecules, but is instead activated by damage-associated molecular patterns (DAMPs), molecules produced from infected and damaged cells. For example, Tsai e*t al*. reported that calgranulin B, which was released by PR8-infected alveolar macrophages and airway epithelial cells, induced TLR4-dependent pro-inflammatory and apoptotic responses in cultured macrophages and in mice (Tsai *et al.*, 2014). Another IAV-associated DAMP that has been identified is oxidised phospholipids, which induce TLR4-mediated pro-inflammatory signalling in mice (Imai *et al.*, 2008). Interestingly, both of these studies found that knockout of TLR4 in mice, reduced IAV-related disease and pathogenesis (Imai *et al.*, 2008; Tsai *et al.*, 2014), similarly to *TLR3*$^{-/-}$ mice (Le Goffic *et al.*, 2006), as inflammatory responses often lead to tissue damage and pathology.

Finally, one study has implicated TLR10 in the detection of IAV infection (Lee *et al.*, 2014). The authors found that TLR10 expression in macrophages was increased following IAV infection and that knockdown of the receptor by RNAi reduced the IAV-induced expression of several cytokines, including IFNβ and IL-6, although the specific viral ligand of TLR10 was not identified (Lee *et al.*, 2014).

1.3.1.2.3. Z-DNA binding protein 1 (ZBP1)

ZBP1 is a cytosolic protein which binds to double stranded DNA with a left-handed helix structure, known as Z-DNA (Ha *et al.*, 2006; Pham *et al.*, 2006). The gene is upregulated in the presence of IFNs, and adopts a nuclear localisation (Pham *et al.*, 2006). ZBP1 has previously been associated with the sensing of DNA viruses, leading

to the activation of IRF3 and programmed cell death (Takaoka *et al.*, 2007; Upton *et al.*, 2012). In 2016, ZBP1 was reported, by two separate studies, to be required for the cell death of IAV-infected cells via necroptosis and apoptosis (Kuriakose *et al.*, 2016; Thapa *et al.*, 2016). Kuriakose *et al*. found that ZBP1 co-precipitated with the NP and PB1 proteins of IAV, and that *Zbp1*$^{-/-}$ cells mice had reduced inflammatory responses to IAV (Kuriakose *et al.*, 2016). Furthermore, they reported that ZBP1 expression was required for the programmed cell death, via apoptosis, necroptosis and pyroptosis, of IAV-infected macrophage and fibroblast cell lines (Kuriakose *et al.*, 2016). Thapa *et al*. also found that ZBP1 was required for IAV-induced cell death, however, they reported that mutant ZBP1, lacking the NP/PB1 binding region, was also capable of inducing cell death in IAV-infected cells, indicating that the viral proteins are not the ligand for ZBP1 (Thapa *et al.*, 2016). Instead, these authors posited that the IAV RNA genome was the PAMP for ZBP1-mediated sensing of the virus. Supporting this hypothesis, vRNA mapping to all eight gene segments were detected with immunoprecipitation of tagged ZBP1 from infected cells (Thapa *et al.*, 2016). Thapa *et al*. posited a model in which cytoplasmic ZBP1 recognises and binds to viral genomic RNA following its nuclear export, leading to ZBP1 oligomerisation and the activation of receptor-interacting serine/threonine-protein kinase 3 (RIPK3), which initiates apoptosis and necroptosis cell death pathways (Nogusa *et al.*, 2016; Thapa *et al.*, 2016). In this model the vRNA is either present in a Z-RNA conformation (double stranded left-handed helix structure) or adopts a Z-RNA conformation following ZBP1-binding (Thapa *et al.*, 2016). Recently, Zhang *et al*. reported that short Z-RNA molecules are produced as part of defective replication of the viral genome (Zhang *et al.*, 2020). Nuclear ZBP1 colocalised with these Z-RNAs and induced both RIPK3-mediated cell death pathways (Zhang *et al.*, 2020).

1.3.1.3. Interferons and interferon stimulated genes

As described above, the recognition of viral PAMPs often leads to the activation of IRF3 and IRF7, which are transcription factors that mediate the expression of type I IFNs (Au *et al.*, 1998; Sato *et al.*, 1998; Schafer *et al.*, 1998). IFNs are antiviral cytokines that were first described in 1957, when they were discovered to interfere with the replication of IAV (Isaacs & Lindenmann, 1957; Isaacs *et al.*, 1957). There are three distinct families of IFN: type I, which in humans includes IFNα, IFNβ, IFNε, IFNκ, and IFNω; type II, which consists of IFNγ only; and type III, which includes IFNλ 1, 2, 3, and 4 (de Weerd & Nguyen, 2012; Pestka *et al.*, 2004). Type I and III IFNs are expressed by most cell types, including respiratory epithelial cells, whereas IFNγ is primarily expressed by NK cells and cytotoxic T cells (Iwasaki & Pillai, 2014; Wu & Metcalf, 2020). Expression of both type I and III is activated by viral infection and these cytokines signal through similar pathways, but via separate receptors, to stimulate the expression of interferon stimulated genes (ISG) (Ank *et al.*, 2006; Onoguchi *et al.*, 2007). Type I IFNs, particularly IFNα and IFNβ, are the most well understood of the families and greatly influence both the innate and adaptive immune response to IAV in mammals (Wu & Metcalf, 2020), so will be the focus of discussion in this section.

When type I IFNs are expressed by IAV infected cells, they are then secreted and bind to receptors on both infected and uninfected neighbouring cells to induce antiviral gene expression to limit the spread of the virus. The type 1 IFN-α/β receptor (IFNAR) is composed of two subunits, IFNAR1 and IFNAR2 (**Figure 1.6**), each containing an extracellular ligand-binding domain and a cytoplasmic tail which is associated with a tyrosine kinase, tyrosine kinase 2 (Tyk2) and Janus kinase 1 (Jak1) respectively (Randall & Goodbourn, 2008). Following ligand binding, the two subunits dimerise and activate their associated tyrosine kinases, which in turn activate the signal

transducers and activators of transcription (STAT) 1 and STAT2 by phosphorylating them. Phosphorylated STAT1 and STAT2 then form a heterodimer, which associates with an IRF9 monomer to form the IFN-stimulated gene factor 3 (ISGF3). ISGF3 is then translocated to the nucleus where the heterotrimer binds to the IFN-stimulated response element (ISRE), present in the promoters of most ISGs to enhance their expression (Randall & Goodbourn, 2008; Wu & Metcalf, 2020). Some of the ISGs that have been associated with anti-IAV immunity are discussed below.

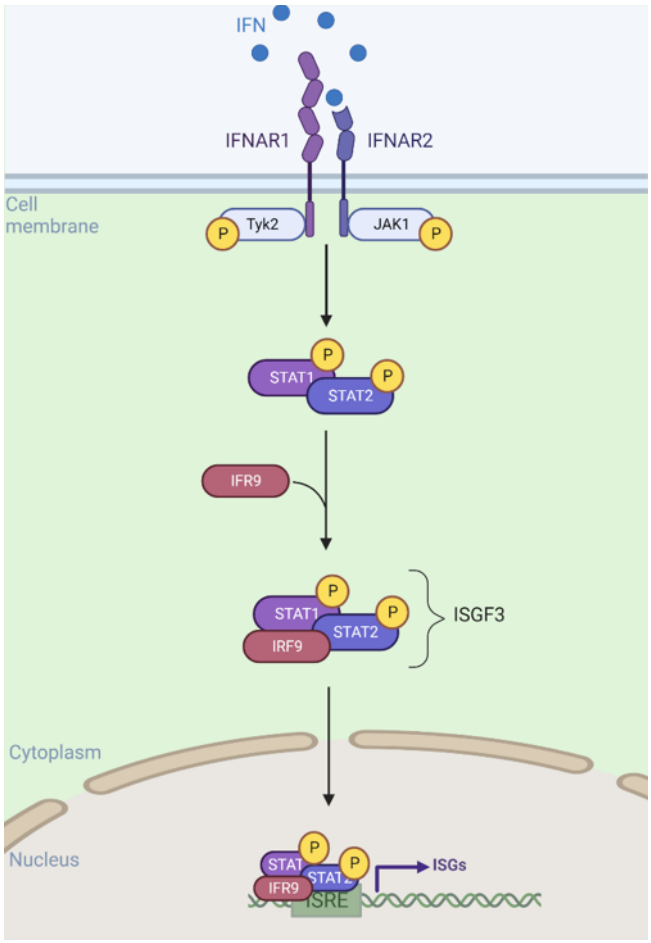

Figure 1.6 IFN type I signalling. *IFN binds to type 1 IFN-α/β receptor (IFNAR) subunits 1 and 2 on the cell surface. The IFNAR subunits activate the associated tyrosine kinases Tyk2 and JAK1, which phosphorylate signal transducer and activator of transcription (STAT)1 and STAT2, activating them to form a heterodimer. The STAT1-STAT2 dimer associates with IRF9 to form IFN-stimulated gene factor 3 (ISGF3), which translocates to the nucleus and regulates the expression of IFN-stimulated genes (ISGs) under the control of an IFN-stimulated response element (ISRE). Created with Biorender.com.*

1.3.1.3.1. Myxovirus resistance protein A (MxA)

MxA is the human orthologue of the murine large GTPase Mx1, both of which are encoded by the *MX1* gene. Both Mx1 and MxA have been found to inhibit the replication of IAV, as well as many other viruses (Haller *et al.*, 2007; Pavlovic *et al.*, 1992). In mice, nuclear Mx1 inhibits the transcription of the IAV genome and thus expression of viral genes (Krug *et al.*, 1985), whereas human MxA accumulates in the cytoplasm, binds to NP, and prevents nuclear import of the vRNP (Turan *et al.*, 2004; Xiao *et al.*, 2013). Mutations in NP that prevent this MxA-mediated restriction are associated with viruses that are capable of cross-species transmission from animal reservoirs into humans (Deeg *et al.*, 2017; Dittmann *et al.*, 2008; Zimmermann *et al.*, 2011).

1.3.1.3.2. IFN-inducible transmembrane (IFITM) proteins

The human genome encodes four functional *IFITM* genes, three of which encode proteins that have been associated with antiviral activity against IAV (Brass *et al.*, 2009). Overexpression of human IFITM1, IFITM2 or IFITM3 in cell culture has been shown to restrict IAV replication whereas knockdown of IFITM3 by RNAi enhanced IAV infection (Brass *et al.*, 2009). Furthermore, deletion of the entire *Ifitm* locus in mice, meaning that no IFITM proteins are expressed, leads to increased IAV replication and enhanced morbidity and mortality (Bailey *et al.*, 2012; Everitt *et al.*, 2012). The specific knockout of *Ifitm3*, but not *Ifitm1* or *Ifitm2*, gives the same results, indicating that IFITM3 is the most potent and important IAV inhibitor of the family in mice (Bailey *et al.*, 2012; Everitt *et al.*, 2012). IFITM3, which is found in the endosomal compartment, inhibits IAV envelope fusion and release of viral components into the cytoplasm, although the exact mechanism of this is not yet known (Feeley *et al.*, 2011; Huang *et al.*, 2011).

1.3.1.3.3. 2'-5'-oligoadenylate synthase (OAS) and RNaseL

Similarly to PRRs, OAS is activated by the binding of dsRNA in the cytoplasm, it then activates RNaseL, which cleaves both viral and cellular ssRNA, inhibiting viral replication (Silverman, 2007). The resulting RNA degradation products may also be recognised by RIG-I, potentiating the antiviral response (Malathi *et al.*, 2007). The OAS/RNaseL pathway is efficiently inhibited by the IAV NS1 protein, which also binds dsRNA, competing with OAS (Min & Krug, 2006). This RNA binding ability of NS1 can be much reduced by a single amino acid substitution (R38A), which greatly attenuates the replication of viruses expressing the mutant NS1. The replication of such viruses can be mostly rescued by the depletion of RNaseL (Min & Krug, 2006).

1.3.1.4. Inflammatory mediators

In addition to IFNs, PRR recognition of IAV also leads to the expression of pro-inflammatory cytokines. A primary function of most inflammatory cytokines is the recruitment and activation of various cells such as macrophages, neutrophils and DCs (Guidotti & Chisari, 2001; Mifsud *et al.*, 2021). They also activate epithelial cells to detect and respond to infection; for example, treatment of A549 cells with TNFα has been shown to induce the expression of RIG-I and TLR3, as well as other factors involved in the signalling of these receptors (Matikainen *et al.*, 2006). Additionally, the signalling induced by pro-inflammatory cytokines can induce programmed cell death in infected cells in order to prevent the spread of infection (Fujikura & Miyazaki, 2018). The composition of the inflammatory environment instructs and directs the development of the adaptive response as it influences the differentiation of activated T cells (Chen *et al.*, 2018; Iwasaki & Pillai, 2014).

1.3.2. Adaptive immunity to IAV infection

1.3.2.1. T cells

As mentioned above, activation of the adaptive immune response in IAV infection is largely mediated by DCs, which acquire viral antigens in the lung, migrate to the

draining lymph nodes, and present antigens to T cells. DCs activate both $CD8^+$ and $CD4^+$ T cells, generally depending on the manner by which they acquired the IAV antigen. DCs that have been infected by IAV present peptides, generated by proteosomal degradation of viral proteins, on MHC class I molecules to naïve $CD8^+$ T cells (Ho *et al.*, 2011). These cells are then activated to differentiate into cytotoxic T lymphocytes (CTLs) which migrate to the sites of infection to clear infected cells and therefore prevent further spread of the virus (Bhardwaj *et al.*, 1994; Ho *et al.*, 2011; Topham *et al.*, 1997). DCs that have phagocytosed virus or apoptotic, virus-infected epithelial cells, are able to present antigen on MHC class I molecules as described above, but also degrade viral proteins in the lysosome to create peptides that are presented on MHC class II molecules to naïve $CD4^+$ T helper cells (van de Sandt *et al.*, 2012). Depending on the cytokines present, activated $CD4^+$ T cells can differentiate into various T helper (Th) effector subtypes. For example, Th1 cells promote the migration and activity of CTLs and macrophages, whereas Th2 cells promote the activation of B cells to produce antibodies (Chen *et al.*, 2018; La Gruta & Turner, 2014; van de Sandt *et al.*, 2012). Additionally, the differentiation of $CD4^+$ T cells in to regulatory T helper cells (Tregs) limit the CTL response in order to minimise damage caused to the host via immune cytotoxicity (La Gruta & Turner, 2014).

1.3.2.2. B cells and antibodies

The activation of naïve B cells by DCs and T helper cells in the lymph nodes causes them to differentiate into antibody-forming plasma cells. During the first infection of a host with an IAV strain, activated B cells produce antibodies of immunoglobulin (Ig) M, IgG, and IgA subtypes, whereas in a secondary infection with the same strain, IgM antibodies are not observed (Chen *et al.*, 2018; van de Sandt *et al.*, 2012). IgA antibodies mediate mucosal neutralisation of virus, whereas IgG is responsible for preventing the systemic spread of the virus (Chiu *et al.*, 2015). Antibodies directed

against HA can neutralise extracellular virions by binding near to the receptor binding site and preventing cell attachment and internalisation into new cells (Jung & Lee, 2020; van de Sandt *et al.*, 2012). NA-specific antibodies do not neutralise IAV but can inhibit the enzymatic activity and thus prevent release of progeny viruses from infected cells (Jung & Lee, 2020; van de Sandt *et al.*, 2012). Furthermore, the binding of NA or M2 on the surface of infected cells can facilitate antibody-dependent cell cytotoxicity by NK cells (Jung & Lee, 2020).

The adaptive immune response to the first infection with an IAV strain is relatively slow to develop, however it produces memory T and B cells. These memory cells allow a rapid, highly specific response to the virus upon secondary exposure to the same strain. Both $CD4^+$ and $CD8^+$ memory T cells have been shown to be important for quickly recognising and clearing infection (Grant *et al.*, 2016; Wilkinson *et al.*, 2012).

1.3.2.3. Antigenic drift and shift

IAV is able to escape host immune memory via a process called antigenic drift. Antigenic drift describes the accumulation of amino acid substitutions in the viral glycoproteins HA and NA. The selection pressure exerted by antibodies and memory immune cells leads to the emergence of new strains of IAV that are no longer recognised as effectively by the memory immunity within a population of hosts (Krammer, 2019; Krammer *et al.*, 2018). This is key contributor to the necessity for annual vaccination and surveillance of circulating IAV strains in order to determine the composition of these vaccines (European Centre for Disease Prevention and Control, 2022; Krammer, 2019).

Additionally, the segmented nature of the IAV genome and the availability of animal reservoirs allows for more drastic changes in antigenicity via reassortment. This occurs when two or more strains of IAV infect the same host and exchange the

genomic segments encoding the surface glycoproteins, creating a progeny virus with radically different surface antigens (Krammer, 2019; Krammer *et al.*, 2018). These new strains, which are antigenically different from circulating strains, may be able to cross the host species barrier into human populations with limited resistance, leading to large scale outbreaks and pandemics (Krammer, 2019; Krammer *et al.*, 2018; Nypaver *et al.*, 2021).

1.4. IAV treatments

1.4.1. Currently available treatments

1.4.1.1. M2 ion channel blockers

The first drug used for treatment of IAV infection was amantadine, a chemical derivative of adamantane, that was approved for clinical use in the UK in 1966 (Davies *et al.*, 1964; Lampejo, 2020). Subsequently, rimantadine, another adamantane derivative, was approved for use in 1993 (Lampejo, 2020). Both drugs work by interacting with the M2 tetramer within the transmembrane "proton gate" structure in order to inhibit the conduction of protons and thus the acidification of the viral core, which is required for the uncoating of the virion (Hay *et al.*, 1985; Khurana *et al.*, 2011; Schnell & Chou, 2008; Stouffer *et al.*, 2008). The efficacy of the adamantanes against clinical disease was initially up to 90%. However IAV strains that were resistant to these drugs were first detected in the 1980s (Hay *et al.*, 1985). Since 2000, there has been a drastic rise in adamantane-resistant strains of IAV. By 2013 approximately 45% of all IAV human subtypes in circulation globally were estimated to be resistant (Hussain *et al.*, 2017) and a more recent analysis estimated that approximately 80% of global human IAV isolates harboured drug resistant M2 genes (He *et al.*, 2021). Due to this widespread resistance, adamantanes are no longer recommended for the treatment of IAV infection (Lampejo, 2020; UK Health Security Agency, 2021).

1.4.1.2. Neuraminidase inhibitors

In the UK, two neuraminidase inhibitors (NAIs), oseltamivir (Tamiflu; oral agent) and zanamivir (Relenza; inhaled or administered intravenously) are approved and recommended for prophylaxis and treatment of IAV infection; additionally peramivir has been licenced but not launched in the UK (Lampejo, 2020; UK Health Security Agency, 2021). Development of NAIs for the treatment of IAV began in the 1960s, and the current inhibitors were designed following the determination of the NA sialic acid binding site in the 1980s (Colman, 1994; Colman *et al.*, 1983). NAIs mimic sialic acid, fitting into the NA active site and competitively inhibiting the binding of the natural substrate (Moscona, 2005). As the sialidase activity of NA is required for the release of progeny virus from infected cells and the movement of virus particles through mucosal layers in the respiratory tract, NAIs inhibit the spread of the virus within and between hosts (Cohen *et al.*, 2013; Griffin *et al.*, 1983; Palese *et al.*, 1974). In the 2007-2008 influenza season, human H1N1 strains were isolated which contained an NA mutation that conferred resistance to oseltamivir (Bloom *et al.*, 2010; Saito *et al.*, 2010). This mutation (H274Y/H275Y) prevents a conformational change in the NA active site which is required for oseltamivir but not zanamivir binding, so zanamivir susceptibility is not reduced (Lampejo, 2020; Moscona, 2009). Extremely high rates (>90%) of oseltamivir resistance, specifically this mutation, were seen during the 2008-2009 influenza season (Baranovich *et al.*, 2010; Dharan *et al.*, 2009; Matsuzaki *et al.*, 2010). However the pandemic H1N1 IAV strain that emerged worldwide in 2009 mostly remained susceptible to oseltamivir, and the susceptibility of subsequent seasonal strains has remained high (Lampejo, 2020).

1.4.1.3. Cap-dependent endonuclease inhibitor

Baloxavir Marboxil (Xofluza) was licenced in Japan and the USA in 2018 and was approved by the UK Medicines and Healthcare products Regulatory Agency (MHRA) in July 2021, but is currently only recommended to be used in the context of research

(UK Health Security Agency, 2021). This drug is an inhibitor of the cap-dependent endonuclease activity required for cap snatching (Noshi *et al.*, 2018; Takashita *et al.*, 2018; Yuan *et al.*, 2009). Baloxavir Marboxil is currently the only drug in this class. Due to its recent release, there is limited data on resistance; however some H3N2 viruses with reduced susceptibility, containing an amino acid substitution in PA (I38T) have been isolated from patients following treatment (Takashita *et al.*, 2019a; Takashita *et al.*, 2019b; Uehara *et al.*, 2020). The PA sequences of these viruses were not the same, indicating that the resistance mutations emerged separately (Takashita *et al.*, 2019a; Takashita *et al.*, 2019b). These mutant strains were associated with higher viral loads and longer duration of infection and symptoms in patients treated with Baloxavir compared to viruses lacking this substitution (Uehara *et al.*, 2020). The transmissibility of the I38T strains has not yet been determined. As with all antimicrobial treatment, careful surveillance and monitoring of emerging resistance is required as Baloxavir Marboxil use continues.

1.4.2. Targeting the host

As with evasion of the immune system, IAV is able to accumulate random mutations that can lead to the emergence of resistance when subjected to the selection pressure of drug treatment. In contrast, humans possess proof reading-competent genome replication machinery so mutations occur less frequently. Furthermore, due to its limited coding capacity, IAV requires the presence and activity of host factors to complete every stage of its lifecycle. This makes the targeting of the host, exploiting the dependency of the virus, an attractive strategy for the design of novel antiviral treatments for IAV (Baillie & Digard, 2013; Ho *et al.*, 2021; Watanabe & Kawaoka, 2015). Ideal targets for antiviral therapeutics are host factors upon which the virus relies heavily but of which the host can tolerate temporary or partial inhibition.

There are a number of routes by which such targets can be identified, including targeted research based on existing knowledge of the virus or host. For example, the role of Rab11a in trafficking of IAV vRNPs was initially investigated due to its known cellular role and because it had previously been implicated in the lifecycles of other viruses (Bruce *et al.*, 2010). Such a targeted approach often comes with established tools, protocols and information about the host factor that can aid in both the investigation of their role in the viral life cycle and in the design of drugs and treatments that target them. An example of specific understanding of host factors being used to develop treatments is Verdinexor, a CRM1 inhibitor that is currently being investigated by Karyopharm Therapeutics (Karyopharm Therapeutics, 2022). Early research into CRM1 in nuclear export of vRNPs showed that treatment of cells with leptomycin B, which irreversibly inactivates CRM1, blocked viral replication (Elton *et al.*, 2001). As leptomycin B is toxic *in vivo*, so would not make a suitable antiviral treatment, Perwitasari *et al*. tested Verdinexor, a compound identified in a screen for specific, reversible inhibitors of CRM1 for the treatment of cancers (Perwitasari *et al.*, 2014). They found that this drug had antiviral effects both *in vitro* and *in vivo* (mice and ferrets), and work on Verdinexor in humans is ongoing (Karyopharm Therapeutics, 2022; Perwitasari *et al.*, 2014; Perwitasari *et al.*, 2016).

Additionally, large scale genome-wide screens are an invaluable tool for the identification of host factors. Many genome-wide RNAi screens examining host genes required for IAV infection have been performed in recent years (Brass *et al.*, 2009; Karlas *et al.*, 2010; Su *et al.*, 2013; Tran *et al.*, 2013). Host factors identified in these screens include COPI, UBR4 and IFITM3 (Brass *et al.*, 2009; Sun *et al.*, 2013; Tripathi *et al.*, 2015). More recently, CRISPR/Cas9 technology has been employed in genome-wide screens to identify host factors (Han *et al.*, 2018; Li *et al.*, 2020a). Such large scale screens have the benefit of potentially revealing unexpected host factors

that might not have been identified otherwise. The downside of screening approaches is that these novel targets often require careful validation to confirm their importance to virus replication, as well as to identify why (or if) they are important.

1.5. Aims

The aim of this thesis was to investigate various human genes that had been implicated in the lifecycle of IAV, with a view to dissect the role of these proteins in the IAV infection and to assess their suitability as drug targets. The host factors investigated in this study had been identified through various routes. In Chapter 2, I investigated the arginine demethylase Jumonji domain containing protein 6 (JMJD6) which previous work has found to have multiple roles in immunity. JMJD6 had been suggested to be a host factor for other viral pathogens, and work in the Roslin Institute by Dr Janice Kwok had found evidence that IAV replication was impaired in the absence of the human enzyme. Next, the cap methyltransferase 1 (CMTR1), which had been identified in a genome-wide CRISPR/Cas9 screen was examined in Chapter 3. Finally, the family of insulin-like growth factor 2 mRNA binding proteins (IGF2BP) was chosen for investigation due to their cellular role as N^6-methyladenosine (m^6A) reader proteins (the emerging role of m^6A RNA modification in IAV is discussed in Chapter 4) and because they had been identified in IAV-host interaction screens.

In each case, I used siRNA knockdown of the host factors to examine IAV replication in their absence. I also used over expression of host proteins and pharmaceutical agents to evaluate their contribution to the IAV lifecycle. This work aimed to dissect the role of these proteins in the viral lifecycle and to assess their suitability as drug targets in the treatment of IAV infection.

Chapter 2: Dissecting the proviral role of JMJD6

2.1. Background and aims

2.1.1. JMJD6

JMJD6 is a highly conserved nuclear protein, part of a family of metalloenzymes containing the Jumonji C domain, that is essential to several cellular functions including the regulation of transcription and of chromatin structure (Kwok *et al.*, 2017). The proteins in this family are oxygenases; capable of catalysing demethylation and hydroxylation reactions (Kwok *et al.*, 2017). JMJD6 was initially proposed to be a phosphatidylserine receptor, expressed on the cell surface of macrophages as well as fibroblastic and epithelial cell lines, allowing the phagocytosis of apoptotic cells (Fadok *et al.*, 2000). This was later disputed when the protein was found to have a nuclear localisation and functions (Böse *et al.*, 2004; Cui *et al.*, 2004).

2.1.1.1. JMJD6 protein

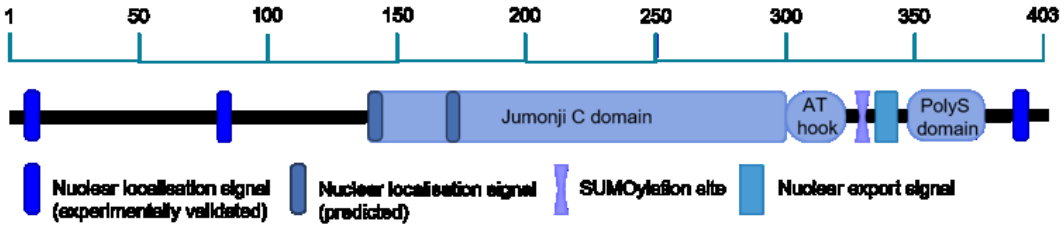

Figure 2.1: The human JMJD6 protein domain structure. Scale bar indicates amino acid coordinates, running from N- to C-terminus. PolyS indicates a poly serine domain. Other features as labelled.

In addition to the central enzymatic Jumonji C domain, JMJD6 contains an AT-hook-like motif. Canonical AT-hook domains facilitate the recognition and binding of DNA (Reeves & Nissen, 1990), and similar domains, extended by basic amino acids in both N- and C-terminal directions, bind RNA (Filarsky *et al.*, 2015). The motif in JMJD6 is extended in the C- but not the N-terminal direction so is neither the classical nor the

extended AT-hook (Kwok *et al.*, 2017). JMJD6 has not been shown to interact directly with DNA but is able to bind efficiently to single stranded RNA (Hong *et al.*, 2010). Furthermore, the in the three-dimensional structure of JMJD6, the AT-hook, as well as a predicted SUMOylation site located in the C-terminal direction, are thought to be accessible for protein-protein interactions (Hahn *et al.*, 2008).

JMJD6 contains five proposed nuclear localisation signals, three of which have been validated (Cikala *et al.*, 2004; Cui *et al.*, 2004). The other two are located in the JmjC domain and are unlikely to have an effect on JMJD6 localisation (Cikala *et al.*, 2004). A nuclear export signal has also been predicted towards the C-terminus (Hahn *et al.*, 2008). A C-terminal poly-serine (polyS) domain of JMJD6 has been shown to be required for the subnuclear localisation of the protein to the nucleoplasm (Wolf *et al.*, 2013). An alternatively spliced variant of JMJD6 lacking the polyS domain shows predominant localisation to the nucleolus and interact with nucleolar proteins (Wolf *et al.*, 2013). **Figure 2.1** shows the domain structure of JMJD6 with its established features.

The enzyme can be found as a monomer or homo-multimers (Hahn *et al.*, 2010; Tibrewal *et al.*, 2007). The purpose and result of the oligomerisation of the protein is not yet understood, but expression of multimers varies between cell types (Kwok *et al.*, 2017), suggesting that the extent of oligomerisation may influence function of the enzyme.

2.1.1.2. JMJD6 functions

Three enzymatic functions of JMJD6 have been reported: arginine demethylation, lysyl hydroxylation and, more recently, tyrosine phosphorylation.

In 2007 JMJD6 was shown to demethylate arginine residues in histones H3 and H4 (Chang *et al.*, 2007). Arginine methylation is an important and common post-

translational modification. Arginine residues of both nuclear and cytoplasmic proteins can be mono- or di-methylated by protein arginine methyltransferase (PRMT) enzymes with various functional consequences (Bedford & Clarke, 2009; Gao *et al.*, 2015). An important example of protein arginine methylation is seen within the histone code in which arginine residues of histone tails are methylated leading to the activation or repression of gene expression (Di Lorenzo & Bedford, 2011). For many years protein arginine methylation was thought to be an irreversible post translational modification until Chang *et al*. reported the arginine demethylase activity of JMJD6 (Chang *et al.*, 2007). However, there has been variable success in reproducing this histone demethylation in subsequent studies (Boeckel *et al.*, 2011; Liu *et al.*, 2013; Webby *et al.*, 2009).

Several other protein substrates for JMJD6 arginine demethylase activity have been proposed, including oestrogen receptor α (ERα), where JMJD6 removes an inhibitory methyl from Arginine 260 (Poulard *et al.*, 2014); and heat shock protein 70 (HSP70), for which removal of the methyl mark at Arginine 469 prevents interaction with chromatin (Gao *et al.*, 2015). Additionally, JMJD6 has been shown to demethylate the 5′-methyl cap of the noncoding 7SK small nuclear RNA (snRNA) as part of RNA polymerase II promoter-proximal pause release (Liu *et al.*, 2013).

Further to its roles in transcriptional regulation via polymerase II promoter-proximal pause release and histone demethylation, JMJD6 is also though to contribute to RNA processing through lysyl hydroxylase activity. This enzymatic activity adds a hydroxyl group to lysine residues in the essential splice factor U2 auxiliary factor 65 kDa subunit (U2AF65) as well as several other proteins involved in alternative splicing (Heim *et al.*, 2014; Webby *et al.*, 2009). Through this involvement in the spliceosome complex, JMJD6 alters alternative splicing patterns of many genes, including its own (Raguz *et al.*, 2020). JMJD6 has also been shown to hydroxylate histones H2a, H2b,

H3 and H4 (Unoki *et al.*, 2013), although the effects of this modification on chromatin structure and gene expression are yet to be discovered.

Recently, JMJD6 has been suggested also to have tyrosine kinase activity. Liu *et al*. found that JMJD6 phosphorylated Tyrosine 39 of the histone variant H2A.X, which altered the expression of various autophagy-related genes (Liu *et al.*, 2019).

Via these many proposed enzymatic activities, JMJD6 is potentially involved in multiple biological processes. Namely, JMJD6 has essential functions in embryogenesis as the protein is required for stem cell differentiation and the development of several tissues (Ji *et al.*, 2022; Kwok *et al.*, 2017) and *JMJD6* knockout in mice is perinatally lethal (Böse *et al.*, 2004). Furthermore, overexpression of JMJD6 has been reported in many human cancers and high levels of expression are associated with poor prognosis (Liu *et al.*, 2019; Vangimalla *et al.*, 2017; Yang *et al.*, 2020). Additionally, JMJD6 has been implicated the regulation of the immune system and in various infectious diseases.

2.1.1.3. JMJD6 and the immune response

JMJD6 is required for the embryonic development of the thymus and of T lymphocytes (Kunisaki *et al.*, 2004), the mechanism of which has been proposed to be via regulation of *Autoimmune Regulator* (*AIRE*) alternative splicing (Yanagihara *et al.*, 2015). In *JMJD6*$^{-/-}$ medullary thymic epithelial cells (mTEC), the *AIRE* transcript was not efficiently spliced leading to reduced abundance of mature AIRE protein, which is required for the deletion of autoreactive T cells. This was partially rescued by the transient expression of wild type JMJD6 but not a lysyl hydroxylase-defective mutant, suggesting that JMJD6-mediated lysyl hydroxylation of splice factors is required for effective *AIRE* splicing (Yanagihara *et al.*, 2015). Moreover, JMJD6 is highly expressed in healthy immune cells, including both $CD4^+$ and $CD8^+$ T cells and

monocytes (Forrest *et al.*, 2014) and has recently been shown to be essential for the maintenance of hematopoietic stem cells (Lawson *et al.*, 2021).

Within the innate immune response, JMJD6 may play a role in TLR signalling by removing inhibitory arginine methylation from TNF receptor-associated factor (TRAF6), which is part of the TLR-induced signalling cascade that leads to NF-κB activation (Tikhanovich *et al.*, 2015). Tikhanovich *et* al. reported that, in Huh7.5 and THP-1 cells, stimulation of TLRs lead to a decrease in the protein arginine methyltransferase 1 (PRMT1)/JMJD6 ratio. This resulted in an increase in the levels of demethylated, and thus active, TRAF6. Two arginine residues in TRAF6, Arginine 88 and Arginine 125, were identified as important targets of PRMT1. Inhibition of arginine methylation, or reduction of PRMT1 protein levels led to increased TRAF6 activity. Increased NF-κB nuclear localisation and activation, as well as transcription of NF-κB target genes, were also observed. This effect was not seen in the absence of JMJD6 and could also be induced by JMJD6 overexpression (Tikhanovich *et al.*, 2015). Proximity ligation assays and co-immunoprecipitation experiments within this study also showed interaction between JMJD6 and TRAF6 (Tikhanovich *et al.*, 2015), further supporting this immune role of JMJD6.

Another suggested role for JMJD6 in immunity is in the formation of stress granules (SG) (Tsai *et al.*, 2017). SGs are RNA-protein complexes which form in the cytoplasm of cells following stress-induced translation inhibition. They are thought to prevent mRNA degradation due to stress and to aid activation of innate immunity, including antiviral immunity (Oh *et al.*, 2016). Included in the complexes are SG-nucleating proteins, overexpression of which induces SG formation. One such protein is the DNA and RNA helicase G3BP1 which is methylated on three arginine residues by PRMT1 and PRMT5. Tsai *et al*. showed that JMJD6 interacted with G3BP1 within SG complexes to demethylate all three of these residues to promote SG formation in

HeLa and U2OS cells (Tsai *et al.*, 2017). JMJD6 demethylase activity was required for maximal induction SG formation in response to various types of stress (Tsai *et al.*, 2017).

Through these described functions within the immune system JMJD6 may broadly impact viral infection. The protein has also been specifically connected to the lifecycles of and immunity to a number of different viruses. This research is described in the next section.

2.1.1.4. JMJD6 and viruses

As mentioned above, JMJD6 has been shown to play important roles in T cell-mediated immunity. This was further supported by research related to hepatitis B virus (HBV) infection, where JMJD6 expression was found to be reduced in the $CD4^+$ T cells of chronic hepatitis B patients (Chen *et al.*, 2014). This finding highlighted a role of JMJD6 in the regulation of T cell proliferation.

Another DNA virus JMJD6 has been associated with is vaccinia virus (VACV). In her PhD thesis, Dr Janice Kwok (The Roslin Institute, University of Edinburgh) investigated VACV infection in JMJD6-deficient bone marrow derived macrophages (BMDM). In these cells, levels of intracellular virus as well as the expression of some late viral genes were decreased compared to wild type BMDM (Kwok, 2018). Furthermore, cell death following VACV infection was greater in the absence of JMJD6 (Kwok, 2018). However, siRNA knockdown of JMJD6 in HeLa cells had no effect on VACV replication or spread (Kwok, 2018), indicating that the reported effect of JMJD6 expression was cell specific. Dr Kwok concluded that JMJD6 had a proviral role in the VACV lifecycle in macrophages, although the mechanism behind this was not defined.

JMJD6 has also been implicated in the lifecycles of RNA viruses. Lawrence *et al*. suggested an indirect proviral role for JMJD6 in foot and mouth disease virus (FMDV), a *Picornavirus* with a single stranded, positive sense genome (Lawrence *et al.*, 2014; Lawrence & Rieder, 2009). Following FMDV infection, levels of non-methylated RNA helicase A (RHA) increased and accumulated in the cytoplasm (Lawrence *et al.*, 2014). RHA acts as a proviral host factor in FMDV infection as it promotes the assembly of the viral replication complex (Lawrence & Rieder, 2009). The increase in non-methylated RHA was due to the demethylation of arginine residues in the C-terminus of the protein which determines its cellular localisation (Smith *et al.*, 2004). Lawrence et al. found that JMJD6 co-precipitated with RHA, and that inhibition of JmjC demethylases with the small molecule inhibitor N-oxalylglycine led to reduced cytoplasmic accumulation of RHA, which in turn lead to reduced production of FMDV viral protein and titres (Lawrence *et al.*, 2014). Thus JMJD6 had a proviral effect on FMDV replication by regulating another host factor.

The arginine demethylase activity of JMJD6 may also play a regulatory role in the type I IFN pathway. Ganesan *et al*. observed that Huh 7.5 cells overexpressing JMJD6 had reduced levels of STAT1 arginine methylation, while cells transfected with JMJD6-targeting siRNA showed the reverse (Ganesan *et al.*, 2018). These data suggested that methylated STAT1 is a substrate of JMJD6. The study also reported that JMJD6 expression affected mRNA expression of the ISGs *OASL* and *OAS-1* in hepatitis C virus (HCV) infected cells following pre-treatment with IFNα. Expression of the ISGs increased following JMJD6 knockdown and decreased with JMJD6 overexpression (Ganesan *et al.*, 2018). Through this STAT1 demethylation, the authors proposed that JMJD6 prevents activated STAT1 from attaching to DNA and activating the transcription of ISGs (Ganesan *et al.*, 2018). The importance of STAT1 methylation had previously been shown. Methylation of STAT1 at the highly

conserved residue Arginine 31 is required for efficient binding of phosphorylated STAT1 to DNA (Mowen *et al.*, 2001). This is due to protein inhibitor of activated STAT1 (PIAS1) binding to the unmethylated STAT1 which prevents the formation of STAT1-STAT2 dimers, a crucial step in the type I IFN signalling pathway (Mowen *et al.*, 2001). This was the first time the role of JMJD6 in the type I IFN signalling pathway had been suggested.

More recently, JMJD6 was again linked to the regulation of type I IFN responses in viral infections, although via a different mechanism than previously presented. Zhang *et al*. reported that overexpression of JMJD6 in HEK293T cells lead to decreased mRNA and protein expression of IFNβ, as well as reduced mRNA expression of the ISGs *ISG15*, *ISG56*, and *MX1*, in response to infection with Sendai virus (SeV) (Zhang *et al.*, 2021). Knockdown of JMJD6 by RNAi in HEK293T cells and knockout by CRISPR-Cas9 editing in HeLa cells showed the inverse effect, with increased IFN response to SeV (Zhang *et al.*, 2021). This was shown to be the result of JMJD6 recruiting the E3 ubiquitin ligase ring finger protein 5 (RNF5) to pIRF3 following SeV infection, which lead to the ubiquitination and degradation of pIRF3 (Zhang *et al.*, 2021). Furthermore, infection of JMJD6 knockout HeLa cells with vesicular stomatitis virus (VSV) resulted in fewer infected cells, reduced viral titres and an increased IFN response compared to wild type cells (Zhang *et al.*, 2021). SeV and VSV are both RNA viruses of the order *Mononegavirales*, with single stranded, negative sense genomes (Kolakofsky *et al.*, 2021). JMJD6 could be considered a proviral host factor in the lifecycle of these viruses. Which, or whether, enzymatic activity of JMJD6 is required for this process was not investigated. However, the authors found that RNF5 binds to JMJD6 between residues 173-288 (Zhang *et al.*, 2021), which are within the JmjC domain and active site (Kwok *et al.*, 2017; Mantri *et al.*, 2010). Further study

may reveal if RNF5 is demethylated, hydroxylated, or phosphorylated by JMJD6 in this interaction.

Zhang *et al*. found that JMJD6 was involved in negatively regulating gene expression triggered by detection of viral RNA via the RIG-I-mediated signalling pathway, whereas Ganesan *et al*. proposed that JMJD6 was a negative regulator of gene expression resulting from activation of the IFN receptor. Involvement of JMJD6 at multiple points in the IFN pathway makes the enzyme an attractive treatment target for many viral infections

Finally, JMJD6 has been proposed as a proviral host factor for IAV. The data supporting this also comes from the PhD thesis of Dr Kwok and, as discussed in the next section, forms the basis of the project presented in this chapter.

2.1.2. JMJD6 and IAV

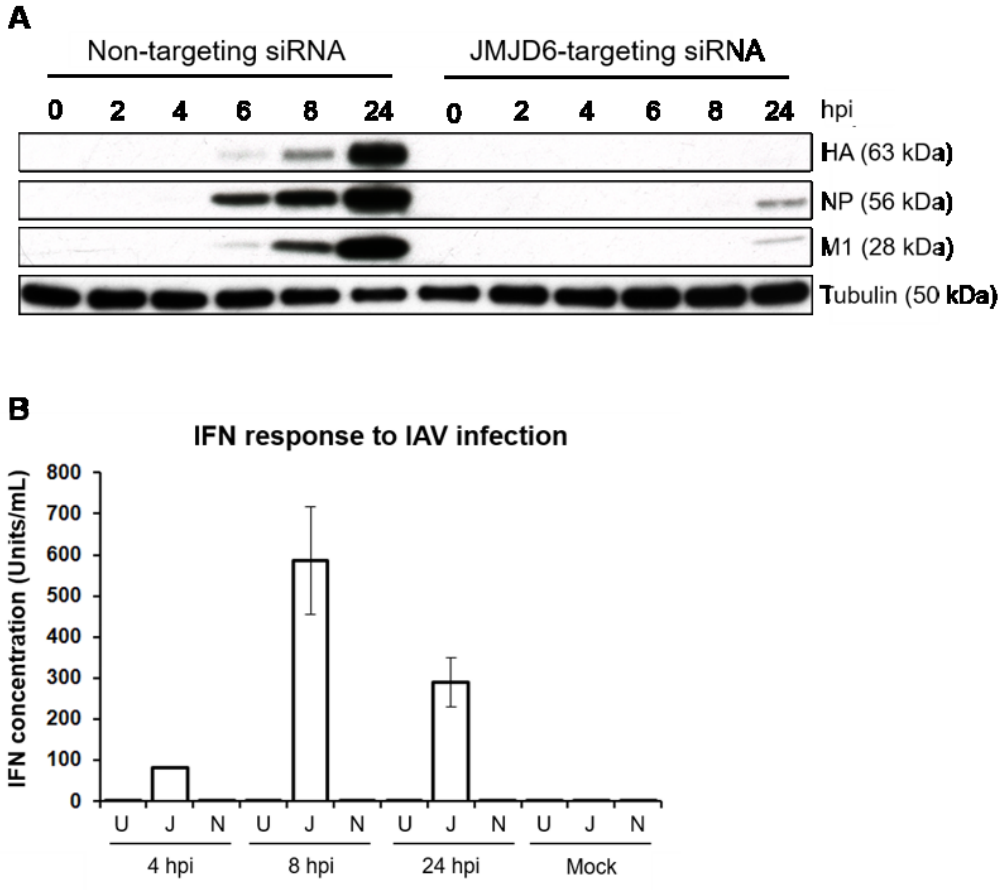

Figure 2.2: Preliminary data suggesting a proviral role of JMJD6 for IAV. *Figures adapted from work by Dr Janice Kwok (**A**) and Dr Jun Hu (**B**). **A:** A549 cells were double transfected with either siRNA-275 or a non-targeting control siRNA, and infected with influenza A/Puerto Rico/8/1934 (PR8) at multiplicity of infection (MOI) 5. Cell lysates were harvested 2, 4, 8, or 24 hours post infection (hpi). Mock infected cells were incubated for 24 hours in virus free media. Cell lysates were examined by western blot and probed with anti-H1N1 anti-sera to detect levels of viral proteins HA, M1 and NP. Western blots were also probed for alpha tubulin as a loading control. **B:** A549 cells were double transfected with either siRNA-275 (J) or a non-targeting control siRNA (N), or left untransfected (U). Cells were then infected with PR8 at MOI 5 and cell supernatants were harvested 4, 8, or 24 hpi. Mock infected cells were incubated for 24 hours in virus free media. IFN levels in the cell supernatant were measured by HEK-Blue™ assay. Bars represent the mean of three biological repeats, error bars represent the standard error of the mean.*

Dr Kwok developed a JMJD6 knockdown protocol from previously published work using an siRNA sequence named siRNA-275 (Heim *et al.*, 2014). A549 cells were

transfected with either siRNA-275 or a non-targeting siRNA control prior to infection with influenza A/Puerto Rico/8/1934 (PR8). Expression of viral proteins was analysed by western blot and infectious virus production was measured by plaque assay. Dr Kwok found that the viral titre measured from these JMJD6 knockdown cells was reduced compared to control cells by more than two orders of magnitude (Kwok, 2018). Similarly, the expression of viral proteins HA, NP and M1 were greatly reduced in JMJD6-deficient A549 cells compared to cells that had been transfected with non-targeting siRNA (**Figure 2.2A**). Levels of viral RNA isolated from JMJD6 knockdown cells were also greatly reduced (Kwok, 2018). Dr Kwok also developed lines of JMJD6 knockout A549 cells which showed reduced IAV replication compared to wild type, although the reduction in these cells was smaller than that seen with siRNA knockdown (Kwok, 2018). These findings strongly suggested that JMJD6 was required for efficient IAV replication.

Further investigation by Dr Kwok aimed to determine the point at which the IAV lifecycle was inhibited by JMJD6 knockdown. No effect of JMJD6 depletion on the cell surface expression of sialic acid was observed, and viral binding at the cell surface was not affected by JMJD6 expression (Kwok, 2018). However, nuclear import of viral RNPs was seen to be reduced in JMJD6 knockdown cells as in immunofluorescence experiments, only 20% of NP staining in JMJD6 knockdown cells was associated with the nucleus, whereas untransfected cells showed 80% nuclear NP staining (Kwok, 2018). From this, it was concluded that JMJD6 has a proviral role in the lifecycle of IAV, after binding at the cell surface, but at or before nuclear import of viral RNPs.

Subsequent work by Dr Jun Hu (The Roslin Institute, University of Edinburgh) showed that, while untransfected A549 cells and cells transfected with non-targeting siRNA did not produce a detectable IFN response to infection with PR8, high concentrations of IFN were produced by JMJD6 knockdown cells following infection (**Figure 2.2B**).

This suggested that the cells deficient in JMJD6 were able to produce a large antiviral IFN immune response to PR8 infection where the control cells could not. This would explain the reduced viral replication seen in these cells and was also consistent with the findings presented in Ganesan *et al*., (2018).

The project presented in this chapter aimed to further dissect this proviral role of JMJD6, and identify the mechanism by which IAV infection was inhibited by JMJD6 depletion. Based on the work by Dr Hu, and previously published work linking JMJD6 to regulation of the IFN response in viral infection, the leading hypothesis at the start of this project was that JMJD6 knockdown allowed an IFN response to IAV infection that JMJD6 would otherwise downregulate.

2.2. Results

2.2.1. Development of JMJD6 knockdown protocols

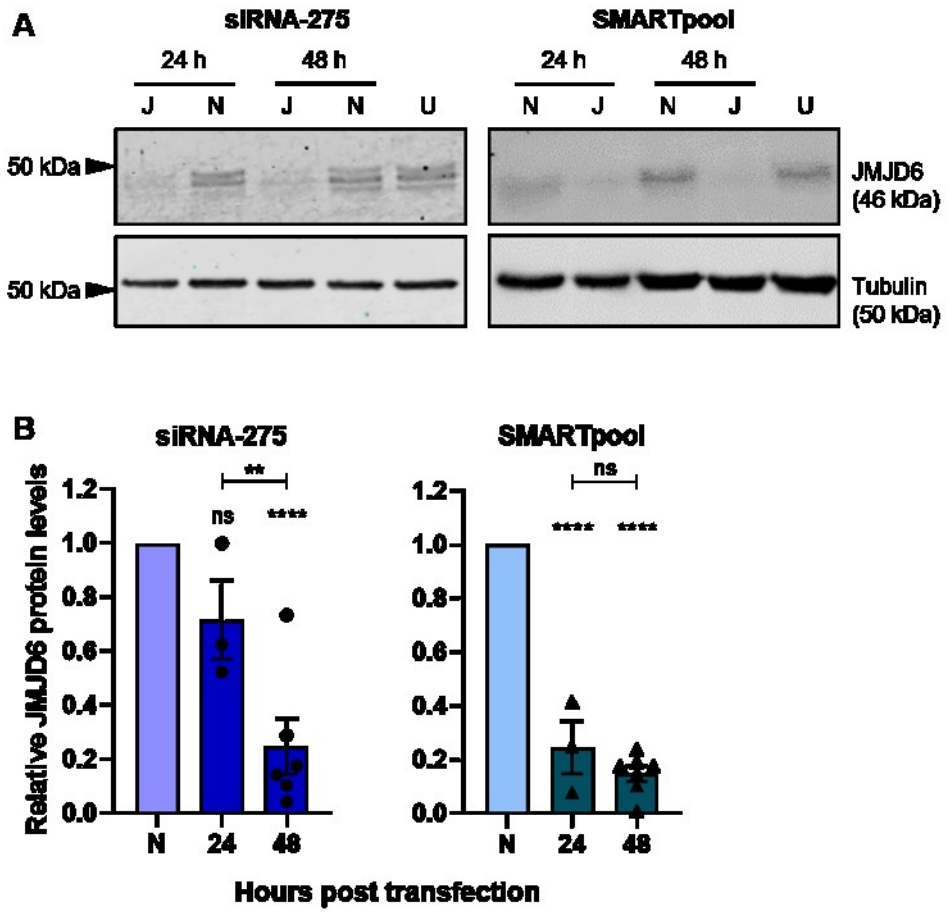

Figure 2.3: Establishment of JMJD6 knockdown conditions. *Using siRNA-275 or SMARTpool, A549 cells were transfected with either JMJD6 targeting (J) or non-targeting (N) siRNA. Cells were harvested and lysed at 24 or 48 hours post transfection. Untransfected cells (U) were harvested 72 hour after seeding.* ***A:*** *Cell lysates were examined via western blot for the indicated proteins, using fluorophore-conjugated secondary antibodies and a LI-COR Odyssey Fc Imaging System; a single representative experiment is shown.* ***B:*** *Protein expression was measured from replicate experiments using LI-COR Image Studio software. JMJD6 levels were normalised to alpha tubulin in the same sample and expressed as a proportion of the matched control. Bars represent the mean of multiple biological repeats (n>3), error bars represent standard error of the mean. Data were analysed by one-way ANOVA with Tukey's multiple comparison test using GraphPad Prism 8. ns: not significant, p≥0.05; **: p≤0.01; ****: p≤0.0001.*

The protocol used previously by Drs Kwok and Hu called for a double transfection of A549 human alveolar epithelial cells, with either siRNA-275 (sequence in Table 6.2) or a non-targeting control 24 hours after seeding, followed by a second transfection after a further 24 hours. Double transfection of A549 cells was not something that the Digard group had previously found necessary to suppress expression of a particular cellular gene with siRNA (e.g. (Bruce *et al.*, 2010)). Furthermore, the preliminary studies by Drs Kwok and Hu relied on a single JMJD6-targeting siRNA (siRNA-275) which had not always been used with an appropriately matched negative control.

Accordingly, to investigate the role of JMJD6 in IAV replication further, an optimised knockdown protocol was established for this study. A fresh stock of siRNA-275 was acquired, as well as a universal siRNA negative control. Additionally, to assess the reproducibility of the findings with siRNA-275, another JMJD6 knockdown system was tested in parallel which used ON-TARGETplus siRNA SMARTpools from Dharmacon. This system involves a pool of four siRNAs, each targeting a different part of the *JMJD6* mRNA sequence (all sequences in Table 6.2) each used at lower concentrations than a single siRNA would be, and a matched non-targeting pool of four scramble siRNAs.

First, A549 cells were transfected with either the non-targeting siRNAs (N) or siRNAs targeting *JMJD6* mRNA (J), or left untransfected (U). Cells were lysed and harvested in order to assess JMJD6 protein levels by western blot. Both double and single transfection protocols were tested. Double transfection of the cells, as previously done by Drs Kwok and Hu, gave unacceptable levels of cytotoxicity in my hands (data not shown). Therefore, single transfection protocols were tested in which cells were harvested either 24 or 48 hours after siRNA transfection. With single siRNA transfection, western blotting for alpha tubulin as a loading control showed consistent recovery of cell lysate from siRNA-275 and control-transfected cells as well as

untransfected cells (**Figure 2.3A**). Probing the same blots with anti-JMJD6 sera showed the expected pattern of three similarly-sized isoforms (Hahn *et al.*, 2008) migrating around 46 kDa (Alahari *et al.*, 2015; Miotti *et al.*, 2017), but in obviously lower amounts in siRNA-treated samples, indicating successful knockdown of expression. Similar results were obtained with the SMARTpool siRNAs; an apparent lack of gross cytotoxicity as indicated by even recovery of tubulin and efficient reduction of JMJD6 accumulation (though note that in the right hand panel of **Figure 2.3A** a lower quality gel did not resolve the JMJD6 isoforms).

To provide quantitative data on the reproducibility and effectiveness of the two approaches to inhibiting JMJD6 expression, replicate experiments were performed and JMJD6 levels quantified by densitometry, expressed relative to non-targeting siRNA-treated samples after normalisation for tubulin levels. JMJD6 protein levels in A549 cells 24 hours after transfection with siRNA-275 (**Figure 2.3B** left) were not significantly lower than control (N) levels. However, 48 hours post siRNA-275 transfection JMJD6 levels were, on average, 75% lower than those from the matched scramble siRNA control ($p<0.0001$). This was deemed to be an acceptable level of knockdown for subsequent infection experiments and was comparable to levels previously achieved by Dr Kwok and Dr Hu (Kwok, 2018). JMJD6 levels 24 hours after transfection with SMARTpool JMJD6-targeting siRNA were reduced by approximately 75% compared to the matched negative control ($p<0.0001$) and by 85% 48 hours post-transfection ($p<0.0001$). However, the difference in knockdown efficiency between the two time points was not statistically significant ($p=0.1566$) (**Figure 2.3B** right). The mean JMJD6 knockdown efficiencies 48 hours post-transfection with either siRNA-275 or JMJD6-targeting SMARTpool siRNA were comparable ($p=0.3886$), although the SMARTpool knockdown system yielded more consistent levels of JMJD6 knockdown. Hence, effective single-transfection protocols for both siRNA-275 and the

SMARTpool system for knockdown were successfully established, using 48 hour incubation before harvest or subsequent infection. These protocols were taken forward and used for the following investigations.

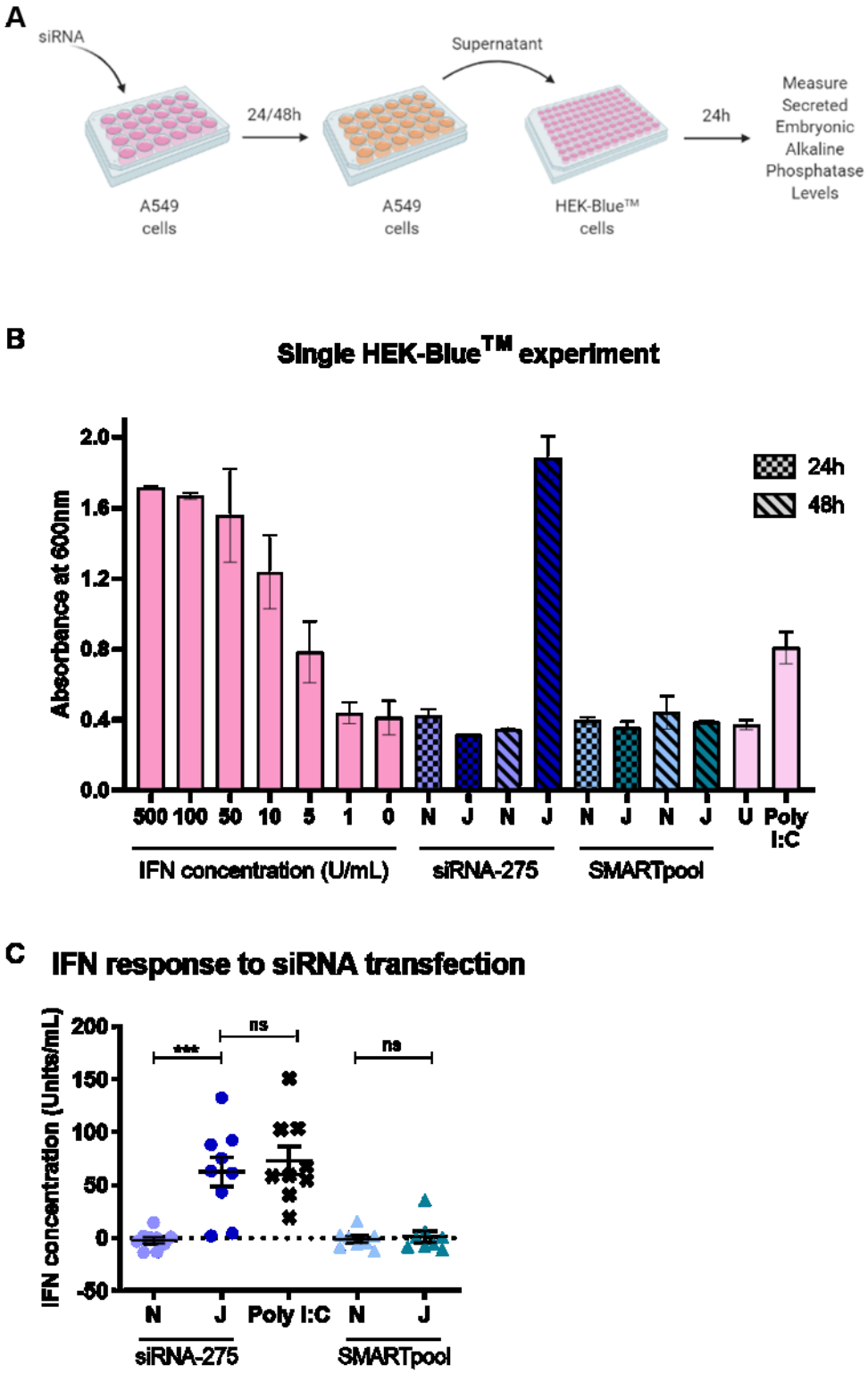

Figure 2.4: IFN responses in JMJD6 knockdown cells. A: *Schematic diagram of experiments in which IFN in the supernatant of cells treated with siRNA was measured by HEK-Blue™ assay. A549 cells were transfected with either JMJD6-targeting (J) or non-targeting siRNA (N) using siRNA-275 or SMARTpool siRNA systems. Cell supernatant was*

harvested either 24 or 48 hours (h) post siRNA transfection. HEK-Blue™ IFN-α/β cells were incubated with this supernatant or with controls for 24 hours before measuring Secreted Embryonic Alkaline Phosphatase (SEAP) levels by determining the colour change of the SEAP substrate, QUANTI-Blue™, via spectrophotometer. Diagram created in BioRender.com. ***B:*** *Spectrophotometer results of a single, representative experiment. An IFN standard curve was generated by incubating HEK-Blue™ cells with known concentrations of universal IFN type I. Baseline levels of IFN and the ability of the A549 cells to produce IFN were established by incubating HEK-Blue™ cells with supernatant from untransfected A549 cells (U) and A549 cells transfected with poly I:C (Poly I:C) respectively. Bars represent mean of two technical replicates, error bars represent standard deviation.* ***C:*** *IFN concentration in the supernatant of cells transfected with siRNA (data from 48 hours post-transfection) or poly I:C. Data points represent means of technical duplicates from independent experiments. Error bars represent standard error of the mean. ns: not significant, p≥0.05; ***: p≤0.001. Data were analysed by one-way ANOVA with Tukey's multiple comparison test using GraphPad Prism 8.*

The preliminary data from Dr Hu showed enhanced IFN production in JMJD6-depleted A549 cells following IAV infection (**Figure 2.2B**). JMJD6 had previously been suggested to have a role in the negative regulation of the type I IFN pathway via demethylation of STAT1 (Ganesan *et al.*, 2018). If this is the case, loss of this inhibition of IFN signalling in JMJD6 knockdown cells could allow a better innate immune response to viral infections, thus higher IFN levels and reduced viral replication.

As part of protocol validation, levels of IFN secreted from siRNA-transfected cells were measured in order to establish the pre-infection environment. Cell supernatants were harvested at 24 and 48 hours post siRNA transfection and IFN levels were measured using HEK-Blue™ IFN-α/β cells. These cells have been engineered to secrete SEAP in response to activation of the IFN receptor by type I IFNs (InvivoGen, 2011). HEK-Blue™ IFN-α/β cells were incubated with the harvested supernatants for 24 hours and levels of SEAP production were assessed by a colour change reaction with QUANTI-Blue™ medium. Absorbance at 600 nm was measured and sample IFN concentrations were estimated by comparison to a standard curve produced by

incubating HEK-Blue™ cells in parallel with a range of known IFN concentrations (**Figure 2.4A**).

The results of a single, representative HEK-Blue™ assay experiment, with two technical replicates for each data point, are shown in **Figure 2.4B**. The reaction of the HEK-Blue™ cells to media containing known concentrations of type I IFN, ranging from 500 to 1 Units/mL (U/mL), was measured, giving a dose-response curve that saturated above 50 U/mL of IFN. Additionally, fresh media containing no IFN (0 U/mL) was used to establish baseline absorbance. Supernatant of untransfected A549 cells (U) was also analysed in order to determine the baseline IFN levels in cell culture. The supernatant of A549 cells transfected with the immunostimulant poly I:C was used as a positive control in order to confirm the ability of the A549 cells to produce IFN. JMJD6 knockdown was confirmed by western blot (data not shown).

At both time points, neither of the non-targeting siRNAs showed a reaction above the baselines of the IFN-free media or the untransfected cell supernatant, indicating no IFN production in response to the transfection of either negative control (**Figure 2.4B**). This was also the case for the cell supernatant harvested 24 hours post transfection with either siRNA-275 or JMJD6-targeting SMARTpool siRNA. However, cell supernatant harvested 48 hours post transfection with siRNA-275 gave a reaction in the HEK-Blue™ assay that was larger than that of both the poly I:C treated positive control, and 500 U/mL type I IFN. This indicated a large IFN reaction following the knockdown of JMJD6 via transfection of siRNA-275. Conversely, cell supernatant harvested 48 hours post transfection with JMJD6-targeting SMARTpool siRNA showed no detectable IFN response above the baseline and negative control. This suggested that the IFN response detected in the siRNA-275-treated cells was due to transfection with the particular siRNA rather than any reduction in JMJD6 protein levels.

IFN levels in supernatants harvested 48 hours post siRNA transfection or following poly I:C treatment from multiple biological replicates were assessed (**Figure 2.4C**), knockdown of JMJD6 was confirmed by western blot for each experiment (data not shown). There was some variability in the responses detected in both siRNA-275 and poly I:C transfected cells, however, siRNA-275 transfection was seen to elicit a statistically significant IFN response compared to both the matched control siRNA ($p=0.0001$), and JMJD6-targeting SMARTpool transfection ($p=0.0005$). This IFN reaction was comparable to that induced by poly I:C transfection ($p=0.9263$).

It can be surmised from these data that transfection of A549 cells with siRNA-275, not the absence of JMJD6, induced IFN production. These high levels of IFN prior to infection may have caused the reduced levels of IAV infection and replication seen in previous experiments. To examine this further, infection experiments were performed following JMJD6 knockdown.

2.2.2. Infection of siRNA-treated cells with IAV

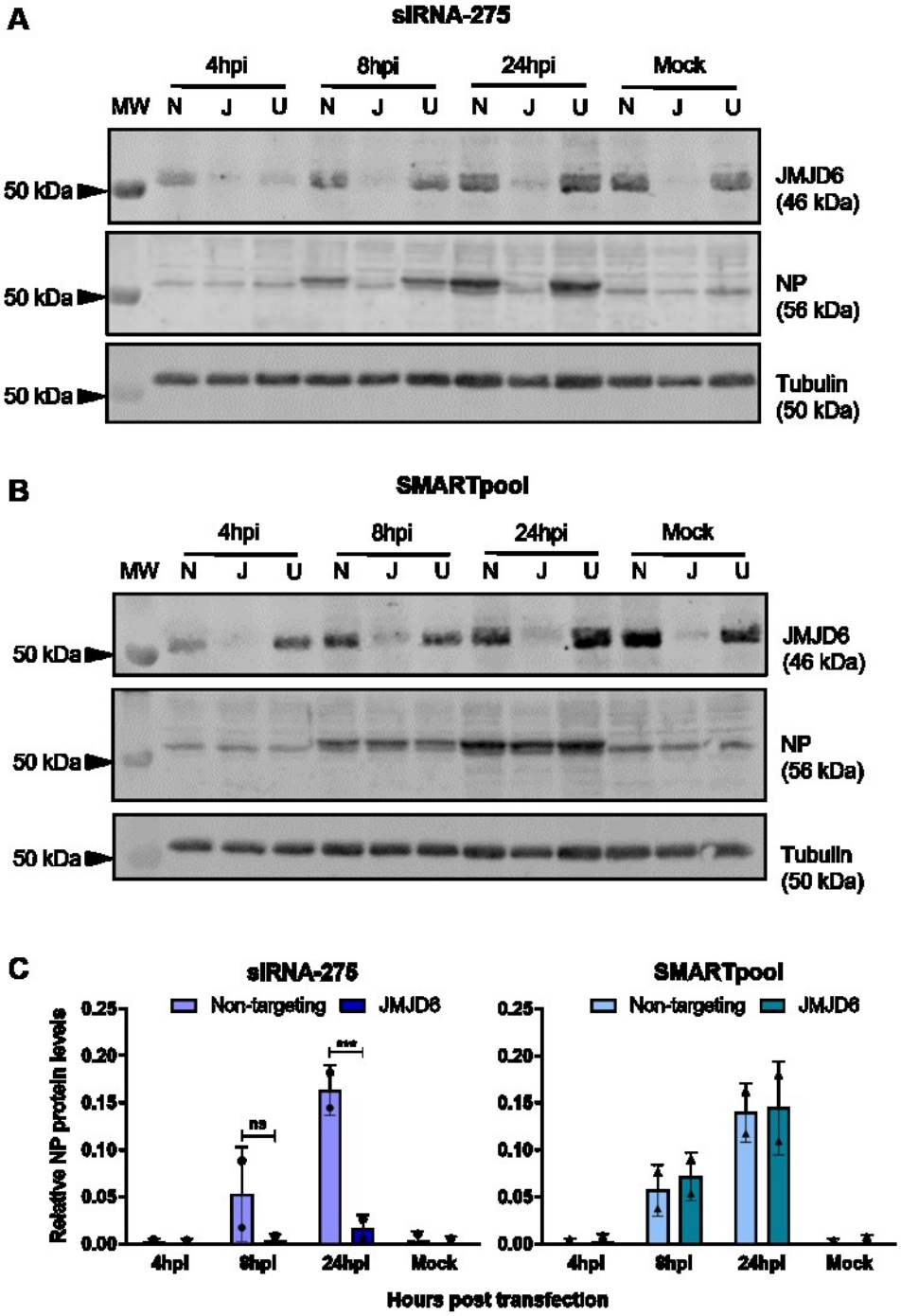

Figure 2.5 Infection of JMJD6 knockdown cells with IAV. *A549 cells were transfected with either JMJD6-targeting (J) or non-targeting (N) siRNA using siRNA-275 or SMARTpool systems, or left untransfected (U). Cells were infected 48 hours post transfection with PR8 at MOI 5. Cell lysates were harvested 4, 8, or 24 hours post infection (hpi). Mock infected cells were incubated for 24 hours in virus free media. Cell lysates were examined by western blot for cellular JMJD6 and viral NP, as well as an alpha tubulin loading control. Protein expression*

was determined by densitometry using LI-COR Image Studio software. NP levels were normalised to tubulin in the same sample. MW indicates a pre-stained ladder of molecular weight markers. ***A, B:*** *Western blot showing a single, representative experiment in which cells were transfected with (**A**) siRNA-275 or the matched non-targeting control or (**B**) SMARTpool siRNA* ***C:*** *Relative protein levels of NP in cells transfected with non-targeting or JMJD6-targeting (JMJD6) siRNA using siRNA-275 (left panel) or SMARTpool (right panel) systems. Bars represent the mean of two biological replicates, error bars represent standard deviation. ns: not significant, p≥0.05; ***: p≤0.001. Data were analysed by two-way ANOVA with Sidak's multiple comparison test using GraphPad Prism 8.*

In order to assess the effect of JMJD6 depletion on IAV infection, A549 cells were transfected with either JMJD6-targeting or non-targeting siRNA from both established knockdown systems. At 48 hours post transfection, cells were infected with PR8 at MOI 5 for 4, 8 or 24 hours. Uninfected cells (Mock) were harvested in parallel with the 24 hour time point. These time points reflect those used previously by Drs Kwok and Hu. Cell lysates were harvested in order to confirm JMJD6 knockdown and examine viral protein expression by western blot. Supernatants were harvested and analysed by plaque assay to measure infectious virus production.

Probing for the tubulin loading control showed consistent recovery of cell lysate from all cells. Concurrent staining for JMJD6 showed the presence of the protein in untransfected cells (U) and in control-siRNA-transfected cells (N) in roughly equal amounts and all time points of infection other than at 4 hours post infection, which showed a higher level of protein in the non-targeting condition (**Figure 2.5A**). Levels of JMJD6 were consistently reduced in the siRNA-275-treated samples. Another blot of the same samples, probed with antisera specific to influenza NP, showed the appearance, above background, of the expected 56 kDa band at 8 hours post infection in untransfected and non-targeting-treated cells. Stronger staining was seen at this molecular weight in these cells at 24 hours post infection. These bands were absent in the mock infected cells. This time-dependent increase of NP was expected in normal infection as IAV goes through its lifecycle, producing more viral proteins,

and thus, more virus particles. However, in siRNA-275-treated samples, the expected viral proteins could not be detected above background and any time point of infection. This indicated a lack of IAV replication in these cells.

When examining SMARTpool siRNA-treated samples by western blot, probing for tubulin similarly indicated equal lysate recovery across all of the conditions (**Figure 2.5B**). Additionally, expression of JMJD6 protein was observed at comparable levels in the non-targeting-siRNA-transfected (N) and untransfected (U) cells, and significantly reduced in cells treated with JMJD6-targeting siRNA at every infection time point and in mock infected cells. However, contrary to the siRNA-275-treated samples, cells treated with JMJD6-targeting SMARTpool siRNA showed levels of NP equivalent to both non-targeting-treated and untransfected cells throughout the course of infection. This implied that the knockdown of JMJD6 with SMARTpool siRNA did not affect the ability of IAV to produce viral proteins in the same way that knockdown with siRNA-275 did.

Replicate experiments were performed and NP levels in the non-targeting- and JMJD6-targeting siRNA-treated cells were quantified and normalised to tubulin levels. Again, viral NP was seen in the control cells after 8 hours and increased at 24 hours post infection (**Figure 2.5C**). In siRNA-275 JMJD6 knockdown cells, however, NP levels were greatly reduced at each time point, similarly to what was previously seen by Drs Kwok and Hu (Kwok, 2018). This reduction was statistically significant at 24 hours post infection ($p=0.0005$).

In contrast, in cells that had been transfected with JMJD6-targeting SMARTpool siRNA, NP levels were comparable to those in control cells at every time point of infection, suggesting that the knockdown of JMJD6 *per se* did not affect the ability of IAV to replicate.

Instead, taking this result together with the pre-infection IFN data (**Figure 2.4**), it seemed possible that siRNA-275 transfection induced an IFN response that inhibited IAV infection and the production of viral proteins, whereas transfection with JMJD6-targeting SMARTpool siRNA did not.

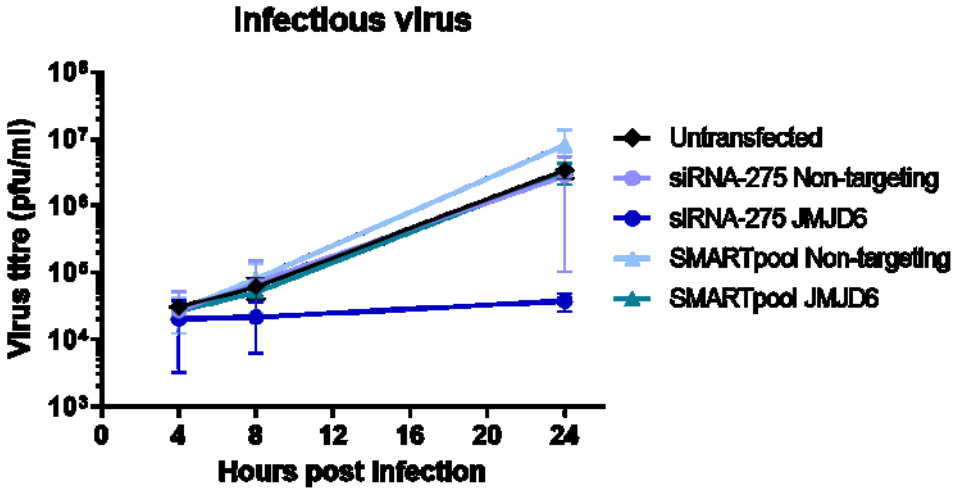

Figure 2.6 Viral replication in JMJD6 knockdown cells. *A549 cells were transfected with either JMJD6-targeting (JMJD6) or non-targeting siRNA using siRNA-275 or SMARTpool siRNA systems or left untransfected. Cells were infected at 48 hours post transfection with PR8 at MOI 5. Cell supernatant was harvested at 4, 8 and 24 hours post infection and virus was titrated by plaque assay on MDCK cells. Points represent the mean of two biological replicates, error bars represent standard deviation. Data were analysed by two-way ANOVA with Tukey's multiple comparison test using GraphPad Prism 8.*

Next, the effect of JMJD6 knockdown on infectious virus production was investigated by plaque titrating supernatants harvested from the infection experiments described above.

Untransfected cells showed increased output of infectious virus with time, with the greatest increase seen between 8 and 24 hours post infection (**Figure 2.6**). A similar pattern of virus production was seen in cells treated with non-targeting siRNA in both siRNA-275 and SMARTpool systems. In both cases, a small increase in virus titre was seen between 4 and 8 hours post infection, followed by a larger increase between

8 and 24 hours. At every time point virus titres were observed in cells transfected with either non-targeting siRNA that were comparable to those of untransfected cells.

Cells transfected with JMJD6-targeting SMARTpool siRNA also presented similar infection kinetics. At every time point these cells showed no significant difference in average titre when compared with either cells transfected with non-targeting SMARTpool ($p=0.76$ at 24 hours) or untransfected cells ($p=0.77$ at 24 hours). Conversely, infectious virus production from cells transfected with JMJD6-targeting siRNA-275 was substantially decreased in comparison with untransfected cells and cells transfected with non-targeting siRNA, displaying almost no increase in titre from the 4 hour time point, which most likely represents residual inoculum. At 24 hours post infection, average infectious virus titre was observed to be approximately two orders of magnitude less in cells transfected with siRNA-275 than untransfected cells. Although this difference was not found to be statistically significant ($p=0.2294$), the reduction in virus titre correlated with the observed reduction in viral protein levels seen in cells transfected with siRNA-275 (**Figure 2.5**). This suggested that transfection with siRNA-275, not depletion of JMJD6 protein levels, restricts the ability of IAV to replicate in A549 cells.

2.2.3. Generation of a clonal population of *JMJD6*$^{-/-}$ A549 cells

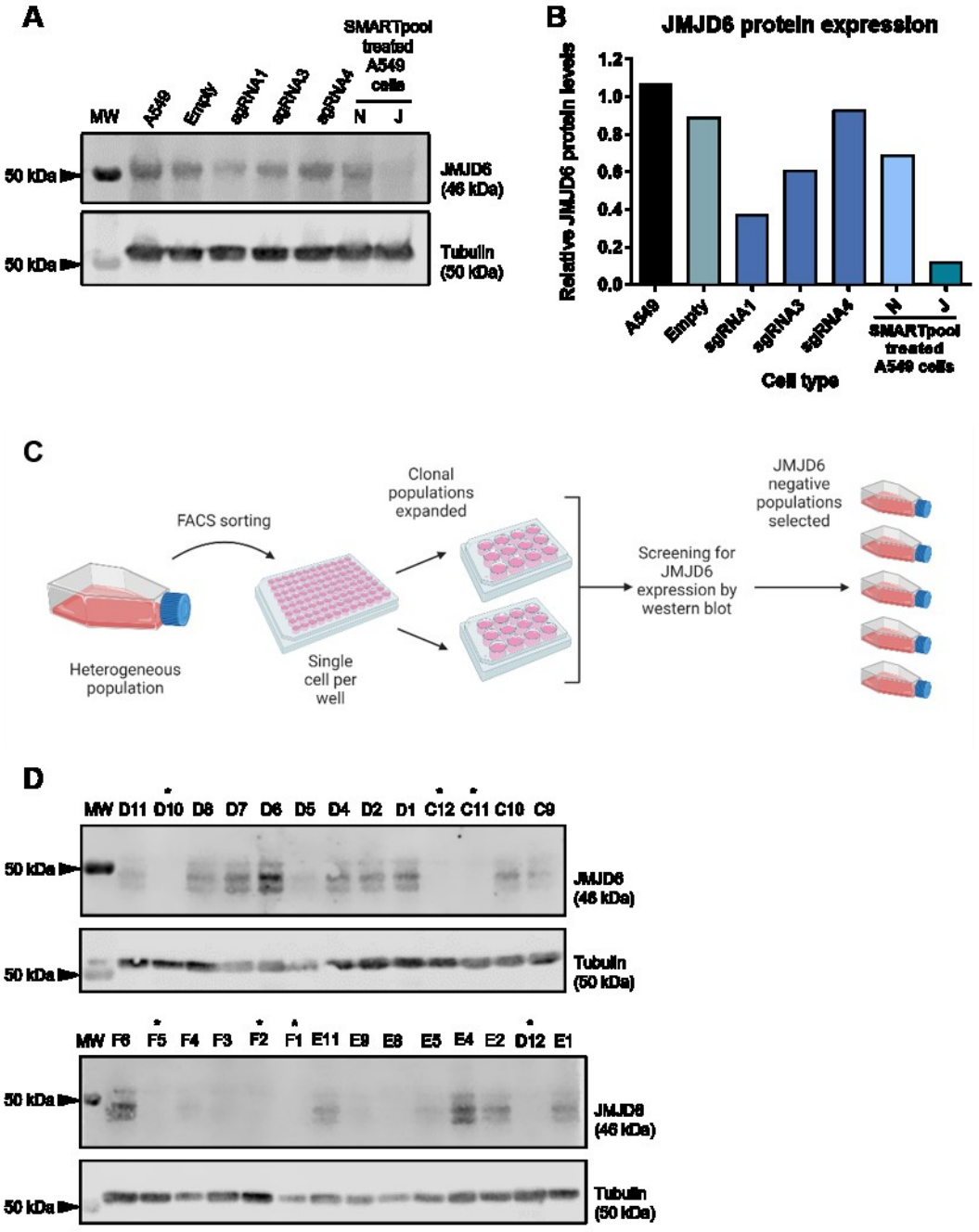

Figure 2.7 Process of making clonal JMJD6 knockout A549 cell populations. A: *Analysis of JMJD6 knockout A549 cell lines created by Dr Kwok. These premade cell lines were recovered from storage at -150°C and passaged three times. Cell lysate samples from each cell population were harvested and analysed by western blot for JMJD6 and tubulin alongside lysates of untreated A549 cells and A549 cells treated with non-targeting (N) or JMJD6-targeting (J) SMARTpool siRNA from previous experiments. MW indicates pre-stained molecular weight markers.* ***B:*** *Graph showing JMJD6 protein levels, determined by*

densitometry and normalised to tubulin. ***C:*** *Schematic diagram of the process used to create clonal JMJD6 $^{-/-}$ cell lines. Diagram created in BioRender.com.* ***D:*** *Examples of analysis of clonal cell lines, screened by western blot for JMJD6 expression. Populations were named by their position in the 96-well cell culture plate following sorting. Populations that were negative for JMJD6 protein expression are indicated with *. These populations were selected and expanded.*

In order to further investigate the effect of siRNA-275 on IAV replication distinct from the reduction of JMJD6 protein expression, populations of *JMJD6*$^{-/-}$ A549 cells were established. Heterogeneous populations of A549 cells which had previously been treated by Dr Janice Kwok to knockout *JMJD6* (Kwok, 2018), were available from frozen stocks. These cells had either been transfected with the pSPCas9(BB)-2A-GFP plasmid containing one of three *JMJD6*-targeting single guide (sg)RNAs or the pSPCas9(BB)-2A-GFP plasmid backbone alone (empty). Following transfection with the CRISPR-Cas9 system, these cells had not been subject to further screening or sorting and were therefore mixed populations, containing both edited and unedited cells.

After these cells were recovered from -150°C, they were passaged in the same way as wild type A549 cells, as described in section 6.2.2.1. After three passages, cells from each of the stock populations, as well as untreated A549 cells were harvested, lysed and analysed by western blot. These cell lysates were compared to those of A549 cells which had been transfected with non-targeting (N) or JMJD6-targeting (J) SMARTpool siRNA. Probing for JMJD6 protein revealed that, although there was some reduction in the level of JMJD6 in one of the CRISPR-treated lines (sgRNA1) compared to untreated A549 cells, the population levels of JMJD6 expression were substantial, and higher even than siRNA knockdown levels (**Figure 2.7A**).

The CRISPR-treated line with the lowest JMJD6 protein level was clonally sorted in order to make cell lines that were homogenously *JMJD6*$^{-/-}$. The control line that had

been transfected with the empty pSPCas9(BB)-2A-GFP plasmid was similarly sorted in order to make a clonal control cell population (denoted Empty). This process is illustrated in **Figure 2.7B**. The starting cell populations were sorted by fluorescence-activated cell sorting (FACS) so that each well of a 96-well plate contained a single cell. FACS was performed by Mr Graeme Robertson from the Roslin Institute Bio-Imaging facility. These single cell populations were cultured and expanded before being screened for JMJD6 protein expression by western blot.

Figure 2.7C shows example western blots from the screening of clonal populations sorted from the "sgRNA1" line. Clonal lines were named for their position in the 96-well plate. Lines negative for JMJD6 protein expression (marked in **Figure 2.7C** by asterisks) in particular, *JMJD6* knockout lines C12 and F2, hereafter termed KOC12 and KOF2, were further expanded to be used in subsequent experiments.

2.2.4. Examination of the effects of siRNA transfection in *JMJD6*$^{-/-}$ A549 cells

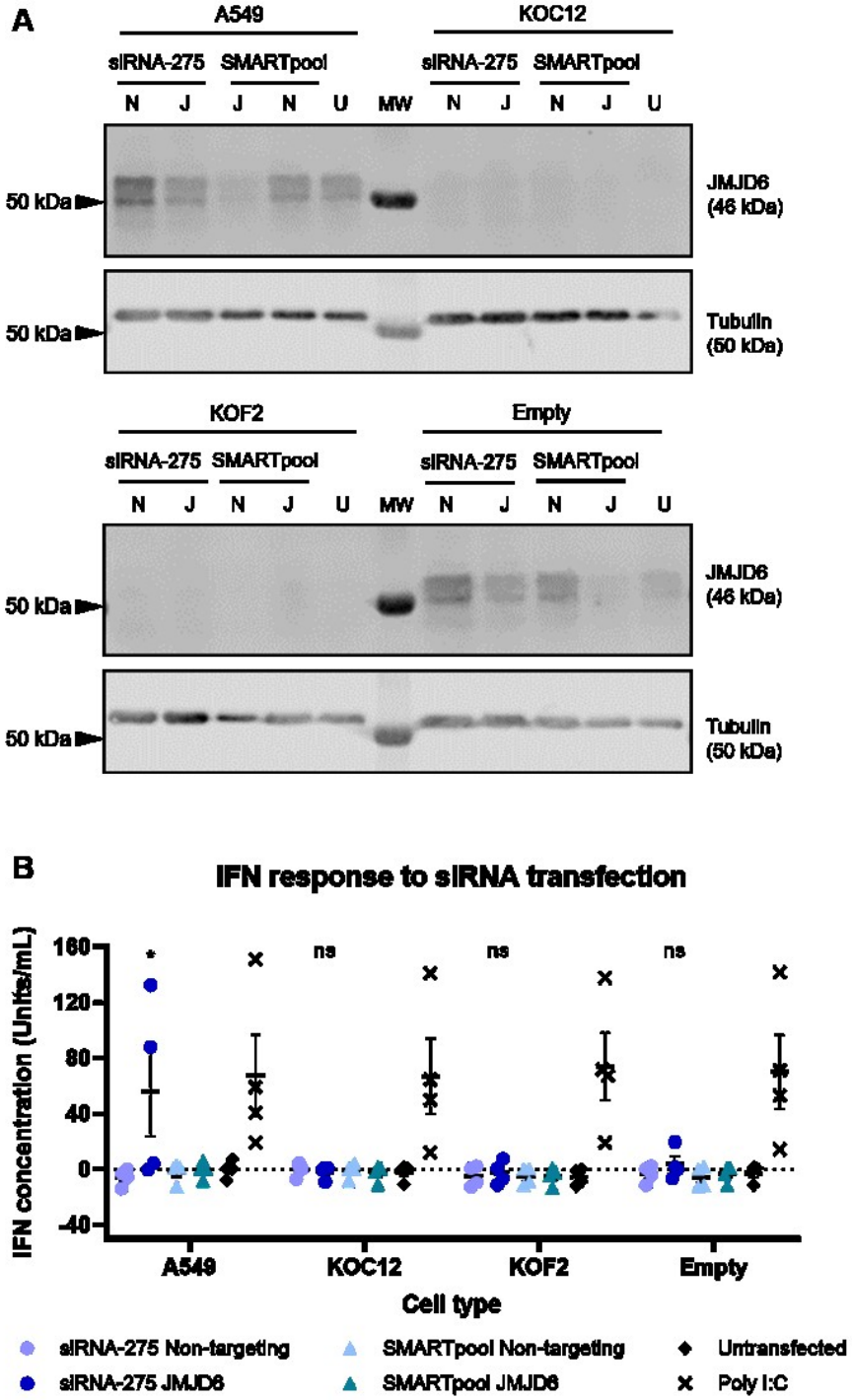

Figure 2.8 Treatment of JMJD6$^{-/-}$ A549 cells with JMJD6-targeting siRNA. *Wild type A549 cells, two clonal populations of JMJD6 knockout A549 cells (KOC12 and KOF2), and a clonal JMJD6$^{+/+}$ control line (Empty) were treated with siRNA. Cells were transfected with non-targeting (N) or JMJD6-targeting (J) siRNA from siRNA-275 or SMARTpool systems, poly I:C,*

or left untransfected (U). Cell lysates and supernatants were harvested 6 hours after transfection with poly I:C and 48 hours post transfection with siRNA. ***A:*** *Cell lysates were examined by western blot for JMJD6 and an alpha tubulin loading control. MW indicates molecular weight markers. Images are from a single experiment in which cells were seeded more densely than usual for a better quality image.* ***B:*** *Cell supernatants were harvested and IFN levels determined by HEK-Blue™ assay. Data points represent means of technical duplicates from independent experiments. Error bars represent standard error of the mean. Significance markers refer to comparison between siRNA-275-treated and untransfected cells within the same cell type. Data were analysed by two-way ANOVA with Tukey's multiple comparison test using GraphPad Prism 8. ns: not significant, p≥0.05; *: p≤0.05. Data points for A549 cells were also included in the analysis of Figure 2.4.*

First, to examine the effect of siRNA-275 transfection, independent of JMJD6 depletion, *JMJD6* knockout lines KOC12 and KOF2 as well as wild type A549 cells and the clonal "Empty" control cell population, were transfected, with siRNA-275 or SMARTpool siRNA systems as before.

To verify knockdown of JMJD6 in the A549 and Empty cells, as well as to confirm continued JMJD6 deficiency in the knock out lines, cell lysates harvested 48hours after transfection were analysed by western blot. The western blot images shown in **Figure 2.8A** are from an experiment in which cells were seeded more densely than is ideal for optimal transfection efficiency, as this approach gave higher quality blots.

Probing for tubulin as a loading control indicated reasonably consistent recovery of cell lysate from all conditions, across all cell types (**Figure 2.8A**). Parallel staining for JMJD6 showed expression of the protein in both untransfected A549 and Empty cells, and although levels appeared lower in untransfected Empty cells, this was not reflected when normalised to tubulin. A549 and Empty cells that had been transfected with siRNA-275 or with JMJD6-targeting SMARTpool siRNA showed reduced levels of JMJD6 protein compared to the same cells transfected with the matched non-targeting siRNA. The reduction in JMJD6 accumulation was greater with SMARTpool than with siRNA-275 siRNAs. Overall, this indicated successful siRNA transfection

and JMJD6 knockdown with both systems and was taken to support the assumption that siRNA transfection was also successful in the knockout cell lines as this could not be confirmed directly. When probing the cell lysates of the knock out cell lines, KOC12 and KOF2, no signal above background was detected, validating the continued *Jmdj6*$^{-/-}$ status of these lines.

The type I IFN response to transfection was assessed via HEK-Blue™ assay (**Figure 2.8B**). The ability of all four cell types to produce an IFN response was tested by transfection with poly I:C. The immunostimulant induced an increase in IFN levels compared to untransfected cells which was statistically significant in all cell lines ($p \leq 0.01$). Although the intensity of response varied between biological repeats for every cell type, the mean IFN responses to poly I:C in KOC12, KOF2 and Empty cells were all comparable to that seen in wild type A549 cells ($p \geq 0.9856$). Wild type A549 cells which had been transfected with siRNA-275 showed, on average, an IFN response that was comparable to that of cells transfected with poly I:C ($p=0.9893$). This response was significantly higher than the baseline levels seen from both untransfected cells ($p=0.0395$) and cells transfected with the matched non-targeting control ($p=0.0167$). However, IFN levels from independent biological repeats were very variable, with one biological repeat showing no IFN production above background. Conversely, no IFN was detected, above baseline, from any of the clonal cell lines transfected using either siRNA-275 or SMARTpool systems. This was expected for the non-targeting siRNAs or *JMJD6*-targeting SMARTpool siRNA but additionally, no IFN response was observed from any of the clonal cell populations transfected with siRNA-275. In both of the *JMJD6* knockout cell lines, KOC12 and KOF2, mean IFN levels were comparable to untransfected cells as well as cells transfected with the matched non-transfecting siRNA ($p \geq 0.9999$ in all cases). This suggested that siRNA-275 transfection did not induce an IFN response in these

JMJD6$^{-/-}$ cell lines as it does in wild type A549 cells. Furthermore, the *JMJD6*$^{+/+}$ Empty cell line, which might have been expected to be equivalent to the parental A549 cell line, also showed no significant IFN response to siRNA-275 transfection.

Taken together, these data did not support the hypothesis that transfection with siRNA-275 induces an IFN response via a route unrelated to JMJD6 depletion. However, as no IFN response to siRNA-275 transfection was observed in Empty cells, which served as a JMJD6-expressing clonal control population, these data also did not suggest that IFN response was associated with loss of JMJD6 expression.

2.2.5. Infection of *JMJD6*$^{-/-}$ A549 cells with IAV

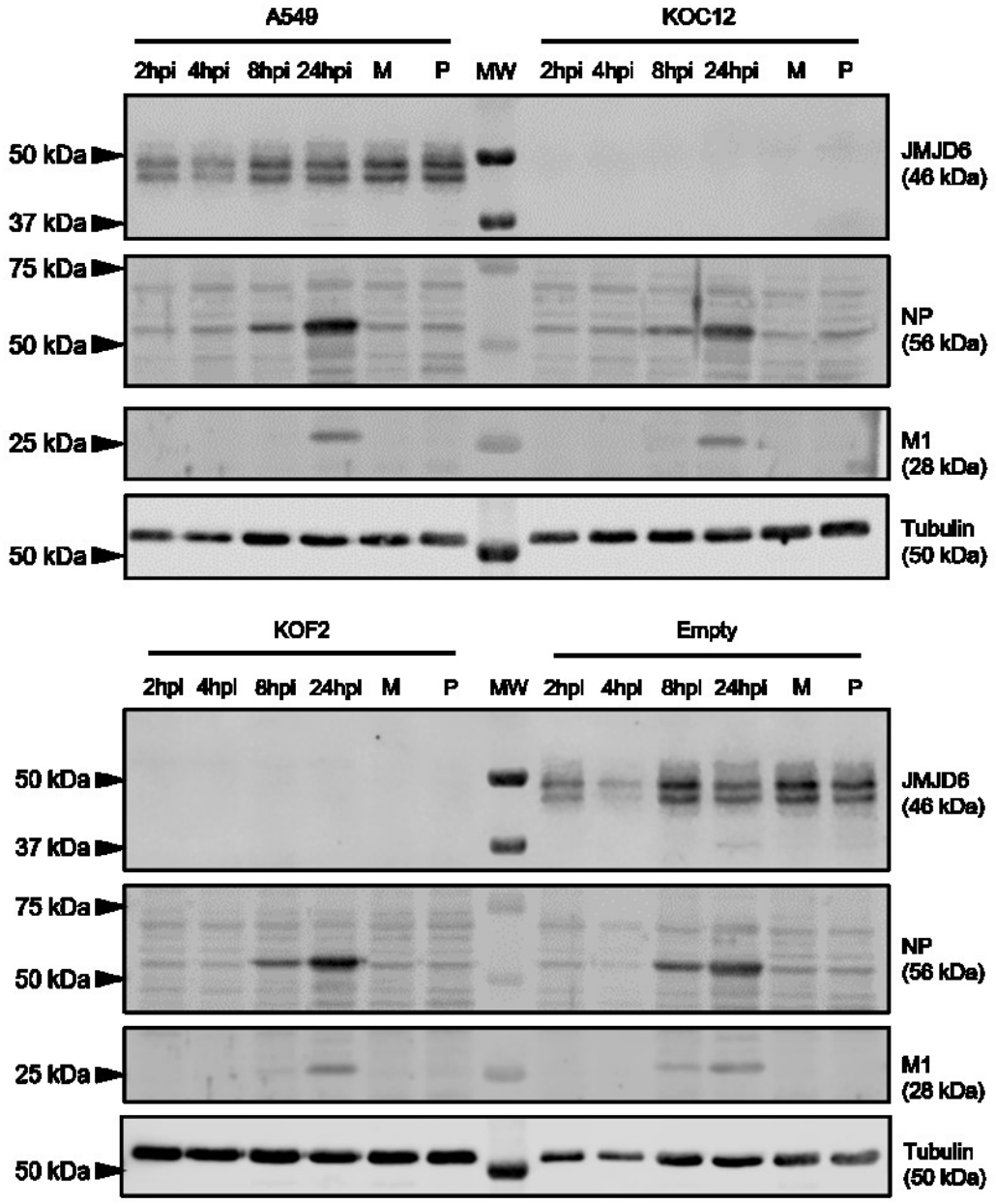

Figure 2.9 Viral protein production in IAV-infected JMJD6$^{-/-}$ A549 cells. *Wild type A549 cells, two clonal populations of JMJD6$^{-/-}$ A549 cells (KOC12 and KOF2), and a clonal JMJD6$^{+/+}$ control line (Empty) were infected with PR8 at MOI 5. Cells were lysed at 2, 4, 8, or 24 hours post infection (hpi). Mock infected cells (M) were incubated for 24 hours in virus free media. Uninfected cells of each line were transfected with poly I:C (P) and cell lysates were harvested at 6 hours post transfection. Cell lysates were examined by western blot for cellular JMJD6, viral NP and M1 and an alpha tubulin loading control. MW indicates molecular weight markers. Figure shows western blot images from a single, representative experiment.*

The *JMJD6*$^{-/-}$ A549 cells were accordingly used to further scrutinise the original hypothesis of a proviral role of JMJD6 by testing their ability to replicate IAV. The clonal populations of *JMJD6*$^{-/-}$ A549 cells, as well as wild type A549 cells and the Empty clonal control cells, were infected with PR8 at MOI 5 for 2, 4, 8 or 24 hours. Lysates of mock infected cells (M) were harvested in parallel with the 24 hour time point, as were lysates of uninfected cells that had been transfected with poly I:C and incubated for 6 hours.

Western blots were used to confirm both continued JMJD6 deficiency in KOC12 and KOF2 cells, as well as consistent JMJD6 protein expression in A549 and Empty cells (**Figure 2.9**). Probing for an alpha tubulin loading control indicated consistent recovery of cell lysate in most conditions, but slightly lower overall protein levels were recovered from both A549 and Empty cells harvested at 2 and 4 hours post infection. JMJD6 protein levels, proportional to tubulin, in A549 and Empty cells remained consistent, both between the two cell lines and over the course of infection. Further, no JMJD6 protein was detected in the cell lysates of KOC12 and KOF2 at any time point. Further western blots of the same samples were probed with anti-NP and anti-M1 sera to determine levels of viral protein. The expected band for NP, around 56 kDa, was detected above background in similar levels across all cell types at 8 and 24 hours post infection, while no NP was detected in uninfected cells. Probing for M1 showed appearance of a signal, above background, at the expected molecular weight of 28 kDa at 24 hours post infection in A549 cells. In Empty cells, similar levels of M1 were detected at 24 hours post infection. Unlike in wild type A549 cells, a small amount of M1 was also detected at the earlier time point of 8 hours post infection. However, this difference was not found to be reproducible over replicate experiments (**Figure 2.10**). M1 was detected at 24 hours post infection in both KOC12 and KOF2 cells at levels comparable to those seen in both A549 and Empty cells at the

equivalent time point (**Figure 2.9**). In KOC12 cells, M1 was first detectable at 24 hours post infection, as in A549 cells. KOF2 cells showed low levels of M1 staining at 8 hours post infection, similar to that seen in Empty cells. Overall, these data gave no indication of a defect in viral protein production in *JMJD6*$^{-/-}$ A549 cells compared to A549 cells expressing JMJD6.

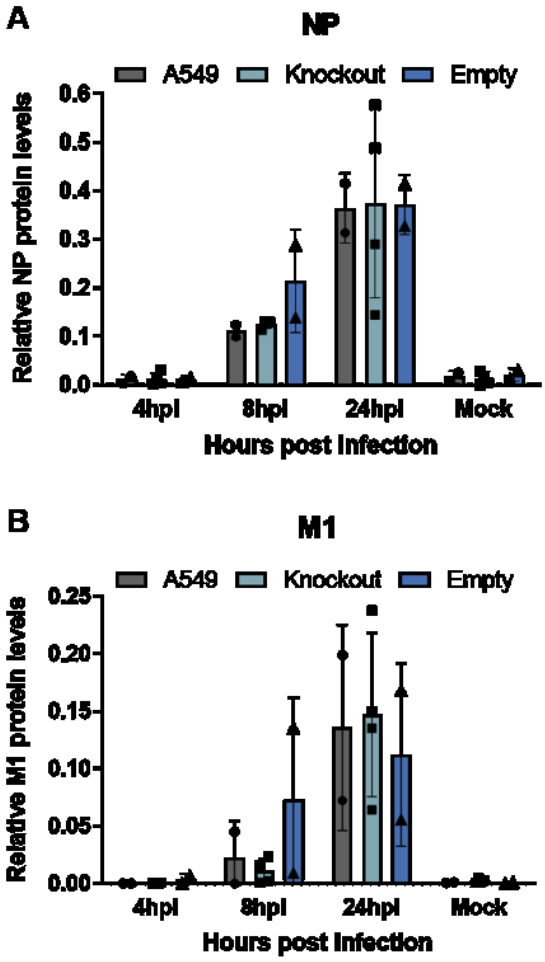

Figure 2.10 Levels of viral proteins detected in IAV-infected JMJD6$^{-/-}$ A549 cells. *Wild type A549 cells, two clonal populations of JMJD6 knockout A549s, and a clonal JMJD6$^{+/+}$ control line (Empty) were infected with PR8 at MOI 5. Cell lysates were harvested at 4, 8, or 24 hours post infection (hpi). Mock cells (M) were incubated for 24 hours in virus free media. Cell lysates were examined by western blot, probing for viral NP and M1, as well as for cellular alpha tubulin as a loading control. Protein expression was determined by densitometry using LI-COR Image Studio software. Viral protein levels were normalised to tubulin in the same sample. Data from the two JMJD6 knockout cell lines were pooled into a single data set named*

*"Knockout". **A:** Relative levels of NP. **B:** Relative levels of M1. Bars represent mean of two biological replicates, error bars represent standard deviation. Data were analysed by two-way ANOVA with Tukey's multiple comparison test using GraphPad Prism 8.*

Replicate infection experiments were performed and viral protein levels were quantified and normalised relative to tubulin levels. Data from the two *JMJD6* knockout cell lines were pooled into a single data set. Again, viral NP was seen in A549 cells after 8 hours and increased at 24 hours post infection (**Figure 2.10A**). In Empty cells, no statistically significant difference in NP levels compared to A549 cells was observed at either 8 (p=0.4402) or 24 (p=0.9964) hours post infection. Equally, *JMJD6* knockout cells showed average levels of NP that were comparable to both control cell groups at both time points. Relative M1 levels, shown in **Figure 2.10B**, were more variable between biological replicates than NP. Nevertheless, mean M1 levels were consistent across cell types as there was no statistically significant difference, at any time point, between *JMJD6* knockout cells and either JMJD6-expressing control cell line. Therefore data from these replicate experiments further demonstrated that IAV protein production was not inhibited by the absence of JMJD6 in these A549 cell lines.

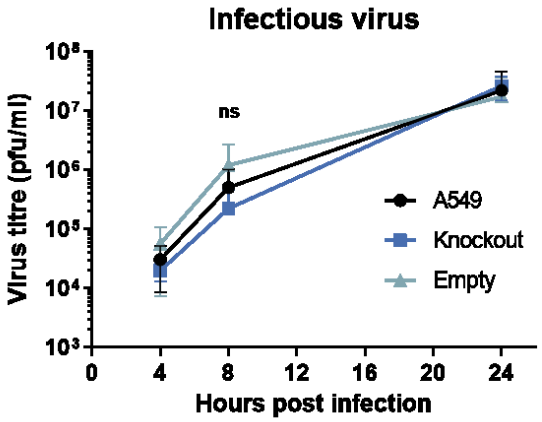

***Figure 2.11 Viral replication in JMJD6 knockout cells.** Wild type A549 cells, two clonal populations of JMJD6 knockout A549 cells (KOC12 and KOF2), and a clonal JMJD6$^{+/+}$ control line (Empty) were infected with PR8 at MOI 5. Cell supernatants were harvested at 4, 8, or 24*

hours post infection and analysed by plaque assay on MDCK cells. Data from two JMJD6 knockout cell lines were pooled into a single data set named "Knockout". Points represent the mean of two biological replicates, error bars represent standard deviation. Data were analysed by two-way ANOVA with Tukey's multiple comparison test using GraphPad Prism 8. ns: not significant.

Finally, the ability of IAV to produce infectious virus from these *JMJD6*$^{-/-}$ A549 cells was investigated. Wild type A549 cells, *JMJD6* knockout cells or the Empty clonal control cells were infected with PR8 at MOI 5 and viral titre in the cell supernatants was measured via plaque assay.

Wild type A549 cells showed the expected kinetics of infection in which the output of infectious virus increased with time and the final virus titre at 24 hours post infection was approximately three orders of magnitude greater than that seen at 4 hours post infection (**Figure 2.11**). The viral output from Empty cells showed a similar pattern to that seen in wild type A549 cells. The mean titre measured at 8 hours post infection appeared to be slightly higher in Empty cells than in A549, however this was minor and not statistically significant (p=0.8318). Likewise, *JMJD6* knockout cells showed infectious virus production at levels and with kinetics that were comparable to wild type A549 cells. The mean titre observed at 8 hours post infection from knockout cells was slightly lower than that seen in A549 cells, however this difference was also found not to be statistically significant (p=0.7903). Overall, these data indicated that IAV replication is not impaired by the absence of JMJD6 in A549 cells. When considered with the data from transient JMJD6 knockdown, this study did not find evidence to support a proviral role of JMJD6 in IAV infection.

2.3. Discussion

2.3.1. JMJD6 as a proviral host factor for IAV

In this project I sought to examine the role of JMJD6 in the IAV lifecycle, with the starting hypothesis that JMJD6 is proviral through being able to downregulate IFN responses to the virus. The results obtained however, did not strongly support this premise.

Arguing against the hypothesis, the work presented in this chapter demonstrated that the siRNA sequence used previously by Drs Kwok and Hu, siRNA-275, induced a large IFN response. This IFN response was not seen with the transfection of a JMJD6-targeting siRNA SMARTpool, indicating that the IFN response was due to transfection with siRNA-275 and not the depletion of JMJD6. Furthermore, JMJD6 knockdown with the non-IFN inducing siRNA SMARTpool did not inhibit the replication of IAV. This suggested that the previously reported proviral role for JMJD6 could well be an artefact of an siRNA-induced IFN response in A549 cells which restricted IAV infection and replication, rather than loss of JMJD6.

Interestingly, Dr Hu did not detect an IFN response in uninfected (mock) knockdown cells (**Figure 2.2B**). It is possible that with the original, longer knockdown protocol the initial IFN response had dissipated past detectable levels, but left cells primed to respond to IAV. Additionally, no antiviral effect on VACV was seen following siRNA treatment of HeLa cells in Dr Kwok's work (Kwok, 2018); this could suggest that the IFN response to siRNA-275 is cell specific. However, IFN was not measured in HeLa cells and, unlike IAV (Xiao *et al.*, 2013), VACV is relatively resistant to a pre-existing IFN response (Smith *et al.*, 2018) so it cannot be assumed that there was no IFN induction by siRNA-275 in HeLa cells.

The original hypothesis was supported by published works implicating JMJD6 in the downregulation of antiviral IFN responses (Ganesan *et al.*, 2018). Work by Ganesan

et al. which showed negative regulation of IFN signalling by JMJD6 did not use siRNA-275 but a commercial pool system from OriGene called Trilencer-27 (Ganesan *et al.*, 2018). They did not detect an IFN response following siRNA transfection and required stimulation of the cells with exogenous IFN to observe the effects of JMJD6 on IFN-induced gene expression (Ganesan *et al.*, 2018). Furthermore, the findings from siRNA knockdown of JMJD6 were also supported with JMJD6 overexpression experiments which showed decreased IFN signalling in response to HCV infection (Ganesan *et al.*, 2018).

Examination of IAV replication in gene edited cells unable to express JMJD6 also failed to support the hypothesis that JMJD6 is proviral for IAV, as the virus displayed normal gene expression and replication in two clonal populations of JMJD6 $^{-/-}$ cells.

Overall, in this study, IAV infection was not inhibited by JMJD6 knockdown using SMARTpool siRNA, and IAV replicated normally in *JMJD6*$^{-/-}$ cells. Therefore, I found no evidence that JMJD6 is directly proviral for IAV, the primary focus of my starting hypothesis. However, the original premise can be broken down into two components – a proviral role for IAV, and a negative regulatory function for JMJD6 in the antiviral response. This latter aspect is discussed below.

2.3.2. JMJD6 and the IFN response

In contrast to the results reported in this thesis, work from others has reinforced the hypothesis that JMJD6 can be proviral for viruses, although others than IAV. Zhang *et al*. reported a role of JMJD6 in the IFN response to SeV and VSV after the work presented here was completed. The siRNA used in that study also does not match siRNA-275 (Zhang *et al.*, 2021). Zhang *et al*. also included overexpression experiments which support the role of JMJD6 as a negative regulator of the IFN response triggered by the detection of viral RNA (Zhang *et al.*, 2021). Furthermore, Zhang *et al*. observed enhanced IFN response to viral infections in JMJD6 knockout

cells (Zhang *et al.*, 2021). Overall, the published data supporting the roles of JMJD6 in the negative regulation of the IFN response to viral infections, both in the pathway resulting from detection of viral RNA and from the activation of the IFN receptor, seem very robust. However, both of the proposed regulatory roles for JMJD6 involve the inhibition of transcription factors activated at the final stage in a signalling pathway (Ganesan *et al.*, 2018; Zhang *et al.*, 2021). IAV possesses mechanisms of antagonising earlier stages of these pathways (Du *et al.*, 2020; Ji *et al.*, 2021), so may circumvent the effects of JMJD6 depletion.

That siRNA-275 transfection induced an IFN response in a manner independent of JMJD6 depletion could not be fully proven here, as no IFN response to siRNA-275 was detected in the clonal *JMJD6*$^{-/-}$ cells. The Digard lab has previously found that clonally sorted edited cells can behave differently to heterogeneous populations, possibly due to the selection of adaptations caused by the loss of a gene (unpublished). This could contribute to the disparity seen between the knockout and wild type cells here. However, no IFN was detected in the "Empty" JMJD6-positive clonal control population transfected with siRNA-275, suggesting that the lack of IFN response was unlikely to be a consequence of editing. The three clonal cell populations used in this study were later found to have been contaminated with bacteria of the *Mycoplasma* genus. Mycoplasma contamination can affect the ability of cells to produce cytokines, including IFN (Drexler & Uphoff, 2002). It is possible that this contamination obscured the detection of an IFN response to siRNA-275 in the edited cells. At the time of writing, work is currently ongoing at The Roslin Institute to develop Mycoplasma-free *JMJD6*$^{-/-}$ A549 cells. These may be used in the future to re-examine the effect of siRNA-275 transfection, as well as to further test the role of JMJD6 in innate immune regulation.

The suggestion that transfection with siRNA-275 may induce an IFN response has implications for studies that have used siRNA-275 to investigate the functions of JMJD6. The sequence was first published in Heim *et al*., 2014, where it, and other JMJD6-targeting siRNA sequences, were used to examine the role of JMJD6 in alternative splicing (Heim *et al.*, 2014). Induction of an IFN response by siRNA-275 could have affected the findings in this work, as there is evidence that IFN itself may alter mRNA splicing factors (Giorelli *et al.*, 2001). At the time of writing, no other published papers specifically name or specify the sequence of this problematic JMJD6-targeting siRNA, although there are many studies that do not give the sequences of siRNAs used. The siRNA-275 sequence, designed and published in the Heim *et al*. study, was custom made and reproduced for the work of Drs Kwok and Hu, as well as the work presented here. The sequence is not commercially available. The findings of this PhD project strongly recommend against the use of siRNA-275 for future work.

Chapter 3: Evaluating CMTR1 as a drug target in IAV infection

3.1. Background and aims

3.1.1. Identification of CMTR1 as a host factor for IAV

CMTR1 was associated with a proviral role in IAV replication by a genome-wide CRISPR screen by Li *et al*. (2020). In this study, A549 cells expressing Cas9 were infected with a lentivirus library which encoded sgRNAs targeting more than 18,000 protein coding genes, as well as non-targeting sgRNA controls. Edited cells, and unedited control cells, were infected with PR8 for 16 hours before being sorted by FACS based on their surface expression of viral HA (Li *et al.*, 2020a). Cells with low HA expression were analysed to identify genetic alterations that restricted IAV replication and the top hits were re-examined in a secondary, more targeted screen. The combined results of these screens gave a list of 121 genes, which included known and predicted IAV host factors as well as genes that had not been previously associated with the IAV lifecycle. One of the genes in this latter group was CMTR1, which, along with three other candidate host factors, were further investigated using polyclonal knockout populations (Li *et al.*, 2020a). CMTR1 knockout cells infected with PR8 showed reduced numbers of infected (HA-positive) cells compared to an unedited population after 16 hours (**Figure 3.1A**), and gave reduced titres of infectious virus over 72 hours (**Figure 3.1B**). This restricted IAV infection was also seen after infection with a lab adapted H3N2 IAV strain as well as with more recent clinical isolates and could be rescued by overexpression of CMTR1 (Li *et al.*, 2020a).

These data strongly suggested that CMTR1 is a proviral host factor for IAV. The protein, its cellular function, and further investigations by the authors of this screen are discussed below.

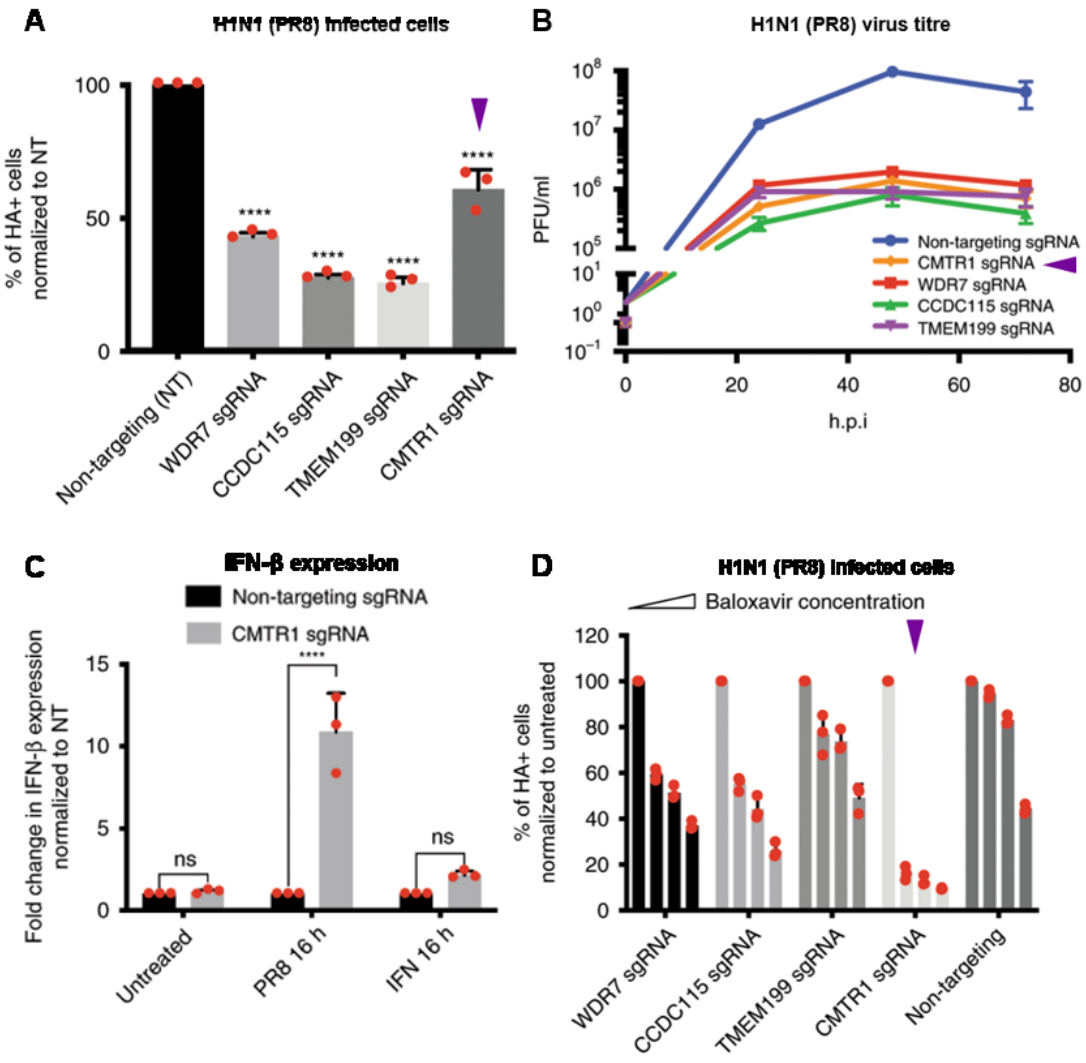

Figure 3.1 Published data indicating a proviral role for CMTR1. *Figures adapted from Li* et al. *(2020). Data for CMTR1 is indicated with purple arrows (added for this thesis).* ***A:*** *A549 cells that had been transduced using the indicated sgRNA were infected with PR8 at MOI 5. Surface expression of HA was analysed at 16 hours post infection. Bars represent the mean of three biological replicates, error bars represent standard deviation.* ***B:*** *Edited cells were infected with PR8 at MOI 0.1. Infectious virus production was measured by plaque assay at 24, 48 and 72 hours post infection (h.p.i.). Points represent the mean of three biological replicates, error bars represent standard deviation.* ***C:*** *A549 cells that had been transduced with either non-targeting or CMTR1-targeting sgRNA were left untreated, infected with PR8 at MOI5, or treated with IFN-β. Levels of IFN-β mRNA, was measured by RT-qPCR at 16 h.p.i. Bars represent the mean of three biological replicates, error bars represent standard deviation.* ***D:*** *Polyclonal populations of edited cells were pre-treated with 0, 1, 5, or 10 nM Baloxavir and infected with PR8 at MOI 5. Surface expression of HA was analysed at 16 hours post infection. Bars represent the mean of three biological replicates, error bars represent standard deviation.*

3.1.2. CMTR1

3.1.2.1. mRNA cap structures

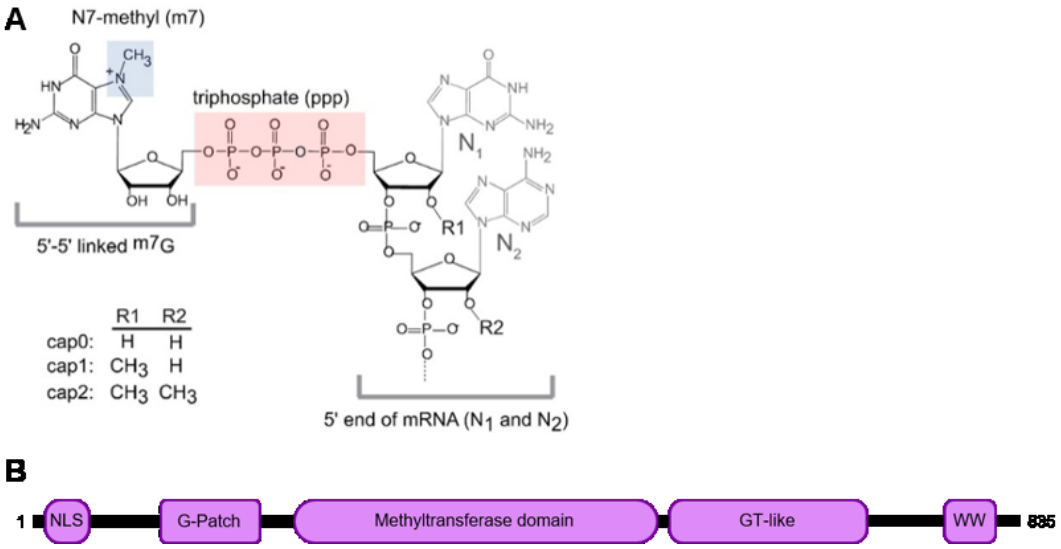

Figure 3.2 Cap structures and CMTR1 domain architecture. A: *Structures of mRNA 5' cap, taken from Schuberth-Wagner et al., 2015.* ***B:*** *Domain architecture of CMTR1. NLS: nuclear localisation signal; GT-like: guanylyltransferase-like domain.*

In eukaryotic cells, mRNA molecules are capped at their 5' end with an N7-methylguanosine (m^7G), linked to the first nucleoside (N) by an inverted 5'-5' triphosphate bridge (ppp) (Shatkin, 1976). This m^7GpppN structure, known as cap0, is added to pre-mRNA molecules co-transcriptionally by enzymes with RNA triphosphatase, RNA guanylyltransferase and RNA guanine-N7 methyltransferase activity, which interact with the C-terminal domain (CTD) of the largest subunit of RNA pol II, RPB1 (Ho *et al.*, 1998). The cap0 structure is essential for the viability of mammalian cells (Shafer *et al.*, 2005).

Subsequent to the formation of the cap0 structure in mammalian cells, the first transcribed nucleotide of the mRNA molecule is methylated at the ribose 2′-O position, resulting in a $m^7GpppNm$ structure called cap1 (Wei *et al.*, 1975). All human mRNA molecules have at least this cap structure, and approximately half are further

methylated at the ribose 2′-O position on the second transcribed nucleoside (m^7GpppNmNm) which gives a cap2 structure (Furuichi *et al.*, 1975) (**Figure 3.2A**).

Cap1 structures have also been found on many viral RNAs and the first 2'-O-methyltransferase enzyme to be isolated and characterised was the VACV VP39 in 1978 (Barbosa & Moss, 1978). Since then, 2'-O-methyltransferase activity has been attributed to proteins encoded by many other viruses including the viral RNA-dependent RNA polymerases of VSV (Hercyk *et al.*, 1988) and Dengue virus (Egloff *et al.*, 2002). CMTR1 was identified as the enzyme responsible for cap1 formation in humans in 2010(Bélanger *et al.*, 2010).

3.1.2.2. CMTR1

CMTR1 had previously been named KIAA0082 when it was first identified as part of the Kazusa cDNA sequencing project (Ohara *et al.*, 1997). It was then reported as a host protein upregulated in chimpanzees following infection with HCV (Su *et al.*, 2002). Expression of the protein was also found to be upregulated in the early stages of VACV infection in HeLa cells (Guerra *et al.*, 2003). Furthermore, expression of KIAA0082 was found to be upregulated in various cell types following type I IFN treatment (Geiss *et al.*, 2003). In all three cases, the gene was identified along with a number of others and was not investigated further. The protein was later renamed ISG95, where the 95 refers to its molecular weight of 95 kDa (Haline-Vaz *et al.*, 2008), prior to the discovery of its role in cap1 formation, when it was renamed again to CMTR1 (Bélanger *et al.*, 2010).

CMTR1 is a multi-domain protein that contains a central RrmJ/FtsJ methyltransferase domain (Haline-Vaz *et al.*, 2008), which binds the cap0 structure and a methyl donor cofactor in order to generate the cap1 (Smietanski *et al.*, 2014). Additionally, the protein has an N-terminal NLS and a G-patch domain, a short motif that is associated with RNA binding proteins (Aravind & Koonin, 1999; Haline-Vaz *et al.*, 2008). The G-

patch domain of CMTR1 has also been reported to interact with other proteins, including the RNA helicase DHX15 (Inesta-Vaquera *et al.*, 2018; Toczydlowska-Socha *et al.*, 2018). A C-terminal WW domain also facilitates protein-protein interactions, including with the RNA pol II RPB1 subunit (Haline-Vaz *et al.*, 2008; Inesta-Vaquera *et al.*, 2018). CMTR1 contains a guanylyltransferase (GT)-like domain C-terminal to the methyltransferase domain (**Figure 3.2B**). Haline-Vaz *et al*. reported that CMTR1 did not rescue cap formation when expressed in yeast mutants lacking the fungal guanylyltransferase enzyme (Haline-Vaz *et al.*, 2008), suggesting that the GT-like domain of CMTR1 does not contribute to formation of the cap0 structure. However, Smietanski *et al*. suggested that the GT-like domain is required for optimal methyltransferase activity of CMTR1, as mutants truncated after the methyltransferase domain showed reduced binding to and methylation of synthetic RNA substrates (Smietanski *et al.*, 2014). However these mutants also lacked the WW domain, so the reduction in methyltransferase activity cannot be fully attributed to the GT-like domain. More work is needed to fully understand the functions of all the CMTR1 domains. Current understanding seems to suggest that CMTR1 is part of a complex of RNA-binding proteins that contributes to co-transcriptional modifications of RNA required for its later processing and function.

3.1.2.3. mRNA cap functions

Cap structures on mRNA are known to promote stability by protecting transcripts from degradation by exonucleases (Furuichi *et al.*, 1977). The cap0 structure is also required for efficient splicing of pre-mRNA (Konarska *et al.*, 1984; Ohno *et al.*, 1987) via the cap binding complex (CBC), which recruits spliceosome components (Pabis *et al.*, 2013). The CBC also mediates export of mRNA to the cytoplasm where it recruits translation initiation factors which then bind to the cap itself (Fortes *et al.*, 2000). It is unclear if the cap1 structure affects splicing, however RNA molecules

containing the 2'-O-methylation have been found to have enhanced ribosomal binding (Muthukrishnan *et al.*, 1976) and translation initiation (Muthukrishnan *et al.*, 1978; Zelus *et al.*, 1989) compared to those without. Furthermore, significantly reduced translation rates have been observed in CMTR1$^{-/-}$ cells compared to wild type cells (Liang *et al.*, 2022). The mechanism behind this is not yet known, however cap0 and cap1 have been shown to bind to the eukaryotic translation Initiation Factor 4E (eIF4E) with similar affinity (Sikorski *et al.*, 2020).

The major role of cap1 seems to be in recognition of mRNAs as self. Inactivation of viral cap 2'-O-methyltransferases has been shown to result in increased susceptibility to antiviral IFN-induced proteins with tetratricopeptide repeats (IFITs) (Daffis *et al.*, 2010). It has been suggested that IFIT proteins have high affinity for uncapped transcripts and for the cap0 structure, but much lower affinity for cap1 (Abbas *et al.*, 2013; Kumar *et al.*, 2014). Similarly, the presence of a cap1 structure on an mRNA transcript greatly reduces the affinity with which RIG-I is able to bind to it. Schuberth-Wagner *et al*. and Devarkar *et al*. both generated synthetic RNA molecules containing the 5'-triphosphate and various features of the cap0, 1 and 2 structures which were transfected into human cells in order to examine the influence of each modification on RIG-I binding and activation. Both groups found that the binding affinity of RIG-I to RNA containing the cap0 structure and to RNA with only a 5'-triphosphate was very similar, and that the binding affinity of RIG-I to RNA containing the cap1 structure was greatly reduced compared to the other RNAs (Devarkar *et al.*, 2016; Schuberth-Wagner *et al.*, 2015). Consequently, RIG-I-mediated IFN responses were induced by RNA oligomers containing the 5'-triphosphate and oligomers with the cap0 structure, however, the IFN response to cap1-containing RNA was greatly reduced, or absent (Devarkar *et al.*, 2016; Schuberth-Wagner *et al.*, 2015) . Mutation of a single histidine in the RNA-binding site of RIG-I, which had previously been seen to interact with the

2'-hydroxyl of the first nucleotide (Lu *et al.*, 2010; Wang *et al.*, 2010), allowed RIG-I to bind to cap1 with equal affinity to cap0, which lead to activation of RIG-I and the induction of IFN expression (Devarkar *et al.*, 2016; Schuberth-Wagner *et al.*, 2015). Interestingly, Schuberth-Wagner *et al*. also saw that RNA oligomers which contained a 2'-O-methyl on the first nucleotide but lacked an m^7G structure (pppNmN) did not induce a RIG-I-mediated IFN response, suggesting that only this 2'-O-methyl is required to inhibit RIG-I recognition of RNA molecules (Schuberth-Wagner *et al.*, 2015). This further highlights the importance of the function of CMTR1 in preventing IFN responses to RNA.

Further supporting the idea that cap methylation can be used to discriminate host from viral mRNA, coronaviruses with inactivated 2'-O-methyltransferases have been found to induce higher MDA5-mediated IFN responses and to be more sensitive to IFN than wild type viruses (Züst *et al.*, 2011). These 2'-O-methyltransferase deficient viruses were able to replicate normally in *MDA5*$^{-/-}$ or *IFIT1*$^{-/-}$ cells (Züst *et al.*, 2011). Thus, the cap1 structure is a marker of self that prevents both the activation of PRRs and the binding of immune effector proteins.

3.1.3. CMTR1 as a host factor for IAV

Due to the importance of cap1 in preventing the activation of an immune response, many viruses encode their own 2'-O-methyltransferase enzyme. IAV does not encode its own capping enzymes, instead acquiring the cap structure from host mRNA molecules via cap-snatching, as described in section 1.2.3.2. Briefly, IAV RNA polymerase subunits bind to RNA pol II and to mRNA cap structures (Engelhardt *et al.*, 2005; Ulmanen *et al.*, 1981) and cleave the nascent host pre-mRNA in order to use the cap and 10-15 nucleotides as a primer for the transcription of IAV genes (Krug *et al.*, 1980a; Krug *et al.*, 1979). Transcription of viral mRNA is dependent on these primers (Plotch *et al.*, 1981). IAV therefore relies on the host 2'-O-methyltransferase

enzyme to generate a cap1 structure in order that viral RNA molecules do not activate RIG-I. Furthermore, IAV cleaves mRNAs with cap1 structures more efficiently than those with a cap0 (Bouloy *et al.*, 1980). As such, Li *et al*. hypothesised that CMTR1 is required for efficient cap snatching by IAV.

Immunoprecipitation experiments in CMTR1 knockout cells showed that a smaller proportion of NP-encoding RNA was associated with eIF4E than in wild type cells (Li *et al.*, 2020a). This lead the authors to conclude that CMTR1 knockout cells contained less capped viral RNA and therefore that CMTR1 is required for IAV cap-snatching. CMTR1 knockout cells also showed increased IFN production (**Figure 3.1C**) and expression of antiviral ISGs in response to IAV infection compared to wild type cells (Li *et al.*, 2020a). This is consistent with the findings that RIG-I is activated by mRNAs with cap0, but not cap1 5'-termini (Devarkar *et al.*, 2016; Schuberth-Wagner *et al.*, 2015). Whether viral RNA molecules are uncapped or capped with cap0 in CMTR1 knockout cells, they are more likely to be bound by RIG-I and thus activate an IFN response.

Finally, Li *et al*. investigated the effects of the IAV antiviral Baloxavir in CMTR1 knockout cells. Baloxavir is the active form of Baloxavir Marboxil (Xofluza) which has been shown to be effective in the treatment of IAV infection in humans (Hayden *et al.*, 2018) and was approved for use in the UK in 2021. The drug inhibits the cap-dependent endonuclease activity of PA, which is required for cap-snatching (Noshi *et al.*, 2018; Takashita *et al.*, 2018). Li *et al*. found that the antiviral effects of Baloxavir were greater in CMTR1 knockout A549s than in unedited cells (**Figure 3.1D**). This suggested potential synergistic action between loss of CMTR1 expression and Baloxavir (Li *et al.*, 2020a).

3.1.4. Aims for this project

The data presented by Li *et al*. showed that IAV replication was reduced and the IFN response increased in the absence of CMTR1, which was hypothesised to be due to impaired cap-snatching in CMTR1 knockout cells. This project aimed to further examine the role of CMTR1 in the IAV lifecycle, with a view to analyse its suitability as a drug target. Initial plans sought to clarify the effects of CMTR1 depletion on the IAV lifecycle. For example, as host mRNAs with cap0 would presumably also be recognised as non-self, cells that lack CMTR1 might be more immunologically primed and therefore have reduced infectability. As the cellular role of CMTR1 is important for normal host functioning, inhibition of the protein may have dangerous side effects. A more detailed understanding of the role of CMTR1 in the IAV life cycle will allow for the better design of CMTR1-targeting antiviral treatments which minimise risk to the host.

For this work, an siRNA knockdown protocol was developed which was used instead of CRISPR-Cas9 knockout for a number of reasons. Primarily, at the time of writing, no specific chemical inhibitors of CMTR1 function are known. Knockdown of gene expression by RNAi is more representative of a drug treatment, as the result is a temporary and incomplete reduction of protein levels rather than its complete, permanent removal. Furthermore, the cap1 structure made by CMTR1 is required for many cellular functions, as described above, therefore knockout may lead to undetected adaptations in edited cells that could confound the results of infection experiments. Although there are also potential issues with siRNA-mediated knockdown, as demonstrated in the previous chapter, using multiple techniques to evaluate the role of CMTR1 in IAV infection makes for robust data.

3.2. Results

3.2.1. Development of a CMTR1 knockdown protocol in A549 cells

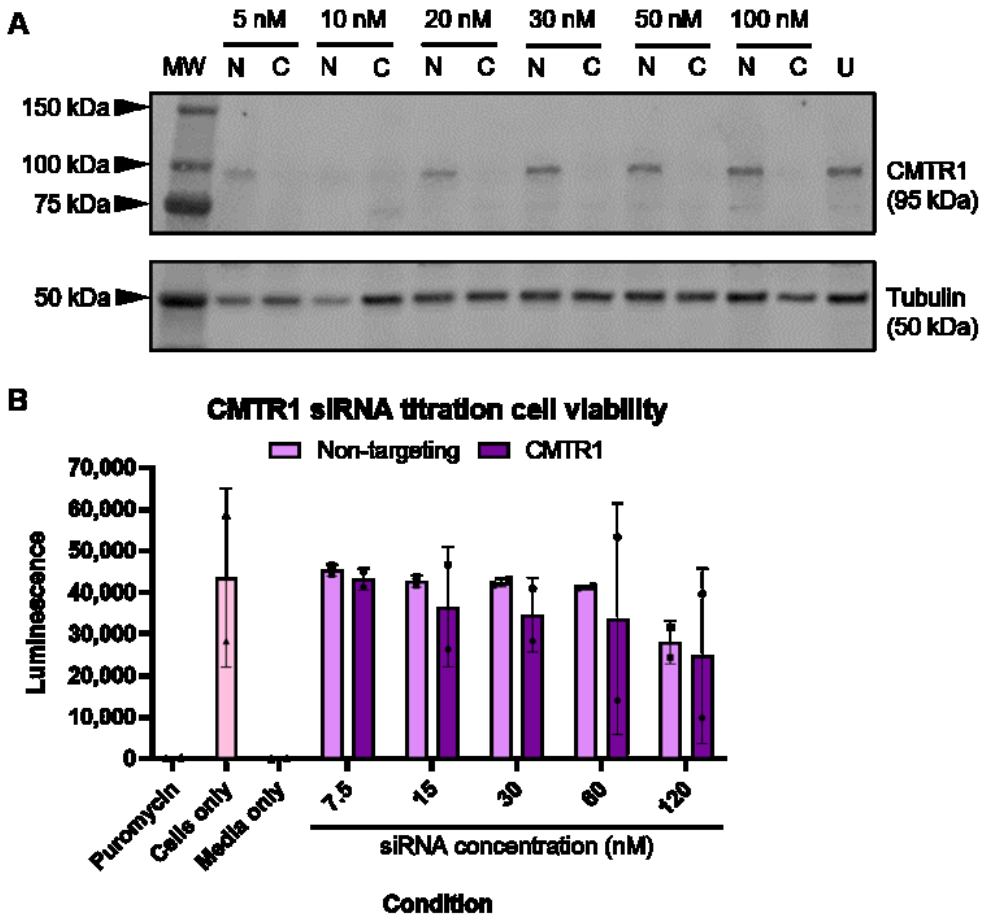

Figure 3.3: CMTR1 knockdown protocol development. A: *A549 cells were transfected with either non-targeting (N) or CMTR1-targeting (C) siRNA at a range of 5-100 nM or left*

untransfected (U). Cells lysates were harvested 48 hours post transfection and examined via western blot for CMTR1 and an alpha tubulin loading control. Images for a single representative experiment are shown. MW indicates molecular weight markers. ***B:*** *A549 cells were transfected with 0-120 nM of either CMTR1-targeting or non-targeting siRNA, treated with 50 µg/µL puromycin, or left untreated (Cells only). After 48 hours cell lysates were analysed using a CellTiter-Glo viability assay kit. Background luminescence was established by incubating cell-free media with the CellTiter-Glo reagent (media only). Points represent the mean of technical duplicates within independent repeats, bars represent the mean of two biological replicates, and error bars represent standard deviation. Data were analysed by one-way ANOVA with Tukey's multiple comparison tests using GraphPad Prism 8.* ***C:*** *CMTR1 levels from western blots were determined using LI-COR Image Studio software and normalised to alpha tubulin in the same sample. Bars represent the mean of nine independent experiments in which cells were transfected with 30nM siRNA, expressed as a proportion of the matched control. Error bars represent standard error of the mean. Data were analysed by unpaired t test using GraphPad Prism 8. ****: p≤0.0001.*

In order to establish a CMTR1 knockdown protocol, an siRNA titration was performed using a CMTR1-targeting ON-TARGETplus siRNA SMARTpool. A549 cells were transfected with either non-targeting (N) or CMTR1-targeting (C) siRNA at concentrations ranging from 5 to 100 nM, or left untransfected (U). Cells were then lysed and CMTR1 protein levels were assessed by western blot. Probing for alpha tubulin as a loading control showed consistent lysate recovery from all samples other than cells treated with 10nM non-targeting siRNA (**Figure 3.3A**). Probing the same western blots with anti-CMTR1 antibody showed a polypeptide migrating at the expected 95 kDa in untransfected cells and in cells transfected with non-targeting siRNA. The same band was seen with much lower intensity in cells transfected with all concentrations of CMTR1-targeting siRNA, indicating successful knockdown even at the lowest concentration of siRNA tested.

CMTR1 plays an important role in the normal functioning of cells; therefore, cell viability following siRNA transfection was assessed in order to assess cytotoxicity in the protocol. A549 cells were transfected with a two-fold dilution series of siRNA concentrations ranging from 7.5 nM to 120 nM. After 48 hours, cells were lysed and

analysed using a CellTiter-Glo viability assay. The assay produced a luminescence signal proportional to the levels of ATP in the lysate which gave an indication of the viability of the cells. In order to establish a baseline for luminescence produced by healthy cells, untreated A549 cells (cells only) were also analysed. Background luminescence was determined by incubating the CellTiter-Glo reagent with cell-free media (media only), and the effect of high levels of cytotoxicity on the assay readout was determined by analysing the lysates of cells that had been treated with the protein synthesis inhibitor, puromycin.

The luminescence signal recorded from cells that had been treated with non-targeting siRNA at the lowest concentration of 7.5 nM was comparable to that produced by untreated cells, as were the signals from cells transfected with 25, 30, and 60 nM non-targeting siRNA (**Figure 3.3B**). Cells transfected with 120 nM non-targeting siRNA showed reduced mean luminescence compared to untreated cells, although this was not statistically significant ($p=0.9801$). The viability of cells that had been transfected with 7.5 nM CMTR1-targeting siRNA was comparable to untreated cells, whereas cells transfected with 15, 30, or 60 nM CMTR1-targeting siRNA showed reduced luminescence compared to untreated cells and to cells treated with the matching concentration of non-targeting siRNA, although this was not significant at any concentration. Luminescence measured from cells treated with 120 nM CMTR1-targeting siRNA was further reduced compared to untreated cells, although this was also not statistically significant ($p=0.9295$). Despite the lack of statistical significance, the CellTiter-Glo assay showed a trend towards reduced cell viability in cells that had been transfected with higher concentrations of siRNA. This cytotoxicity appeared to be greater in cells transfected with CMTR1-targeting siRNA.

On balance, 30 nM siRNA was chosen to be used for subsequent experiments, and any reduction in cell viability seen with transfection with this concentration of CMTR1-

targeting siRNA was deemed to be acceptable for use in the context of this study. To provide quantitative data on the reproducibility and effectiveness of this protocol at depleting CMTR1 expression, CMTR1 levels from replicate siRNA titration experiments, as well as subsequent experiments in which the 30 nM protocol was used, were collated and expressed relative to the matched non-targeting siRNA-treated samples (**Figure 3.3C**). An average knockdown efficiency of approximately 85% was observed in cells transfected with 30 nM CMTR1-targeting siRNA compared to 30 nM non-targeting siRNA ($p<0.0001$). This level of CMTR1 depletion was judged to be sufficient for this type of study.

Together with the cell viability data, this showed CMTR1 protein levels in A549 cells could be greatly reduced using 30nM siRNA and that cells could tolerate this temporary depletion with minimal cytotoxicity.

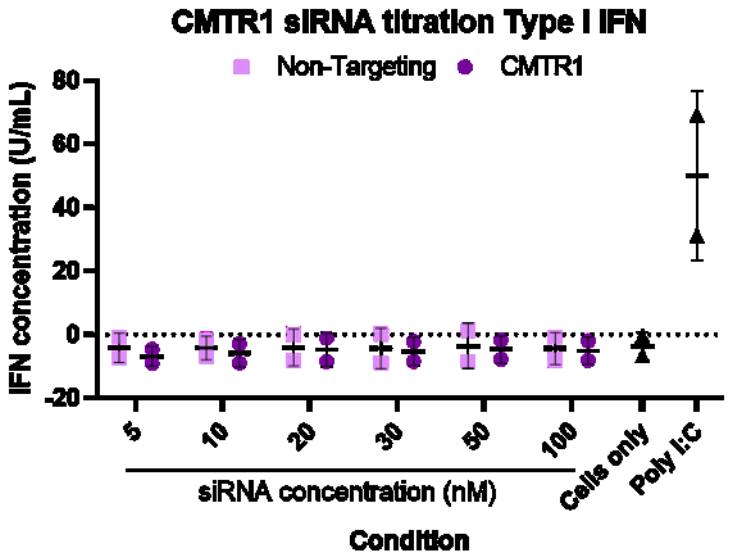

Figure 3.4: IFN response to siRNA titration. *A549 cells were transfected with 5-100 nM of either CMTR1-targeting or non-targeting siRNA for 48 hours, 5 µg poly I:C for 6 hours or left untransfected (Cells only). Cell supernatants were harvested and type I IFN was measured by HEK-Blue™ assay. Data points represent the means of technical duplicates from independent experiments, error bars represent standard deviation. Data were analysed by one-way ANOVA with Tukey's multiple comparison tests using GraphPad Prism 8.*

The final step of this protocol development and validation was investigating IFN response to CMTR1 knockdown. The cap1 2′-O-methylation of host transcripts by CMTR1 is thought to act as a marker for recognition as self, by reducing the affinity with which RIG-I can bind to the RNA molecules and thus induce IFN responses (Devarkar *et al.*, 2016; Schuberth-Wagner *et al.*, 2015). Accordingly, at least one previously published study has observed the induction of an IFN response, indicated by increased levels of IFN-β mRNA, following siRNA-mediated knockdown of CMTR1 (Schuberth-Wagner *et al.*, 2015). However other studies in which siRNA was used to knockdown CMTR1 did not report an IFN response to the depletion (Bélanger *et al.*, 2010; Lee *et al.*, 2020; Williams *et al.*, 2020). Nor was an IFN response observed in CRISPR-edited CMTR1 knockout cells without further stimulation (Li *et al.*, 2020a).

To test the IFN response to this CMTR1 knockdown protocol, A549 cell supernatants were harvested from the experiments described above, 48 hours post transfection with 5-100 nM of either non-targeting or CMTR1-targeting siRNA. Supernatants of untransfected cells and cells that had been transfected with poly I:C were also harvested. These samples were assessed by HEK-Blue™ assay, and standard curves of known concentrations of type I IFN were used to calculate approximate IFN levels. Untransfected cells (cells only), showed no detectable IFN and cells transfected with poly I:C acted as a positive control to confirm the ability of the cells to produce an IFN response (**Figure 3.4**). Cells which had been transfected with non-targeting siRNA showed no IFN response above the limit of detection of the HEK-Blue™ assay, and at all concentrations were found to be comparable to untransfected cells. Similarly, cells that had been transfected with CMTR1-targeting siRNA, and hence were expressing reduced levels of CMTR1 protein, showed no IFN response.

Therefore, the depletion of CMTR1 protein did not result in a detectable IFN response in this system, suggesting that, within the timeframe of these experiments, reduced

CMTR1 expression did not lead to an immune reaction against cellular RNA molecules. The CMTR1 knockdown protocol developed above, in which cells were transfected with 30 nM siRNA, was therefore deemed suitable to be used for examining the effects of CMTR1 depletion on IAV infection.

3.2.2. Infection of CMTR1 knockdown cells

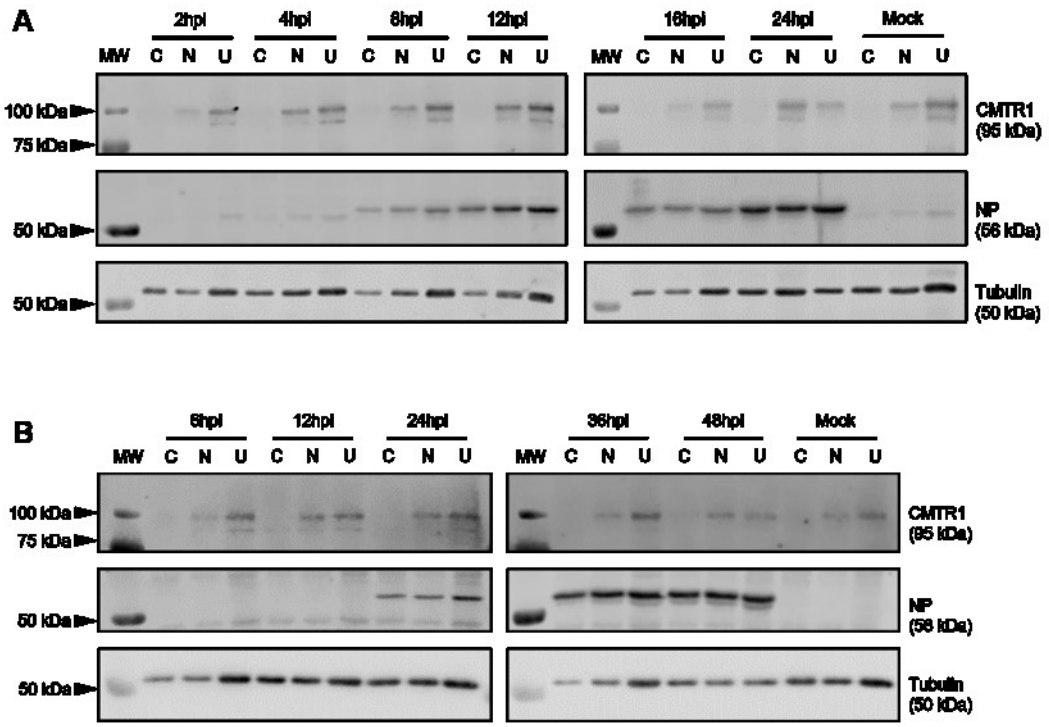

Figure 3.5: Viral NP levels in infected CMTR1 knockdown cells. *A549 cells were transfected with CMTR1-targeting (C) or non-targeting (N) siRNA or left untransfected (U) and incubated for 48 hours. Cells were infected with PR8 and cell lysates were harvested at the indicated time points. Mock infected cells were incubated for 24 hours in virus free media. Lysates were examined by western blot for cellular CMTR1, viral NP and an alpha tubulin loading control. Single representative western blots are shown for experiments in which cells were infected with PR8 at* ***A****: MOI 5 or* ***B*****:** *MOI 0.01. hpi: hours post infection. MW indicates molecular weight markers.*

In order to determine if siRNA-mediated CMTR1 depletion had a similar inhibitory effect on IAV replication as CMTR1 knockout (Li *et al.*, 2020a), siRNA-treated cells were infected with PR8. A549 cells were transfected with either CMTR1-targeting or non-targeting siRNA or left untransfected; 48 hours post transfection cells were

infected with PR8 at MOI 5 or 0.01. Cell lysates were harvested at various time points and analysed by western blot to confirm CMTR1 knockdown. Viral NP was also probed for in order to determine the effect of CMTR1 depletion on IAV protein production.

For single cycle infections at MOI 5, in which nearly all cells should be infected, lysates were harvested at time points up to 24 hours post infection. Examining these by western blot for an alpha tubulin loading control showed somewhat variable lysate recovery between the sets of samples (**Figure 3.5A**); this was considered when judging the levels of CMTR1 and NP. Staining the same western blots with anti-CMTR1 antibody indicated maintained and consistent expression of CMTR1, relative to tubulin, in untransfected cells over the course of infection. Similarly, cells that had been transfected with non-targeting (N) siRNA showed expression of CMTR1 protein at a consistent level throughout the course of infection, and equivalent to those seen in untransfected cells, relative to tubulin. Further, cells that had been transfected with CMTR1-targeting siRNA showed greatly reduced levels of the protein compared with both control groups, confirming successful knockdown. Probing a separate western blot of the same samples with anti-NP antisera produced signal at the expected size of 56 kDa, above background in untransfected cells at 8 hours post infection. This band was not observed above background levels in mock infected cells of any siRNA treatment condition. Comparable levels of NP, relative to tubulin, were seen at 8 hours post infection in cells that had been transfected with non-targeting siRNA. CMTR1 knockdown cells also showed similar relative expression of NP at this time point. Throughout the course of infection NP levels were seen to increase. This was seen to be true for all conditions and at each time point, and NP levels observed in CMTR1 knockdown cells were comparable to the corresponding non-targeting siRNA-treated

and untransfected cells. This indicated that NP production in IAV infected cells was not inhibited by CMTR1 knockdown.

Multi-cycle infections at MOI 0.01 were also performed. In this type of infection, a small proportion of cells are infected for a longer time in order to scrutinise the ability of the virus to spread from cell to cell. Cells that had been infected at this lower MOI were harvested at 6 hours post infection and then every 12 hours up to 48 hours. Again, lysates were analysed by western blot in order to confirm CMTR1 knockdown. Staining for alpha tubulin indicated variable levels of lysate recovery across samples (**Figure 3.5B**), but this was not specific to any siRNA treatment condition. Staining for CMTR1 gave the expected band at consistently equal intensities, relative to tubulin, in untransfected cells and cells transfected with non-targeting siRNA throughout the course of infection. CMTR1 reactivity was seen at much lower intensity, if at all, in all samples that had been transfected with CMTR1-targeting siRNA indicating successful knockdown. At this lower MOI, NP was not detected until 24 hours post infection. Here, the level of NP was seen to be consistent between conditions, with similar signal intensity observed in CMTR1 knockdown cells as in both CMTR1-expressing control groups. Higher levels of the viral protein were seen at later time points for all conditions. Again, no difference in NP protein expression was seen in CMTR1 knockdown cells compared to cells that had been transfected with non-targeting siRNA or to untransfected cells.

Overall these data showed that CMTR1 expression in A549 cells was not increased by IAV infection at either MOI. Furthermore, accumulation of a major IAV protein was not inhibited by CMTR1 knockdown, suggesting that IAV gene expression may not be inhibited by CMTR1 depletion, as it was reported to be in CRISPR-edited CMTR1 knockout cells.

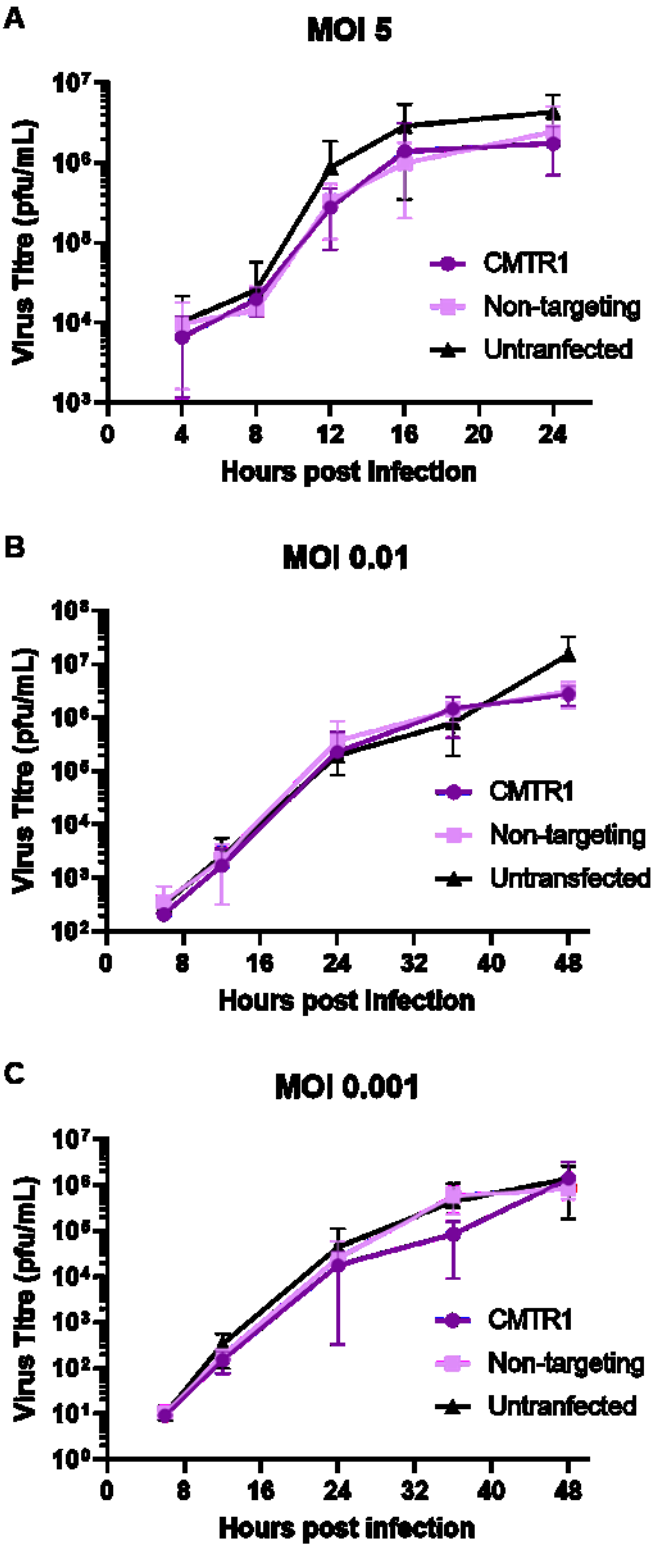

Figure 3.6: Infectious virus production in CMTR1 knockdown cells. *A549 cells were transfected with either CMTR1-targeting or non-targeting siRNA or left untransfected. After 48 hours, cells were infected with PR8 at the indicated MOIs. Cell supernatants were harvested*

at various time points and analysed by plaque assay on MDCK cells. ***A:*** *Points represent the mean of three biological replicates, error bars represent standard deviation.* ***B:*** *Points represent the mean of two biological replicates, error bars represent standard deviation.* ***C:*** *Points represent the mean of three biological replicates, error bars represent standard deviation. Data were analysed by two-way ANOVA with Tukey's multiple comparison test using GraphPad Prism 8. No significant differences were found.*

In addition to analysing viral gene expression, IAV replication in CMTR1 knockdown cells was assessed by measuring the production of infectious virus. Cell supernatants were harvested from the infection experiments described above, as well as from similar experiments in which cells were infected at MOI 0.001, and viral output was measured by plaque assay and growth curves were generated.

First, the effect of CMTR1 knockdown on virus titre in a single cycle infection was examined using MOI 5 (**Figure 3.6A**). Virus titre was measured at 4, 8, 12, 16 and 24 hours post infection. Titres from untransfected cells showed the expected pattern for high MOI IAV infection, of a sharp rise after 8 hours that plateaued by 16 hours post infection. Cells which had been transfected with non-targeting siRNA showed the same kinetics of infection as untransfected cells, but actual titre values were slightly lower, although not statistically significantly different from those from untreated cells. Cells which had been transfected with CMTR1-targeting siRNA showed infection kinetics and mean titres comparable to both untransfected cells and cells transfected with non-targeting siRNA. As with the non-targeting condition, titres produced by CMTR1 knockdown cells appeared slightly lower than those produced by untransfected cells. However, again, this reduction was not statistically significant at any time point. As there was no difference in titre seen between cells transfected with either siRNA, any reduction compared to untransfected cells was likely an artefact of the transfection process rather than an effect of CMTR1 depletion.

In order to examine the ability of IAV to spread between CMTR1 knockdown cells, multicycle infections were performed using MOI 0.01 and MOI 0.001 (**Figure 3.6B** and **C** respectively). In both cases, virus titres measured from CMTR1 knockout cells were comparable to those from cells transfected with non-targeting siRNA and from untransfected cells throughout the course of infection. This indicated normal IAV replication and spread despite depletion of CMTR1 protein.

CMTR1 knockout edited cells, exhibited greatly reduced PR8 titres compared to unedited cells (Li *et al.*, 2020a). However no defect in infectious virus production was observed in the CMTR1 knockdown cells. Overall, CMTR1 knockdown cells showed viral protein expression, infectious virus production and viral spread that was equivalent to cells expressing normal levels of CMTR1. Together the data presented here do not support an essential role for CMTR1 in IAV infection, contrary to what was seen in knockout cells (Li *et al.*, 2020a).

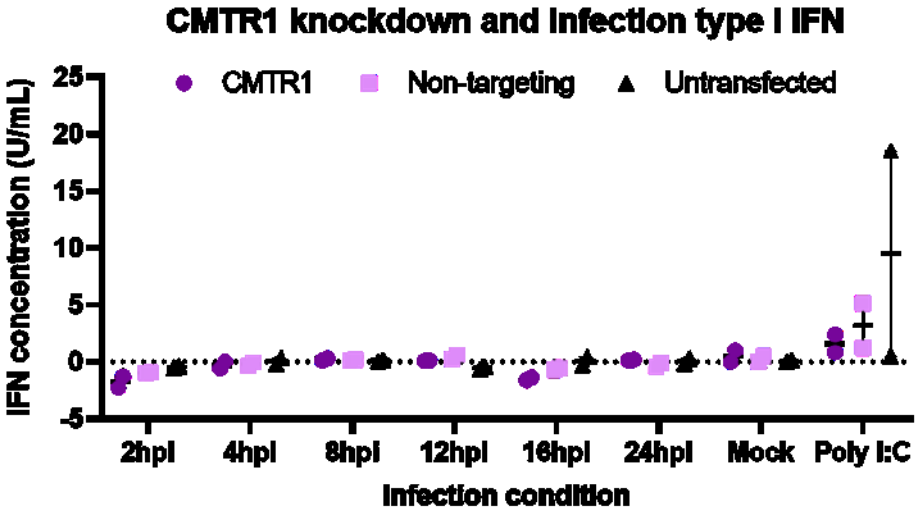

Figure 3.7: IFN response in CMTR1 knockdown cells infected with IAV. *A549 cells were transfected with either CMTR1-targeting or non-targeting siRNA or left untransfected. At 48 hours post transfection, cells were infected with PR8 at MOI 5 and incubated in trypsin-free media. Mock infected cells were incubated for 24 hours in virus-free media. Cell supernatants were harvested at the indicated times post infection (hpi) and virus was inactivated using*

ultraviolet radiation. A positive control group of uninfected cells were transfected with poly I:C and cell supernatant was harvested 6 hours post transfection. IFN levels in the supernatants were measured by HEK-Blue™ assay. Data points represent the means of technical duplicates from independent biological repeats, error bars represent standard error of the mean. Data were analysed by two-way ANOVA with Dunnett's multiple comparison tests using GraphPad Prism 8.

Li *et al.* also reported increased levels of *IFN-β* mRNA in IAV infected CMTR1 knockout cells compared to unedited cells. Therefore, the IFN response to IAV infection was examined in CMTR1 knockdown cells. Cell supernatant was harvested from siRNA-treated or untransfected cells which had been infected with PR8 at MOI 5 for examination by HEK-Blue™ assay. For this analysis, the infection overlay omitted trypsin, which is required for IAV to spread between cells in tissue culture, but would inhibit the colorimetric SEAP reaction of the HEK-Blue™ assay. Therefore IFN response to low MOI, multi-cycle infections could not be measured in this way.

Transfection with poly I:C was used to confirm the ability of the cells to produce IFN. Within these experiments, untransfected cells that were treated with poly I:C showed great variation in the levels of IFN produced, and overall much lower levels than had been previously seen in this study (**Figure 3.7**). In fact, in one biological repeat, no IFN response was detected above background in the untransfected cells. Cells that had been transfected with non-targeting siRNA 48 hours prior to transfection with poly I:C showed a small IFN response, the mean of which was also much lower than that seen in untransfected cells previously. CMTR1 knockdown cells transfected with poly I:C also showed a small IFN response that was even weaker than the response from either control group. This weak response to the positive control indicated either a defect in the ability of the cells to produce IFN or a fault with the assay. No IFN was detected above background in any of the siRNA treatment conditions at any time point of infection, which correlates with the lack of IAV inhibition seen in these cells. However, due to the lack of robust positive controls, these data did not permit the

strong conclusion of a lack of an IFN response to PR8 infection in CMTR1 knockdown cells.

In summary, using siRNA to deplete CMTR1 protein in A549 cells did not result in inhibition of IAV infection, as indicated by maintained viral gene expression (**Figure 3.5**) and infectious virus titres (**Figure 3.6**). This was not consistent with the findings presented in Li *et al.* (2020), who suggested CMTR1 is an essential host protein for IAV replication. Due to the difference in the two systems used to manipulate CMTR1 expression, the data presented here did not completely disprove a proviral role for CMTR1 in IAV infection; however they did suggest that CMTR1 alone may not be a suitable drug target for the treatment of IAV.

3.2.3. Examination of CMTR1 knockdown for potential synergistic action with Baloxavir

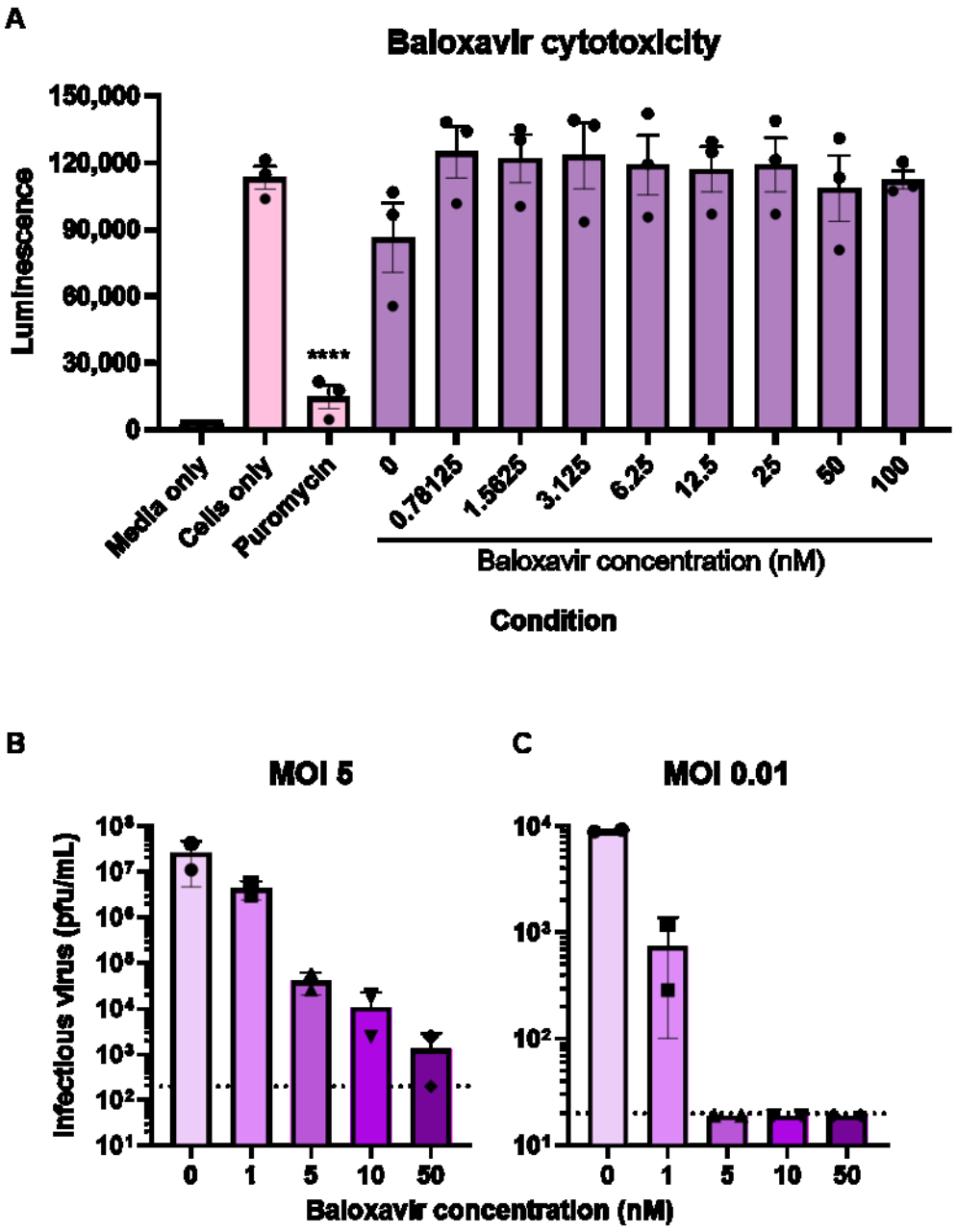

Figure 3.8: Baseline Baloxavir activity. A: *A549 cells were incubated with at a range of concentrations of Baloxavir, DMSO vehicle only (0 nM), 50 µg/µL puromycin, or left untreated (Cells only) for 24 hours. Cell lysates were analysed using a CellTiter-Glo viability assay. Background luminescence was established by incubating cell-free media with the CellTiter-Glo reagent (media only). Points represent the mean of technical duplicates, bars represent the mean of three biological replicates, and error bars represent standard error of the mean. Data were analysed by one-way ANOVA with Tukey's multiple comparison tests using*

*GraphPad Prism 8. Significance marker refers to comparison with cells only. ****: p≤0.0001* ***B:*** *A549 cells were pre-treated with 1, 5, 10, or 50 nM Baloxavir or DMSO only (0 nM) for 24 hours prior to infection with PR8 at either MOI 5 or MOI 0.01. Cell supernatants were harvested 16 hours post infection and analysed by plaque assay on MDCK cells. Bars represent the mean of two biological replicates, error bars represent standard deviation. The dotted lines indicate the limit of detection for the assay.*

In order to examine the potential suitability of CMTR1 as a target alongside a combination treatment, CMTR1 knockdown was combined with Baloxavir treatment. Li *et al.* found that CMTR1 knockout cells showed greater IAV inhibition with Baloxavir pre-treatment than wild-type cells (**Figure 3.2D**), which suggested a potential synergistic interaction between the loss of CMTR1 and Baloxavir treatment. In my study, no inhibition of IAV was seen with CMTR1 knockdown alone. However, the potential for CMTR1 protein depletion as an enhancer of Baloxavir antiviral activity was examined.

First, appropriate Baloxavir concentrations for use in this system were determined by assessing cytotoxicity of the drug. A549 cells were incubated with a range of concentrations of Baloxavir or with DMSO vehicle only (0 nM) for 24 hours. Cell lysates were analysed by CellTiter-Glo assay, using untreated cells (cells only) as a measure of the luminescence produced by healthy cells, and puromycin treatment to show the effect of high levels of cytotoxicity on the assay readout. Background luminescence was determined by incubating the CellTiter-Glo reagent with cell free media (media only).

Cells that had been treated with DMSO only (0 nM Baloxavir), appeared to show reduced cell viability compared to untreated cells (**Figure 3.8A**), although this was not statistically significant (p=0.8297). The luminescence signal measured from these cells was significantly higher than that seen in puromycin-treated cells. In cells treated with Baloxavir, no significant difference was observed in cell viability compared to

cells only or DMSO only, even with increased Baloxavir concentrations. Therefore, it was determined that the concentrations used by Li *et al*. (1, 5, and 10 nM) as well as an additional, higher concentration of 50 nM, were suitable for use in this study.

To demonstrate baseline levels of Baloxavir antiviral activity, A549 cells were treated with increasing concentrations of Baloxavir or with DMSO vector only 24 hours prior to infection with PR8 at MOI 5 or 0.01. After a further 16 hour incubation, cell supernatants were harvested and analysed by plaque assay. Cells that had been pre-treated with DMSO only showed normal levels of infectious virus production at both MOIs tested here (**Figure 3.8B**). At MOI 5, cells pre-treated with the lowest concentration of Baloxavir (1 nM) showed virus titres reduced by an order of magnitude compared to 0 nM. At 5 nM, cells showed titres approximately three orders of magnitude lower than those seen with DMSO only. Further reduction in infectious virus was seen at 10 nM and cells pre-treated with 50 nM Baloxavir showed mean titres approaching the limit of detection for the assay. Similarly, in cells infected at MOI 0.01, pre-treatment with 1 nM Baloxavir also greatly reduced the observed titres compared with vector only (**Figure 3.8C**). Furthermore, pre-treatment with Baloxavir at 5 nM or higher reduced infectious virus output to below the limit of detection of the assay. Overall, the Baloxavir concentrations used in the Li *et al*. (2020) study caused a dose-dependent reduction in virus titre with no effect on host cell viability. These concentrations were then used in combination with siRNA knockdown, and due to the data shown here, plaque assays with a lower limit of detection were performed to analyse low MOI infections with CMTR1 knockdown.

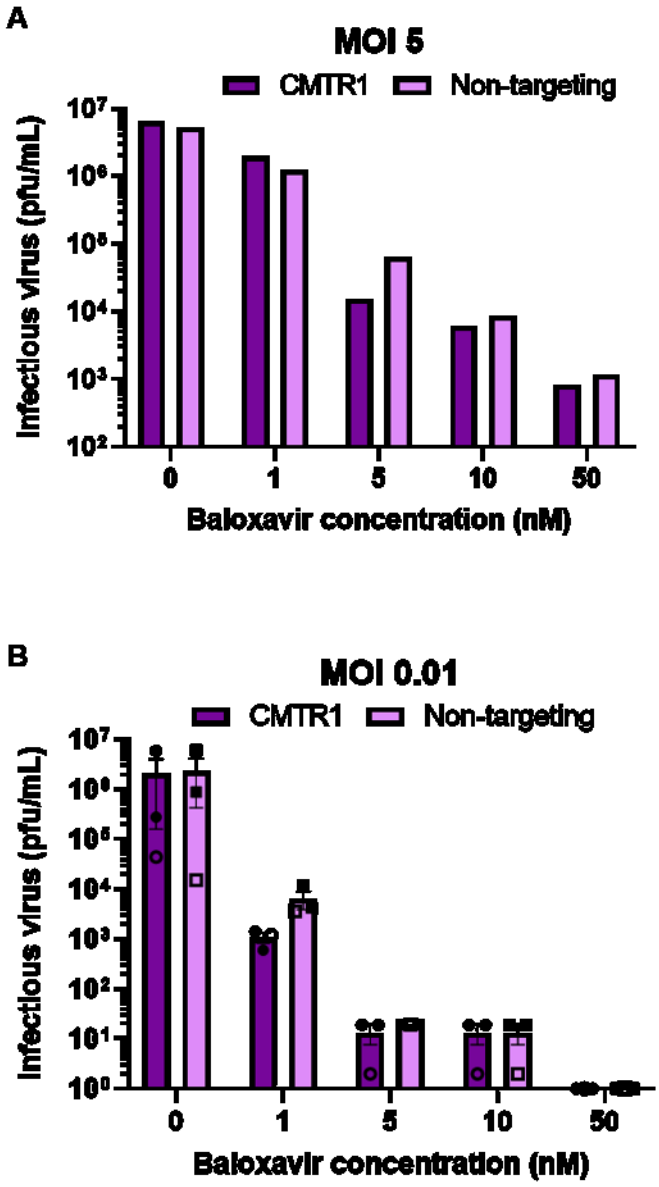

Figure 3.9: Infection of CMTR1 knockdown cells pre-treated with Baloxavir. *A549 cells were transfected with either CMTR1-targeting (CMTR1) or non-targeting siRNA. At 48 hours post transfection cells were treated with 0, 1, 5, 10 or 50 nM Baloxavir for a further 24 hours prior to infection with PR8. Infected cell supernatants were analysed by plaque assay on MDCK cells.* ***A:*** *Virus titres from cells infected at MOI 5 at 16 hours post infection. Bars represent the titres measured in a single experiment.* ***B:*** *Virus titres from cells infected at MOI 0.01. Filled points represent titres measured at 16 and 24 hours post infection in one independent experiment, empty points represent titres measured at 16 hours post infection in a separate independent repeat. Bars represent the mean of these points, error bars represent standard error of the mean. Data were analysed by two-way ANOVA with Sidak's multiple comparison test; no significant differences were seen.*

In order to match the experiments done with Baloxavir in knockout cells, CMTR1 knockdown cells and cells that had been transfected with non-targeting siRNA were treated with a range of concentrations of Baloxavir for 24 hours prior to infection with PR8 at MOI 5. Cell supernatants were harvested 16 hours post infection to be analysed by plaque assay and knockdown was confirmed by western blot (data not shown). Due to time constraints, only a single experiment was performed.

Cells that had been pre-treated with DMSO only showed titres within the expected range (**Figure 3.9A**) and similar levels of infectious virus were measured from CMTR1 knockdown cells as from cells that had been transfected with non-targeting siRNA. Pre-treatment with 1 nM of the drug lead to decreased titres from both cell types, although the reduction seen here was not as great as that previously seen in untransfected cells (**Figure 3.8B**). Further reductions in titres were observed with greater concentrations of Baloxavir in a dose dependent manner for both siRNA conditions (**Figure 3.9A**). In this single experiment, titres measured from CMTR1 knockdown cells pre-treated with 1 nM Baloxavir were marginally higher than from the control cells but with 5 nM and higher concentrations of drug this difference was reversed; titres were up to four times lower from the cells treated with CMTR1-targeting siRNA compared to non-targeting siRNA. However, as these were the results of only a single biological repeat, no relationship between CMTR1 knockdown and Baloxavir could be interpreted without further experimentation.

Additionally, treatment of CMTR1 knockdown cells with Baloxavir was tested with infection at MOI 0.01. In this case, two independent experiments were performed. Titres were measured 16 hours post infection in one repeat, and at two time points of 16 and 24 hours post infection in the other. The three titre values are shown in **Figure 3.9B**. Infectious virus production from these cells decreased with increasing Baloxavir concentration. Based on the titre reduction seen in normal A549 cells, plaque assays

with a limit of detection of 2 pfu/mL were used to measure virus levels from cells treated with higher concentrations of Baloxavir. Titres measured at 5 and 10 nM Baloxavir were approaching this limit of detection and no plaques were observed from samples pre-treated with 50 nM. When comparing titres from CMTR1 knockdown cells and cells transfected with non-targeting siRNA, no difference was seen with DMSO only pre-treatment. However, CMTR1 knockdown cells pre-treated with 1 nM Baloxavir showed mean titres six times lower than control cells treated with the same concentration of drug. No difference in titres was observed between the cell types with 5 or 10 nM Baloxavir. As these data represent the results from only two biological replicates, no conclusions about interaction between CMTR1 depletion and Baloxavir treatment could be made. Nevertheless, these preliminary results suggested that with further experimentation, an interaction might be detected, despite the fact that CMTR1 knockdown alone had no effect on IAV. Also, these data indicate that further investigation at this MOI could gain more insight by using lower Baloxavir concentrations.

3.2.4. Overexpression of inactive CMTR1

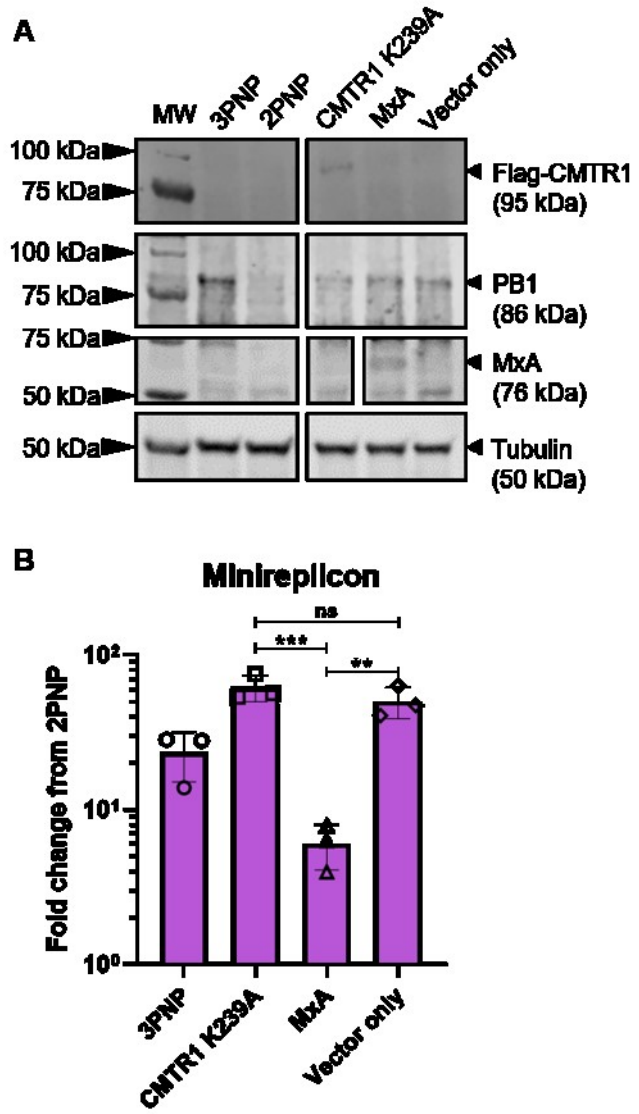

Figure 3.10: Minireplicon experiment with overexpression of methyltransferase dead CMTR1. *293T cells were transfected with plasmids encoding PR8 PB2, PB1, PA and NP (3PNP) as well as a firefly luciferase vRNA reporter plasmid. Experimental groups were also transfected with overexpression plasmids encoding Flag-CMTR1 K239A or MxA (untagged), or empty pcDNA plasmid (vector only). As a negative control, cells were transfected with the IAV polymerase, omitting PB1 (2PNP). Cells were lysed 48 hours post transfection and either were examined by western blot or for luciferase activity.* ***A:*** *Western blots probed for Flag-CMTR1 K239A, PB1, MxA and an alpha tubulin loading control. MxA strip is interrupted due to altered loading order between blots. MW indicates molecular weight markers.* ***B:*** *Luciferase activity measured from cell lysates, expressed as fold change in luminescence compared to 2PNP. Bars represent the mean of three technical replicates; error bars represent standard*

*deviation. Data were analysed by one-way ANOVA with Tukey's multiple comparison tests using GraphPad Prism 8. ns: not significant, p≥0.05; **: p≤0.01; ***: p≤0.001.*

A final examination of CMTR1 as a host factor for IAV was designed using overexpression and an IAV minireplicon luminescence assay. A minireplicon assay assesses the transcriptional activity of the IAV polymerase using plasmids encoding the viral polymerase proteins (PB2, PB1 and PA) and NP under the control of a RNA pol II promoter to express the viral proteins. A plasmid encoding a luciferase reporter, flanked by IAV UTR sequences, under an RNA polymerase I promoter is simultaneously transfected. The transcription of this, by the cellular RNA polymerase I produces a vRNA-like molecule that can be transcribed into mRNA by the IAV polymerase, to be translated into luciferase protein by the cell (Lutz *et al.*, 2005). Therefore luciferase levels indicate the transcriptional activity of the viral polymerase.

If CMTR1 has a proviral role in IAV replication, overexpression of an inactive form of the protein might inhibit the normal function of the endogenous protein through dominant-negative effects (Sheppard, 1994) and thus inhibit the activity of the viral replication machinery. A plasmid containing a Flag-tagged CMTR1 gene with the mutation K239A, which leads to an inactive methyltransferase domain (Lee *et al.*, 2020; Smietanski *et al.*, 2014), was successfully cloned by Dr Nisha Kriplani in our laboratory. It was considered that since endogenous CMTR1 interacts host RNA pol II (Haline-Vaz *et al.*, 2008), wild type CMTR1 might be displaced from this complex by overexpression of the CMTR1 K239A and that this would be another way to model inhibition of CMTR1 activity. With this in mind, a minireplicon assay was performed using the methyltransferase inactivated CMTR1. Due to time limitations, this experiment could be performed once.

X293T cells were transfected with plasmids encoding the three PR8 polymerase proteins and NP (3PNP), and a firefly luciferase reporter vRNA under the control of

the IAV polymerase promoter. Additionally, cells were transfected with overexpression plasmids containing CMTR1 K23A or the ISG MxA which is known to inhibit IAV gene expression (Turan *et al.*, 2004). For a vector only control, cells were transfected with 3PNP and an empty pcDNA plasmid. Baseline luminescence was measured from cells transfected with PR8 PB2, PA and NP, but no PB1, termed 2PNP. After 48 hours, expression of CMTR1 K239A, MxA and PB1 were examined by western blot and luciferase expression was determined by measuring enzymatic activity via luminescence.

When examining cell lysates by western blot, probing for tubulin showed consistent lysate retrieval between conditions (**Figure 3.10A**). Staining with anti-PB1 antisera was used to confirm expression of the protein in the relevant samples, as well as to determine transfection efficiency across the conditions. This gave a band migrating at around 86 kDa, the expected molecular weight, from cells that had been transfected with 3PNP. This band was not seen in the 2PNP sample. Cells that had been transfected with 3PNP and with additional overexpression plasmids also showed expression of PB1, although at lower levels than cells transfected with 3PNP alone. Probing a separate blot of the same samples for MxA showed expression of the protein only in the cells that had been transfected with the relevant overexpression plasmid, indicating successful transfection as well as the absence of endogenous MxA. Similarly, the same samples were examined on another blot using an anti-Flag antibody. This staining only gave signal in cells that had been transfected with the Flag tagged CMTR1 K239A overexpression plasmid, at approximately 95 kDa, thus all cells were seen to be expressing the expected proteins.

In order to determine the level at which the IAV polymerase had transcribed luciferase, cell lysates were treated with luciferase reagent and luminescence was measured. **Figure 3.10B** shows the fold change in luminescence compared to the 2PNP

condition. Cells that had been transfected with 3PNP alone showed luciferase activity that was more than an order of magnitude greater than the 2PNP condition. This demonstrated the baseline replication activity of the IAV polymerase in this system. The luminescence measured from cells transfected with 3PNP and an empty plasmid vector was significantly higher than that from the 3PNP only condition ($p=0.0308$). This did not correlate with transfection efficiency or expression of PB1. Cells that were overexpressing MxA showed reduced luciferase activity compared to the 3PNP condition, although this was not significant ($p=0.1794$). However, the luminescence measured from these samples was significantly lower than that from the vector only condition ($p=0.0017$), demonstrating the effective antiviral activity of MxA. Luciferase activity in cells overexpressing CMTR1 K239A was significantly higher than the 3PNP samples ($p=0.0043$) but comparable to the vector only condition ($p=0.4766$). Furthermore, the luminescence from these cells was also significantly higher than from cells expressing MxA ($p=0.0004$). These data represented the results of only a single biological repeat and therefore no definitive conclusions could be inferred. However at this preliminary stage, there was no suggestion of a relationship between the overexpression of a methyltransferase dead CMTR1 and the activity of the IAV polymerase.

3.3. Discussion

In this chapter I set out to examine the role of CMTR1 in IAV infection in order to gain understanding that could inform the design of antiviral treatments. Previous work by Li *et al*. showed that IAV replication was inhibited and the IFN response to infection was enhanced in CMTR1 knockout cells (Li *et al.*, 2020a). This was hypothesised to be due to a requirement for CMTR1 and its generation of cap1 structures for IAV cap-snatching (Li *et al.*, 2020a). However, in my study, IAV replication was not inhibited by transient CMTR1 knockdown, as viral NP protein levels and infectious virus production was comparable to those in cells expressing normal amounts of CMTR1. This did not support the published findings that CMTR1 was required for efficient IAV replication (Li *et al.*, 2020a).

Of note, when Bélanger *et al*. first characterised the role of CMTR1 as a cap 1 2'-O-methyltransferase, they tested the effect of its knockdown on influenza A virus but saw no significant effect on viral replication, and therefore did not did not publish the associated data but simply referred to it as "data not shown" (Bélanger *et al.*, 2010). This lends confidence to the validity of the findings presented in this chapter.

The difference in techniques used between the three studies could contribute to the disparity seen between findings. Namely, the knockdown of CMTR1 in this study (and presumably in that of Bélanger and colleagues) was incomplete, with an average reduction in protein expression of approximately 85%. The remaining CMTR1 protein could be sufficient for IAV replication. Similarly, CMTR1 was depleted for less time with knockdown than with knockout, as the knockdown cells in the project described here were infected two days post transfection, whereas Li *et al*. infected nine days after transduction with the editing sgRNAs (Li *et al.*, 2020a). It is therefore possible residual cap1-containing mRNA in the siRNA-treated cells allowed IAV to replicate at normal levels. This would presumably require cap-snatching from mature mRNA

molecules independent of RNA pol II, which is not normally thought to occur in infected cells (Amorim & Digard, 2006; Lukarska *et al.*, 2017). The influenza viral polymerase can certainly use mature mRNAs as a primer substrate *in vitro* though (Beaton & Krug, 1981; Bouloy *et al.*, 1978) and the *Arenaviridae* and *Bunyaviridae* cap-snatch in the cytoplasm (Olschewski *et al.*, 2020; Rosenthal *et al.*, 2017), so this may not be implausible.

Another possibility is that adaptations may have been made in CRISPR edited CMTR1 knockout cells in order to compensate for the loss of an important gene. That the knockout cells were reported to show normal levels of viability and proliferation rates (Li *et al.*, 2020a), despite the importance of CMTR1 and the cap1 in cellular processes such as translation (Liang *et al.*, 2022; Muthukrishnan *et al.*, 1978; Zelus *et al.*, 1989), may support this hypothesis. Such modifications may not be detected and could obscure the effects of CMTR1 deficiency on IAV. However, Li *et al*. reported that transfection of CMTR1 knockout cells with plasmids encoding CMTR1 rescued IAV replication in these cells (Li *et al.*, 2020a). This strongly suggests that the reduction of IAV replication was due to CMTR1 deficiency rather than additional modifications.

An experiment was designed for this study, in which CMTR1 would be overexpressed in 293T cells with the minireplicon system in order to assess if IAV replication was enhanced. However, the wild type CMTR1 overexpression plasmid could not be made within the time frame. Preliminary experiments with methyltransferase-inactive CMTR1 did not indicate a relationship with IAV replication. Future work with CMTR1 overexpression and IAV would give more insight to this potential virus-host interaction.

Overall, the findings presented here do not suggest that a treatment targeting CMTR1 alone would be effective against IAV, as complete ablation of the protein and its

function may be required for antiviral effects to be seen. However, preliminary data from experiments treating CMTR1 knockdown cells with Baloxavir, suggested that further investigation may show enhancement of drug treatment by targeting CMTR1. Of note, the timing of treatment used in my study and by Li *et al*. meant that the drug was not present in the media during viral replication. Further experiments with Baloxavir treatment concurrent with infection may be more appropriate. Therefore, the research into CMTR1 and the treatment of IAV should be continued with a view to target CMTR1 in a combination treatment.

Since the completion of the work in this chapter, a meta-analysis of gene expression in chickens following IAV infection was published, which associated upregulation of the galline orthologue of CMTR1 with infection with highly pathogenic IAV strains (Pirbaluty *et al.*, 2022). This is consistent with previous studies that saw CMTR1 upregulation following HCV (Su *et al.*, 2002) and VACV (Guerra *et al.*, 2003) infection, although CMTR1 protein was not seen to be upregulated with IAV infection in this study. This finding supports the association of CMTR1 with IAV infection, but does not provide insight to a possible mechanism.

Chapter 4: Examining IGF2BP proteins as host factors for IAV

4.1. Background and aims

4.1.1. The N^6-methyladenosine (m^6A) epitranscriptome

Many posttranscriptional or epitranscriptomic modifications to RNA molecules can alter their function and expression. Within the mammalian epitranscriptome the most prevalent modification is the addition of a methyl group at the N^6 position of internal adenosine residues (Desrosiers *et al.*, 1975). When this modification was first discovered in the 1970s, it was estimated that the average cellular mRNA transcript (approximately 2.2 kb) contained three internal N^6-methyladenosine (m^6A) residues (Desrosiers *et al.*, 1974; Desrosiers *et al.*, 1975). Since then it has been reported that highly regulated mRNA molecules may contain 10 or more internal m^6A residues (Linder *et al.*, 2015).

The m^6A epitranscriptome is dynamically regulated by so called “writers” and “erasers”: methyltransferase and demethylase enzymes, respectively, that add and remove the m^6A modification from RNA. The first writer to be identified was methyltransferase-like 3 (METTL3) (Bokar *et al.*, 1994; Bokar *et al.*, 1997), a highly conserved protein that acts as the core methyltransferase subunit of a large m^6A methyltransferase complex (Bokar *et al.*, 1994; Bujnicki *et al.*, 2002). More recently, methyltransferase-like 14 (METTL14) was reported to form a stable heterodimer with METTL3 and facilitate m^6A deposition (Liu *et al.*, 2014). Crystal structure analysis of this dimer has suggested that METTL14 does not exert methyltransferase activity within this complex, but is instead required for binding to the RNA substrate and enhances the catalytic activity of METTL3 (Śledź & Jinek, 2016; Wang *et al.*, 2016). *In vitro*, knockdown (Wang *et al.*, 2014b) or knockout (Batista *et al.*, 2014; Geula *et al.*, 2015) of either METTL3 or METTL14 in mammalian cells has been reported to

result in 60 to 99% reduction in detectable m^{6}A (Batista *et al.*, 2014; Geula *et al.*, 2015; Wang *et al.*, 2014b), strongly suggesting that the METTL3-METTL14 complex is responsible for the majority of m^{6}A methylation. A second m^{6}A methyltransferase, METTL16, has also been identified, which appears to act as a monomer and has a smaller range of known substrates than the METTL3-METTL14 complex (Doxtader *et al.*, 2018; Pendleton *et al.*, 2017).

The known m^{6}A erasers, or demethylases are fat mass and obesity-associated protein (FTO) and α-ketoglutarate-dependent dioxygenase AlkB homologue 5 (ALKBH5). FTO was found to have mRNA m^{6}A demethylase activity in 2011, which proved that this RNA modification was reversible (Jia *et al.*, 2011). Later, ALKBH5, a homologue of FTO was also shown to demethylate m^{6}A residues (Zheng *et al.*, 2013).

This dynamic modification of RNA has been implicated in several processes of mRNA regulation, including splicing (Dominissini *et al.*, 2012), stability (Wang *et al.*, 2014a) and both cap-dependent (Heilman *et al.*, 1996; Karikó *et al.*, 2008), and cap-independent (Meyer *et al.*, 2015) translation. These functions are mediated by m^{6}A "reader" proteins, RNA-binding proteins which preferentially bind m^{6}A modified RNA. Some readers can bind directly to m^{6}A residues, as has been shown for the YTH domain family (YTHDF) and YTH domain containing (YTHDC) proteins (Li *et al.*, 2020b; Xu *et al.*, 2015; Xu *et al.*, 2014; Zhu *et al.*, 2014). Other, more indirect reader proteins bind to motifs made accessible by m^{6}A-dependent changes in RNA structure, in a mechanism called the "m^{6}A switch" (Liu *et al.*, 2015b). This was first observed by Liu *et al.*, who reported that m^{6}A modifications destabilised double stranded RNA within hairpin structures, increasing the accessibility of the single stranded binding site for heterogeneous nuclear ribonucleoprotein (hnRNP)-C (Liu *et al.*, 2015b). Approximately 7% of the hnRNP-C binding sites identified in this study were predicted to be regulated by an m^{6}A switch (Liu *et al.*, 2015b). Other hnRNP proteins have also

been shown to indirectly recognise m^{6}A sites via this switch mechanism (Liu *et al.*, 2017b; Wu *et al.*, 2018).

Whether binding to m^{6}A directly or identifying binding sites via the m^{6}A switch mechanism, reader proteins exert a wide range of effects. The first reader proteins to be identified were the YTHDF and YTHDC proteins (Dominissini *et al.*, 2012), which have been very well studied. YTHDF1 has been shown to bind to mRNA transcripts and enhance their translation efficiency, as siRNA-mediated knockdown of this m^{6}A reader lead to reduced ribosomal binding of its target mRNA (Wang *et al.*, 2015). YTHDF1 interacts with ribosomal subunits and translation initiation factor eIF3 to promote ribosomal loading of the modified mRNA (Wang *et al.*, 2015). Conversely, YTHDF2, which may share approximately 50% of its target transcripts with YTHDF1 (Wang *et al.*, 2015), has been shown to enhance mRNA degradation and turnover by recruiting deadenylation complexes (Du *et al.*, 2016) and shuttling RNA to processing bodies (Wang *et al.*, 2014a). YTHDC1 was initially described as a component of the spliceosome, as overexpression *in vitro* was shown to alter splicing patterns (Hartmann *et al.*, 1999). It was later reported to bind m^{6}A modified pre-mRNA, and knockout of the gene was associated with splicing defects in its targets (Kasowitz *et al.*, 2018). These are a small selection of a large range of proteins that demonstrate the diversity of effects mediated by m^{6}A reader proteins.

4.1.2. m^{6}A and IAV

Soon after the discovery of internal m^{6}A in mammalian cells, Krug *et al*. reported that IAV viral mRNA also contained the modification (Krug *et al.*, 1976). This was the first instance of a virus being shown to bear these modifications, and since then m^{6}A residues have been found in many others, including herpesviruses (Moss *et al.*, 1977), retroviruses (Kane & Beemon, 1985; Lichinchi *et al.*, 2016), and more recently, coronaviruses (Liu *et al.*, 2021). Krug *et al*. found that viral mRNA contained similar

levels of m^{6}A residues to host mRNA; approximately three per mRNA chain (Krug *et al.*, 1976). This was later disputed by Narayan *et al*. who reported differing levels of m^{6}A content between IAV genes (Narayan *et al.*, 1987). Despite the discovery of internal m^{6}A residues in IAV in the 1970s, little investigation into their function in the lifecycle of the virus has been conducted until recently, most likely because the cell biological significance of the methylation was not known.

In 2017 Courtney *et al*. used a technique called photo-crosslinking-assisted m6A sequencing (PA-m^{6}A-seq) (Chen *et al.*, 2015a) to map m^{6}A modifications on both the mRNA (positive sense) and the genomic vRNA (negative sense) of PR8 (Courtney et al., 2017). This gave a more detailed picture of the IAV m^{6}A epitranscriptome than had been seen previously. They found multiple m^{6}A sites on both vRNA and mRNA molecules encoding the HA, NP, NA, M and NS genes and lower levels on those encoding PB2, PB1 and PA (Courtney *et al.*, 2017). Courtney *et al*. also showed that IAV replication was impaired in *METTL3*$^{-/-}$ A549s compared to unedited cells, with reduced expression of the examined viral proteins: NP, NS1 and M2, and lower levels of spliced M2 mRNA detected in the absence of the m^{6}A methyltransferase (Courtney *et al.*, 2017). Furthermore, infectious virus production in *METTL3* knockout cells was almost an order of magnitude lower than in control cells (Courtney *et al.*, 2017). Earlier studies had reported that IAV replication is inhibited by 3-deazaadenosine, a methyltransferase inhibitor that depletes SAM, the methyl donor of METTL3 (Fischer *et al.*, 1990; Woyciniuk *et al.*, 1995). Courtney *et al*. also reproduced this finding (Courtney *et al.*, 2017). However SAM is also the methyl donor for many other methyltransferases, including those involved in cap formation such as CMTR1 (Bélanger *et al.*, 2010; Byszewska *et al.*, 2014), so inhibition by 3-deazaadenosine is not m^{6}A-specific, and the role of m^{6}A could not be dissected from this. Therefore, the work by Courtney *et al*. was the first to specifically show that m^{6}A modification of IAV

RNA enhances viral gene expression. Levels of m^{6}A following METTL3 knockout were not examined, so whether METTL3 is the only m^{6}A methyltransferase for IAV is unknown.

Moreover, Courtney *et al*. used synonymous point mutations to remove multiple m^{6}A sites from either the mRNA or vRNA of the HA segment. Both of these mutant viruses showed reduced mRNA and protein expression of HA over the course of infection in A549 cells, where other viral genes, NS1 and M2, were unaffected (Courtney *et al.*, 2017). Interestingly, this reduction appeared more pronounced in the mutant virus lacking m^{6}A on the negative sense (vRNA) strand. Furthermore, both mutants showed reduced pathogenicity in mice (Courtney *et al.*, 2017). These findings further supported that m^{6}A modifications in IAV RNA function to enhance gene expression and infection. Although, the mutation of so many nucleotides at once, 14 for the mRNA mutant and 15 for vRNA, could have had effects on gene expression or vRNA packaging independent of m^{6}A, which was not controlled for in this study.

Furthermore, Courtney *et al*. investigated how three major m^{6}A readers, YTHDF1-3, interacted with IAV by ectopically expressing each protein in A549 cells prior to infection with PR8. They found that the expression of viral proteins, as well as the production of infectious virus was increased in cells overexpressing YTHDF2 (Courtney *et al.*, 2017). This is similar to effects seen with YTHDF2 overexpression in human immunodeficiency virus 1 (HIV-1) infection (Kennedy *et al.*, 2016), but is at odds with the reported cellular role of YTHDF2 as a mediator of mRNA degradation (Du *et al.*, 2016; Wang *et al.*, 2014a). This potentially demonstrates that this m^{6}A reader exerts different functions depending on the RNA target.

No effect on IAV gene expression was observed with overexpression of YTHDF1 or YTHDF3 in A549 cells (Courtney *et al.*, 2017). However, using photoactivatable ribonucleoside-enhanced crosslinking and immunoprecipitation (PAR-CLIP) in IAV-

infected, YTHDF-overexpressing 293T cells, binding sites for all three of the m^{6}A reader proteins on both IAV vRNA and mRNA were identified (Courtney *et al.*, 2017). Furthermore, these binding sites largely correlated with the m^{6}A modifications mapped using PA-m6A-seq (Courtney *et al.*, 2017).

Currently, the Courtney study represents the primary work on m^{6}A readers in IAV infection, and presents a proviral function for YTHDF2, although the mechanism of this is not yet understood. However many questions remain. For example, do methyltransferases other than the METTL3-METTL14 complex catalyse the addition of m^{6}A modifications to IAV RNA? Are patterns of m^{6}A deposition consistent between IAV strains and host cells? Do other m^{6}A readers interact with IAV RNA to influence its lifecycle?

In this chapter, I aimed to address this last question.

4.1.3. IGF2BPs

With a view to investigate m^{6}A readers as potential host factors for IAV, a literature search was conducted. This search found the insulin-like growth factor 2 mRNA binding proteins (IGF2BP), which had recently been shown to preferentially bind m6A-modified RNA and to promote stability and enhance translation of their targets (Huang *et al.*, 2018), in the Host-Pathogen Interaction Database (HPIDB) 3.0 (Kumar & Nanduri, 2010). This database lists host proteins from multiple species that have been reported to interact with the proteins of pathogens (Kumar & Nanduri, 2010). Here, IGF2BP1, IGF2BP2 and IGF2BP3 were all listed as potentially interacting with the NS1 protein from multiple strains of IAV. This came from a large screen which aimed to identify host proteins that interact with viral immune-modulating proteins (Pichlmair *et al.*, 2012). These human proteins and their galline and bovine orthologues were also listed as interactors for several other viral and bacterial pathogens (Kumar &

Nanduri, 2010). Furthermore, another study investigating the interactome of PR8 NS1 also identified IFG2BP1 and IGF2BP3 (Rahim *et al.*, 2018).

IGF2BP1-3 constitute a highly conserved family of RNA binding proteins that bind specific mRNAs and recruit other proteins in order to stabilise their targets (Doyle *et al.*, 1998), and repress (Hüttelmaier *et al.*, 2005; Nielsen *et al.*, 1999) or enhance (Dai *et al.*, 2011; Liao *et al.*, 2005) translation. The proteins all contain four hnRNP-K homology (KH) domains in their C-terminal two-thirds, which mediate m^6A recognition and RNA binding (Farina *et al.*, 2003; Huang *et al.*, 2018), as well as two N-terminal RNA-recognition motifs (RRMs) which have been suggested to stabilise IGF2BP-RNA interactions (Nielsen *et al.*, 2004) (**Figure 4.1A**). The three genes share high levels of similarity in both the DNA and amino acid sequences, particularly IGF2BP1 and IGF2BP3, which share 73% amino acid sequence identity (Bell *et al.*, 2013) (**Figure 4.1B**). This is reflected in a large overlap of RNA targets, as Huang et al. identified more than 2,000 mRNA transcripts that are bound by all three proteins (Huang *et al.*, 2018).

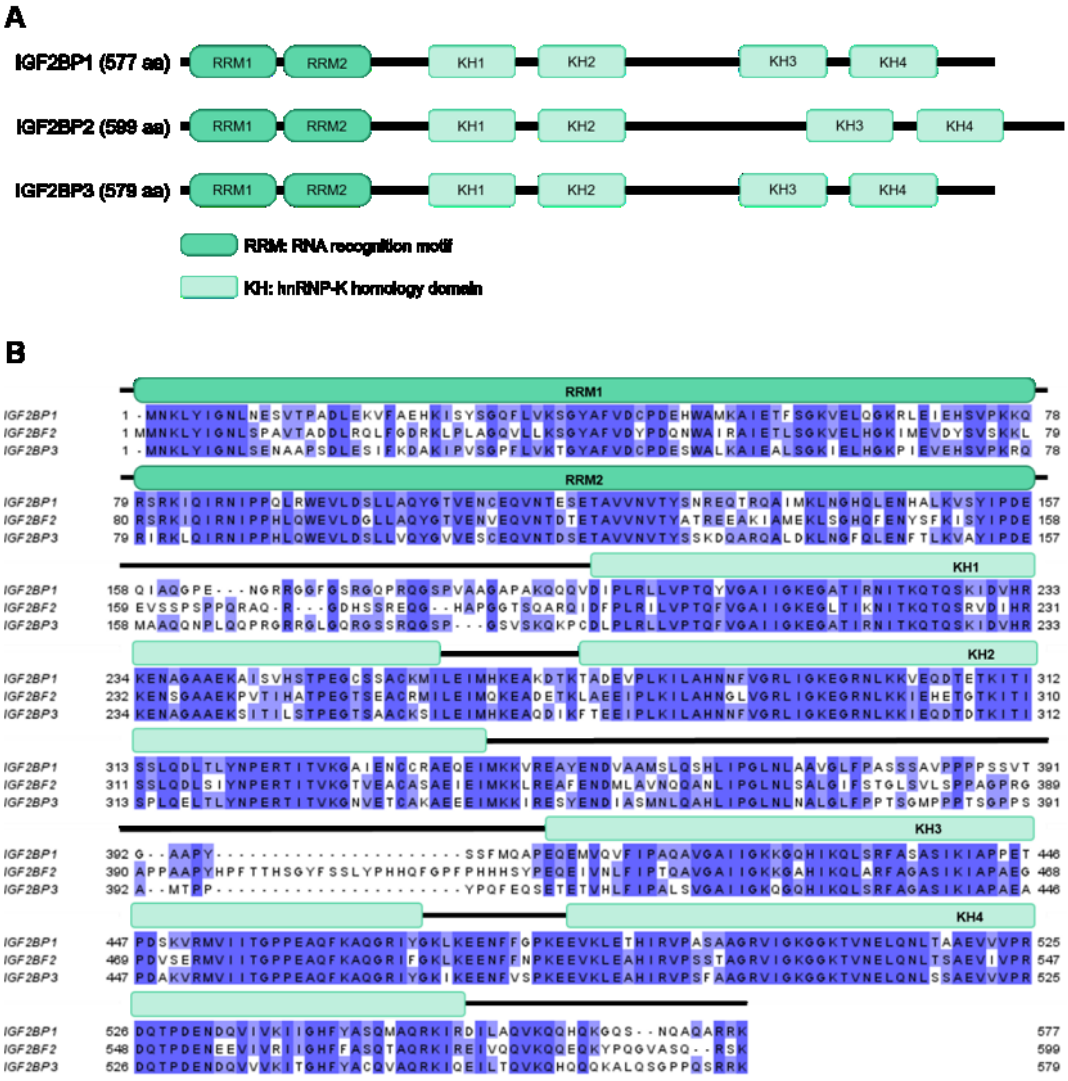

Figure 4.1 Primary protein structures of the IGF2BP family. A: *Domain architecture of proteins in the IGF2BP family.* ***B:*** *Alignment of the amino acid sequences of the human IGF2BP1 (reference sequence NM_006546.4), IGF2BP2 (reference sequence NM_006548.6) and IGF2BP3 (reference sequence NM_006547.3), with the corresponding domains indicated above.*

In 2018, Huang *et al*. reported that more than 80% of the mRNA targets of the IGF2BP family contained m^{6}A modifications and used pull-down experiments to demonstrate that they preferentially bound RNA bait that was m^{6}A-modified (Huang *et al.*, 2018). They mapped m^{6}A sites on the IGF2BP1 target transcript, *c-Myc*, using methylated RNA immunoprecipitation sequencing (MeRIP-seq/m^{6}A-seq) and found strong correlation between the binding sites of all three IGF2BPs (Huang *et al.*, 2018). The

authors suggested that the third and fourth KH domains of each protein bind directly to m^{6}A (Huang *et al.*, 2018), however, Sun *et al*. reported in 2019 that IGF2BP3 bound certain RNA probes in a manner dependent on the m^{6}A switch (Sun *et al.*, 2019). Therefore the mechanism by which the IGF2BPs identify m^{6}A-modified sites may differ between RNA targets.

Huang *et al*. showed that the IGF2BPs recruited known mRNA stabilising proteins such as Hu antigen R (HuR) in order to stabilise their m^{6}A-containing targets (Huang *et al.*, 2018). Since this finding, the known functions of IGF2BPs as m^{6}A readers have expanded: IGF2BP3 has been implicated in micro RNA processing (Li *et al.*, 2022b); and both IGF2BP2 (Zhao *et al.*, 2022) and IGF2BP3 (Xueqing *et al.*, 2020) have been reported to regulate alternative splicing.

Therefore, on the basis of the data described above, the IGF2BPs were selected to be investigated as potential host factors in IAV due to their m^{6}A reader function and probable interaction with NS1. This project thus combined a knowledge-driven approach and the results of large screens to identify targets for investigation.

4.2. Hypothesis and aims

This project aimed to examine whether the IGF2BP m^{6}A readers are involved in the IAV lifecycle and if they would make suitable targets for the design of IAV treatments. The IGF2BPs preferentially bind to RNA containing the m^{6}A modification, which is prevalent in the IAV genome and in IAV mRNA (Courtney *et al.*, 2017; Krug *et al.*, 1976; Narayan *et al.*, 1987). They have also been suggested to interact with the IAV immunomodulatory protein, NS1. Therefore, I hypothesised that host IGF2BPs may contribute to the IAV lifecycle via a combination of interaction with NS1 protein and m^{6}A-modified viral RNA.

4.3. Results

4.3.1. Development of knockdown protocols

4.3.1.1. siRNA titrations

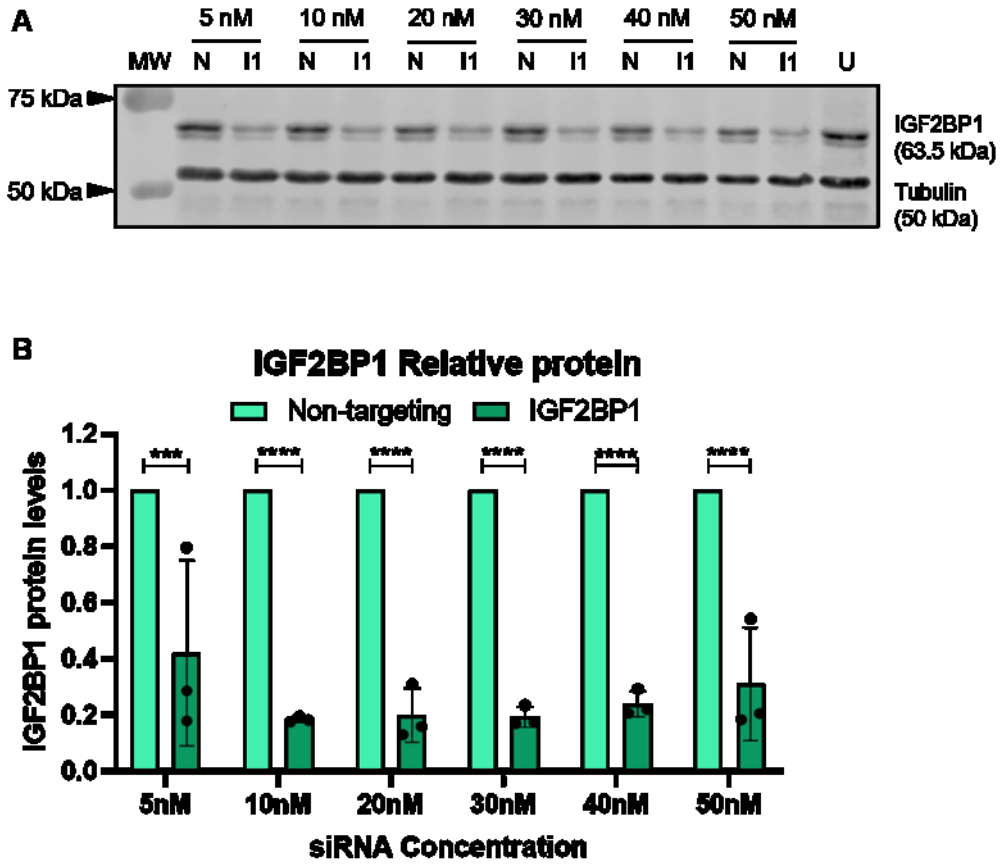

Figure 4.2 Titration of IGF2BP1-targeting siRNA. A: *A549 cells were transfected with either non-targeting (N) or IGF2BP1-targeting (I1) siRNA at a range of concentrations or left untransfected (U). Cell lysates were harvested 48 hours post transfection and examined via western blot for IGF2BP1 and an alpha tubulin loading control. Images from a single representative experiment are shown. MW indicates molecular weight markers.* ***B:*** *IGF2BP1 protein levels were determined from western blots using LI-COR Image Studio software, normalised to tubulin in the same sample and expressed as a proportion of the matched non-targeting control. Bars represent the mean of three independent experiments. Error bars represent standard deviation, Data were analysed by two-way ANOVA with Tukey's multiple comparisons test using GraphPad Prism 8. ***: p≤0.001; ****: p≤0.0001.*

In order to develop an IGF2BP1 knockdown protocol, an siRNA titration was performed using a IGF2BP1-targeting ON-TARGETplus siRNA SMARTpool. A549

cells were transfected with a range of concentrations of either non-targeting (N) or IGF2BP1-targeting siRNA, or left untransfected (U). Cells were lysed and knockdown was evaluated by western blot for IGF2BP1 and an alpha tubulin loading control. Signal measured from the loading control indicated consistent lysate recovery from all conditions (**Figure 4.2A**). Probing the blots with anti-IGF2BP1 anti-sera gave strong signal at 63.5 kDa, the expected molecular weight, from untransfected cells and cells transfected with any concentration of non-targeting siRNA. A second polypeptide migrating at a slightly lower apparent molecular weight was also observed in these cells with lower signal intensity. This band did not correspond with the known alternative isoform of IGF2BP1, which is approximately 50 kDa (Fakhraldeen *et al.*, 2015). In cells that had been transfected with IGF2BP1-targeting siRNA, signal for the band at 63.5 kDa was seen at much lower intensity than in untransfected cells and cells treated with non-targeting siRNA. The second, lower molecular weight band was also seen to be reduced in cells treated with IGF2BP1 targeting siRNA, suggesting that the band does represent IGF2BP1 protein, perhaps resulting from some form of post-translational modification or which had been incompletely denatured. In this initial experiment, the level of IGF2BP1 reduction did not noticeably vary across the various concentrations of siRNA tested.

To provide quantitative data on knockdown efficiency relative to siRNA concentration, this titration experiment was repeated twice further. IGF2BP1 protein levels were calculated by densitometry and expressed as a proportion of the matched non-targeting siRNA-treated samples. Cells that had been treated with 5 nM IGF2BP1-targeting siRNA showed an average knockdown efficiency of approximately 60% compared to cells transfected with 5 nM non-targeting siRNA (**Figure 4.2B**). This was statistically significant ($p=0.0001$), although there was some variability between repeats. Cells that had been transfected with 10, 20, 30, or 40 nM of IGF2BP1-

targeting siRNA showed an average of 80% less IGF2BP1 protein than each matched control, which was reproducible between repeats ($p<0.0001$ for all). The mean knockdown efficiency measured from cells transfected with 50 nM IGF2BP1-targeting siRNA was 70% ($p<0.0001$). The differences in knockdown efficiency between different concentrations of siRNA were not found to be statistically significant. Overall, it was found that IGF2BP1 knockdown could be achieved even at low concentrations of siRNA. The maximum knockdown efficiency reached was 80%, using between 10 and 40 nM siRNA targeting the *IGF2BP1* mRNA. For subsequent IGF2BP1 knockdown experiments, 30 nM siRNA was used.

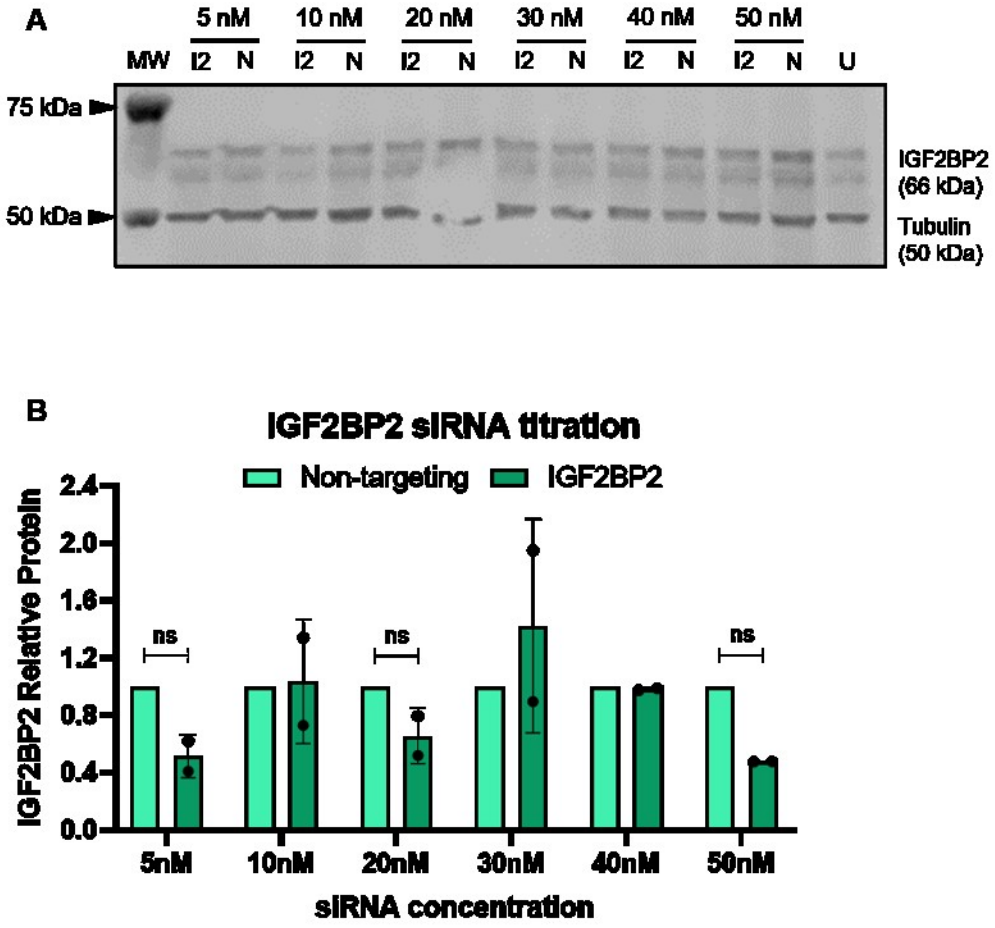

Figure 4.3 Titration of IGF2BP2-targeting siRNA. A: *A549 cells were transfected with either non-targeting (N) or IGF2BP2-targeting (I2) siRNA at a range of concentrations or left untransfected (U). Cell lysates were harvested 48 hours post transfection and examined via western blot for IGF2BP2 and an alpha tubulin loading control. Images from a single representative experiment are shown. MW indicates molecular weight markers.* ***B:*** *IGF2BP2 protein levels were determined from western blots using LI-COR Image Studio software, normalised to tubulin in the same sample and expressed as a proportion of the matched non-targeting control. Bars represent the mean of two independent experiments, error bars represent standard deviation. Data were analysed by two-way ANOVA with Tukey's multiple comparison test using GraphPad Prism 8. ns: not significant, p≥0.05.*

Similarly, a range of concentrations of IGF2BP2-targeting siRNA, also an ON-TARGETplus siRNA SMARTpool, were tested in order to establish a knockdown system for the second protein in the family. Again, A549 cells were transfected with either non- (N) or IGF2BP2 (I2) -targeting siRNA at a range of concentrations or left

untransfected (U) and harvested after 48 hours. Cell lysates were then analysed by western blot. Probing for alpha tubulin gave consistent signal across all conditions (**Figure 4.3A**). The same blot was also stained with anti-IGF2BP2 anti-sera, which resulted in a band migrating around the expected size of 66 kDa. This staining also showed another band at around 60 kDa which may correspond to a known IGF2BP2 isoform, generated by alternative translation initiation, which is expressed at lower levels than the full length protein (Le *et al.*, 2012). The intensity of both bands was seen to be consistent across all samples regardless of siRNA treatment or concentration indicating that knockdown of IGF2BP2 was not achieved here.

This siRNA titration was repeated and IGF2BP2 protein levels were calculated using the band at 66 kDa normalised to tubulin in the same sample. **Figure 4.3B** shows the result of the two biological repeats. In cells transfected with 5 nM IGF2BP2-targeting siRNA, mean IGF2BP2 protein levels were approximately 50% lower than those seen with the matched non-targeting control, however this was not statistically significant ($p=0.4154$). There was no difference in mean IGF2BP2 levels between cells that had been transfected with 10 nM or 40 nM targeting siRNA and cells treated with non-targeting siRNA, while a non-significant reduction in IGF2BP2 was seen in cells transfected with 20 nM or 50 nM IGF2BP2-targeting siRNA ($p=0.7563$ and $p=0.3310$ respectively) and a non-significant increase was seen with 30 nM ($p=0.5563$). On the whole, these siRNA titration experiments showed no effective knockdown of IGF2BP2 with these concentrations of siRNA. Higher concentrations of siRNA gave unacceptable levels of cytotoxicity (data not shown). Therefore an IGF2BP2 knockdown protocol could not be developed with this system.

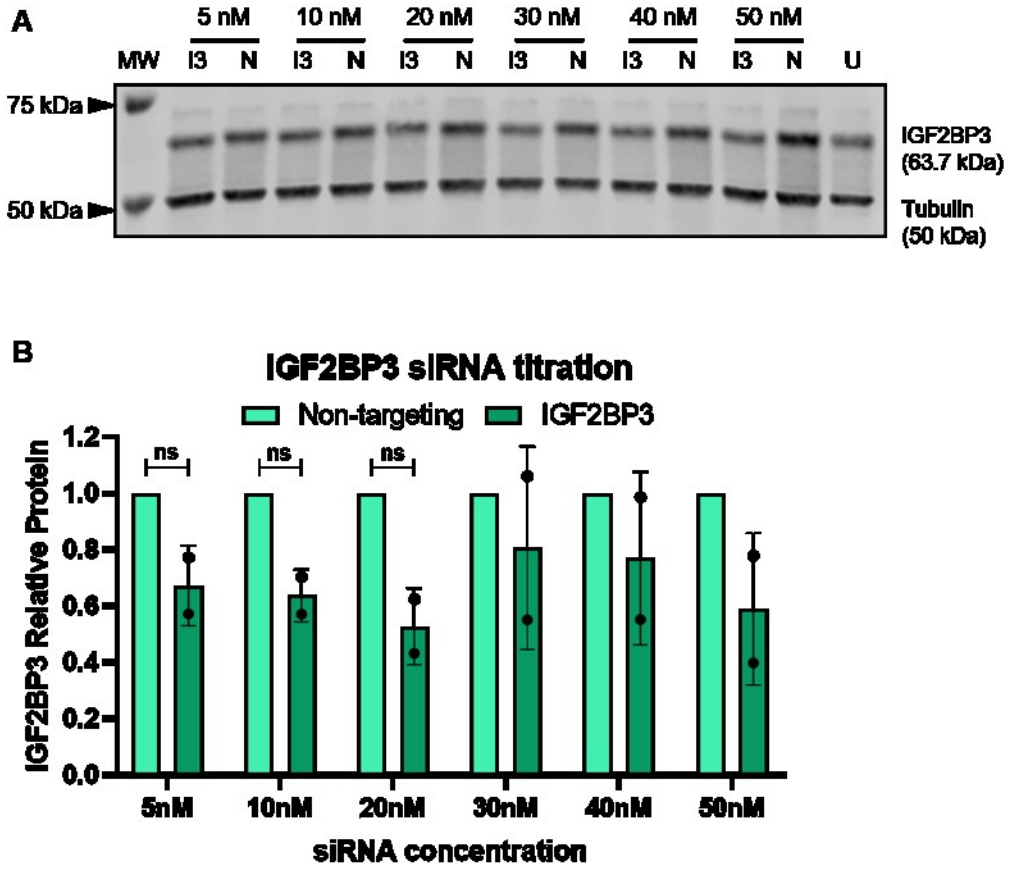

Figure 4.4 Titration of IGF2BP3-targeting siRNA. A: *A549 cells were transfected with either non-targeting (N) or IGF2BP3-targeting (I3) siRNA at a range of concentrations or left untransfected (U). Cell lysates were harvested 48 hours post transfection and examined via western blot for IGF2BP3 and an alpha tubulin loading control. Images from a single representative experiment are shown. MW indicates molecular weight markers.* ***B:*** *IGF2BP3 protein levels were determined from western blots using LI-COR Image Studio software, normalised to tubulin in the same sample and expressed as a proportion of the matched non-targeting control. Bars represent the mean of two independent experiments, error bars represent standard deviation. Data were analysed by two-way ANOVA with Tukey's multiple comparison test using GraphPad Prism 8. ns: not significant, p≥0.05.*

Finally, a titration of an IGF2BP3-targeting siRNA SMARTpool was performed. A549 cells were treated and harvested as above and cell lysates were analysed by western blot with anti-IGF3BP and anti-alpha tubulin antibodies. Uniform recovery of cell lysates across conditions was confirmed by the tubulin staining (**Figure 4.4A**). Probing for IGF2BP3 gave a band from all cells which corresponded with the

canonical isoform of the protein at 63.7 kDa. This band was expressed highly in all cells that had been transfected with non-targeting siRNA and in untransfected cells. In cells that had been treated with lower concentrations of IGF2BP3-targeting siRNA, 5, 10 or 20 nM, the signal detected at this band was slightly lower than that in the control cells. At higher concentrations of the siRNA, IGF2BP3 levels were reduced further, compared to the matched non-targeting controls. The greatest reduction, observed with 50 nM siRNA, was still small, suggesting only partial knockdown of IGF2BP3 was achieved, even with this highest concentration of siRNA.

The IGF2BP3 levels from this titration, as well as a second biological repeat, were calculated as before and expressed relative to the matched non-targeting controls. Cells that had been transfected with 5 nM IGF2BP3-targeting siRNA showed a non-significant decrease in mean IGF2BP3 protein levels of approximately 30% compared to the matched non-targeting control ($p=0.3802$; **Figure 4.4B**). With transfection of 10 nM and 20 nM siRNA, the mean reduction increased to 35% and then to 40%, although these were also not significant ($p=0.2811$ and $p=0.0951$ respectively). This trend in reduction did not continue with higher concentrations of siRNA, IGF2BP3 levels measured from cells that had been transfected with 30, 40, or 50 nM siRNA were also not significantly reduced compared to the matched controls and were variable between the two repeats. None of these siRNA concentrations gave sufficient, reproducible knockdown to be used for further experiments.

As knockdown protocols apparently could not be developed here for either IGF2BP2 or IGF2BP3, it was considered that the similarity in gene sequences within this family could have reduced the specificity and thus effectiveness of siRNA targeting them. That is, siRNA targeting one gene could have also bound to the mRNA of another, reducing the amount of siRNA targeting the intended gene. Further, the high amino acid sequence identity between the proteins could have caused cross-reactivity

between the antibodies used, which would have masked the knockdown efficiency of the siRNAs. These possibilities were investigated next.

4.3.1.2. Evaluation of siRNA specificity

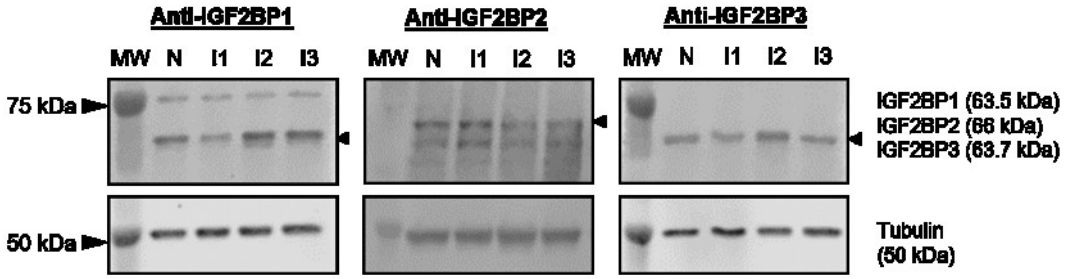

Figure 4.5 Examination of siRNA specificity. *The lysates of cells from siRNA titration experiments that had been transfected with 50 nM non-targeting (N) siRNA or IGF2BP1 (I1)-IGF2BP2 (I2)-, or IGF2BP3 (I3)-targeting siRNA were analysed by western blot. Membranes were probed with the indicated antibodies and an alpha tubulin loading control. MW indicates molecular weight markers. Western blotting with anti-IGF2BP2 (middle panel) was performed by Dr Hui-Min Lee.*

In order to investigate the specificity of the siRNAs targeting each of the three genes, the lysates of A549 cells that had been transfected with 50 nM non-targeting (N), or IGF2BP1 (I1)-, IGF2BP2 (I2)-, or IGF2BP3 (I3)-targeting siRNA were examined by western blot for the expression of all three proteins. When probing with anti-IGF2BP1 antibody, the expected band at 63.5 kDa was seen in the cells treated with non-targeting siRNA (**Figure 4.5**, left). As in **Figure 4.2A**, the same band intensity was reduced in cells that had been transfected with IGF2BP1-targeting siRNA. In cells that had been treated with siRNA targeting either *IGF2BP2* or *IGF2BP3* mRNA, IGF2BP1 protein levels, relative to tubulin in the same sample, were comparable to those seen with the non-targeting control (**Figure 4.5**, left). This suggested that neither of these siRNA pools had significant off target binding with *IGF2BP1* mRNA.

Staining a duplicate western blot of the same samples with anti-IGF2BP2 antibody (performed by Dr Hui-Min Lee in our group) gave the two expected polypeptides migrating at 66 and 60 kDa from all samples (**Figure 4.5**, middle). The signal intensity

of both bands was marginally reduced in cells transfected with IGF2BP2-targeting siRNA compared to the non-targeting control. Conversely, IGF2BP2 protein levels in the cells treated with IGF2BP1-targeting siRNA were apparently higher than in the matched control, particularly the 60 kDa isoform. No difference in expression was observed between cells treated with the IGF2BP3-targeting and the non-targeting siRNA. These data did not indicate off target knockdown of the other proteins by the IGF2BP2-targeting siRNA.

Finally, another western blot of the samples was probed with anti-IGF2BP3 antibody. As seen in the siRNA titration experiment, the IGF2BP3 band at approximately 64 kDa had slightly lower intensity in cells that had been transfected with IGF2BP3-targeting siRNA compared to non-targeting siRNA (**Figure 4.5**, right). Further, the IGF2BP3 band in cells that had been treated with IGF2BP1-targeting siRNA also appeared reduced compared to the matched control. The IGF2BP3 levels in these cells were comparable to the cells treated with IGF2BP3-targeting siRNA, which suggested a potential off target knockdown by the IGF2BP1-targeting siRNA pool. Cells that had been transfected with IGF2BP2-targeting siRNA showed higher signal at the IGF2BP3 band than all other samples.

Together these data did not suggest off target effects of IGF2BP2- or IGF2BP3-targeting siRNAs on the other genes in the family, but did indicate a potential reduction in IGF2BP3 protein by the IGF2BP1-targeting siRNA. However, due to the variable efficacy of both IGF2BP2 and IGF2BP3 knockdown, meaning that successful transfection of the siRNA was hard to prove, conclusive examination of the effects of these siRNAs on the other genes was also difficult.

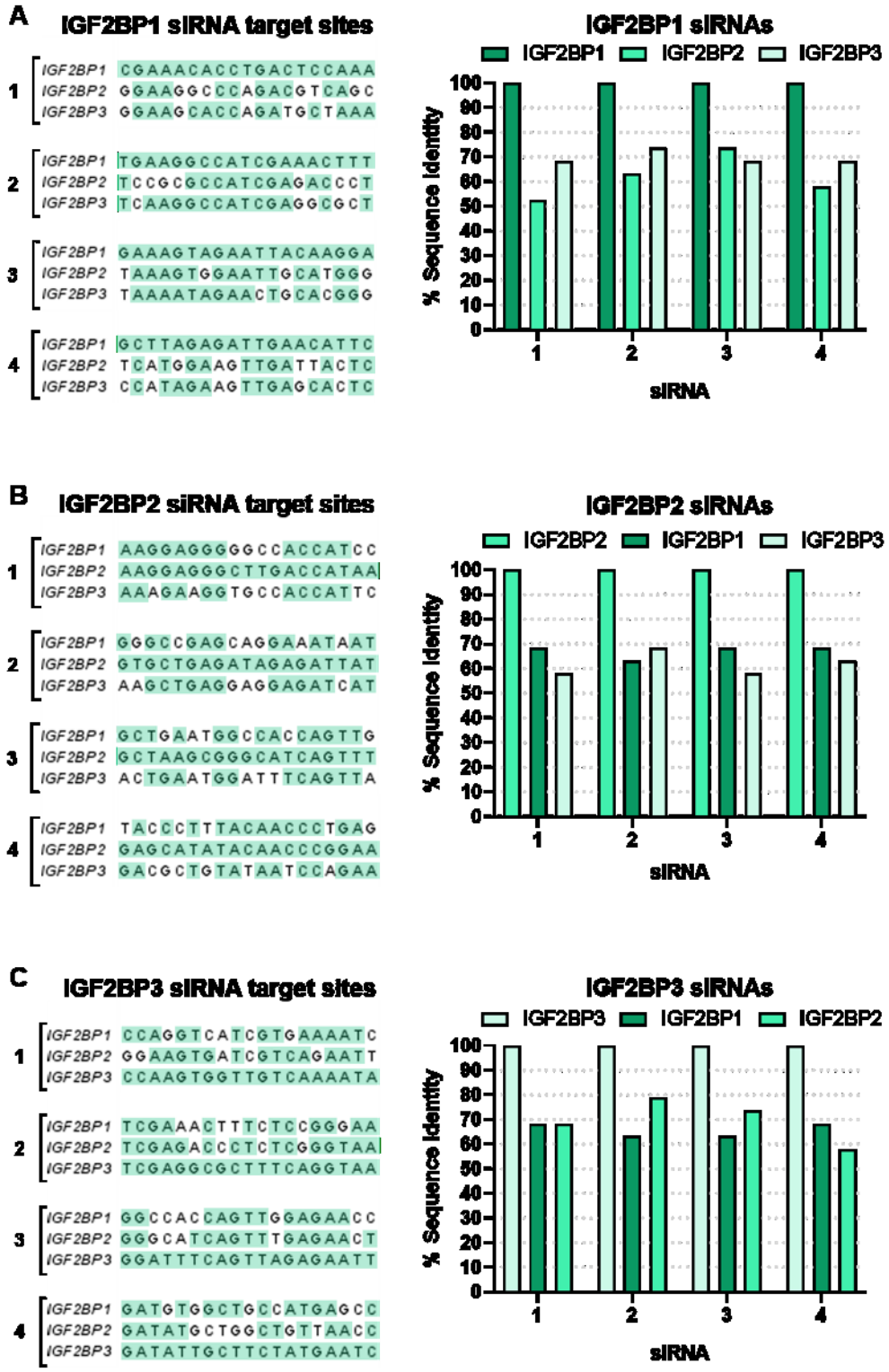

Figure 4.6 Alignment of siRNA target sites. *The canonical cDNA sequences of the three IGF2BP genes were aligned using Clustal Omega. The target sites of each of the four siRNA sequences from the SMARTpools for IGF2BP1 (**A**), IGF2BP2 (**B**) and IGF2BP3 (**C**) are shown. Nucleotides matching the target sequence are highlighted (left). siRNA sequences in each*

pool were arbitrarily assigned a number 1-4 which corresponds to graphs showing percentage sequence identity to the siRNA target sequences for each gene, calculated using an online tool from bioinformatics.org (right).

As further investigation of the possibility of off target knockdown within the IGF2BP family, the cDNA sequences of each gene were aligned and examined for sequence identity with the siRNA targets. When examining the sequences of IFG2BP1-targeting siRNA, all four were found to share 100% identity with sites in the target gene (**Figure 4.6A**). The same sites in the *IGF2BP2* cDNA sequence showed between 52 and 74% identity with *IGF2BP1*, and an average of 62% identity. In the *IFG2BP3* gene, the target sites shared an average of 70% identity with *IGF2BP1*. None of the siRNA sequences matched either *IGF2BP2* or *IGF2BP3* mRNA sequences to a degree that would suggest substantial off target binding would be likely.

The IFG2BP2-targeting siRNA sequences also matched the target gene with 100% identity (**Figure 4.6B**). The mean identity at these points was 67% with *IGF2BP1* and 62% with *IGF2BP3*. Further, neither gene shared more than 68% identity at any site with the target. Again, these data did not suggest that any of these siRNA sequences was likely to bind to the wrong gene.

Finally, the target sites for the IGF2BP3-targeting siRNA were examined. As with the other two genes, the target sites in the *IGF2BP3* gene shared 100% identity with the siRNAs targeting it (**Figure 4.6C**). *IGF2BP1*, the more closely related gene, showed between 63 and 68% identity with the target gene at these sites. In the case of *IGF2BP2*, three of the four sites showed similar identity to *IGF2BP3* as had been seen with the other genes and target sites. The second site shared 79% identity with *IGF2BP3*, with only four nucleotide mismatches. Neither *IGF2BP1* nor *IGF2BP2* showed enough similarity to the target gene to strongly suggest the potential off target binding and knockdown. The siRNA sequence most likely to bind off target was the

second IGF2BP3-targeting siRNA, which could possibly bind to *IGF2BP2* mRNA; however there was no suggestion of this in the western blot data (**Figure 4.5**). Overall, no off target binding of siRNA to the other genes in the family was predicted with any of the siRNA pools.

4.3.1.3. Examination of antibody cross-reactivity

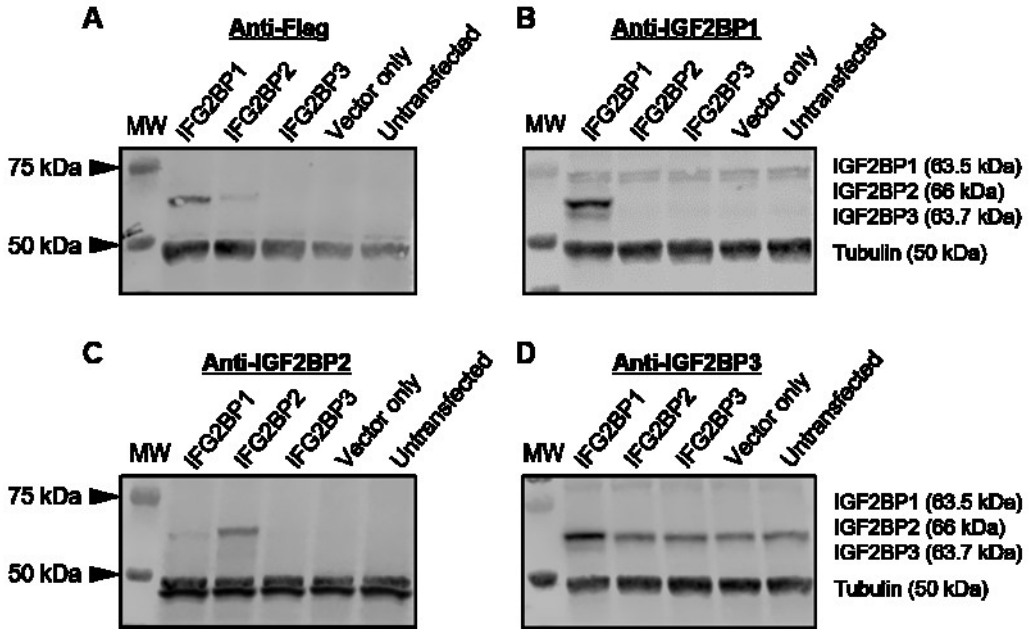

Figure 4.7 Examination of IGF2BP antibody cross reactivity with overexpressed Flag-tagged proteins. *BSR-T7 cells were transfected with plasmids containing Flag-tagged IGF2BP1, IGF2BP2, or IGF2BP3 genes under the control of a T7 RNA polymerase promotor, empty pMiniT plasmid (vector only), or left untransfected. After 24 hours, cells were lysed and cell lysates were analysed by western blot using anti-Flag (**A**), anti-IGF2BP1 (**B**), anti-IGF2BP2 (**C**), or anti-IGF2BP3 (**D**) antibody. Alpha tubulin was probed for as a loading control. MW indicates molecular weight markers.*

In order to examine potential cross-reactivity of the antibodies used that could have masked knockdown effects, overexpression plasmids encoding each of the *IGF2BP* genes were generated. Dr Nisha Kriplani cloned the cDNA sequence of each *IFG2BP* gene, along with an N-terminal Flag-tag (DYKDDDDK) into pMiniT plasmids oriented to be under the control of a T7 RNA polymerase promoter. The sequences of these plasmids were validated by diagnostic digests and Sanger sequencing (data not

shown). These plasmids were then transfected into BSR-T7 cells, a hamster kidney fibroblast cell line that stably expresses T7 RNA polymerase (Buchholz *et al.*, 1999). A vector only control was generated by transfecting cells with linear pMiniT plasmid lacking an insert. The lysates of these, as well as of untransfected cells, were analysed by western blot.

Firstly, the samples were probed with an anti-Flag antibody and an alpha tubulin loading control. Tubulin staining indicated slightly reduced lysate recovery in the vector only and untransfected samples (**Figure 4.7A**); subsequent loading of the samples was adjusted to account for this. Probing with the anti-Flag antibody gave no signal in either of the vector only or untransfected controls. Cells that had been transfected with Flag-IGF2BP1 overexpression plasmid showed strong staining of a single band at approximately 63.5 kDa, indicating successful overexpression of IGF2BP1. Anti-Flag staining in cells transfected with the Flag-IGF2BP2 overexpression plasmid was weaker, with a band migrating slightly more slowly than the smaller IGF2BP1 protein, suggesting that the cells were expressing Flag-IGF2BP2, but at a lower level. No Flag signal was detected in the cells transfected with the Flag-IGF2BP3 overexpression plasmid. Multiple unsuccessful attempts were made to express Flag-IGF2BP3 using this plasmid, and other plasmid backbones (data not shown), which suggested an undetected issue with the synthetic DNA sequence that could not be determined within this study.

Another western blot of the same samples was probed with anti-IGF2BP1 antibody. The tubulin loading control of this blot indicated that the samples were loaded equally (**Figure 4.7B**). In cells that had been transfected with the Flag-IGF2BP1 overexpression plasmid, anti-IGF2BP1 staining gave a double band, as seen previously with this antibody (**Figure 4.2A** and **Figure 4.5**, left). Both bands were absent in all other samples (**Figure 4.7B**), however, as Flag-IGF2BP2 expression was

very weak this could not rule out cross reactivity of the antibody. Furthermore, Flag-IGF2BP3 expression was not achieved, so off target binding to this protein could not be examined here.

Parenthetically, with anti-Flag staining, only the primary IGF2BP1 band was detected in cells that had been transfected with the Flag-IGF2BP1 overexpression plasmid, and not the additional, lower molecular weight band detected with the anti-IGF2BP1 antibody. The lower molecular weight band, was not seen in the absence of the IGF2BP1 overexpression plasmid, which suggested that this band did not represent nonspecific binding of the anti-IGF2BP1 antibody. It could represent an isoform lacking the N-terminus of the protein and thus the Flag tag, although no IGF2BP1 isoform of this molecular weight has been described to date.

Next, the samples were examined with anti-IGF2BP2 antibody on a separate western blot. In all samples, this reacted with a polypeptide migrating at around 45 kDa, just faster than the tubulin band (**Figure 4.7C**). This was uniform across all conditions and was likely due to off target antibody binding to a golden hamster protein. At the expected molecular weight of IGF2BP2, no signal was detected from the control cells or the cells that had been transfected with Flag-IGF2BP3 overexpression plasmid. As the Flag-IGF2BP3 plasmid had failed to express the protein, no data on the cross-reactivity of the anti-IGF2BP2 antibody with IGF2BP3 protein could be gathered here. In cells that had been transfected with the Flag-IGF2BP2 plasmid, strong signal was detected at approximately 66 kDa at much greater intensity than the corresponding band detected with anti-Flag antibody. No signal was detected at 60 kDa, suggesting that the smaller isoform was not translated from the plasmid in these cells. A faint signal was detected from cells transfected with Flag-IGF2BP1 overexpression plasmid, indicating some cross-reactivity of this antibody with IGF2BP1. As the two IGF2BP polypeptides are so similar in size, it would not be possible to resolve them

in the same sample by standard SDS-PAGE. Therefore the binding of IGF2BP1 by anti-IGF2BP2 may have obscured the detection of IGF2BP2 knockdown.

Lastly, the cell lysates, on another western blot, were probed with anti-IGF2BP3. In the untransfected and vector only cells, a band was detected at the expected molecular weight (**Figure 4.7D**), which likely represented the hamster IGF2BP3 orthologue. This band was also detected, at the same intensity, in the cells transfected with the Flag-IGF2BP3 expression plasmid which had not detectably expressed the Flag antigen. Cells that had been transfected with the Flag-IGF2BP2 plasmid also showed comparable signal to both control groups, suggesting that the anti-IGF2BP3 antibody did not cross-react with IGF2BP2; however the expression level of IGF2BP2 was low in these cells and cross-reactivity might have been detected if greater expression had been achieved. The anti-IGF2BP3 signal was greatly increased in the cells transfected with Flag-IGF2BP1 overexpression plasmid. Further, the second, lower molecular weight band, seen with anti-IGF2BP1 antibody, was also detected here. This demonstrated strong cross-reactivity of the anti-IGF2BP3 antibody with IGF2BP1 which would inhibit the detection of IGF2BP3 knockdown by western blot.

In summary, both the anti-IGF2BP2 and anti-IGF2BP3 antibodies were found to cross-react with IGF2BP1, which meant that western blot with these antibodies could not be used to accurately measure knockdown of the target proteins. Poor and failed overexpression of IGF2BP2 and IGF2BP3, respectively, meant that the cross-reactivity of the anti-IGF2BP1 antibody could not be fully examined here. Instead the sequences of the antibody binding sites were considered.

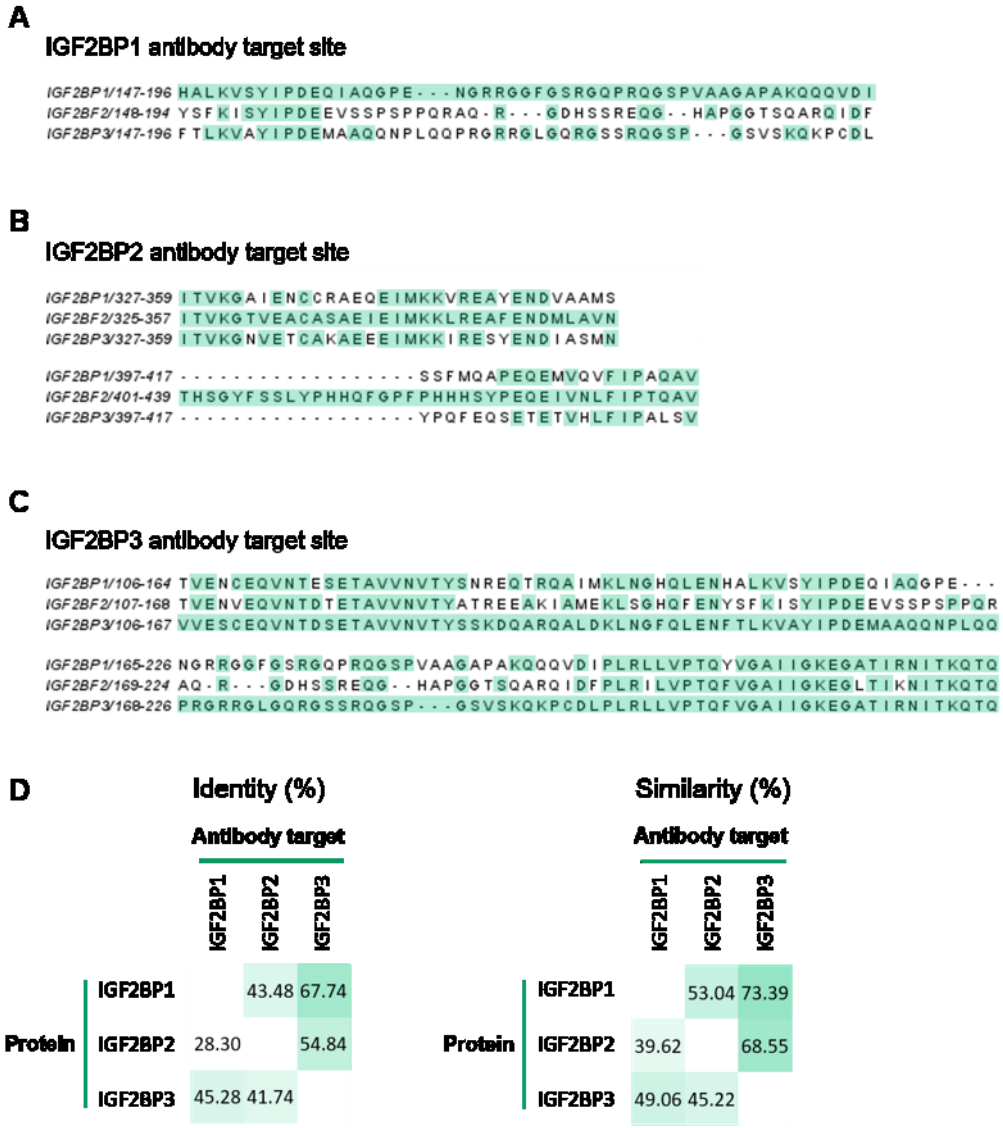

Figure 4.8 Analysis of antibody target sites. *The amino acid sequences of IGF2BP1, IGF2BP2 and IGF2BP3 were aligned using Clustal Omega. The alignment at sites corresponding to the antigen sequences used to generate anti-IGF2BP1 (**A**), anti-IGF2BP2 (**B**), and anti-IGF2BP3 (**C**) antibodies are shown. Amino acids matching the antigen sequence are highlighted. The antigen sequence for the IGF2BP2 antibody (**B**) was given as corresponding to two sites in the protein separated by 44 amino acids, the intermediate sequence is omitted here. Identity and similarity between the proteins at these sites were calculated using an online tool from bioinformatics.org and presented in heat maps (**D**). Darker green indicates greater percentage identity or similarity to the antigen sequence.*

Due to poor overexpression of IGF2BP2 and IGF2BP3, cross-reactivity of antibodies with these proteins could not be properly evaluated. Therefore the antibody target

sites (as given in the datasheets of each anti-serum) of all three IGF2BPs were compared in order to predict the likelihood of off target binding within the family. The amino acid sequences of the three proteins were aligned using Clustal Omega, and the antigen sequences used to generate the polyclonal rabbit antibodies were identified. **Figure 4.8A**, **B** and **C** show the alignments at each of these sites with the residues matching the antigen sequences highlighted in green. The identity and similarity between the proteins at these sites was calculated and presented as heat maps in **Figure 4.8D**. The 100% identity and similarity with their own antibody target sequence was omitted from the heat maps.

IGF2BP1 protein was found to have 43.48% identity with the IGF2BP2 antigen sequence and 53.04% similarity (**Figure 4.8D**). It is stated that 75-85% homology with an immunogenic sequence indicates a high likelihood of cross-reactivity (Abcam, 2021; Proteintech, 2020); however the anti-IGF2BP2 antibody bound to IGF2BP1 (**Figure 4.7**) despite having this lower level of similarity. The identity and similarity of IGF2BP1 to the IGF2BP3 antigen sequence was greater, 67.74% and 73.39% respectively (**Figure 4.8D**), which correlated with the higher cross-reactivity of the anti-IGF2BP3 antibody with IGF2BP1 than the anti-IGF2BP2 antibody (**Figure 4.7**).

The identity and similarity between IGF2BP2 and the IGF2BP1 immunogenic sequences were much lower, at 28.30% and 39.62% respectively (**Figure 4.8D**). No cross-reactivity of anti-IGF2BP1 antibody with the poorly overexpressed IGF2BP2 was detected (**Figure 4.7**). These alignment data suggest that, even with greater levels of IGF2BP2 expression, cross-reactivity would be unlikely. Conversely, high levels of identity (54.84%) and similarity (68.55%) were found between IGF2BP2 and the IGF2BP3 antibody binding site (**Figure 4.8D**). This homology was greater than that seen between IGF2BP1 and the IGF2BP2 antigen sequence, which lead to observable cross-reactivity. This suggested that cross-reactivity of anti-IGF2BP3

antibody with IGF2BP2 protein was probable and might have been detected via western blot if greater IGF2BP2 overexpression had been achieved.

Overexpression of Flag-IGF2BP3 was not achieved in previous experiments (**Figure 4.7**) which meant that cross-reactivity of anti-IGF2BP1 and anti-IGF2BP2 antibodies with IGF2BP3 could not be assessed. The likelihood of off target binding was instead considered using the homology between IGF2BP3 and the antigen sequences used to generate these antibodies. At the IGF2BP1 antibody target site, IGF2BP3 was found to have 45.28% identity with the immunogenic sequence (**Figure 4.8D**), which was greater than that seen to cause cross-reactivity of the anti-IGF2BP2 antibody with IGF2BP1 protein. This suggested that anti-IGF2BP1 antibody could bind to IGF2BP3 protein. Both the identity and similarity between IGF2BP3 and the IGF2BP2 antigen sequence were lower than any that had been seen to cause cross-reactivity here, which suggested that anti-IGF2BP2 antibody was less likely to bind to IGF2BP3.

Overall, while the anti-IGF2BP1 anti-sera does not show cross-reactivity with IGF2BP2, the homology data presented here suggested that off target binding of IGF2BP3 was likely. This could have disguised the efficacy of IGF2BP1-targeting siRNA, although high knockdown efficiency was detected. The anti-IGF2BP2 anti-sera moderately cross-reacted with IGF2BP1, however off target binding to IGF2BP3 was predicted using the alignment data to be less likely and weaker. Anti-IGF2BP3 anti-sera was found to be highly cross-reactive with IGF2BP1 and homology data suggested that it was also likely to bind IGF2BP2. Antibody cross-reactivity, likely obscured the extent of knockdown achieved with both IGF2BP2- or IGF2BP3-targeting siRNA. Due to the difficulties developing knockdown protocols for IGF2BP2 and IGF2BP3, it was decided to focus on investigating the role of IGF2BP1 in IAV infection going forward.

4.3.2. Infection of IGF2BP1 knockdown cells with IAV

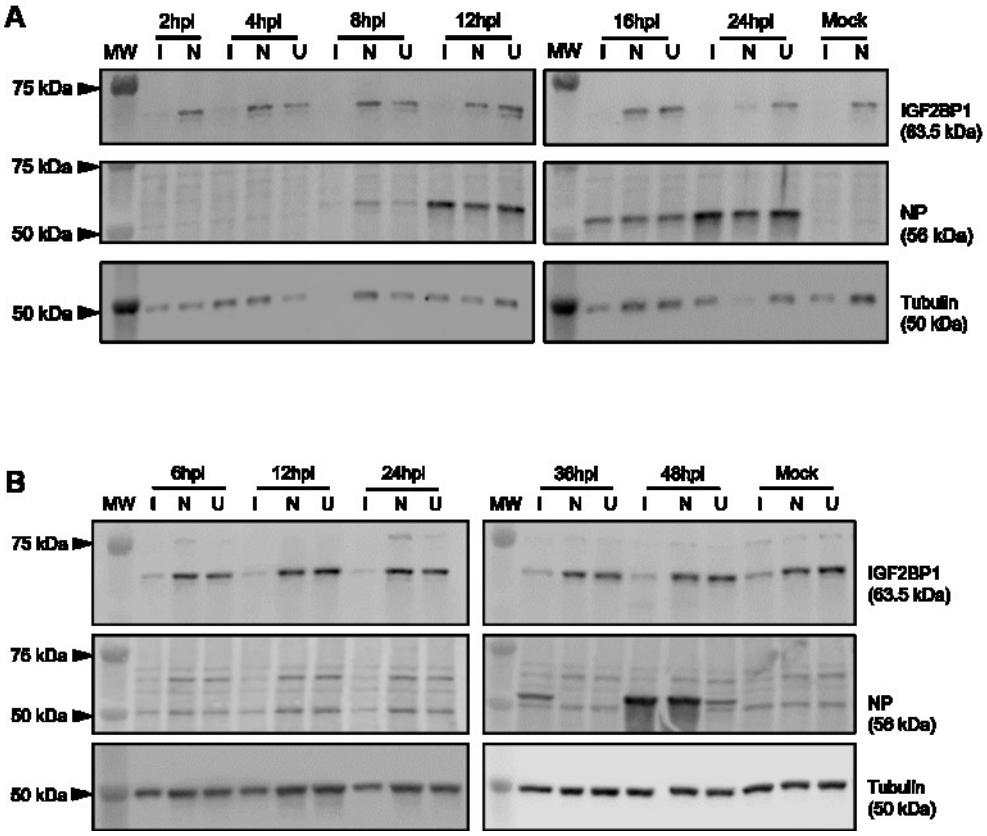

Figure 4.9 Viral protein levels in infected IGF2BP1 knockdown. *A549 cells were transfected with IGF2BP1-targeting (I) or non-targeting (N) siRNA or left untransfected (U) and incubated for 48 hours. Cells were infected with PR8 and cell lysates were harvested at various time points (hpi: hours post infection). Mock infected cells were incubated for 24 hours in virus free media. Lysates were examined by western blot for cellular IGF2BP1, viral NP and an alpha tubulin loading control. MW indicates molecular weight markers.* ***A:*** *Western blots of a single representative experiment in which cells were infected with PR8 at MOI 5.* ***B:*** *Western blot images from a single representative experiment in which cells were infected with PR8 at MOI 0.01.*

With the aim of investigating the effect of IGF2BP1 knockdown on IAV replication, A549 cells were transfected with 30 nM IGF2BP1-targeting (I) or non-targeting (N) siRNA or left untransfected 48 hours prior to infection with PR8. Cells were infected at either MOI 5 or 0.01 and cell lysates were harvested at various time points to be analysed by western blot for IGF2BP1, viral NP, and an alpha tubulin loading control.

First, the lysates of cells infected at MOI 5 were analysed. Probing for the alpha tubulin loading control showed variable lysate recovery between samples including one sample with no tubulin detected (**Figure 4.9A**). Low lysate recovery was not specific to a time point or siRNA treatment. The absence of protein in the sample harvested at 8 hours post infection was likely due to error in the wash step of sample harvest. Probing the same western blot with anti-IGF2BP1 anti-sera showed the expected staining of a band at 63.5 kDa and a smaller, lower molecular weight band in all untransfected cells and cells transfected with non-targeting siRNA. In cells that had been treated with IGF2BP1-targeting siRNA, this band was either absent or present at a much lower level, confirming successful knockdown. The western blot was then probed for NP in order to assess viral protein production. No NP was detected in mock infected cells, or in infected cells at 2 or 4 hours post infection. NP was first detected above background at 8 hours post infection in the untransfected cells and in cells transfected with non-targeting siRNA. NP expression at this time in the cells transfected with IFG2BP1-targeting siRNA could not be determined due to poor sample recovery. At 12 hours post infection, NP was detected at higher levels in the both control cell samples and was also seen in cells treated with IGF2BP1-targeting siRNA. Relative to tubulin, expression of the viral protein at this time point was comparable between all conditions. NP was expressed at a similar level at 16 hours post infection, and was consistent regardless of IGF2BP1 expression. The highest levels of NP were seen at 24 hours post infection. Again, expression of the viral protein in untransfected cells and in cells transfected with non-targeting siRNA was similar to that seen in IGF2BP1 knockdown cells. This data suggested that knockdown of IGF2BP1 did not affect the production of viral protein.

When examining the lysates of cells infected at MOI 0.01, tubulin staining showed more consistent lysate recovery across all samples (**Figure 4.9B**). Staining with anti-

IGF2BP1 showed the band at 63.5 kDa was expressed highly in all untransfected cells and cells transfected with non-targeting siRNA. The lower molecular weight band was present in these cells but the signal was weaker here than had been seen previously. Cells that had been transfected with IGF2BP1-targeting siRNA showed greatly reduced IGF2BP1 protein expression at every time point, and average knockdown efficiency for this experiment was calculated to be approximately 85%. At this MOI, NP protein was not detected above background until 36 hours post infection, when it was seen in IGF2BP1 knockdown cells but not in either of the control cells. This earlier expression of NP was not reproducible across repeats (data not shown). At 48 hours post infection, NP was detected in all conditions but expression of the protein was lower in untransfected cells than in cells treated with either siRNA. However, IGF2BP1 knockdown did not alter NP levels compared to treatment with non-targeting siRNA.

Together, these data did not suggest that IGF2BP1 knockdown either inhibited or enhanced expression of viral NP.

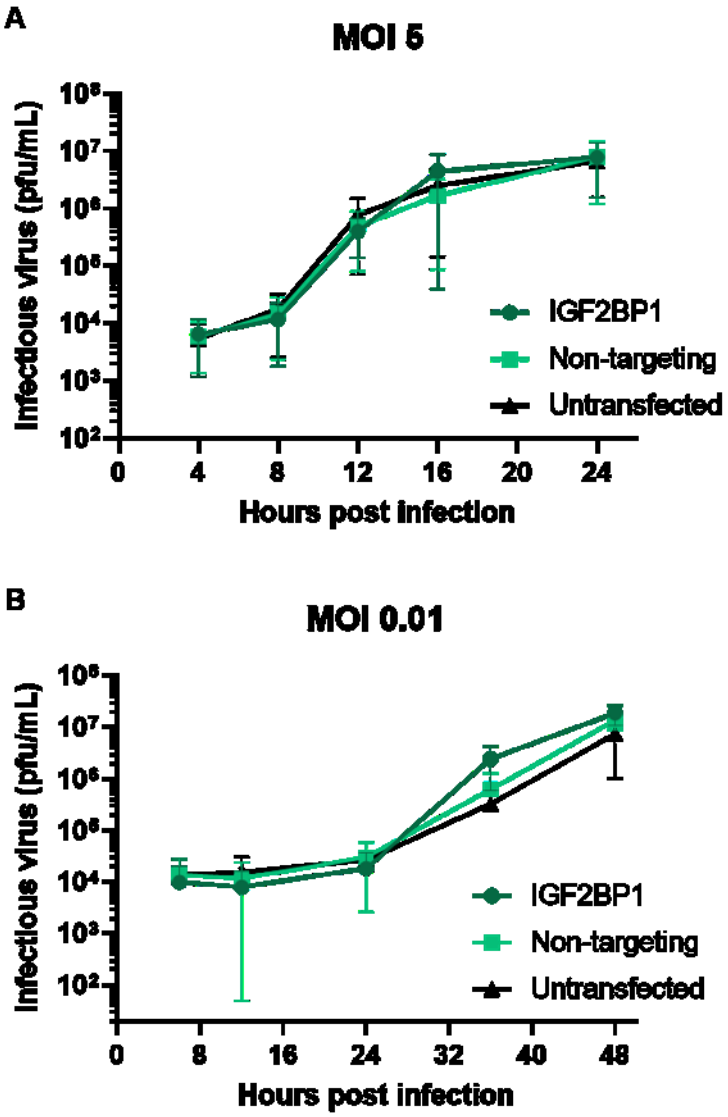

Figure 4.10 IAV replication in IGF2BP1 knockdown cells. *A549 cells were transfected with either IGF2BP1-targeting (IGF2BP1) or non-targeting siRNA or left untransfected. After 48 hours, cells were infected with PR8. Cell supernatants were harvested at various time points and analysed by plaque assay on MDCK cells.* ***A:*** *Virus titres from cells infected at MOI 5.* ***B:*** *Virus titres from cells infected at MOI 0.01. Points represent the mean of two biological replicates, error bars represent standard deviation. Data were analysed by two-way ANOVA with Tukey's multiple comparison test using GraphPad Prism 8.*

IAV replication in IGF2BP1 knockdown cells was also assessed using plaque assay of cell supernatants, harvested from the infection experiments described above, to measure infectious virus production. With infection at MOI 5, cells transfected with either siRNA showed comparable viral titres and the same infection kinetics as

untransfected cells (**Figure 4.10A**), suggesting that IGF2BP1 knockdown did not affect the replication of PR8. Similarly, IGF2BP1 knockdown cells infected at MOI 0.01 produced viral titres at the same level as both IGF2BP1 expressing control groups up to 24 hours post infection (**Figure 4.10B**). At 36 hours post infection, viral levels measured from cells transfected with non-targeting siRNA were marginally, but not significantly, higher than those from untransfected cells (p=0.9972). IGF2BP1 knockdown cells at this time showed mean titres that were almost an order of magnitude greater than untransfected cells, although this was not statistically significant (p=0.8685). At 48 hours post infection, titres from IGF2BP1 knockdown cells were still higher than those from untransfected cells, although to a lesser extent and again, this was not statistically significant (p=0.3670). Further, the titres measured from cells transfected with non-targeting siRNA were comparable to those from knockout cells at this time point.

Overall, these data did not suggest that knockdown of IGF2BP1 inhibited the replication or spread of IAV in A549 cells. Infection at low MOI showed a potential proviral effect of knockdown at 36 hours post infection, which correlated with the earlier detection of NP seen in these cells (**Figure 4.9B**). However, in both cases, this was not consistent between biological repeats so was not found to be a real effect. This does not support the hypothesis that IGF2BP1 is involved in IAV infection.

4.3.3. Pharmaceutical inhibition of IGF2BP1 and IAV infection

IGF2BP proteins, IGF2BP1 in particular, have been found to bind to and stabilise the mRNA of many oncogenic genes and so make an attractive target for pharmaceutical inhibition in the treatment of many cancers. For this reason, in 2017, a small molecule screen was carried out to find inhibitors of IGF2BP1 (Mahapatra *et al.*, 2017). The compound 2-[[(5-bromo-2-thienyl)methylene]amino]-benzamide (BTYNB) was identified and found to selectively inhibit the binding of IGF2BP1 to *c-Myc* mRNA, as

well as the mRNA of several other oncogenes and genes associated with tumour cell proliferation and migration (Mahapatra *et al.*, 2017; Müller *et al.*, 2020). The mechanism by which BTYNB inhibits IGF2BP1-mRNA binding and specificity within the IGF2BP family has not been described.

In this study, BTYNB was used to further investigate any potential role of IGF2BP1 in the IAV lifecycle. The compound was acquired from Cayman Chemical Company and various infection experiments were carried out. Later, shortly before I finished experimental work for this thesis, testing by Cayman Chemical Company found that the compound in the batch I had received had the incorrect structure and was not BTYNB. A replacement confirmed to contain the correct BTYNB compound was acquired and tested. Due to the volume of work performed using the incorrect compound, the data gathered is presented here. The compound is referred to as “BTYNB”. The concentrations used were based on the molar mass of BTYNB, as the actual molecular structure of the compound are unknown, these are not accurate but indicate relative concentrations within experiments.

4.3.3.1. Incorrect compound

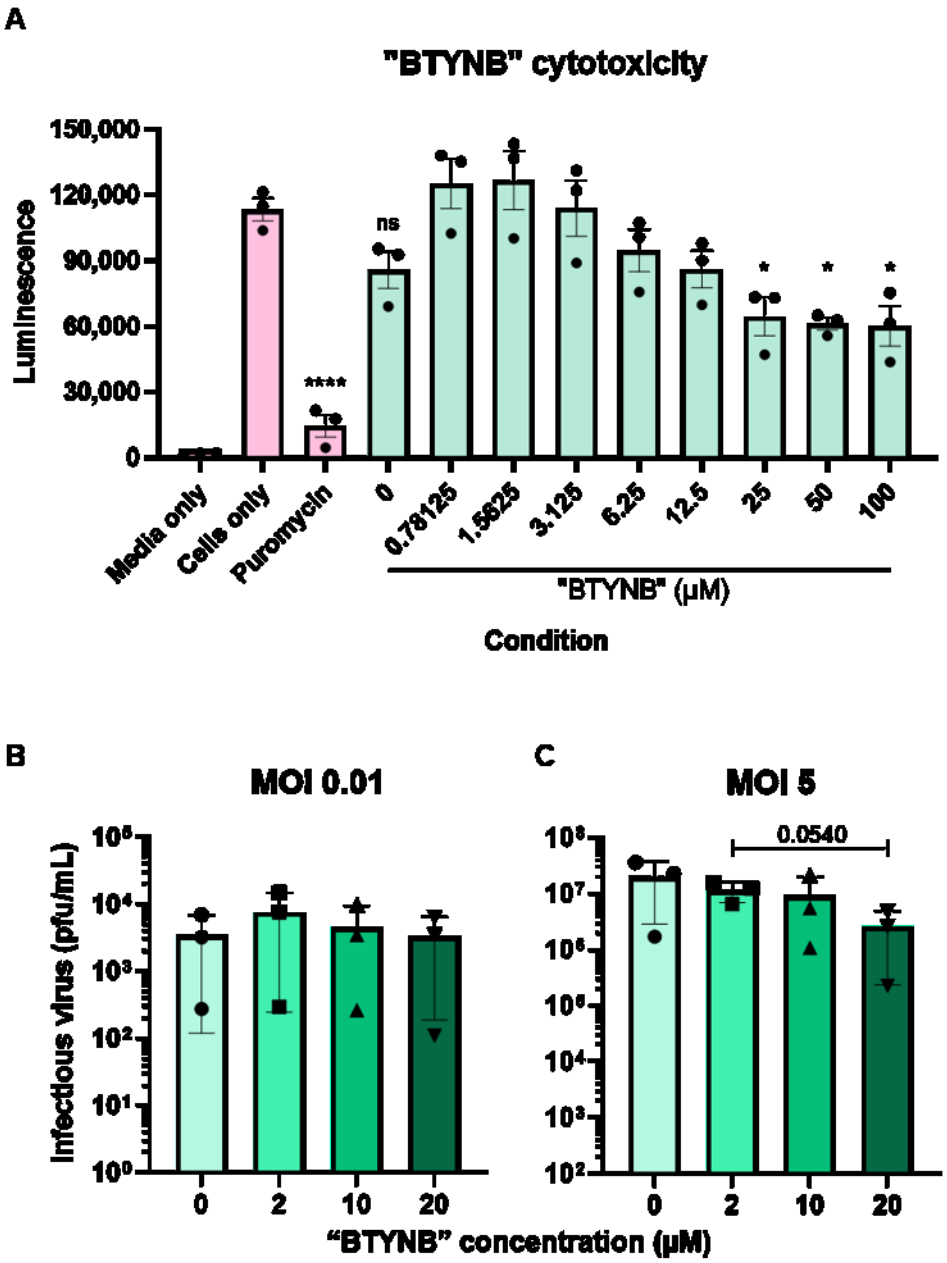

Figure 4.11 "BTYNB" cytotoxicity and effect on IAV titre. A: *A549 cells were incubated with at a range of concentrations of "BTYNB", DMSO vector only (0 μM "BTYNB"), 50 μg/μL puromycin, or left untreated (cells only) for 24 hours. Cell lysates were analysed using a CellTiter-Glo viability assay. Background luminescence was established by incubating cell-free media with the CellTiter-Glo reagent (media only). Points represent the mean of technical duplicates; bars represent the mean of three biological replicates; and error bars represent standard error of the mean. Data were analysed by one-way ANOVA with Tukey's multiple comparison tests using GraphPad Prism 8. Significance markers refer to comparison with cells*

*only. ****: p≤0.0001; *: p≤0.05.* ***B and C:*** *A549 cells were infected with PR8 at either MOI 5 (**B**) or MOI 0.01 (**C**), 1 hour post infection, cells were overlaid with media containing 2, 10, or 20 μM "BTYNB" or DMSO only (0 μM). Cell supernatants were harvested at 16 hours post infection and analysed by plaque assay on MDCK cells. Bars represent the mean of three biological replicates, error bars represent standard deviation. Data were analysed by one-way ANOVA with Tukey's multiple comparison tests using GraphPad Prism 8.*

In order to ascertain an appropriate range of drug concentrations to use, cytotoxicity of the compound was examined using a CellTiter-Glo assay. A two-fold dilution series of "BTYNB" in DMSO was set up and A549 cells were incubated with the drug or DMSO only (0 μM "BTYNB") for 24 hours. The lysates of these cells, as well as of untreated cells (cells only) and cells treated with puromycin, were incubated with CellTiter-Glo reagent. The luminescence signal produced was proportional to the metabolic activity, and therefore viability, of the cells. Background luminescence was determined using cell free media (media only) incubated with the CellTiter-Glo reagent. The luminescence data from the media only, cells only and puromycin controls presented here (**Figure 4.11A**) were also shown in **Figure 3.8** in relation to Baloxavir cytotoxicity, as the two compounds were tested concurrently using the same control conditions.

Luminescence measured from untreated cells (cells only) established the assay readout with normal levels of cell viability. Cells that had been treated with puromycin showed an 87% reduction in luminescence compared to cells only (**Figure 4.11A**; $p<0.0001$), demonstrating high levels of cytotoxicity. The mean luminescence measured from cells that had been treated with DMSO only (0 μM "BTYNB") was 25% lower than that from untreated cells, however this reduction was not statistically significant ($p=0.5501$). Cells that had been treated with the two lowest concentrations of drug, 0.78 and 1.56 μM, showed mean luminescence that was marginally higher than that from cells only, and treatment with 3.13 μM "BTYNB" gave signal at similar levels to untreated cells. The viability of cells treated with 6.25 μM of the drug was

slightly, but not significantly reduced compared to cells only (p=0.9229). Further reduction was seen with 12.5 μM “BTYNB”, however this was also not found to be significantly different from cells only (p=0.5638) and was equivalent to the luminescence measured from cells treated with DMSO only. Significant loss of cell viability was seen with 25 μM “BTYNB” as luminescence measured from these cells was approximately 45% of that seen in cells only (p=0.0243). Similar levels of cytotoxicity were observed at 50 and 100 μM “BTYNB”, with no significant decrease in viability seen between these three highest concentrations. However the luminescence measured from these cells was not found to be significantly lower than that from cells treated with DMSO only (p>0.65 for all three concentrations).

Overall, these data show a trend of increased cytotoxicity with increased concentration of this compound, although at lower concentrations cell viability was not reduced significantly. BTYNB had been previously shown to inhibit the interaction of IGF2BP1 with oncogenic mRNAs at 10 μM (Mahapatra *et al.*, 2017). Based on this and the cytotoxicity data, 10 μM was deemed an appropriate concentration for initial tests with IAV infection. Concentrations that were substantially higher (20 μM) and lower (2 μM) were also tested in order to detect any dose dependent effects of the drug.

Accordingly, infections were carried out in which A549 cells were infected with PR8 at MOI 5 and 0.01 and overlaid 1 hour post infection with media containing DMSO only or the chosen concentrations of “BTYNB”. Supernatants were harvested 16 hours post infection and analysed by plaque assay. In cells that had been treated with DMSO only and infected at MOI 0.01, the mean titre measured was approximately $3.5x10^3$ pfu/mL (**Figure 4.11C**). In comparison, twice as much infectious virus was seen in cells treated with 2 μM “BTYNB”, although this difference was not statistically significant (p=0.7475). There appeared to be a slight reduction in mean virus titre from

cells that had been treated with 10 μM “BYTNB”, and another reduction with 20 μM “BTYNB”. However, virus titres from both of these conditions were comparable to those from DMSO only and the 2 μM “BTYNB” treatments. Altogether, the differences in titre seen between “BTYNB” treatment concentrations were minimal and none were statistically significant. These data did not suggest that the protein was involved with IAV replication or spread.

Cells that had been infected at MOI 5 and overlaid with media containing DMSO showed average titres after 16 hours of approximately $2x10^7$ pfu/mL (**Figure 4.11B**). Virus titres measured from cells treated with 2 μM “BTYNB” were marginally lower, however this was not statistically significant (p=0.7454). With 10 μM BTYNB, titres were reduced further, and infectious virus produced by cells treated with 20 μM was almost an order of magnitude lower than that from cells treated with DMSO only. Compared to the 0 μM titres, neither of these differences were statistically significant (p=0.3800 and p=0.4405 respectively), but the difference in titres produced following treatment with 2 and 20 μM “BTYNB” approached significance (p=0.0540). There was likely a slight loss of cell viability at this concentration of the drug compared to 0 μM, however this seemed unlikely to account for the level of titre reduction. Therefore the compound may have had some minor antiviral effects at the higher concentration. At the point in the project when the compound was still thought to be the IGF2BP1 inhibitor, this was taken to support a potential non-essential or redundant role of the protein in IAV infection.

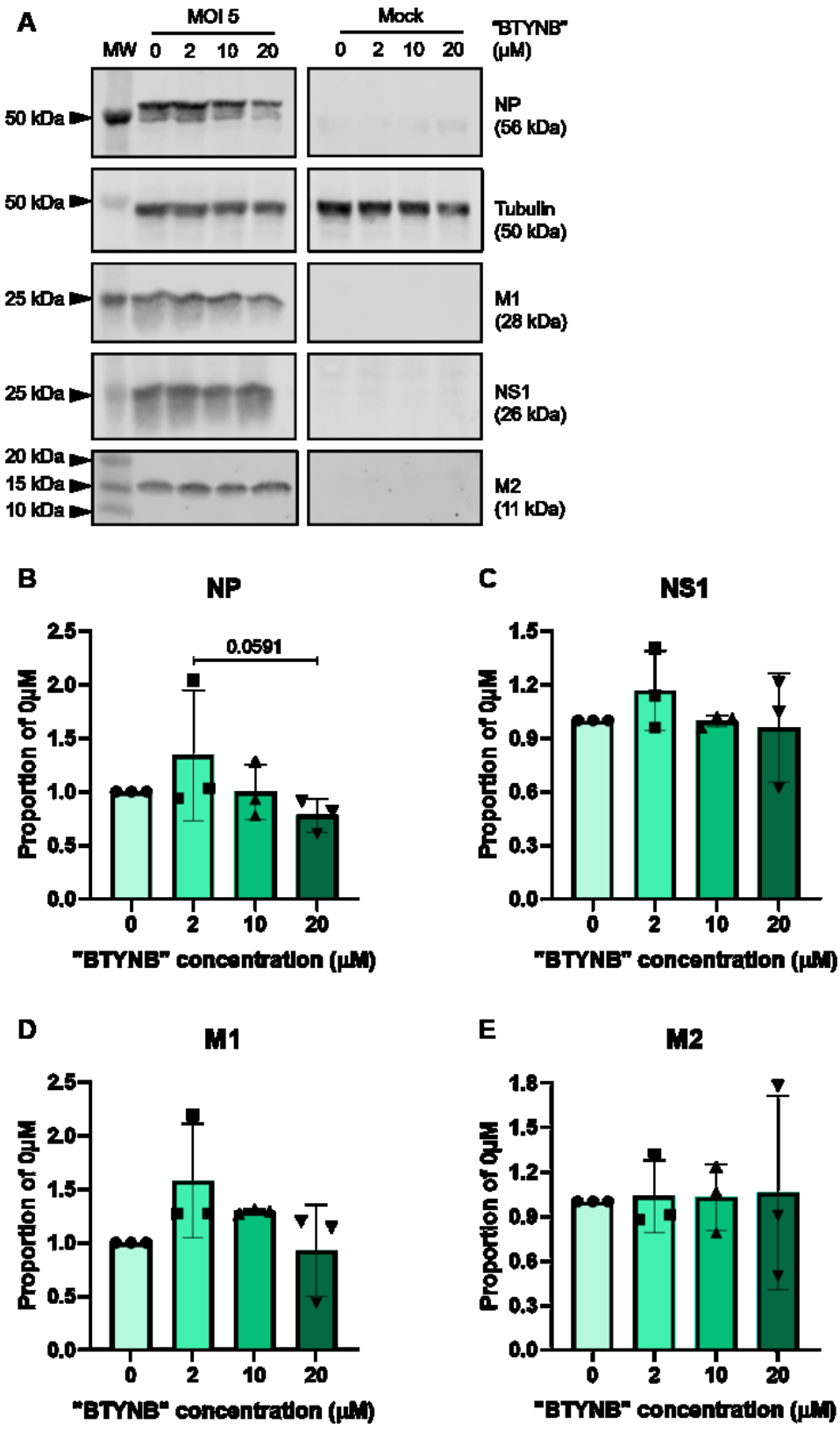

Figure 4.12 Viral protein levels in cells treated with "BTYNB". *A549 cells were infected with PR8 at MOI 5. One hour post infection, cells were overlaid with media containing 2, 10,*

or 20 μM "BTYNB" or DMSO only (0 μM). Cell lysates were harvested at 16 hours post infection and analysed by western blot for the indicated viral proteins and alpha tubulin loading controls. Mock infected cells were incubated with the drug in virus free media for 16 hours. ***A:*** *Western blots of a single representative experiment. The alpha tubulin blot shows the loading control from simultaneous staining with NP and M1 and is representative of the loading controls for NS1 and M2 which were probed for on a separate membrane. MW indicates molecular weight markers. Protein expression was measured from replicate experiments using LI-COR Image Studio software. Levels of NP (**B**), NS1 (**C**), M1 (**D**) and M2 (**E**) were normalised to alpha tubulin in the same sample and expressed as a proportion of protein detected in cells treated with 0 μM "BTYNB". Bars represent the mean of three biological repeats, error bars represent standard deviation. Quantification data were analysed by one-way ANOVA with Tukey's multiple comparison test using GraphPad Prism 8.*

The virus titres produced in cells infected at MOI 5 appeared to be slightly reduced with "BTYNB" treatment (**Figure 4.11B**). In order to further scrutinise this trend, the cell lysates of the infected cells were analysed by western blot to measure the expression of viral proteins in the presence of "BYTNB". The western blots were probed with anti-alpha tubulin antibody which showed equal lysate recovery and loading across samples (**Figure 4.12A**). Staining with anti-NP anti-sera gave no signal above background in mock infected cells, and in cells infected at MOI 5, a band was observed at the expected size of 56 kDa. Slightly increased levels of NP were detected in infected cells treated with 2 μM "BTYNB". With 10 μM "BTYNB" treatment, NP was marginally reduced compared to cells treated with either 0 μM or 2 μM. Further reduction in NP expression was seen in cells that had been treated with 20 μM of the drug. The levels of viral protein were measured from three independent experiments, normalised to tubulin in the same sample and expressed as a proportion of the levels observed in cells treated with DMSO only. Mean NP levels were greater in cell treated with 2 μM "BTYNB" than with DMSO only (**Figure 4.12B**), although this was largely due to particularly high expression in one of the replicates. NP levels following treatment with 10 μM "BTYNB" were comparable to those seen with 0 μM ($p=0.9963$). Cells treated with 20 μM of the drug showed mean NP levels that were

approximately 24% lower than those in cells treated with DMSO, although this reduction, was not statistically significant (p=0.4697). Similarly to the titre data in these infections, the difference in mean NP levels between cells treated with 2 μM and 20 μM “BTYNB” was approaching significance (p=0.0591).

IGF2BP1 has been found to interact with NS1 protein (Pichlmair *et al.*, 2012; Rahim *et al.*, 2018), although the consequences of this interaction are unknown. In order to test for altered NS1 protein levels with IGF2BP1 inhibition, the same samples were probed with anti-NS1 anti-sera on a separate western blot. Again, no viral protein was detected in mock infected cells (**Figure 4.12A**). A band was seen at approximately 26 kDa, the molecular weight of NS1, in cells that had been treated with DMSO only. Slightly greater NS1 staining was seen in cells treated with 2 μM “BTYNB” than with 0 μM, however in cells treated with 10 μM of the compound, the viral protein was detected at lower levels. In cells treated with 20 μM “BTYNB”, NS1 levels were comparable to those from cells treated with 2 μM. Across biological repeats, mean levels of NS1 protein were slightly, although not significantly, higher in cells treated with 2 μM “BTYNB” (**Figure 4.12C**; p=0.9940). Cells treated with either 10 μM or 20 μM showed mean NS1 levels that were comparable to those in cells treated with DMSO only. This did not suggest any effect of “BTYNB” treatment on the expression of NS1 protein.

One of the functions of m^6A reader proteins binding to mRNA is the regulation of alternative splicing (Dominissini *et al.*, 2012), which has been shown for both IGF2BP2 (Zhao *et al.*, 2022) and IGF2BP3 (Xueqing *et al.*, 2020). In order to examine the effects of IGF2BP1 inhibition on the alternative splicing of an IAV gene, the expression of viral M1 and M2 proteins in the “BYTNB”-treated A549 cells was analysed. The western blot for NP was also stained with anti-M1 anti-sera, and M2 was probed for on the blot used to examine NS1 expression. No signal was seen in

mock infected cells for either protein (**Figure 4.12A**). In infected cells treated with 0 μM “BTYNB”, anti-M1 staining showed a band migrating at approximately 28 kDa. The same band was seen with slightly higher signal intensity in cells treated with either 2 or 10 μM “BTYNB”. However, expression of M1 detected in cells treated with 20 μM “BTYNB” was reduced compared to all other drug concentrations. Staining for M2 gave a band at approximately 15 kDa, slightly higher than the expected 11 kDa. This signal intensity of this band was higher in cells treated with 2 μM of the compound than with DMSO only. With 10 μM treatment, lower M2 levels were observed and the highest expression of the protein was seen in cells treated with 20 μM “BTYNB”. Mean expression of these two segment 7 proteins were examined across biological repeats. M1 protein levels were found to be higher in cells that had been treated with 2 μM “BTYNB” than in cells treated with DMSO only (**Figure 4.12D**), however this difference was not statistically significant ($p=0.4222$). With increased “BTYNB” concentrations, mean M1 levels decreased, and in cells treated with 20 μM of the compound, M1 was comparable to that in cells treated with DMSO and none of the differences in protein accumulation between conditions were statistically significant. Mean M2 levels were consistent across all “BTYNB” concentrations, although there was great variation between biological repeats (**Figure 4.12E**). As M1 protein levels decreased with “BTYNB” treatment but M2 levels did not, the ratio between the two proteins did change with increased drug concentration, but not significantly (data not shown; one-way ANOVA, $p=0.8145$). Therefore, as the compound used was thought to be the IGF2BP1 inhibitor, there was no indication here that IGF2BP1 bound to the mRNA of PR8 segment 7 to affect alternative splicing.

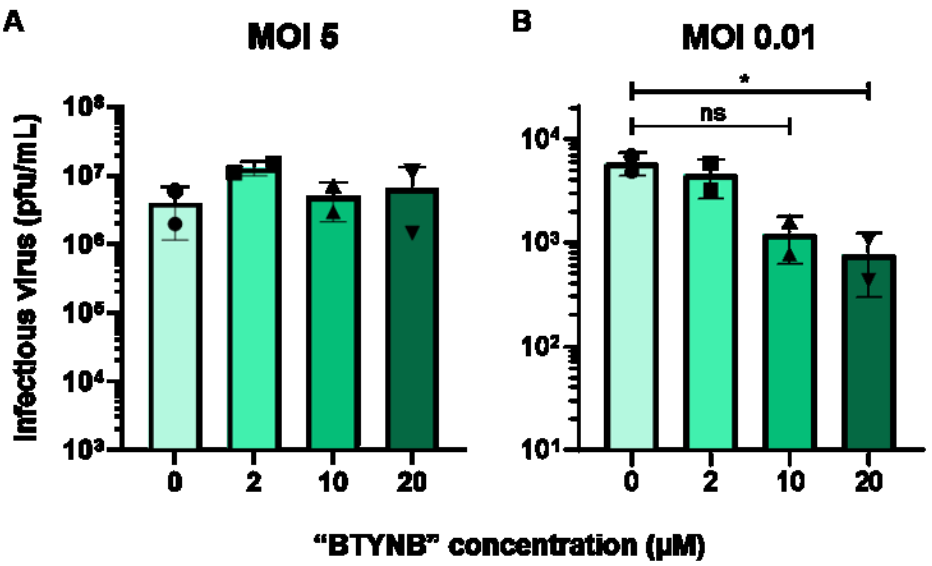

Figure 4.13 Infectious virus production in cells pre-treated with "BTYNB". *A549 cells were incubated with "BTYNB" or DMSO vector only (0 μM "BTYNB") for 24 hours prior to infection with PR8 at either MOI 5 (**A**) or 0.01 (**B**). At 16 hours, post infection, cell supernatants were harvested and analysed by plaque assay on MDCK cells. Bars represent the mean of two biological repeats, error bars represent standard deviation. Data were analysed by one-way ANOVA with Tukey's multiple comparison test using GraphPad Prism 8. Ns: not significant, p≥0.05; *: p≤0.05.*

The apparent inhibition of IGF2BP1 had no obvious direct effect on IAV replication, but I considered whether indirect effects through its altering of normal cellular processes were possible. Accordingly, the effect of "BTYNB" on IAV replication was further scrutinised using infection experiments in which A549 cells were pre-treated with drug 24 hours prior to infection in order to allow any effects of IGF2BP1 inhibition to take hold. The supernatants of cells infected at MOI 5 or 0.01 were harvested at 16 hours post infection and analysed by plaque assay. In cells pre-treated with 2 μM "BTYNB" and infected at MOI 5, the mean infectious virus measured at 16 hours was double that seen in cells pre-treated with DMSO only (**Figure 4.13A**), although this difference was not statistically significant (p=0.3012). Conversely, the mean virus titres from cells pre-treated with 10 μM or 20 μM "BTYNB" were both comparable to that from cells pre-treated with DMSO. Unlike the infections at MOI 5 with "BTYNB"

in the virus overlay, no effect of the drug on infectious virus production was observed here.

With infection at MOI 0.01, infectious virus produced by cells pre-treated with 2 μM "BTYNB" was slightly reduced compared to that from cells treated with DMSO only (**Figure 4.13B**), although this difference was not statistically significant (p=0.7250). The mean titre measured from cells that had been pre-treated with 10 μM "BTYNB" was approximately 80% lower than that measured from cells treated with 0 μM, but this also did not reach statistical significance (p=0.0629). Virus production was further reduced with 20 μM pre-treatment and was significantly lower than that observed from cells treated with DMSO only (p=0.0474). Although statistical significance was only reached at the highest concentration of "BTYNB", these data showed a trend of reduced infectious virus output with increased concentrations of "BTYNB" pre-treatment. This trend was not seen when the drug was administered in the infection overlay (**Figure 4.11C**). When the compound was thought to inhibit IGF2BP1, these data suggested that inhibition of the protein prior to infection reduced multicycle IAV replication, which implied an indirect role in the viral lifecycle. However, at this point, Cayman Chemicals contacted me to explain that they had supplied the incorrect compound. Furthermore, the actual identity or structure of the compound could not be determined, and therefore the mechanism that lead to this reduction in virus replication could not be identified.

4.3.3.2. Correct compound

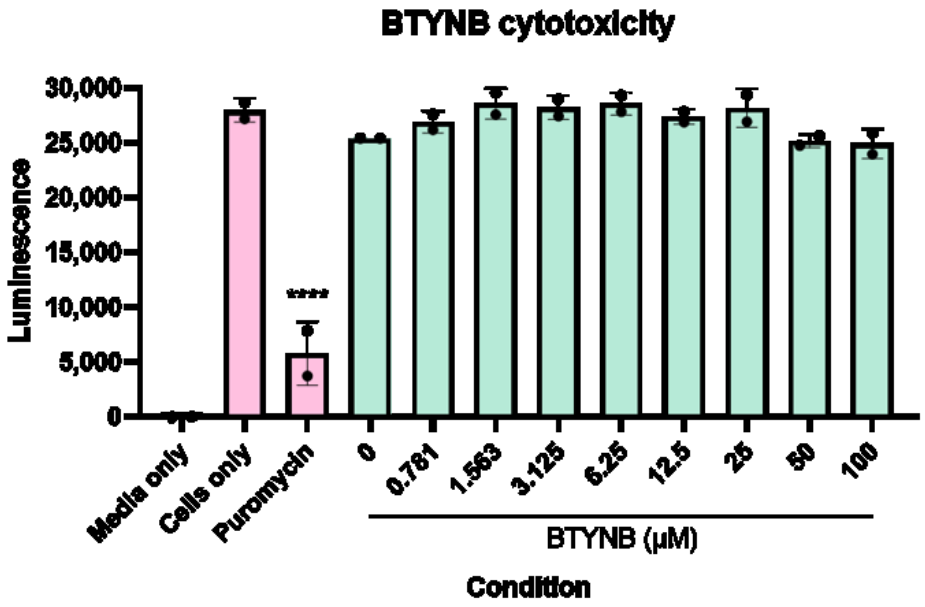

Figure 4.14 BTYNB cytotoxicity. *A549 cells were incubated with at a range of concentrations of BTYNB, DMSO vector only (0 μM BTYNB), 50 μg/μL puromycin, or left untreated (Cells only) for 24 hours. Cell lysates were analysed using a CellTiter-Glo viability assay. Background luminescence was established by incubating cell-free media with the CellTiter-Glo reagent (media only). Points represent the means of technical duplicates, bars represent the mean of two biological replicates, and error bars represent standard deviation. Data were analysed by one-way ANOVA with Tukey's multiple comparison tests using GraphPad Prism 8. Significance markers refer to comparison with cells only. ****: p≤0.0001.*

When Cayman Chemicals realised their error, they supplied the correct BTYNB compound. Accordingly, a CellTiter-Glo assay was performed to determine an appropriate range of concentrations to be used for infection experiments. As before, a two-fold dilution series of the drug was made and A549 cells were incubated with either BTYNB, puromycin or drug-free media (cells only) for 24 hours before the ATP content of the cell lysates was analysed. The mean luminescence detected from cells treated with DMSO only (0 μM) was slightly, but not significantly (p=0.7116), reduced compared to cells only (**Figure 4.14**), indicating minimal loss of cell viability. With all concentrations of BTYNB tested, mean luminescence was not significantly different to that from either cells only or cells treated with DMSO, indicating that the drug did

not cause cytotoxicity at these concentrations. Using this data and the concentration at which inhibitory activity of BTYNB had been previously seen, 10 μM (Mahapatra *et al.*, 2017), a range of 0 to 50 μM was chosen for IAV infection experiments.

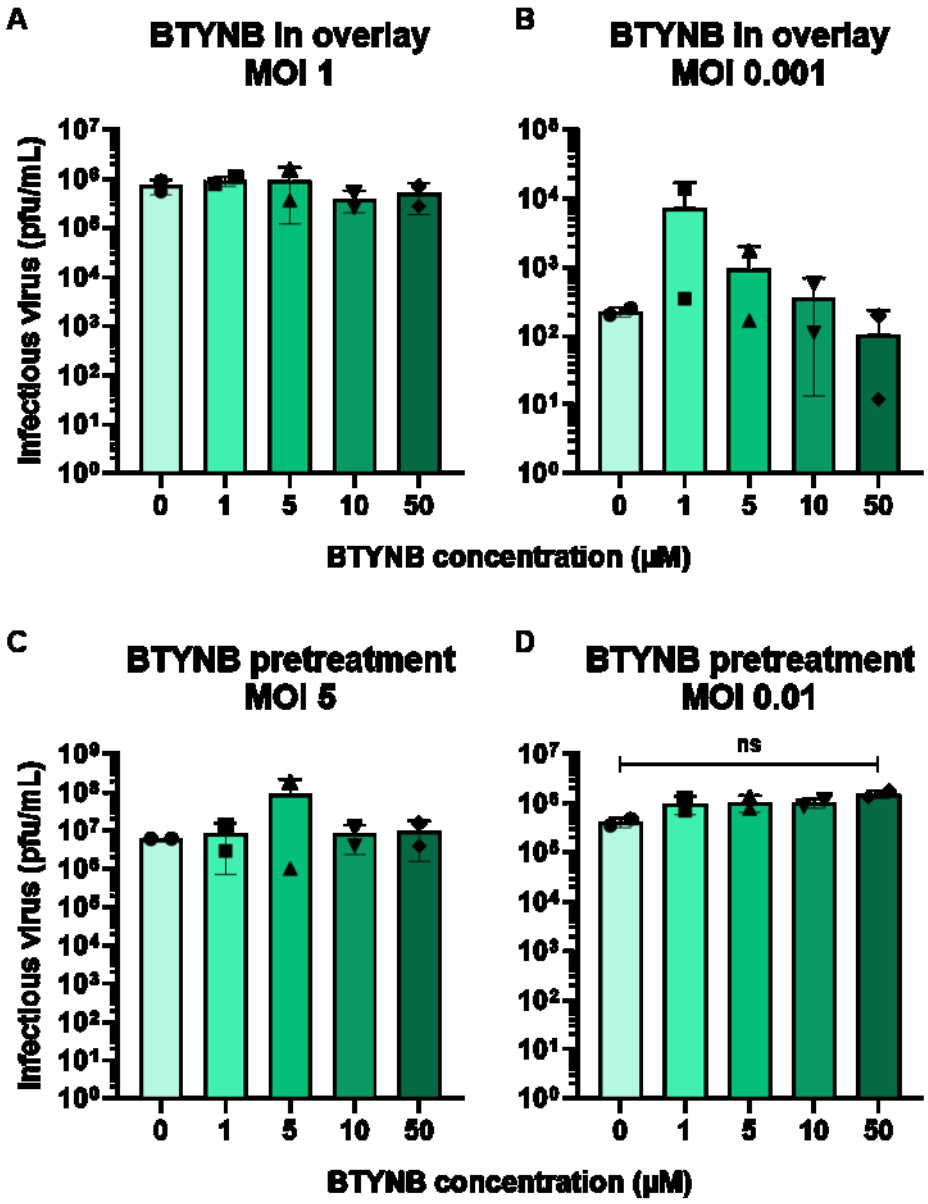

Figure 4.15 Infectious virus production in cells treated with BTYNB. A and B: *A549 cells were infected with PR8 at either MOI 1 or MOI 0.001 and 1 hour post infection, cells were overlaid with media containing BTYNB or DMSO only (0 μM). Cell supernatants were harvested at 16 hours post infection and analysed by plaque assay on MDCK cells.* ***C and D:*** *A549 cells were pre-treated with BTYNB or DMSO vector only (0 μM BTYNB) for 24 hours prior to infection with PR8 at either MOI 5 or 0.01. At 16 hours post infection, cell supernatants*

were harvested and analysed by plaque assay on MDCK cells. Bars represent the mean of two biological repeats, error bars represent standard deviation. Data were analysed by one-way ANOVA with Tukey's multiple comparison test using GraphPad Prism 8.

In order to investigate the effects of IGF2BP1 inhibition on IAV, A549 cells were infected with PR8 and BTYNB was added to the infection overlay media. Supernatants were harvested at 16 hours post infection and analysed by plaque assay to assess infectious virus production. Due to calculation errors, the cells were infected at approximately MOI 1 instead of the usual MOI 5. Here, no significant differences in virus titre were seen between cells treated with DMSO only and cells treated with any concentration of BTYNB (**Figure 4.15A**). In cells infected at MOI 0.001, 1 μM BTYNB treatment apparently increased virus replication by more than an order of magnitude compared to that from cells treated with DMSO (**Figure 4.15B**). Higher concentrations of drug then led to lower titres more comparable to the DMSO control. However overall titres from these experiments were unexpectedly low, there was great variation between the biological replicates at 1 μM and no differences were statistically significant. Due to this, no conclusions could confidently be made using this data. Overall, no effect of IGF2BP1 inhibition during IAV replication was seen here.

As with the incorrect compound, further infection experiments were conducted in which cells were pre-treated with BTYNB prior to infection. Cells were incubated with BTYNB or DMSO for 24 hours, infected with PR8 at either MOI 5 or MOI 0.01 and released virus titred by plaque assay at 16 hours post infection as before. At all concentrations of BTYNB pre-treatment other than 5 μM, mean virus titres measured from cells infected at MOI 5 were comparable to those seen from cells pre-treated with DMSO only (**Figure 4.15C**). Although on average higher, the titres from cells treated with 5 μM BTYNB were variable and none of these differences were statistically significant ($p>0.6$ in all cases). Therefore no relationship between

IGF2BP1 inhibition and IAV replication was seen at this MOI. With infection at MOI 0.01, the mean titres were more consistent and showed a trend, although still not statistically significant, towards increased infectious virus output with increased BTYNB concentrations (**Figure 4.15D**). Due to time limitations, only two independent repeats of these experiments could be performed and more power was needed to determine whether this increase was real. If it were, this could suggest a minor antiviral role for IGF2BP1; however with the data presented here, no effect of IGF2BP1 on IAV replication could be proven.

4.3.4. Overexpression of IGF2BP1

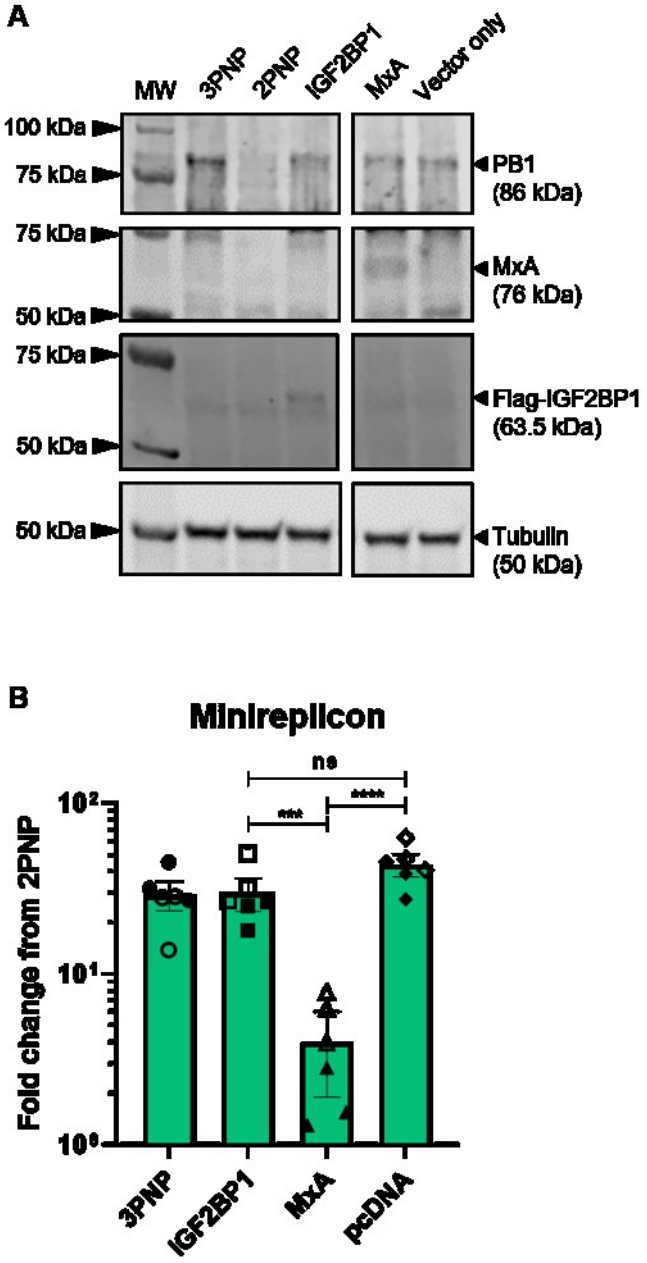

Figure 4.16 IAV gene expression in cells overexpressing IGF2BP1. *293T cells were transfected with plasmids encoding PR8 PB2, PB1, PA and NP (3PNP) and a vRNA firefly luciferase reporter plasmid. Experimental groups were also transfected with overexpression plasmids encoding Flag-IGF2BP1 or untagged MxA, or empty pcDNA3.1 plasmid (vector only). As a negative control, cells were transfected with the IAV polymerase, omitting PB1 (2PNP). Cells were lysed 48 hours post transfection and either were examined by western blot or for luciferase activity.* ***A:*** *Western blots of a single representative experiment in X293T cells, probed for Flag-IGF2BP1, PB1, MxA and an alpha tubulin loading control. MW indicates*

molecular weight markers. The western blot images for PB1, MxA and Tubulin were also shown in ***Figure 3.10****.* ***B:*** *Cell lysates were treated with luciferase reagent, luminescence signal was measured and expressed as fold change compared to 2PNP. Filled points represent the technical replicates from HEK293T cells, empty points represent technical replicates from X293T cells. Control data from X293T cells were also presented in section 3.2.4 in a minireplicon experiment with CMTR1 K23A overexpression. Bars represent the mean of two biological repeats; error bars represent standard error of the mean. Data were analysed by one-way ANOVA with Tukey's multiple comparison tests using GraphPad Prism 8. ns: not significant, p≥0.05; ***: p≤0.001; ****: p≤0.0001.*

Finally, the effects of IGF2BP overexpression on IAV gene expression in a mini-replicon system were examined. For this, 293T cells were transfected with pDUAL plasmids encoding the components of the viral RNP (3PNP) and a luciferase reporter plasmid encoding a vRNA-like molecule to be transcribed by the IAV polymerase (Lutz *et al.*, 2005). Additionally, cells were also transfected with a pcDNA3.1 plasmid encoding Flag-IGF2BP1 (cloned by Dr Nisha Kriplani), an untagged MxA overexpression pcDNA3.1 plasmid or empty pcDNA3.1 (vector only). A 2PNP negative control was included, in which cells were transfected with the reporter plasmid and an incomplete viral RNP, omitting PB1. At 48 hours post transfection, cells were lysed and luciferase activity was analysed as a measure of viral polymerase activity and expressed relative to 2PNP. Two independent repeats were performed, one in HEK293T cells and the other in X293T cells; the data from these are presented together.

To confirm successful transfection and appropriate protein expression, cell lysates were analysed by western blot. Equal alpha tubulin staining was seen across samples (**Figure 4.16A**). Probing with anti-PB1 anti-sera showed signal for the viral protein in cells that had been transfected with 3PNP that was absent in the 2PNP sample. The same band was also present, though to a lesser extent, in cells that had been co-transfected with 3PNP and pcDNA plasmids. The western blots were also probed with anti-MxA antibody, which showed expression of the antiviral ISG in cells that had been

transfected with the corresponding plasmid but not in other cells, indicating that MxA was not endogenously expressed in this experiment. Lastly, overexpression of IGF2BP1 in the relevant cells was confirmed by probing the samples, on a separate blot, with anti-Flag antibody. Here, signal was detected in cells transfected with the Flag-IGF2BP1 overexpression plasmid at the expected molecular weight, around 63.5 kDa but again, not seen in the other cells. Therefore, the cells were determined to be expressing the correct proteins so that the IAV polymerase activity could then be analysed. The gene expression activity of the viral RNP was determined by treating cell lysates with luciferase reagent and measuring the luminescence signal produced, expressing the values as fold change from the background signal measured from cells transfected with 2PNP. The baseline activity of the viral polymerase in cells transfected with 3PNP was approximately 30 times greater than background signal (**Figure 4.16B**). Cells that had been transfected with 3PNP and an empty plasmid vector showed increased luminescence signal compared cells transfected with 3PNP alone. However this difference was not statistically significant ($p=0.0694$). Luminescence measured from cells expressing MxA was significantly reduced compared to both the 3PNP positive control ($p=0.0012$) and cells transfected with 3PNP and empty pcDNA3.1 ($p<0.0001$), demonstrating the effect of an antiviral protein on the minireplicon assay. With overexpression of Flag-IGF2BP1 no significant difference in mean luminescence was seen compared to cells transfected with 3PNP alone ($p=0.9987$), or to cells transfected with 3PNP and empty vector ($p=0.0934$). The replicative activity of the IAV RNP in these cells was also significantly higher than in cells expressing MxA ($p=0.0008$). Overall, these data did not suggest any effect, either pro- or anti-viral of IGF2BP1 overexpression on the activity of the IAV polymerase.

4.4. Discussion

4.4.1. Development of tools to study IGF2BP proteins and IAV

In this chapter, I aimed to investigate whether the IGF2BP m^6A readers were involved in the lifecycle of IAV. In order to do this, I attempted to develop knockdown protocols for each of the proteins in the family. IGF2BP1 knockdown was achieved with an average knockdown efficiency of approximately 80%. In the process of investigating IGF2BP1, western blotting showed a band at a lower molecular weight than expected, which did not correspond to a known isoform of the protein (Fakhraldeen *et al.*, 2015), and was reduced in cells transfected with IGF2BP1-targeting siRNA (**Figure 4.2**). When examining antibody staining using IGF2BP1 with an N-terminal Flag tag, this band was seen with anti-IGF2BP1 staining but not with anti-Flag (**Figure 4.7**). This suggested that the band seen here may represent an undescribed IGF2BP1 isoform lacking the N-terminus of the protein. Whether this has any biological relevance, in IAV replication or otherwise, is not clear.

Knockdown of IGF2BP2 or IGF2BP3 could not be definitively established in this study. This was partly due to antibody cross-reactivity between IGF2BPs that obscured the measurement of knockdown. Therefore, depletion of IGF2BP2 or IGF2BP3 may have been better evaluated using qPCR measurements of transcript levels. Two recent studies have been able to achieve reproducible knockdown of IGF2BP2 mRNA in the lung bronchial epithelial cell line BEAS-2B using single siRNA (Dong *et al.*, 2021) or short hairpin (sh)RNA (Wang *et al.*, 2021) molecules. Furthermore, other groups have achieved IGF2BP3 knockdown via shRNA transduction in A549 cells (Zhao *et al.*, 2017) or with siRNA in gastric cancer cell lines (Jiang *et al.*, 2021; Zhou *et al.*, 2017). These studies demonstrate that knockdown of IGF2BP2 or IGF2BP3 is achievable and could be used to guide protocol optimisation for any future work on IGF2BPs and

IAV. Furthermore, the antibodies used in these studies to confirm knockdown of IGF2BP3 expression may serve better than the ones used here.

An attempt to study the effects of overexpression of the IGF2BP proteins on IAV was also made. Plasmids for the overexpression of all three IGF2BP proteins with N-terminal Flag tags were developed by Dr Nisha Kriplani. Plasmids encoding Flag-IGF2BP1 in both a pMiniT and pcDNA3.1 backbone were successfully cloned, and transfection of these into mammalian cells resulted in translation of the tagged protein (**Figure 4.7** and **Figure 4.16**, respectively). A pMiniT plasmid encoding Flag-IGF2BP2 was also produced, however the resulting protein expression was poor (**Figure 4.7**). Multiple other plasmid backbones were tested without success; it was therefore hypothesised that an unknown product of the sequence was toxic to the bacteria used for cloning. pMiniT and pcDNA3.1 plasmids containing the Flag-IGF2BP3 gene were produced and confirmed by diagnostic digest and sequencing (data not shown). However, transfection of either plasmid into cells did not give expression of the tagged protein, suggesting that there was a problem with the sequence used to generate these plasmids, although the specific issue could not be determined within the time frame of this study.

Nevertheless, the IGF2BP1 knockdown system was used, in addition to inhibition and overexpression experiments, to investigate whether IGF2BP1 is involved in IAV infection.

4.4.2. IGF2BP1 in IAV infection

In IGF2BP1 knockdown cells, there was no consistent evidence for either inhibition or enhancement of IAV infection. Courtney et al. reported that m^6A modifications in IAV RNA enhance viral gene expression and infectious virus production (Courtney *et al.*, 2017). However, knockout of METTL3 reduced titres by less than an order of magnitude (Courtney *et al.*, 2017), so under the assumption that METTL3 is the only

enzyme responsible for IAV m^{6}A methylation, this suggests that the modification amplifies infection, but is not strictly required. If IGF2BP1 is a host factor via its m^{6}A reader function, any reduction in IAV replication due to loss of IGF2BP1 expression would be modest. Furthermore, large overlap in the RNA targets of the three proteins in the IGF2BP family likely causes redundancy that could not be explored here without conclusively establishing systems to deplete IGF2BP2 or IGF2BP3. Future research in this area could use gene editing techniques to create single, double and triple knockout cells in order to dissect the contribution, if any, of the individual proteins and of the whole family.

An IGF2BP1 inhibitor was also used to investigate any contribution of the protein to IAV infection. BTYNB was reported to inhibit the binding of IGF2BP1 to its mRNA targets (Mahapatra *et al.*, 2017), although the mechanism, binding site and specificity of the drug have not been clarified. I initially received a compound that appeared to have minor antiviral effects. However, retroactive quality control experiments by the supplier revealed that the batch received contained the wrong compound. The actual structure of the compound could not be discerned by myself or the supplier. Therefore the cause of the antiviral effect is unknown. With the correct compound, no antiviral effect was detected, which was consistent with the knockdown data.

Finally, minireplicon experiments with overexpression of IGF2BP1 showed no effect on IAV replication. This supported the other data here that suggest IGF2BP1 is not involved in the lifecycle of IAV. However, these experiments only analyse the activity of the IAV polymerase (indirectly, relying on mRNA translation). IGF2BP1 has been reported to interact with NS1 (Pichlmair *et al.*, 2012; Rahim *et al.*, 2018) and this interaction was not examined using this experimental technique. Overexpression of the Flag-tagged IGF2BP1 could be used to investigate this interaction over the course of infection and whether this influences the localisation or activity of the viral protein.

These investigations were not possible within the time frame of this study, and are unlikely to directly aid in the development of treatment strategies, however they may provide insight into the functioning of the viral immunomodulatory NS1.

Overall, the data presented in this chapter could not support a role for IGF2BP1 in the lifecycle of IAV and thus IGF2BP1 alone is not a suitable drug target for the treatment of IAV. However, this evidence was not sufficient to exclude IGF2BP1 or the other proteins in the family and should not deter future investigation in this area.

Chapter 5: Final discussion

5.1. Concluding remarks

The work presented in this thesis aimed to investigate cellular factors in the lifecycle of IAV with a view to assess whether these factors were suitable targets for the design of antiviral therapies. For various reasons, none of these factors were determined to be suitable drug targets; nevertheless my findings may provide some direction for future work. First JMJD6, a factor that had been selected for investigation via a knowledge-driven route, had previously been suggested to be involved in the replication of IAV. However, the data presented in Chapter 2 showed that a published JMJD6-targeting siRNA sequence induced an IFN response when transfected into cells that would obscure any effects of the depletion of JMJD6 expression on IAV infection. Using an alternative method of RNAi knockdown that did not induce IFN, as well as *JMJD6*$^{-/-}$ cells, I found that IAV could replicate normally with reduced or ablated expression of JMJD6. I next investigated CMTR1, which had been identified in a genome wide CRISPR/Cas9 screen for IAV host dependency factors. However the data presented in this thesis suggested that IAV replication is not inhibited without complete removal of CMTR1 or its activity, which could not realistically be achieved with drug treatment. Nevertheless, this work did not rule out that targeting CMTR1 may enhance the antiviral activity of the cap-dependent endonuclease inhibitor Baloxavir, which should be investigated further. Finally, the IGF2BP family of RNA binding proteins was examined, based on a focused literature search of various IAV-host factor screens. The investigation of IGF2BPs in IAV infection was hindered by issues with knockdown development, time restrictions and being supplied with an incorrect chemical inhibitor. However, while the work presented here does not support these cellular proteins as host dependency factors, they also could not be excluded

as such. Suggestions for experiments that may determine whether IGF2BPs are involved in the lifecycle of IAV are discussed in section 4.4.

Together, this work highlights the difficulties of validation studies when developing treatment strategies for infectious disease. Furthermore, Chapters 2 and 3 in particular demonstrate that published research regarding IAV host factors, as with all research, should be regarded with a certain level of scrutiny and that work building on published studies should be approached with caution. The examination of the same host factor in different hands, using different tools can yield varying results and highlight as yet unseen issues. Therefore collaboration and validation between different research groups is invaluable for the advancement of the understanding of IAV infection and the design of treatments.

5.2. Future directions: identifying new targets

Experiments for future investigation into CMTR1 and the IGF2BPs are discussed in Chapters 3 and 4, respectively. Here, I will briefly discuss how new host factors and drug targets for the treatment of IAV may be identified in the future.

Three different routes were used to identify the potential host factors examined in this thesis. The direct selection of individual genes that have known functions that may translate to IAV infection, as with JMJD6, has benefits, such as the existence of tools and literature to support the design of an investigation. However this is limited in that only one factor, or group of factors is examined at once. Large scale, hypothesis-free RNAi and CRISPR screens, such as that performed by Li *et al*. which highlighted CMTR1, allow for the examination of many genes at once and may reveal genes or pathways that may not have been considered based on pre-existing knowledge of the pathogen (Li *et al.*, 2020a). However, the results of screens often vary greatly between research groups and studies (Chou *et al.*, 2015). Additionally, as demonstrated in this

thesis with CMTR1, these screens can potentially over-represent the importance of some host factors.

Combining knowledge of the pathogen with the results of large scale screens, as was done here with IGF2BP1, is a way to exploit the benefits of both. Specifically, a large number of potential candidates can be considered in a more focused way that could reduce examination of irrelevant false positives. Targeted examination of larger scale screens, or smaller more focused screens may yield more useful and successful hits. For example, screening the genes of specific pathways, such as spliceosome components that may be required for the expression of IAV M2 or NEP genes, or genes associated with anti-IAV immunity such as ISGs.

Large scale screens in which host genes are knocked down or out (Li *et al.*, 2020a), and interaction screens, in which tagged IAV proteins are overexpressed in cell culture and examined using immunoprecipitation (Pichlmair *et al.*, 2012) were briefly discussed in this thesis. Other types of larger scale screens that have been used to examine IAV and the human host include genetic association studies, examining the genomes of patients that suffer serious IAV infections compared to those with mild disease or exposed, uninfected individuals, which can be focused on specific pathways, or genome-wide (Chen *et al.*, 2015b; Clohisey & Baillie, 2019; To *et al.*, 2014). Additionally transcriptomic studies of IAV infected cells, animals and patients can reveal host gene expression patterns that are altered in IAV infection that may have pro- or anti-viral effects (Cao *et al.*, 2019; Hancock *et al.*, 2018; Josset *et al.*, 2010; Zhou *et al.*, 2021).

In 2019, Pizzorno *et al*. used the data gathered from transcriptomic profiles of IAV-infected patients in order to refine a list of FDA-approved host-targeted inhibitors that were then screened for antiviral activity in IAV infection (Pizzorno *et al.*, 2019). The authors reported that diltiazem, an antagonist of voltage-gated calcium channels,

inhibited IAV replication in mice and a cultured airway epithelium model (Pizzorno *et al.*, 2019). Voltage-gated calcium channels had separately been reported to mediate IAV cell entry (Fujioka *et al.*, 2018), but not all inhibitors of this channel show significant antiviral activity against IAV (Pizzorno *et al.*, 2019). Pizzorno *et al*. also identified off-target effects of diltiazem that could have contributed to IAV restriction and which will likely be the focus of future study and antiviral design (Pizzorno *et al.*, 2019). This study demonstrates the benefits of combining different tools and techniques for the investigation of IAV host factors and drug targets. With the development and advancement of new technologies, many study and screen types may be used in collaborations in the future in order to inform the design of IAV treatments.

Chapter 6: Materials and Methods

6.1. Materials

6.1.1. General reagents

General purpose reagents were supplied by Sigma-Aldrich, Scientific Laboratory Supplies and Fisher Scientific. The Roslin Institute Central Services Unit (CSU) prepared and provided sterile water and phosphate-buffered saline (PBS). Additional specific reagents and kits and their respective suppliers are listed below in **Table 6.1**.

Table 6.1 General reagents.

Reagent or kit	**Source**
30% acrylamide:bisacrylamide (37.5:1)	BioRad
Agarose (UltraPureTM)	Invitrogen
Avicel	FMC Biopolymer
Cell-Titre Glo	Promega
DharmaFECT1	Dharmacon
Dimethyl sulphoxide (DMSO)	ThermoFisher Scientific
1kb DNA Ladder	Promega
Gel Loading Dye, Purple (6X)	New England Biolabs
Lipofectamine 2000	ThermoFisher Scientific
Luciferase Assay Reagent	Promega
Mini-PROTEAN® TGX™ Precast Gels	BioRad
Neutral Buffered Formalin (NBF)	Leica
Nitrocellulose membrane (0.45µm)	BioRad
Nuclease free water	Qiagen
Precision Plus Dual Colour Molecular Weight Marker	BioRad
Polyinosinic:polycytidylic acid (poly I:C)	InvivoGen
QIAGEN Plasmid Midi Kit	Qiagen
QUANTI-Blue™	InvivoGen
Reporter Lysis Buffer	Promega
Resolving buffer for acrylamide gels	Protogel
Stacking buffer for acrylamide gels	Protogel
SYBR DNA gel stain	Invitrogen
Tetramethylethylenediamine (TEMED)	Protogel
Trans-Blot Turbo 5x Transfer Buffer	BioRad
Tween20	Sigma-Aldrich
Universal type I IFN	Bio-Techne

6.1.2. siRNAs

***Table 6.2 Sequences of targeting siRNA**.*

Gene target	Sequence	Source
Jmjd6 (siRNA-275)	GGAAAUAUCGGAACCAGAAGUUCAA	Sigma-Aldrich (custom)
Jmjd6 (SMARTpool)	GGAGAGCACUCGAGAUGAU	Dharmacon (L-010363-00-0005)
	GGACCCGGCACAACUACUA	
	GGUAUAGGAUUUUGAAGCA	
	GGAUAACGAUGGCUACUCA	
CMTR1	GAAUUCAGCUUGCCGAGAA	Dharmacon (L-014142-01-0005)
	UGGAUAACACAGAUCGCAA	
	GGGAUUACCUCUUCGCAGU	
	GAUCAAAGCUCUGGCGAAA	
IGF2BP1	CGAAACACCUGACUCCAAA	Dharmacon (L-003977-00-0005)
	UGAAGGCCAUCGAAACUUU	
	GAAAGUAGAAUUACAAGGA	
	GCUUAGAGAUUGAACAUUC	
IGF2BP2	AAGGAGGGCUUGACCAUAA	Dharmacon (L-017705-00-0005)
	GUGCUGAGAUAGAGAUUAU	
	GCUAAGCGGGCAUCAGUUU	
	GAGCAUAUACAACCCGGAA	
IGF2BP3	CCAAGUGGUUGUCAAAAUA	Dharmacon (L-003976-00-0005)
	UCGAGGCGCUUUCAGGUAA	
	GGAUUUCAGUUAGAGAAUU	
	GAUAUUGCUUCUAUGAAUC	

6.1.3. Plasmids

Table 6.3 Plasmids used throughout the study.

<table>
<tr><th>Name</th><th colspan="2">Description</th><th>Source</th></tr>
<tr><td>pDual</td><td colspan="2">Reverse genetics plasmid. Bidirectional pol I and pol II promoters either side of insert lead to mRNA and vRNA-like RNA synthesis. Used to make A/Puerto Rico/8/1934 H1N1 (PR8) stocks and to reconstitute the PR8 polymerase in minireplicon assays.
Segment | Accession number
PB2 | EF467818
PB1 | EF467819
PA | EF467820
HA | EF467821
NP | EF467822
NA | EF467823
M | EF467824
NS | EF467817</td><td>Dr Rute dos Santos Pinto (The Roslin Institute, The University of Edinburgh, UK); (de Wit et al., 2004)</td></tr>
<tr><td>pcDNA3.1</td><td colspan="2">CMV pol II promoter upstream of insert leads to constitutive high protein expression. Used for overexpression of IGF2BP1, CMTR1 K23A and Mx.</td><td>Dr Nisha Kriplani; Dr Hui-Min Lee (The Roslin Institute, The University of Edinburgh, UK); Invitrogen</td></tr>
<tr><td>pMiniT 2.0</td><td colspan="2">Cloning vector used as part of NEB® PCR Cloning Kit, T7 and SP6 promoters upstream of restriction sites allows induced expression of insert.</td><td>Dr Nisha Kriplani (The Roslin Institute, The University of Edinburgh, UK); New England Biolabs</td></tr>
</table>

Name	Description	Source
pPol I FF Luciferase	Reporter for minireplicon assay. Contains firefly luciferase reporter gene in reverse orientation. Flanked by UTRs of PR8 segment 8 under the control of a pol I promotor.	Dr Laurence Tiley (The University of Cambridge, UK)

6.1.4. Antibodies

Table 6.4 Primary antibodies and antisera raised against IAV proteins.

Antibody	Application	Source
Rabbit polyclonal anti-PR8 M1 (A2917)	WB (1:500)	(Amorim *et al.*, 2007)
Mouse monoclonal anti-M2 (14C2)	WB (1:500)	Abcam (ab20343)
Rabbit polyclonal anti-MBP-NP (A2915)	WB (1:1000)	(Noton *et al.*, 2007)
Rabbit polyclonal anti-NS1 (V29)	WB (1:500)	(Carrasco *et al.*, 2004)
Rabbit polyclonal anti-PB1 (V19)	WB (1:1000)	(Digard *et al.*, 1989)

Table 6.5 Primary antibodies raised against human cellular proteins, and tags.

Antibody	Application	Source
Rabbit polyclonal anti-CMTR1	WB (1:1000)	Atlas Antibodies via Cambridge Biosciences (HPA029979)
Rabbit polyclonal anti-Flag	WB (1:1000)	Sigma-Aldrich (SAB4301135)
Rabbit polyclonal anti-IGF2BP1	WB (1:1000)	Atlas Antibodies via Cambridge Biosciences (HPA062273)
Rabbit polyclonal anti-IGF2BP2	WB (1:500)	Atlas Antibodies via Cambridge Biosciences (HPA035145)
Rabbit polyclonal anti-IGF2BP3	WB (1:1000)	Atlas Antibodies via Cambridge

Antibody	Application	Source
		Biosciences (HPA002037)
Mouse monoclonal anti Jmjd6 (H-7)	WB (1:2000)	Santa Cruz Biotechnology (sc-28348)
Goat polyclonal anti-MxA/Mx1	WB (1:1000)	R&D systems (AF7946)
Rat monoclonal anti-tubulin (YL1/2)	WB (1:2000)	Thermo Fisher (MA180017)

Table 6.6 Secondary antibodies.

Antibody	Application	Source
IRDye 800CW Donkey anti-Rabbit IgG (H + L) Secondary Antibody	WB (1:10000)	LI-COR (926-32213)
IRDye 800CW Donkey anti-Mouse IgG (H + L) Secondary Antibody	WB (1:10000)	LI-COR (926-32212)
IRDye 800CW Donkey anti-Goat IgG (H + L) Secondary Antibody	WB (1:10000)	LI-COR (926-32214)
IRDye 680RD Goat anti-Human IgG Secondary Antibody	WB (1:10000)	LI-COR (926-68078)

6.1.5. Mammalian cell lines

Table 6.7 Mammalian cell lines used throughout the study.

Cell	Description	Source
A549	Human Adenocarcinomic Alveolar Basal Epithelial cells	Sigma/ Dr Nikki Smith (The Roslin Institute, The University of Edinburgh, UK); (Turnbull *et al.*, 2016)

Cell	Description	Source
MDCK	Madin-Darby Canine Kidney cells	Sigma/ Dr Nisha Kriplani (The Roslin Institute, The University of Edinburgh, UK); (Wise *et al.*, 2012)
HEK293T	Human Embryonic Kidney cells	Sigma/ Dr Hui-Min Lee (The Roslin Institute, The University of Edinburgh, UK); (Clements *et al.*, 2021)
X293T	Lenti-X 293T subclone of the transformed HEK 293 which is highly transfectable	ATCC/ Dr Nisha Kriplani (The Roslin Institute, The University of Edinburgh, UK); (Kriplani *et al.*, 2021)
HEK-Blue™	HEK-Blue™ IFNα/β cells	InvivoGen /Dr Rute dos Santos Pinto (The Roslin Institute, The University of Edinburgh, UK); (Turnbull *et al.*, 2016)
BSR-T7	Clone of BHK-21 (Baby Hamster Kidney fibroblasts) which stably expresses T7 RNA polymerase	(Buchholz *et al.*, 1999)/ Olga Diebold (The Roslin Institute, The University of Edinburgh, UK)

6.1.6. Solutions and Media

6.1.6.1. Eukaryotic cell culture media and cell passage solutions

Table 6.8 Reagents used in the preparation of media for eukaryotic cell culture.

Reagent	**Source**
0.25% Trypsin- Ethylenediamine tetraacetic acid (EDTA)	Life Technologies
Blasticidin	InvivoGen
Bovine serum albumin (BSA)	ThermoFisher Scientific
Dulbecco's Modified Eagle Medium (D-MEM)	Sigma-Aldrich
Foetal Bovine Serum (FBS)	Life Technologies
Glasgow's Modified Eagle Medium (G-MEM)	Life Technologies
L-1-Tosylamide-2-phenylethyl chloromethyl ketone- -(TPCK)-treated bovine pancreatic trypsin	Sigma-Aldrich
L-Glutamine	Life Technologies
Opti-MEM	Life Technologies
Penicillin/Streptomycin	Life Technologies
Tryptose Phosphate Broth solution (TPB)	Sigma-Aldrich
Zeocin	InvivoGen

The previously listed supplies were used to prepare the following media:

- Complete D-MEM: D-MEM supplemented with 10% (v/v) heat inactivated (HI) -FBS, 2 mM glutamine, 100 U/mL penicillin, and 100 µg/mL streptomycin.
- Serum free medium: Complete D-MEM without FBS.
- Virus growth medium: D-MEM supplemented with 2 mM glutamine, 100 U/mL penicillin, 100 µg/mL streptomycin, 0.14% (w/v) BSA, and 1 µg/mL N-tosyl-L-phenylalanine chloromethyl ketone (TPCK)-treated trypsin.
- Transfection medium: Complete D-MEM without penicillin and streptomycin.
- BSR-T7 culture medium: G-MEM supplemented with 10% (v/v) HI-FBS, 10% (v/v) TPB, 100 U/mL penicillin, and 100 µg/mL streptomycin.

6.1.6.2. Bacterial media

Bacterial growth media and agar were prepared and provided by the Roslin Institute CSU according to the following formulae:

- Luria-Bertani (LB) Broth: 10 g/L tryptone, 5 g/L yeast extract, 5 g/L sodium chloride (pH 7.0).

- Super Optimal Broth (SOB): 20 g/L tryptone, 5 g/L yeast extract, 10 mM NaCl, 2.5 mM KCl, 10 mM $MgCl_2$, and 10 mM $MgSO_4$.
- LB agar 15 g/L agar, 20g/L tryptone, 5 g/L yeast extract, 10 g/L sodium chloride (pH 7.0).

Ampicillin sodium salt (used at 100 µg/mL) was sourced from Sigma-Aldrich.

6.1.6.3. Competent bacteria preparation solutions

- Calcium/Manganese Based (CCMB) transformation buffer: 10 mM potassium acetate, 10% (v/v) glycerol, 80 mM $CaCl_2$, 20 mM $MnCl_2$, 10 mM $MgCl_2$, pH 6.4.

6.1.6.4. Protein buffers and solutions

6.1.6.4.1. Lysis buffer

Laemmli's sample buffer: 20% (v/v) glycerol, 2% (w/v) sodium dodecyl sulphate (SDS), 100 mM dithiothreitol (DTT), 24 mM Tris pH 6.8, 0.016% (v/v) bromophenol blue, 0.016% (v/v) xylene cyanol solution.

6.1.6.4.2. Acrylamide gel electrophoresis

- SDS-PAGE running buffer. 25 mM Tris, 192 mM glycine, 0.1% (w/v) SDS.
- 4 x resolving buffer (Protogel) 1.5 M Tris-HCl, 0.4% (w/v) SDS, pH 8.8.
- 4 x stacking buffer (Protogel) 0.5 M Tris-HCl, 0.4% (w/v) SDS, pH 6.8.
- Resolving polyacrylamide gel: 7-15% acrylamide:bisacrylamide (37.5:1), 1× resolving buffer, 0.1% (w/v) APS, 0.1% (v/v) TEMED. This formula was adapted to make gels containing 7-15% polyacrylamide by altering the added amounts 30% acrylamide solution and water.
- Stacking polyacrylamide gel: 4% acrylamide:bisacrylamide (37.5:1), 1× stacking buffer, 0.5% (w/v) APS, 0.1% (v/v) TEMED.

6.1.6.4.3. Western blotting

- Protein transfer buffer: Trans-Blot Turbo Transfer Buffer (BioRad), 20% (v/v) ethanol.
- Blocking Buffer: PBS/0.1% (v/v) Tween20, 5% (w/v) skimmed milk (local supermarkets).
- Washing solution (PBST): PBS/0.1% (v/v) Tween20

6.1.6.5. Nucleic acid gel electrophoresis buffers

Tris acetate EDTA (TAE) buffer was prepared and supplied by the Roslin Institute CSU according to the following formulae:

- TAE buffer: 40 mM Tris, 20 mM acetic acid, 1 mM EDTA.
- 6x DNA loading buffer: 10 mM Tris-HCl (pH 7.6) 0.15% (w/v) Orange G dye, 0.03% (w/v) xylene cyanol FF, 60% (v/v) glycerol, 60 mM EDTA.

6.1.7. Drugs

Table 6.9 Compounds used throughout the study.

Reagent (solvent; concentrations)	Source
Baloxavir (DMSO; used at 1, 5, 10 and 50 nM)	LKT Laboratories via Cambridge Bioscience
BTYNB (DMSO used at 1, 5, 10 and 50 µM)	Cayman Chemical Company via Cambridge Bioscience
BTYNB incorrect compound (DMSO used at 2, 10 and 20 µM)	Cayman Chemical Company via Cambridge Bioscience

6.2. Methods

6.2.1. Molecular techniques

6.2.1.1. Preparation of agar plates

LB agar was heated in a microwave until all agar had dissolved. After cooling, the appropriate selection antibiotic was added and mixed. Molten LB agar was poured into sterile 10 cm dishes, working under the flame of a Bunsen burner to reduce contamination. The agar was then allowed to set at room temperature and stored at 4°C until further use.

6.2.1.2. Preparation of competent DH5α bacterial cells

Stocks of *Escherichia coli* bacteria (strain DH5α) were used to produce competent cells. Briefly, at least 10 µL of a starter culture was propagated overnight in 5 mL of antibiotic-free SOB medium at 37ºC on an orbital shaker. The next day, the culture was diluted 1:100 in 60 mL of SOB and incubated at 37ºC for a further 3 hours on an

orbital shaker until the optical density at 550 nm (OD_{550}) was approximately 0.3. Spectrophotometry was performed using 1 mL of the bacterial culture, using blank SOB medium as a reference. For the first two hours, the OD_{550} was measured once every hour, however in the last hour measurements were taken every 15-30 minutes. Once the desired OD_{550} was reached, the bacteria were incubated on ice for 10 minutes, followed by centrifugation at 3000 rpm at 4ºC for 10 minutes. The supernatant was removed and the pellet were resuspended in 1/4 of the initial volume (15 mL) of cold CCMB buffer (Hanahan *et al.*, 1991) and incubated on ice for 4 hours. Bacteria were pelleted as before, resuspended in 1/12 of the starting volume (5 mL) of cold CCMB buffer, and 100 µL aliquots were snap frozen on dry ice and stored at -80ºC.

6.2.1.3. Transformation of competent DH5α bacterial cells

The competent DH5α *E. coli* cells prepared before were used to amplify plasmid DNA using the heat shock transformation method. Briefly, approximately 50 ng of plasmid DNA was added to 50 µL of bacteria. This mixture was incubated on ice for 30 minutes, heated at 42ºC for 45 seconds, then immediately incubated on ice for 5 minutes. LB broth (800 µL) was added and the cells were placed in a shaker (180-200 rpm) for 1 hour at 37ºC to recover. Bacterial cells were then spread onto agar plates containing the appropriate antibiotic, using a sterile spreader whilst working under a flame. Agar plates were incubated in an inverted position overnight at 37ºC. The remaining volume of the transformation reaction was stored at 4ºC until confirmation of successfully transformed colonies along with the absence of colonies in water-transformed bacteria under antibiotic selection.

To amplify plasmid DNA from the transformed bacteria, single colonies were picked with a P200 pipette tip and incubated in 100 mL of LB with antibiotic selection at 37ºC in a shaker (180-200 rpm). Following overnight incubation, the bacterial cells were

pelleted at 4300 rpm at 4ºC for 15 minutes and the supernatant discarded. Cells were then used to prepare the plasmid DNA or stored at -20ºC.

6.2.1.4. Plasmid extraction and quantification

Plasmid DNA midi-preps were performed using QIAGEN Plasmid Midi Kit according to the manufacturer's instructions. DNA was diluted in nuclease free water and the final concentration was determined by measuring absorbance at 260 nm using a NanoDrop ND-1000 spectrophotometer. Plasmid integrity was also checked by agarose gel electrophoresis.

6.2.1.5. Agarose gel electrophoresis of DNA

Agarose gel electrophoresis was carried out using 0.8-2% (w/v) agarose gels depending on the size of DNA fragments to be separated. Gels were prepared by dissolving agarose in TAE buffer using a microwave. After cooling, 1X SYBR DNA gel stain was added (1:10,000) and mixed. The melted agarose was poured into a gel tray with a comb containing the desired number of wells. Once set, the gel was immersed in TAE buffer. DNA samples were mixed with 1X gel loading dye (final concentration) and loaded into the set agarose gel alongside 1kb DNA ladder. Gels were typically run at 80-100 V for 45-60 minutes in a horizontal electrophoresis tank (Bio-Rad). Gels were imaged using a LI-COR Odyssey Fc Imaging System.

6.2.1.6. Restriction enzyme digestion

DNA endonuclease enzymes were obtained from New England Biolabs (NEB), and digests were performed as instructed by the manufacturer. Typically, 1 µg of DNA was digested in a 50 µL reaction. The buffer used, amount of enzyme added, and incubation conditions were determined using the NEBcloner tool from NEB (https://nebcloner.neb.com/#!/).

6.2.2. Eukaryotic cell culture, isolation and manipulation

6.2.2.1. Cell passage

MDCK cells, 293T cells and A549 cells were all grown in complete D-MEM. HEK-Blue™ cells were cultured in complete D-MEM supplemented with 30 µg/mL blasticidin and 100 µg/mL Zeocin. BSR-T7 cells were cultured inBSR-T7 culture medium. All cells were grown at 37°C in 5% CO_2. Cells were typically passaged twice weekly by washing cells once with PBS and detaching using 0.25% trypsin-EDTA solution or without trypsin for HEK-Blue™ cells. Cells were resuspended in the relevant fresh medium and typically split 1 in 10.

6.2.2.2. Cell counting

All cell types were counted using a haemocytometer (Neubauer counting chamber). Usually, 10 µL of cell suspension was added into each side of the chamber under a glass cover slip. Under a light microscope, the number of cells was counted in a designated squared area equivalent to 0.1 mm^3 (1×10^{-4}mL). Cell concentration was then estimated (cell concentration (cells/mL) = number of counted cells x 10^4).

6.2.2.3. Cytotoxicity assays

Drug cytotoxicity was measured using the CellTiter-Glo viability assay kit, which quantifies the ATP content of cells. Cells were seeded at 1.5×10^4 cells/well in a flat clear bottom, opaque-walled 96-well plate. On the following day, cells were incubated with increasing concentrations of drug and/or DMSO (vehicle) in a total volume of 100 µL of complete D-MEM at 37°C in 5% CO_2 for 24 hours. An equal volume of the CellTiter-Glo reagent was added to each well and mixed for 2 minutes on an orbital shaker to induce cell lysis. The plate was incubated at room-temperature for 10 minutes to stabilise the luminescent signal before imaging with a micro plate reader (BioTek) using Gen5 software.

CellTiter-Glo viability assay kit was also used as described above to determine cytotoxicity caused by the transfection of siRNAs. The day following seeding, cells were transfected with increasing concentrations of targeting or non-targeting siRNA in a total volume of 100 µL transfection medium. Following 24 hours incubation at 37°C in 5% CO_2, the siRNA and transfection medium was removed and cells were overlaid with 100 µL complete D-MEM and incubated for a further 24 hours at 37°C in 5% CO_2. The CellTiter-Glo protocol was then followed as above.

6.2.2.4. siRNA transfection of A549 cells

A549 cells were transfected with siRNA in order to deplete protein levels of the candidate genes targeted in this study. Initial knockdown of Jmjd6 was performed using a protocol adapted from the Ph.D. thesis of Dr Janice Kwok (Kwok, 2018) and a published siRNA sequence termed siRNA-275 (Heim *et al.*, 2014). All other targeting siRNAs used were ON-TARGETplus siRNA SMARTpool from Dharmacon. All targeting siRNA sequences are listed in **Table 6.2**. MISSION® siRNA Universal Negative Control #1 (Sigma-Aldrich; SIC001) was used as a matched non-targeting control siRNA for siRNA-275. ON-TARGETplus Non-targeting Control Pool (Dharmacon; D-001810-10) was used matched non-targeting control for all SMARTpool siRNAs.

A549 cells were seeded in 1 mL complete D-MEM per well of a 24-well plate to achieve 60-70% confluence the following day for transfection. Prior to transfection, the complete D-MEM was removed, the cells were washed once with PBS and overlaid with transfection medium. SMARTpool siRNA transfections used 400 µL/well transfection medium as described above in section *6.1.6.1*. Transfection of siRNA-275 used 150 µL/well of a different transfection medium, D-MEM supplemented with 5% HI-FBS and 2 mM L-glutamine.

DharmaFECT1 transfection reagent and siRNA were diluted in separate volumes of either transfection medium, for siRNA-275, or Opti-MEM, for SMARTpool siRNAs, and incubated at room temperature for 5 minutes. The DharmaFECT1 and siRNA mixtures were combined and gently mixed. Following 20 minutes incubation at room temperature, 100 µL of the DharmaFECT1/siRNA mixture was dripped slowly into each well, making final total volume per well 250 µL for siRNA-275 and 500 µL for SMARTpool.

The concentration of siRNA used for SMARTpool transfections was determined by performing siRNA titration experiments, in which increasing concentrations of siRNAs (5-100 nM) were transfected into A549 cells and knockdown efficiency was determined using western blotting. For each gene that was targeted in subsequent infection experiments, 30 nM siRNA was determined to be optimal. The final composition of transfection mixtures that cells were incubated with are described below:

siRNA-275: 224.75 µL DMEM (5% HI-FBS, 2 mM L-glutamine), 0.75 µL DharmaFECT1 (Dharmacon) and 100 nM siRNA per well.

SMARTpool siRNAs: 400 µL D-MEM (10% HI-FBS, 2 mM L-glutamine), 96 µL Opti-MEM, 1 µL DharmaFECT1, and 30 nM siRNA per well.

Cells were incubated at 37°C in 5% CO_2 for 24 hours, after which either the samples were harvested or the transfection medium was removed and cells were overlaid with complete D-MEM. Cells were incubated for a further 24 hours (48 hours total) and either harvested or used for further infection experiments. For sample harvest, supernatants were removed and stored at -80°C, cells were washed with PBS and lysed with 150 µL/well 2X Laemmli sample buffer (10% DTT). Cell lysates were stored at -20°C.

6.2.2.5. Plasmid transfection of mammalian cells

Mammalian cell lines X293T, HEK293T, and BSR-T7 were transfected with overexpression plasmids using Lipofectamine2000. Briefly, cells were seeded in 1 mL of the relevant culture medium per well of a 24-well plate to achieve 60-70% confluence the following day for transfection. Prior to transfection, media was removed, the cells were washed once with PBS and overlaid with 400 µL either transfection medium (293T lines) or G-MEM supplemented with 10% (v/v) heat inactivated (HI)-FBS, 10% (v/v) TPB, without penicillin and streptomycin (BSR-T7). Lipofectamine2000 (2 µL) and 100 ng plasmid were each diluted separately in 50 µL Opti-MEM. After 5 minutes incubation at room temperature, these mixtures were combined, gently mixed, and incubated at room temperature for a further 20 minutes. The Lipofectamine2000/plasmid mixture (100 µL total) was then added to cells dropwise. Cells were incubated for 24 hours and lysed with 150 µL/well 2X Laemmli sample buffer (10% DTT). Cell lysates were stored at -20°C.

6.2.2.6. Generation of Jmjd6 knockdown cells

Frozen stocks of heterogeneous populations of A549 cells, which had previously been treated by Dr Janice Kwok to knockout *Jmjd6* (Kwok, 2018) were recovered from storage at -150°C and passaged as normal A549 cells (as described in section *6.2.2.1*).

After three passages, the heterogeneous cell lines were prepared for single cell cloning by FACS. Cells were pelleted by centrifugation at 3000 rpm at 4°C for 10 minutes, washed once in PBS and pelleted again under the same conditions. Media removed from the cells was filtered through a 0.2 µm filter (Sigma-Aldrich), mixed 1:1 with complete D-MEM and filtered again to make conditioned medium. The cells were resuspended in serum free medium at an approximate density of $5x10^6$ cells/mL, passed through a Falcon® 70 µm cell strainer and kept on ice until sorting.

FACS was performed by Mr Graeme Robertson from the Roslin Institute Bio-Imaging facility. Cells were sorted so that each well of a 96-well plate contained a single cell in 100 µL conditioned medium and were incubated at 37°C in 5% CO_2. Cells were checked by microscopy every 24 hours. After 1 week cells that had survived and divided were detached using 0.25% trypsin-EDTA solution and resuspended in 1 mL conditioned medium. Resuspended cells were seeded into two wells of a 24-well plate and incubated at 37°C in 5% CO_2. When cells reached 70-80% confluency, one well was passaged into a t25 flask and the other was lysed with 150 µL/well 2X Laemmli sample buffer (10% DTT). Cell lysates were stored at -20°C prior to screening for Jmjd6 expression by western blot. Populations determined to be Jmjd6 negative were then passaged as wild type A549 cells.

6.2.3. Virus work

6.2.3.1. Generation of P0 stocks

Wild type influenza A/Puerto Rico/8/1934 H1N1 (PR8) was rescued as previously described using an eight plasmid reverse genetics system (de Wit *et al.*, 2004). This system uses eight pDUAL plasmid vectors (**Table 6.3**), each encoding a single IAV genome segment, transfected into 70-80% confluent monolayers of HEK293T cells in 6-well plates. Briefly, 250 ng of each plasmid was diluted in 100 µL Opti-MEM and 4 µL Lipofectamine2000 was separately mixed with 100 µL Opti-MEM. Following 5 minutes incubation at room temperature, these were mixed gently and incubated for a further 20 minutes at room temperature. The HEK293T cells were washed once with PBS and overlaid with 800 µL transfection medium. The Lipofectamine2000/ DNA/ Opti-MEM mixture was dripped slowly over the cells and incubated overnight at 37°C in 5% CO_2. The following day, the transfection medium was replaced with 2 mL virus growth medium and the cells were incubated for a further 48 hours at 37°C in 5% CO_2. Cell supernatant was harvested and cleared by low-speed centrifugation (5

minutes at 1500 rpm), giving a “passage zero” (P0) viral stock which was aliquoted and stored at -80°C to be used to make a P1 virus stock.

6.2.3.2. Generation of P1 stocks

A first passage (P1) PR8 stock was generated using confluent monolayers of MDCK cells in T75 flasks. Cells were washed twice with PBS, inoculated with 200 µL of the P0 stock diluted in 2 mL serum free medium and incubated for 1 hour at 37°C in 5% CO_2. The cells were overlaid with 18 mL serum free medium and incubated for a further 48 hours at 37°C. Supernatants were harvested and cleared by centrifugation at 3000 rpm for 5 minutes at 4°C. P1 stocks were aliquoted and stored at -80 °C.

6.2.3.3. Growth of virus in embryonated chicken eggs

P0 viral stocks were obtained as described above and 100 µL used to infect 10-day old embryonated chicken eggs (Henry Stewart & Co.) via the allantoic cavity. Mock-infected eggs were inoculated with 100 µL of serum free medium. Eggs were incubated for 48 hours at 37ºC with 40-50% humidity. Prior to infection, eggs were candled to check viability of the embryo. The shell was sterilised with 70% ethanol (v/v) and a small hole was punctured in the egg shell, just below the line of the air sac. Using a 1 mL syringe and 25 gauge needle, P0 virus stock or serum free medium was inoculated into the allantoic cavity via this hole. The punctures were sealed with Scotch Magic Tape and eggs were incubated for a further 48 hours at 37°C in 40-50% humidity.

Eggs were culled by chilling overnight at 4ºC. The top of the shell was removed using curved forceps and the air sac membrane was punctured using a P1000 Gilson tip. Allantoic fluid was collected using a P1000 Gilson, clarified at 4000 rpm for 10 minutes and aliquoted and stored at -80°C until further use.

6.2.3.4. Quantification of virus by plaque assay

Viral titre determination was performed on monolayers of MDCK cells, which were seeded in 6-well plates in complete D-MEM and grown to 100% confluence. Virus P1 or supernatant from virally infected cells was serially diluted 10-fold (10^{-1} to 10^{-8}) in serum free medium. Prior to infection, cells were washed once with PBS and infected with 500 µL of virus dilutions per well. Cells were incubated with the virus dilutions for 1 hour at 37°C in 5% CO_2, then overlaid with Avicel overlay (virus growth medium supplemented with 1.2% (w/v) Avicel, 0.14% BSA and 1 µg/mL TPCK-treated trypsin). Following 48 hours incubation at 37°C, cells were fixed with 2 mL of 10% neutral buffer formalin (NBF) per well for 1 hour at room temperature. The NBF and remaining Avicel overlay were removed and the cells stained with 0.1% Toluidine blue. After 20 minutes to 1 hour incubation at room temperature, staining solution was rinsed under tap water, plates were air dried and plaques were counted. The value for plaque forming unit (pfu)/mL was determined by multiplying the plaques per well by 2 and then by the dilution factor of that well.

6.2.3.5. Viral infections

A549 cells were either seeded in to 24-well plates the day prior to infection to achieve approximately 90% confluence on the day of infection, or seeded and transfected with siRNA as described above. Cells were washed once with PBS to remove FBS. Virus stocks were diluted in serum free medium to the required MOI and 100 µL was applied to cells for 1 hour at 37°C in 5% CO_2.

For multi-cycle infections (MOI 0.01 and MOI 0.001), inoculum was removed and cells were overlaid with 1 mL virus growth medium. For single-cycle infections (MOI 5 and MOI 1), inoculum was aspirated, 250 µL acid wash buffer (10 mM HCl, 150 mM NaCl, pH3) was applied for 1 minute to inactivate non-internalised particles, and cells were washed three times with PBS. Single-cycle infections for which measurement of IFN

secretion by HEK-Blue^{TM} type I IFN assay was intended were overlaid with serum free medium supplemented with 0.14% (w/v) BSA. All other single-cycle infections were overlaid with virus growth medium, the make-up of which is described in section *6.1.6.1*.

Supernatants and cell lysates were harvested 1 hour post acid wash and at various time points post infection. Supernatants were harvested and stored at -80°C. Cells were washed once with PBS and lysed with 100 µL/well 2X Laemmli sample buffer (10% DTT). Cell lysates were stored at -20°C.

6.2.3.6. Minireplicon assays

HEK293T or X293T cells were seeded in 24-well plates to achieve 60-70% confluence the following day for transfection. Lipofectamine2000 (1 µL) was mixed with 50 µL Opti-MEM and incubated for 5-10 minutes. Separately, 50 ng pDUAL plasmids encoding PR8 PB2, PB1, PA and NP (abbreviated as 3PNP), along with 20 ng pPol I FF Luciferase and 50 ng of various overexpression pcDNA3.1 plasmids, or empty pcDNA3.1, were diluted in 50 µL Opti-MEM. As a negative control, transfections lacking the PB1 plasmid (empty vector was used to balance plasmid intake) were also performed (2PNP).

The Lipofectamine2000 mixture and the plasmid mixture were combined, gently mixed and incubated for 20 minutes at room temperature. Medium on the 293T cells was removed, the cells were washed once with PBS and overlaid with 500 µL Opti-MEM. The Lipofectamine2000/ DNA/ Opti-MEM mixture (100 µL total) was dripped slowly over the cells. Following 24 hours incubation at 37°C in 5% CO_2, the transfection mixture was removed, the cells were overlaid with complete D-MEM and incubated for a further 24 hours at 37°C in 5% CO_2.

Medium was removed and 150 µL Reporter Lysis Buffer (Promega) added per well, cells were lysed by freezing and thawing, and lysates were collected into clean tubes. Lysates were clarified by centrifugation at 3000 rpm for 5 minutes at 4°C. The supernatant was removed, 60 µL was transferred to an opaque-walled 96-well plate and an equal volume of Luciferase Assay Reagent (Promega) was added. Luminescence was immediately read using a micro plate reader (BioTek) and Gen5 software.

6.2.4. Protein Analysis

6.2.4.1. SDS-PAGE

Proteins were separated using sodium dodecyl sulphate polyacrylamide gel electrophoresis (SDS-PAGE). Both precast polyacrylamide gels (BioRad) and polyacrylamide gels made in-house were used. Stacking gels were cast at 4% (v/v) acrylamide and resolving gels were cast at various acrylamide concentrations (7-15%) depending on the size of the proteins being separated. Both were prepared using reagents supplied by Protogel according to the manufacturer's instructions; recipes for these are shown in section *6.1.6.4.2*.

Prior to SDS-PAGE, cell lysates were heated at 95 °C for 5 minutes, vortexed briefly and centrifuged for 1 minute. Each lane was loaded with 5-20 µL of sample and 3 µL of Precision Plus Dual Colour Molecular Weight Marker (BioRad) was added to the end lanes. All electrophoresis was performed in a Bio-Rad tank (Mini-Protean tetra system) at 80 V for 30 minutes to cross the stacking gel, followed by 120 V for the desired length of time.

6.2.4.2. Western blotting

Proteins separated by SDS-PAGE were transferred to 0.45 µm nitrocellulose membrane using the Transfer-blot® Turbo™ semi-dry transfer system (BioRad) according to the manufacturer's instructions (2.5 A, 25.0 V for 7 minutes). Membranes

were blocked for at least 1 hour with 5% (w/v) milk blocking buffer (described above in section *6.1.6.4.3*) and probed with a primary antibody diluted in blocking buffer overnight at 4°C on a platform rocker. Membranes were washed 3 times for 5 minutes in PBST and incubated at room temperature for 45-60 minutes with secondary antibody (**Table 6.6**) diluted in blocking buffer. Membranes were again washed 3 times for 5 minutes and imaged using a LI-COR Odyssey Fc Imaging System and LI-COR Image Studio version 5.2.5 software.

6.2.4.3. Densitometry

Protein quantification following western blotting was determined by densitometry using the LI-COR Image Studio Lite version 5.2.5 software.

6.2.5. HEK-Blue™ type I interferon assays

Positive controls were acquired for each experiment by transfecting cells with polyinosinic:polycytidylic acid (poly I:C) to induce a type I IFN response via the RIG-I pathway. Confluent A549 cells in 24-well plates were overlaid with transfection medium. Poly I:C (5 µg) and 2 µL Lipofectamine2000 were separately diluted in 100 µL Opti-MEM and incubated at room temperature for 5 minutes. The two mixtures were combined, gently mixed and incubated at room temperature for 20 minutes. The poly I:C/ Lipofectamine2000/ Opti-MEM mixture was dripped slowly over the cells. After 6 hours incubation at 37°C in 5% CO_2, supernatants were harvested and stored at -80°C. Cells were washed once with PBS and lysed with 100 µL/well 2X Laemmli sample buffer (10% DTT). Cell lysates were stored at -20°C.

Cell supernatants harvested from experiments described above in sections 6.2.2.4 and 6.2.3.5 were thawed on ice. Samples from infection experiments were UV-treated to inactivate infectious virus particles by transferring 300 µL of sample to a 24-well plate, kept on ice with lid removed, and treating at 120000 µJ/cm^2 for 10 minutes in a

CL-1000 Ultraviolet Crosslinker. Inactivation of the virus was confirmed by plaque assay.

HEK-Blue™ cells were suspended in complete D-MEM at 2.8 x 10^5 cells/mL and180 µL of cell suspension was added to 20 µL of either original or UV-inactivated samples in 96-well. An IFN standard curve was produced by incubating known quantities of universal type I IFN (Bio-Techne) alongside experimental samples. After 24 hours incubation at 37°C in 5% CO_2, 20 µL of HEK-Blue™ cell supernatant was transferred to 180 µL of QUANTI-Blue™ reagent (InvivoGen) in a separate 96-well plate and incubated for 1 hour at 37°C. Absorbance values at 600 nm were acquired using a GLOMAX® multidetection system.

6.2.6. Alignment of cDNA and protein sequences

In order to assess potential siRNA and antibody cross reactivity between the proteins in the IGF2BP family, alignments of protein and cDNA sequences of the genes were generated and analysed. Protein sequences were exported from UniProt and cDNA sequences were exported from Ensembl. Alignments were generated using Clustal Omega (https://www.ebi.ac.uk/Tools/msa/clustalo/) and exported to Jalview 2.11.0 (https://www.jalview.org/development/release-history/Jalview-2110). Identity and similarity was calculated using the Sequence Manipulation Suite (version 2) Ident and Sim online analysis tool from bioinformatics.org (https://www.bioinformatics.org/sms2/ident_sim.html). Identification numbers for the genes are shown in **Table 6.10**.

Table 6.10 IGF2BP gene and protein sequence identification numbers.

Gene	Ensembl gene ID	NCBI Reference Sequence	UniProt Accession number
IGF2BP1	ENSG00000159217	NM_006546.4	Q9NZI8-1 (Canonical sequence: 577aa)
IGF2BP2	ENSG00000073792	NM_006548.6	Q9Y6M1-2 (Canonical sequence: 599aa)

Gene	Ensembl gene ID	NCBI Reference Sequence	UniProt Accession number
IGF2BP3	ENSG00000136231	NM_006547.3	O00425-1 (Canonical sequence: 579aa)

6.2.7. Statistical analysis

Statistical analysis was performed using GraphPad Prism 8 Software.

Chapter 7: Bibliography

Abbas, Y. M., Pichlmair, A., Górna, M. W., Superti-Furga, G. & Nagar, B. (2013) Structural basis for viral 5'-PPP-RNA recognition by human IFIT proteins. *Nature*, 494(7435), 60-4.

Abcam (2021) *Will this antibody cross-react?* Available online: https://www.abcam.com/help/will-this-antibody-cross-react [Accessed 2022].

Abdoli, A., Soleimanjahi, H., Tavassoti Kheiri, M., Jamali, A. & Jamaati, A. (2013) Determining influenza virus shedding at different time points in madin-darby canine kidney cell line. *Cell J*, 15(2), 130-5.

Akarsu, H., Burmeister, W. P., Petosa, C., Petit, I., Müller, C. W., Ruigrok, R. W. & Baudin, F. (2003) Crystal structure of the M1 protein-binding domain of the influenza A virus nuclear export protein (NEP/NS2). *Embo j*, 22(18), 4646-55.

Alahari, S., Post, M. & Caniggia, I. (2015) Jumonji Domain Containing Protein 6: A Novel Oxygen Sensor in the Human Placenta. *Endocrinology*, 156(8), 3012-25.

Ali, A., Avalos, R. T., Ponimaskin, E. & Nayak, D. P. (2000) Influenza virus assembly: effect of influenza virus glycoproteins on the membrane association of M1 protein. *J Virol*, 74(18), 8709-19.

Amorim, M. J., Bruce, E. A., Read, E. K., Foeglein, A., Mahen, R., Stuart, A. D. & Digard, P. (2011) A Rab11- and microtubule-dependent mechanism for cytoplasmic transport of influenza A virus viral RNA. *J Virol*, 85(9), 4143-56.

Amorim, M. J. & Digard, P. (2006) Influenza A virus and the cell nucleus. *Vaccine*, 24(44-46), 6651-5.

Amorim, M. J., Read, E. K., Dalton, R. M., Medcalf, L. & Digard, P. (2007) Nuclear export of influenza A virus mRNAs requires ongoing RNA polymerase II activity. *Traffic*, 8(1), 1-11.

Anderson, S. G., Burnet, F. M. & et al. (1948) Mucins and mucoids in relation to influenza virus action; general discussion. *Aust J Exp Biol Med Sci*, 26(Pt 5), 403-11.

Ank, N., West, H., Bartholdy, C., Eriksson, K., Thomsen, A. R. & Paludan, S. R. (2006) Lambda interferon (IFN-lambda), a type III IFN, is induced by viruses and IFNs and displays potent antiviral activity against select virus infections in vivo. *J Virol*, 80(9), 4501-9.

Aravind, L. & Koonin, E. V. (1999) G-patch: a new conserved domain in eukaryotic RNA-processing proteins and type D retroviral polyproteins. *Trends Biochem Sci*, 24(9), 342-4.

Arnon, T. I., Achdout, H., Lieberman, N., Gazit, R., Gonen-Gross, T., Katz, G., Bar-Ilan, A., Bloushtain, N., Lev, M., Joseph, A., Kedar, E., Porgador, A. & Mandelboim, O. (2004) The mechanisms controlling the recognition of tumor- and virus-infected cells by NKp46. *Blood*, 103(2), 664-72.

Arnon, T. I., Lev, M., Katz, G., Chernobrov, Y., Porgador, A. & Mandelboim, O. (2001) Recognition of viral hemagglutinins by NKp44 but not by NKp30. *Eur J Immunol*, 31(9), 2680-9.

Au, W. C., Moore, P. A., LaFleur, D. W., Tombal, B. & Pitha, P. M. (1998) Characterization of the interferon regulatory factor-7 and its potential role in the transcription activation of interferon A genes. *J Biol Chem*, 273(44), 29210-7.

Bailey, C. C., Huang, I. C., Kam, C. & Farzan, M. (2012) Ifitm3 limits the severity of acute influenza in mice. *PLoS Pathog*, 8(9), e1002909.

Baillie, J. K. & Digard, P. (2013) Influenza--time to target the host? *N Engl J Med*, 369(2), 191-3.

Baranovich, T., Saito, R., Suzuki, Y., Zaraket, H., Dapat, C., Caperig-Dapat, I., Oguma, T., Shabana, II, Saito, T. & Suzuki, H. (2010) Emergence of H274Y oseltamivir-resistant A(H1N1) influenza viruses in Japan during the 2008-2009 season. *J Clin Virol*, 47(1), 23-8.

Barber, M. R., Aldridge, J. R., Jr., Webster, R. G. & Magor, K. E. (2010) Association of RIG-I with innate immunity of ducks to influenza. *Proc Natl Acad Sci U S A*, 107(13), 5913-8.

Barbosa, E. & Moss, B. (1978) mRNA(nucleoside-2'-)-methyltransferase from vaccinia virus. Purification and physical properties. *J Biol Chem*, 253(21), 7692-7.

Barman, S. & Nayak, D. P. (2000) Analysis of the transmembrane domain of influenza virus neuraminidase, a type II transmembrane glycoprotein, for apical sorting and raft association. *J Virol*, 74(14), 6538-45.

Basu, A., Shelke, V., Chadha, M., Kadam, D., Sangle, S., Gangodkar, S. & Mishra, A. (2011) Direct imaging of pH1N1 2009 influenza virus replication in alveolar pneumocytes in fatal cases by transmission electron microscopy. *J Electron Microsc (Tokyo)*, 60(1), 89-93.

Batista, P. J., Molinie, B., Wang, J., Qu, K., Zhang, J., Li, L., Bouley, D. M., Lujan, E., Haddad, B., Daneshvar, K., Carter, A. C., Flynn, R. A., Zhou, C., Lim, K. S., Dedon, P., Wernig, M., Mullen, A. C., Xing, Y., Giallourakis, C. C. & Chang, H. Y. (2014) m(6)A RNA modification controls cell fate transition in mammalian embryonic stem cells. *Cell Stem Cell*, 15(6), 707-19.

Baudin, F., Bach, C., Cusack, S. & Ruigrok, R. W. (1994) Structure of influenza virus RNP. I. Influenza virus nucleoprotein melts secondary structure in panhandle RNA and exposes the bases to the solvent. *Embo j*, 13(13), 3158-65.

Baudin, F., Petit, I., Weissenhorn, W. & Ruigrok, R. W. (2001) In vitro dissection of the membrane and RNP binding activities of influenza virus M1 protein. *Virology*, 281(1), 102-8.

Beaton, A. R. & Krug, R. M. (1981) Selected host cell capped RNA fragments prime influenza viral RNA transcription in vivo. *Nucleic Acids Res*, 9(17), 4423-36.

Beaulieu, A., Gravel, É., Cloutier, A., Marois, I., Colombo, É., Désilets, A., Verreault, C., Leduc, R., Marsault, É. & Richter, M. V. (2013) Matriptase proteolytically activates influenza virus and promotes multicycle replication in the human airway epithelium. *J Virol*, 87(8), 4237-51.

Bedford, M. T. & Clarke, S. G. (2009) Protein arginine methylation in mammals: who, what, and why. *Mol Cell*, 33(1), 1-13.

Bélanger, F., Stepinski, J., Darzynkiewicz, E. & Pelletier, J. (2010) Characterization of hMTr1, a human Cap1 2'-O-ribose methyltransferase. *J Biol Chem*, 285(43), 33037-33044.

Bell, J. L., Wächter, K., Mühleck, B., Pazaitis, N., Köhn, M., Lederer, M. & Hüttelmaier, S. (2013) Insulin-like growth factor 2 mRNA-binding proteins (IGF2BPs): post-transcriptional drivers of cancer progression? *Cell Mol Life Sci*, 70(15), 2657-75.

Benitez, A. A., Panis, M., Xue, J., Varble, A., Shim, J. V., Frick, A. L., López, C. B., Sachs, D. & tenOever, B. R. (2015) In Vivo RNAi Screening Identifies MDA5 as a Significant Contributor to the Cellular Defense against Influenza A Virus. *Cell Rep*, 11(11), 1714-26.

Bhagwat, A. R., Le Sage, V., Nturibi, E., Kulej, K., Jones, J., Guo, M., Tae Kim, E., Garcia, B. A., Weitzman, M. D., Shroff, H. & Lakdawala, S. S. (2020) Quantitative live cell imaging reveals influenza virus manipulation of Rab11A transport through reduced dynein association. *Nat Commun*, 11(1), 23.

Bhardwaj, N., Bender, A., Gonzalez, N., Bui, L. K., Garrett, M. C. & Steinman, R. M. (1994) Influenza virus-infected dendritic cells stimulate strong proliferative and cytolytic responses from human CD8+ T cells. *J Clin Invest*, 94(2), 797-807.

Blaas, D., Patzelt, E. & Kuechler, E. (1982) Identification of the cap binding protein of influenza virus. *Nucleic Acids Res*, 10(15), 4803-12.

Bloom, J. D., Gong, L. I. & Baltimore, D. (2010) Permissive secondary mutations enable the evolution of influenza oseltamivir resistance. *Science*, 328(5983), 1272-5.

Boeckel, J. N., Guarani, V., Koyanagi, M., Roexe, T., Lengeling, A., Schermuly, R. T., Gellert, P., Braun, T., Zeiher, A. & Dimmeler, S. (2011) Jumonji domain-containing protein 6 (Jmjd6) is required for angiogenic sprouting and regulates splicing of VEGF-receptor 1. *Proc Natl Acad Sci U S A*, 108(8), 3276-81.

Bokar, J. A., Rath-Shambaugh, M. E., Ludwiczak, R., Narayan, P. & Rottman, F. (1994) Characterization and partial purification of mRNA N6-adenosine methyltransferase from HeLa cell nuclei. Internal mRNA methylation requires a multisubunit complex. *J Biol Chem*, 269(26), 17697-704.

Bokar, J. A., Shambaugh, M. E., Polayes, D., Matera, A. G. & Rottman, F. M. (1997) Purification and cDNA cloning of the AdoMet-binding subunit of the human mRNA (N6-adenosine)-methyltransferase. *Rna*, 3(11), 1233-47.

Böse, J., Gruber, A. D., Helming, L., Schiebe, S., Wegener, I., Hafner, M., Beales, M., Köntgen, F. & Lengeling, A. (2004) The phosphatidylserine receptor has essential functions during embryogenesis but not in apoptotic cell removal. *J Biol*, 3(4), 15.

Böttcher-Friebertshäuser, E., Freuer, C., Sielaff, F., Schmidt, S., Eickmann, M., Uhlendorff, J., Steinmetzer, T., Klenk, H. D. & Garten, W. (2010) Cleavage of influenza virus hemagglutinin by airway proteases TMPRSS2 and HAT differs in subcellular localization and susceptibility to protease inhibitors. *J Virol*, 84(11), 5605-14.

Böttcher-Friebertshäuser, E., Klenk, H. D. & Garten, W. (2013) Activation of influenza viruses by proteases from host cells and bacteria in the human airway epithelium. *Pathog Dis*, 69(2), 87-100.

Böttcher, E., Matrosovich, T., Beyerle, M., Klenk, H. D., Garten, W. & Matrosovich, M. (2006) Proteolytic activation of influenza viruses by serine proteases TMPRSS2 and HAT from human airway epithelium. *J Virol*, 80(19), 9896-8.

Bouloy, M., Plotch, S. J. & Krug, R. M. (1978) Globin mRNAs are primers for the transcription of influenza viral RNA in vitro. *Proc Natl Acad Sci U S A*, 75(10), 4886-90.

Bouloy, M., Plotch, S. J. & Krug, R. M. (1980) Both the 7-methyl and the 2'-O-methyl groups in the cap of mRNA strongly influence its ability to act as primer for influenza virus RNA transcription. *Proc Natl Acad Sci U S A*, 77(7), 3952-6.

Bourmakina, S. V. & García-Sastre, A. (2003) Reverse genetics studies on the filamentous morphology of influenza A virus. *J Gen Virol*, 84(Pt 3), 517-27.

Braam, J., Ulmanen, I. & Krug, R. M. (1983) Molecular model of a eucaryotic transcription complex: functions and movements of influenza P proteins during capped RNA-primed transcription. *Cell*, 34(2), 609-18.

Brass, A. L., Huang, I. C., Benita, Y., John, S. P., Krishnan, M. N., Feeley, E. M., Ryan, B. J., Weyer, J. L., van der Weyden, L., Fikrig, E., Adams, D. J., Xavier, R. J., Farzan, M. & Elledge, S. J. (2009) The IFITM proteins mediate cellular resistance to influenza A H1N1 virus, West Nile virus, and dengue virus. *Cell*, 139(7), 1243-54.

Bruce, E. A., Digard, P. & Stuart, A. D. (2010) The Rab11 pathway is required for influenza A virus budding and filament formation. *J Virol*, 84(12), 5848-59.

Buchholz, U. J., Finke, S. & Conzelmann, K. K. (1999) Generation of bovine respiratory syncytial virus (BRSV) from cDNA: BRSV NS2 is not essential for virus replication in tissue culture, and the human RSV leader region acts as a functional BRSV genome promoter. *J Virol*, 73(1), 251-9.

Bui, M., Whittaker, G. & Helenius, A. (1996) Effect of M1 protein and low pH on nuclear transport of influenza virus ribonucleoproteins. *J Virol*, 70(12), 8391-401.

Bujnicki, J. M., Feder, M., Radlinska, M. & Blumenthal, R. M. (2002) Structure prediction and phylogenetic analysis of a functionally diverse family of proteins homologous to the MT-A70 subunit of the human mRNA:m(6)A methyltransferase. *J Mol Evol*, 55(4), 431-44.

Bullough, P. A., Hughson, F. M., Skehel, J. J. & Wiley, D. C. (1994) Structure of influenza haemagglutinin at the pH of membrane fusion. *Nature*, 371(6492), 37-43.

Byszewska, M., Śmietański, M., Purta, E. & Bujnicki, J. M. (2014) RNA methyltransferases involved in 5' cap biosynthesis. *RNA Biol*, 11(12), 1597-607.

Calder, L. J., Wasilewski, S., Berriman, J. A. & Rosenthal, P. B. (2010) Structural organization of a filamentous influenza A virus. *Proc Natl Acad Sci U S A*, 107(23), 10685-90.

Campbell, P. J., Danzy, S., Kyriakis, C. S., Deymier, M. J., Lowen, A. C. & Steel, J. (2014) The M segment of the 2009 pandemic influenza virus confers increased neuraminidase activity, filamentous morphology, and efficient contact transmissibility to A/Puerto Rico/8/1934-based reassortant viruses. *J Virol*, 88(7), 3802-14.

Cao, S., Liu, X., Yu, M., Li, J., Jia, X., Bi, Y., Sun, L., Gao, G. F. & Liu, W. (2012) A nuclear export signal in the matrix protein of Influenza A virus is required for efficient virus replication. *J Virol*, 86(9), 4883-91.

Cao, Y., Zhang, K., Liu, L., Li, W., Zhu, B., Zhang, S., Xu, P., Liu, W. & Li, J. (2019) Global transcriptome analysis of H5N1 influenza virus-infected human cells. *Hereditas*, 156, 10.

Carr, S. M., Carnero, E., García-Sastre, A., Brownlee, G. G. & Fodor, E. (2006) Characterization of a mitochondrial-targeting signal in the PB2 protein of influenza viruses. *Virology*, 344(2), 492-508.

Carrasco, M., Amorim, M. J. & Digard, P. (2004) Lipid raft-dependent targeting of the influenza A virus nucleoprotein to the apical plasma membrane. *Traffic*, 5(12), 979-92.

Carrique, L., Fan, H., Walker, A. P., Keown, J. R., Sharps, J., Staller, E., Barclay, W. S., Fodor, E. & Grimes, J. M. (2020) Host ANP32A mediates the assembly of the influenza virus replicase. *Nature*, 587(7835), 638-43.

Chaipan, C., Kobasa, D., Bertram, S., Glowacka, I., Steffen, I., Tsegaye, T. S., Takeda, M., Bugge, T. H., Kim, S., Park, Y., Marzi, A. & Pöhlmann, S. (2009) Proteolytic activation of the 1918 influenza virus hemagglutinin. *J Virol*, 83(7), 3200-11.

Chang, B., Chen, Y., Zhao, Y. & Bruick, R. K. (2007) JMJD6 is a histone arginine demethylase. *Science*, 318(5849), 444-7.

Chen, B. J., Leser, G. P., Jackson, D. & Lamb, R. A. (2008) The influenza virus M2 protein cytoplasmic tail interacts with the M1 protein and influences virus assembly at the site of virus budding. *J Virol*, 82(20), 10059-70.

Chen, B. J., Leser, G. P., Morita, E. & Lamb, R. A. (2007) Influenza virus hemagglutinin and neuraminidase, but not the matrix protein, are required for assembly and budding of plasmid-derived virus-like particles. *J Virol*, 81(13), 7111-23.

Chen, C. F., Feng, X., Liao, H. Y., Jin, W. J., Zhang, J., Wang, Y., Gong, L. L., Liu, J. J., Yuan, X. H., Zhao, B. B., Zhang, D., Chen, G. F., Wan, Y., Guo, J., Yan, H. P. & He, Y. W. (2014) Regulation of T cell proliferation by JMJD6 and PDGF-BB during chronic hepatitis B infection. *Sci Rep*, 4, 6359.

Chen, K., Lu, Z., Wang, X., Fu, Y., Luo, G. Z., Liu, N., Han, D., Dominissini, D., Dai, Q., Pan, T. & He, C. (2015a) High-resolution N(6) -methyladenosine (m(6) A) map using photo-crosslinking-assisted m(6) A sequencing. *Angew Chem Int Ed Engl*, 54(5), 1587-90.

Chen, W., Calvo, P. A., Malide, D., Gibbs, J., Schubert, U., Bacik, I., Basta, S., O'Neill, R., Schickli, J., Palese, P., Henklein, P., Bennink, J. R. & Yewdell, J. W. (2001) A novel influenza A virus mitochondrial protein that induces cell death. *Nat Med*, 7(12), 1306-12.

Chen, X., Liu, S., Goraya, M. U., Maarouf, M., Huang, S. & Chen, J. L. (2018) Host Immune Response to Influenza A Virus Infection. *Front Immunol*, 9, 320.

Chen, Y., Zhou, J., Cheng, Z., Yang, S., Chu, H., Fan, Y., Li, C., Wong, B. H., Zheng, S., Zhu, Y., Yu, F., Wang, Y., Liu, X., Gao, H., Yu, L., Tang, L., Cui, D., Hao, K., Bossé, Y., Obeidat, M., Brandsma, C. A., Song, Y. Q., To, K. K., Sham, P. C., Yuen, K. Y. & Li, L. (2015b) Functional variants regulating LGALS1 (Galectin 1) expression affect human susceptibility to influenza A(H7N9). *Sci Rep*, 5, 8517.

Cheung, P. H., Lee, T. T., Kew, C., Chen, H., Yuen, K. Y., Chan, C. P. & Jin, D. Y. (2020) Virus subtype-specific suppression of MAVS aggregation and activation by PB1-F2 protein of influenza A (H7N9) virus. *PLoS Pathog*, 16(6), e1008611.

Chiu, C., Ellebedy, A. H., Wrammert, J. & Ahmed, R. (2015) B cell responses to influenza infection and vaccination. *Curr Top Microbiol Immunol*, 386, 381-98.

Chlanda, P., Schraidt, O., Kummer, S., Riches, J., Oberwinkler, H., Prinz, S., Kräusslich, H. G. & Briggs, J. A. (2015) Structural Analysis of the Roles of Influenza A Virus Membrane-Associated Proteins in Assembly and Morphology. *J Virol*, 89(17), 8957-66.

Chou, Y. C., Lai, M. M., Wu, Y. C., Hsu, N. C., Jeng, K. S. & Su, W. C. (2015) Variations in genome-wide RNAi screens: lessons from influenza research. *J Clin Bioinforma*, 5, 2.

Chou, Y. Y., Heaton, N. S., Gao, Q., Palese, P., Singer, R. H. & Lionnet, T. (2013) Colocalization of different influenza viral RNA segments in the cytoplasm before viral budding as shown by single-molecule sensitivity FISH analysis. *PLoS Pathog*, 9(5), e1003358.

Choudhury, N. R., Trus, I., Heikel, G., Wolczyk, M., Szymanski, J., Bolembach, A., Dos Santos Pinto, R. M., Smith, N., Trubitsyna, M., Gaunt, E., Digard, P. & Michlewski, G. (2022) TRIM25 inhibits influenza A virus infection, destabilizes viral mRNA, but is redundant for activating the RIG-I pathway. *Nucleic Acids Res*, 50(12), 7097-114.

Chu, C. M., Dawson, I. M. & Elford, W. J. (1949) Filamentous forms associated with newly isolated influenza virus. *Lancet*, 1(6554), 602.

Chutiwitoonchai, N. & Aida, Y. (2016) NXT1, a Novel Influenza A NP Binding Protein, Promotes the Nuclear Export of NP via a CRM1-Dependent Pathway. *Viruses*, 8(8).

Cikala, M., Alexandrova, O., David, C. N., Proschel, M., Stiening, B., Cramer, P. & Bottger, A. (2004) The phosphatidylserine receptor from Hydra is a nuclear protein with potential Fe(II) dependent oxygenase activity. *BMC Cell Biol*, 5, 26.

Clements, A. L., Peacock, T. P., Sealy, J. E., Lee, H. M., Hussain, S., Sadeyen, J. R., Shelton, H., Digard, P. & Iqbal, M. (2021) PA-X is an avian virulence factor in H9N2 avian influenza virus. *J Gen Virol*, 102(3).

Clohisey, S. & Baillie, J. K. (2019) Host susceptibility to severe influenza A virus infection. *Crit Care*, 23(1), 303.

Cohen, M., Zhang, X. Q., Senaati, H. P., Chen, H. W., Varki, N. M., Schooley, R. T. & Gagneux, P. (2013) Influenza A penetrates host mucus by cleaving sialic acids with neuraminidase. *Virol J*, 10, 321.

Colman, P. M. (1994) Influenza virus neuraminidase: structure, antibodies, and inhibitors. *Protein Sci*, 3(10), 1687-96.

Colman, P. M., Varghese, J. N. & Laver, W. G. (1983) Structure of the catalytic and antigenic sites in influenza virus neuraminidase. *Nature*, 303(5912), 41-4.

Coloma, R., Valpuesta, J. M., Arranz, R., Carrascosa, J. L., Ortín, J. & Martín-Benito, J. (2009) The structure of a biologically active influenza virus ribonucleoprotein complex. *PLoS Pathog*, 5(6), e1000491.

Compans, R. W., Content, J. & Duesberg, P. H. (1972) Structure of the ribonucleoprotein of influenza virus. *J Virol*, 10(4), 795-800.

Compans, R. W., Klenk, H. D., Caliguiri, L. A. & Choppin, P. W. (1970) Influenza virus proteins. I. Analysis of polypeptides of the virion and identification of spike glycoproteins. *Virology*, 42(4), 880-9.

Costa, T., Chaves, A. J., Valle, R., Darji, A., van Riel, D., Kuiken, T., Majó, N. & Ramis, A. (2012) Distribution patterns of influenza virus receptors and viral attachment patterns in the respiratory and intestinal tracts of seven avian species. *Vet Res*, 43(1), 28.

Courtney, D. G., Kennedy, E. M., Dumm, R. E., Bogerd, H. P., Tsai, K., Heaton, N. S. & Cullen, B. R. (2017) Epitranscriptomic Enhancement of Influenza A Virus Gene Expression and Replication. *Cell Host Microbe*, 22(3), 377-386.e5.

Cros, J. F., García-Sastre, A. & Palese, P. (2005) An unconventional NLS is critical for the nuclear import of the influenza A virus nucleoprotein and ribonucleoprotein. *Traffic*, 6(3), 205-13.

Cui, P., Qin, B., Liu, N., Pan, G. & Pei, D. (2004) Nuclear localization of the phosphatidylserine receptor protein via multiple nuclear localization signals. *Exp Cell Res*, 293(1), 154-63.

Cui, S., Eisenächer, K., Kirchhofer, A., Brzózka, K., Lammens, A., Lammens, K., Fujita, T., Conzelmann, K. K., Krug, A. & Hopfner, K. P. (2008) The C-terminal regulatory domain is the RNA 5'-triphosphate sensor of RIG-I. *Mol Cell*, 29(2), 169-79.

Dadonaite, B., Gilbertson, B., Knight, M. L., Trifkovic, S., Rockman, S., Laederach, A., Brown, L. E., Fodor, E. & Bauer, D. L. V. (2019) The structure of the influenza A virus genome. *Nat Microbiol*, 4(11), 1781-89.

Dadonaite, B., Vijayakrishnan, S., Fodor, E., Bhella, D. & Hutchinson, E. C. (2016) Filamentous influenza viruses. *J Gen Virol*, 97(8), 1755-64.

Daffis, S., Szretter, K. J., Schriewer, J., Li, J., Youn, S., Errett, J., Lin, T. Y., Schneller, S., Zust, R., Dong, H., Thiel, V., Sen, G. C., Fensterl, V., Klimstra, W. B., Pierson, T. C., Buller, R. M., Gale, M., Jr., Shi, P. Y. & Diamond, M. S. (2010) 2'-O methylation of the viral mRNA cap evades host restriction by IFIT family members. *Nature*, 468(7322), 452-6.

Dai, N., Rapley, J., Angel, M., Yanik, M. F., Blower, M. D. & Avruch, J. (2011) mTOR phosphorylates IMP2 to promote IGF2 mRNA translation by internal ribosomal entry. *Genes Dev*, 25(11), 1159-72.

Daniels, R., Kurowski, B., Johnson, A. E. & Hebert, D. N. (2003) N-linked glycans direct the cotranslational folding pathway of influenza hemagglutinin. *Mol Cell*, 11(1), 79-90.

Davies, W. L., Grunert, R. R., Haff, R. F., McGahen, J. W., Neumayer, E. M., Paulshock, M., Watts, J. C., Wood, T. R., Hermann, E. C. & Hoffmann, C. E. (1964) ANTIVIRAL ACTIVITY OF 1-ADAMANTANAMINE (AMANTADINE). *Science*, 144(3620), 862-3.

de Castro Martin, I. F., Fournier, G., Sachse, M., Pizarro-Cerda, J., Risco, C. & Naffakh, N. (2017) Influenza virus genome reaches the plasma membrane via a modified endoplasmic reticulum and Rab11-dependent vesicles. *Nat Commun*, 8(1), 1396.

de Marcken, M., Dhaliwal, K., Danielsen, A. C., Gautron, A. S. & Dominguez-Villar, M. (2019) TLR7 and TLR8 activate distinct pathways in monocytes during RNA virus infection. *Sci Signal*, 12(605).

de Rozières, C. M., Pequeno, A., Shahabi, S., Lucas, T. M., Godula, K., Ghosh, G. & Joseph, S. (2022) PABP1 Drives the Selective Translation of Influenza A Virus mRNA. *J Mol Biol*, 434(5), 167460.

de Vries, E., Tscherne, D. M., Wienholts, M. J., Cobos-Jiménez, V., Scholte, F., García-Sastre, A., Rottier, P. J. & de Haan, C. A. (2011) Dissection of the influenza A virus endocytic routes reveals macropinocytosis as an alternative entry pathway. *PLoS Pathog*, 7(3), e1001329.

de Weerd, N. A. & Nguyen, T. (2012) The interferons and their receptors--distribution and regulation. *Immunol Cell Biol*, 90(5), 483-91.

de Wit, E., Spronken, M. I., Bestebroer, T. M., Rimmelzwaan, G. F., Osterhaus, A. D. & Fouchier, R. A. (2004) Efficient generation and growth of influenza virus A/PR/8/34 from eight cDNA fragments. *Virus Res*, 103(1-2), 155-61.

Deeg, C. M., Hassan, E., Mutz, P., Rheinemann, L., Götz, V., Magar, L., Schilling, M., Kallfass, C., Nürnberger, C., Soubies, S., Kochs, G., Haller, O., Schwemmle, M. &

Staeheli, P. (2017) In vivo evasion of MxA by avian influenza viruses requires human signature in the viral nucleoprotein. *J Exp Med*, 214(5), 1239-48.

Deng, T., Engelhardt, O. G., Thomas, B., Akoulitchev, A. V., Brownlee, G. G. & Fodor, E. (2006a) Role of ran binding protein 5 in nuclear import and assembly of the influenza virus RNA polymerase complex. *J Virol*, 80(24), 11911-9.

Deng, T., Vreede, F. T. & Brownlee, G. G. (2006b) Different de novo initiation strategies are used by influenza virus RNA polymerase on its cRNA and viral RNA promoters during viral RNA replication. *J Virol*, 80(5), 2337-48.

Desrosiers, R., Friderici, K. & Rottman, F. (1974) Identification of methylated nucleosides in messenger RNA from Novikoff hepatoma cells. *Proc Natl Acad Sci U S A*, 71(10), 3971-5.

Desrosiers, R. C., Friderici, K. H. & Rottman, F. M. (1975) Characterization of Novikoff hepatoma mRNA methylation and heterogeneity in the methylated 5' terminus. *Biochemistry*, 14(20), 4367-74.

Devarkar, S. C., Wang, C., Miller, M. T., Ramanathan, A., Jiang, F., Khan, A. G., Patel, S. S. & Marcotrigiano, J. (2016) Structural basis for m7G recognition and 2'-O-methyl discrimination in capped RNAs by the innate immune receptor RIG-I. *Proc Natl Acad Sci U S A*, 113(3), 596-601.

Dharan, N. J., Gubareva, L. V., Meyer, J. J., Okomo-Adhiambo, M., McClinton, R. C., Marshall, S. A., St George, K., Epperson, S., Brammer, L., Klimov, A. I., Bresee, J. S. & Fry, A. M. (2009) Infections with oseltamivir-resistant influenza A(H1N1) virus in the United States. *Jama*, 301(10), 1034-41.

Di Lorenzo, A. & Bedford, M. T. (2011) Histone arginine methylation. *FEBS Lett*, 585(13), 2024-31.

Dias, A., Bouvier, D., Crépin, T., McCarthy, A. A., Hart, D. J., Baudin, F., Cusack, S. & Ruigrok, R. W. (2009) The cap-snatching endonuclease of influenza virus polymerase resides in the PA subunit. *Nature*, 458(7240), 914-8.

Diebold, S. S., Kaisho, T., Hemmi, H., Akira, S. & Reis e Sousa, C. (2004) Innate antiviral responses by means of TLR7-mediated recognition of single-stranded RNA. *Science*, 303(5663), 1529-31.

Digard, P., Blok, V. C. & Inglis, S. C. (1989) Complex formation between influenza virus polymerase proteins expressed in Xenopus oocytes. *Virology*, 171(1), 162-9.

Dittmann, J., Stertz, S., Grimm, D., Steel, J., García-Sastre, A., Haller, O. & Kochs, G. (2008) Influenza A virus strains differ in sensitivity to the antiviral action of Mx-GTPase. *J Virol*, 82(7), 3624-31.

Dominissini, D., Moshitch-Moshkovitz, S., Schwartz, S., Salmon-Divon, M., Ungar, L., Osenberg, S., Cesarkas, K., Jacob-Hirsch, J., Amariglio, N., Kupiec, M., Sorek, R. & Rechavi, G. (2012) Topology of the human and mouse m6A RNA methylomes revealed by m6A-seq. *Nature*, 485(7397), 201-6.

Doms, R. W., Lamb, R. A., Rose, J. K. & Helenius, A. (1993) Folding and assembly of viral membrane proteins. *Virology*, 193(2), 545-62.

Dong, L., Geng, Z., Liu, Z., Tao, M., Pan, M. & Lu, X. (2021) IGF2BP2 knockdown suppresses thyroid cancer progression by reducing the expression of long non-coding RNA HAGLR. *Pathol Res Pract*, 225, 153550.

Dou, D., Revol, R., Östbye, H., Wang, H. & Daniels, R. (2018) Influenza A Virus Cell Entry, Replication, Virion Assembly and Movement. *Front Immunol*, 9, 1581.

Doxtader, K. A., Wang, P., Scarborough, A. M., Seo, D., Conrad, N. K. & Nam, Y. (2018) Structural Basis for Regulation of METTL16, an S-Adenosylmethionine Homeostasis Factor. *Mol Cell*, 71(6), 1001-1011.e4.

Doyle, G. A., Betz, N. A., Leeds, P. F., Fleisig, A. J., Prokipcak, R. D. & Ross, J. (1998) The c-myc coding region determinant-binding protein: a member of a family of KH domain RNA-binding proteins. *Nucleic Acids Res*, 26(22), 5036-44.

Drexler, H. G. & Uphoff, C. C. (2002) Mycoplasma contamination of cell cultures: Incidence, sources, effects, detection, elimination, prevention. *Cytotechnology*, 39(2), 75-90.

Du, H., Zhao, Y., He, J., Zhang, Y., Xi, H., Liu, M., Ma, J. & Wu, L. (2016) YTHDF2 destabilizes m(6)A-containing RNA through direct recruitment of the CCR4-NOT deadenylase complex. *Nat Commun*, 7, 12626.

Du, Y., Yang, F., Wang, Q., Xu, N., Xie, Y., Chen, S., Qin, T. & Peng, D. (2020) Influenza a virus antagonizes type I and type II interferon responses via SOCS1-dependent ubiquitination and degradation of JAK1. *Virol J*, 17(1), 74.

Dudek, S. E., Wixler, L., Nordhoff, C., Nordmann, A., Anhlan, D., Wixler, V. & Ludwig, S. (2011) The influenza virus PB1-F2 protein has interferon antagonistic activity. *Biol Chem*, 392(12), 1135-44.

Egloff, M. P., Benarroch, D., Selisko, B., Romette, J. L. & Canard, B. (2002) An RNA cap (nucleoside-2'-O-)-methyltransferase in the flavivirus RNA polymerase NS5: crystal structure and functional characterization. *Embo j*, 21(11), 2757-68.

Ehre, C., Worthington, E. N., Liesman, R. M., Grubb, B. R., Barbier, D., O'Neal, W. K., Sallenave, J. M., Pickles, R. J. & Boucher, R. C. (2012) Overexpressing mouse model demonstrates the protective role of Muc5ac in the lungs. *Proc Natl Acad Sci U S A*, 109(41), 16528-33.

Elton, D., Simpson-Holley, M., Archer, K., Medcalf, L., Hallam, R., McCauley, J. & Digard, P. (2001) Interaction of the influenza virus nucleoprotein with the cellular CRM1-mediated nuclear export pathway. *J Virol*, 75(1), 408-19.

Engelhardt, O. G., Smith, M. & Fodor, E. (2005) Association of the influenza A virus RNA-dependent RNA polymerase with cellular RNA polymerase II. *J Virol*, 79(9), 5812-8.

European Centre for Disease Prevention and Control (2022) *Factsheet about seasonal influenza* Available online: https://www.ecdc.europa.eu/en/seasonal-influenza/facts/factsheet [Accessed 2022].

Everitt, A. R., Clare, S., Pertel, T., John, S. P., Wash, R. S., Smith, S. E., Chin, C. R., Feeley, E. M., Sims, J. S., Adams, D. J., Wise, H. M., Kane, L., Goulding, D., Digard, P., Anttila, V., Baillie, J. K., Walsh, T. S., Hume, D. A., Palotie, A., Xue, Y., Colonna, V., Tyler-Smith, C., Dunning, J., Gordon, S. B., Smyth, R. L., Openshaw, P. J., Dougan, G., Brass, A. L. & Kellam, P. (2012) IFITM3 restricts the morbidity and mortality associated with influenza. *Nature*, 484(7395), 519-23.

Fadok, V. A., Bratton, D. L., Rose, D. M., Pearson, A., Ezekewitz, R. A. & Henson, P. M. (2000) A receptor for phosphatidylserine-specific clearance of apoptotic cells. *Nature*, 405(6782), 85-90.

Fakhraldeen, S. A., Clark, R. J., Roopra, A., Chin, E. N., Huang, W., Castorino, J., Wisinski, K. B., Kim, T., Spiegelman, V. S. & Alexander, C. M. (2015) Two Isoforms of the RNA Binding Protein, Coding Region Determinant-binding Protein (CRD-BP/IGF2BP1), Are Expressed in Breast Epithelium and Support Clonogenic Growth of Breast Tumor Cells. *J Biol Chem*, 290(21), 13386-400.

Fan, H., Walker, A. P., Carrique, L., Keown, J. R., Serna Martin, I., Karia, D., Sharps, J., Hengrung, N., Pardon, E., Steyaert, J., Grimes, J. M. & Fodor, E. (2019) Structures of influenza A virus RNA polymerase offer insight into viral genome replication. *Nature*, 573(7773), 287-290.

Farina, K. L., Huttelmaier, S., Musunuru, K., Darnell, R. & Singer, R. H. (2003) Two ZBP1 KH domains facilitate beta-actin mRNA localization, granule formation, and cytoskeletal attachment. *J Cell Biol*, 160(1), 77-87.

Feeley, E. M., Sims, J. S., John, S. P., Chin, C. R., Pertel, T., Chen, L. M., Gaiha, G. D., Ryan, B. J., Donis, R. O., Elledge, S. J. & Brass, A. L. (2011) IFITM3 inhibits influenza A virus infection by preventing cytosolic entry. *PLoS Pathog*, 7(10), e1002337.

Filarsky, M., Zillner, K., Araya, I., Villar-Garea, A., Merkl, R., Längst, G. & Németh, A. (2015) The extended AT-hook is a novel RNA binding motif. *RNA Biol*, 12(8), 864-76.

Fischer, A. A., Müller, K. & Scholtissek, C. (1990) Specific inhibition of the synthesis of influenza virus late proteins and stimulation of early, M2, and NS2 protein synthesis by 3-deazaadenosine. *Virology*, 177(2), 523-31.

Flerlage, T., Boyd, D. F., Meliopoulos, V., Thomas, P. G. & Schultz-Cherry, S. (2021) Influenza virus and SARS-CoV-2: pathogenesis and host responses in the respiratory tract. *Nat Rev Microbiol*, 19(7), 425-41.

Fodor, E. & Smith, M. (2004) The PA subunit is required for efficient nuclear accumulation of the PB1 subunit of the influenza A virus RNA polymerase complex. *J Virol*, 78(17), 9144-53.

Fonteneau, J. F., Gilliet, M., Larsson, M., Dasilva, I., Münz, C., Liu, Y. J. & Bhardwaj, N. (2003) Activation of influenza virus-specific CD4+ and CD8+ T cells: a new role for plasmacytoid dendritic cells in adaptive immunity. *Blood*, 101(9), 3520-6.

Forrest, A. R., Kawaji, H., Rehli, M., Baillie, J. K., de Hoon, M. J., Haberle, V., Lassmann, T., Kulakovskiy, I. V., Lizio, M., Itoh, M., Andersson, R., Mungall, C. J., Meehan, T. F., Schmeier, S., Bertin, N., Jørgensen, M., Dimont, E., Arner, E., Schmidl, C., Schaefer, U., Medvedeva, Y. A., Plessy, C., Vitezic, M., Severin, J., Semple, C., Ishizu, Y., Young, R. S., Francescatto, M., Alam, I., Albanese, D., Altschuler, G. M., Arakawa, T., Archer, J. A., Arner, P., Babina, M., Rennie, S., Balwierz, P. J., Beckhouse, A. G., Pradhan-Bhatt, S., Blake, J. A., Blumenthal, A., Bodega, B., Bonetti, A., Briggs, J., Brombacher, F., Burroughs, A. M., Califano, A., Cannistraci, C. V., Carbajo, D., Chen, Y., Chierici, M., Ciani, Y., Clevers, H. C., Dalla, E., Davis, C. A., Detmar, M., Diehl, A. D., Dohi, T., Drabløs, F., Edge, A. S., Edinger, M., Ekwall, K., Endoh, M., Enomoto, H., Fagiolini, M., Fairbairn, L., Fang, H., Farach-Carson, M. C., Faulkner, G. J., Favorov, A. V., Fisher, M. E., Frith, M. C., Fujita, R., Fukuda, S., Furlanello, C., Furino, M., Furusawa, J., Geijtenbeek, T. B., Gibson, A. P., Gingeras, T., Goldowitz, D., Gough, J., Guhl, S., Guler, R., Gustincich, S., Ha, T. J., Hamaguchi, M., Hara, M., Harbers, M., Harshbarger, J., Hasegawa, A., Hasegawa, Y., Hashimoto, T., Herlyn, M., Hitchens, K. J., Ho Sui, S. J., Hofmann, O. M., Hoof, I., Hori, F., Huminiecki, L., et al (2014) A promoter-level mammalian expression atlas. *Nature*, 507(7493), 462-70.

Fortes, P., Inada, T., Preiss, T., Hentze, M. W., Mattaj, I. W. & Sachs, A. B. (2000) The yeast nuclear cap binding complex can interact with translation factor eIF4G and mediate translation initiation. *Mol Cell*, 6(1), 191-6.

Fouchier, R. A., Munster, V., Wallensten, A., Bestebroer, T. M., Herfst, S., Smith, D., Rimmelzwaan, G. F., Olsen, B. & Osterhaus, A. D. (2005) Characterization of a novel influenza A virus hemagglutinin subtype (H16) obtained from black-headed gulls. *J Virol*, 79(5), 2814-22.

Fragaszy, E. B., Warren-Gash, C., White, P. J., Zambon, M., Edmunds, W. J., Nguyen-Van-Tam, J. S. & Hayward, A. C. (2018) Effects of seasonal and pandemic influenza on health-related quality of life, work and school absence in England: Results from the Flu Watch cohort study. *Influenza Other Respir Viruses*, 12(1), 171-82.

Fujikura, D. & Miyazaki, T. (2018) Programmed Cell Death in the Pathogenesis of Influenza. *Int J Mol Sci*, 19(7), 2065.

Fujioka, Y., Nishide, S., Ose, T., Suzuki, T., Kato, I., Fukuhara, H., Fujioka, M., Horiuchi, K., Satoh, A. O., Nepal, P., Kashiwagi, S., Wang, J., Horiguchi, M., Sato, Y., Paudel, S., Nanbo, A., Miyazaki, T., Hasegawa, H., Maenaka, K. & Ohba, Y. (2018) A Sialylated Voltage-Dependent Ca(2+) Channel Binds Hemagglutinin and Mediates Influenza A Virus Entry into Mammalian Cells. *Cell Host Microbe*, 23(6), 809-18.e5.

Fukuyama, S. & Kawaoka, Y. (2011) The pathogenesis of influenza virus infections: the contributions of virus and host factors. *Curr Opin Immunol*, 23(4), 481-6.

Furuichi, Y., LaFiandra, A. & Shatkin, A. J. (1977) 5'-Terminal structure and mRNA stability. *Nature*, 266(5599), 235-9.

Furuichi, Y., Morgan, M., Shatkin, A. J., Jelinek, W., Salditt-Georgieff, M. & Darnell, J. E. (1975) Methylated, blocked 5 termini in HeLa cell mRNA. *Proc Natl Acad Sci U S A*, 72(5), 1904-8.

Gack, M. U., Albrecht, R. A., Urano, T., Inn, K. S., Huang, I. C., Carnero, E., Farzan, M., Inoue, S., Jung, J. U. & García-Sastre, A. (2009) Influenza A virus NS1 targets the ubiquitin ligase TRIM25 to evade recognition by the host viral RNA sensor RIG-I. *Cell Host Microbe*, 5(5), 439-49.

Ganesan, M., Tikhanovich, I., Vangimalla, S. S., Dagur, R. S., Wang, W., Poluektova, L. I., Sun, Y., Mercer, D. F., Tuma, D., Weinman, S. A., Kharbanda, K. K. & Osna, N. A. (2018) Demethylase JMJD6 as a New Regulator of Interferon Signaling: Effects of HCV and Ethanol Metabolism. *Cell Mol Gastroenterol Hepatol*, 5(2), 101-12.

Gao, W. W., Xiao, R. Q., Peng, B. L., Xu, H. T., Shen, H. F., Huang, M. F., Shi, T. T., Yi, J., Zhang, W. J., Wu, X. N., Gao, X., Lin, X. Z., Dorrestein, P. C., Rosenfeld, M. G. & Liu, W. (2015) Arginine methylation of HSP70 regulates retinoid acid-mediated RARbeta2 gene activation. *Proc Natl Acad Sci U S A*, 112(26), E3327-36.

García-Sastre, A., Egorov, A., Matassov, D., Brandt, S., Levy, D. E., Durbin, J. E., Palese, P. & Muster, T. (1998) Influenza A virus lacking the NS1 gene replicates in interferon-deficient systems. *Virology*, 252(2), 324-30.

Garfinkel, M. S. & Katze, M. G. (1993) Translational control by influenza virus. Selective translation is mediated by sequences within the viral mRNA 5'-untranslated region. *J Biol Chem*, 268(30), 22223-6.

Gaush, C. R. & Smith, T. F. (1968) Replication and plaque assay of influenza virus in an established line of canine kidney cells. *Appl Microbiol*, 16(4), 588-94.

Gee, P., Chua, P. K., Gevorkyan, J., Klumpp, K., Najera, I., Swinney, D. C. & Deval, J. (2008) Essential role of the N-terminal domain in the regulation of RIG-I ATPase activity. *J Biol Chem*, 283(14), 9488-96.

Geiss, G. K., Carter, V. S., He, Y., Kwieciszewski, B. K., Holzman, T., Korth, M. J., Lazaro, C. A., Fausto, N., Bumgarner, R. E. & Katze, M. G. (2003) Gene expression profiling of the cellular transcriptional network regulated by alpha/beta interferon and its partial attenuation by the hepatitis C virus nonstructural 5A protein. *J Virol*, 77(11), 6367-75.

George, S. T., Lai, J., Ma, J., Stacey, H. D., Miller, M. S. & Mullarkey, C. E. (2021) Neutrophils and Influenza: A Thin Line between Helpful and Harmful. *Vaccines (Basel)*, 9(6), 597.

Geula, S., Moshitch-Moshkovitz, S., Dominissini, D., Mansour, A. A., Kol, N., Salmon-Divon, M., Hershkovitz, V., Peer, E., Mor, N., Manor, Y. S., Ben-Haim, M. S., Eyal, E., Yunger, S., Pinto, Y., Jaitin, D. A., Viukov, S., Rais, Y., Krupalnik, V., Chomsky, E., Zerbib, M., Maza, I., Rechavi, Y., Massarwa, R., Hanna, S., Amit, I., Levanon, E. Y., Amariglio, N., Stern-Ginossar, N., Novershtern, N., Rechavi, G. & Hanna, J. H. (2015) Stem cells. m6A mRNA methylation facilitates resolution of naïve pluripotency toward differentiation. *Science*, 347(6225), 1002-6.

GeurtsvanKessel, C. H., Willart, M. A., van Rijt, L. S., Muskens, F., Kool, M., Baas, C., Thielemans, K., Bennett, C., Clausen, B. E., Hoogsteden, H. C., Osterhaus, A. D., Rimmelzwaan, G. F. & Lambrecht, B. N. (2008) Clearance of influenza virus from the lung depends on migratory langerin+CD11b- but not plasmacytoid dendritic cells. *J Exp Med*, 205(7), 1621-34.

Giorelli, M., Livrea, P., Defazio, G., Ricchiuti, F., Pagano, E. & Trojano, M. (2001) IFN-beta1a modulates the expression of CTLA-4 and CD28 splice variants in human mononuclear cells: induction of soluble isoforms. *J Interferon Cytokine Res*, 21(10), 809-12.

Gómez-Puertas, P., Albo, C., Pérez-Pastrana, E., Vivo, A. & Portela, A. (2000) Influenza virus matrix protein is the major driving force in virus budding. *J Virol*, 74(24), 11538-47.

Gorden, K. B., Gorski, K. S., Gibson, S. J., Kedl, R. M., Kieper, W. C., Qiu, X., Tomai, M. A., Alkan, S. S. & Vasilakos, J. P. (2005) Synthetic TLR agonists reveal functional differences between human TLR7 and TLR8. *J Immunol*, 174(3), 1259-68.

Graef, K. M., Vreede, F. T., Lau, Y. F., McCall, A. W., Carr, S. M., Subbarao, K. & Fodor, E. (2010) The PB2 subunit of the influenza virus RNA polymerase affects virulence by interacting with the mitochondrial antiviral signaling protein and inhibiting expression of beta interferon. *J Virol*, 84(17), 8433-45.

Grant, E. J., Quiñones-Parra, S. M., Clemens, E. B. & Kedzierska, K. (2016) Human influenza viruses and CD8(+) T cell responses. *Curr Opin Virol*, 16, 132-142.

Griffin, J. A., Basak, S. & Compans, R. W. (1983) Effects of hexose starvation and the role of sialic acid in influenza virus release. *Virology*, 125(2), 324-34.

Guerra, S., López-Fernández, L. A., Pascual-Montano, A., Muñoz, M., Harshman, K. & Esteban, M. (2003) Cellular gene expression survey of vaccinia virus infection of human HeLa cells. *J Virol*, 77(11), 6493-506.

Guidotti, L. G. & Chisari, F. V. (2001) Noncytolytic control of viral infections by the innate and adaptive immune response. *Annu Rev Immunol*, 19, 65-91.

Ha, S. C., Van Quyen, D., Hwang, H. Y., Oh, D. B., Brown, B. A., 2nd, Lee, S. M., Park, H. J., Ahn, J. H., Kim, K. K. & Kim, Y. G. (2006) Biochemical characterization and preliminary X-ray crystallographic study of the domains of human ZBP1 bound to left-handed Z-DNA. *Biochim Biophys Acta*, 1764(2), 320-3.

Hahn, P., Böse, J., Edler, S. & Lengeling, A. (2008) Genomic structure and expression of Jmjd6 and evolutionary analysis in the context of related JmjC domain containing proteins. *BMC Genomics*, 9, 293.

Hahn, P., Wegener, I., Burrells, A., Böse, J., Wolf, A., Erck, C., Butler, D., Schofield, C. J., Böttger, A. & Lengeling, A. (2010) Analysis of Jmjd6 cellular localization and testing for its involvement in histone demethylation. *PLoS One*, 5(10), e13769.

Haline-Vaz, T., Silva, T. C. & Zanchin, N. I. (2008) The human interferon-regulated ISG95 protein interacts with RNA polymerase II and shows methyltransferase activity. *Biochem Biophys Res Commun*, 372(4), 719-24.

Haller, O., Staeheli, P. & Kochs, G. (2007) Interferon-induced Mx proteins in antiviral host defense. *Biochimie*, 89(6-7), 812-8.

Hamilton, B. S., Whittaker, G. R. & Daniel, S. (2012) Influenza virus-mediated membrane fusion: determinants of hemagglutinin fusogenic activity and experimental approaches for assessing virus fusion. *Viruses*, 4(7), 1144-68.

Han, J., Perez, J. T., Chen, C., Li, Y., Benitez, A., Kandasamy, M., Lee, Y., Andrade, J., tenOever, B. & Manicassamy, B. (2018) Genome-wide CRISPR/Cas9 Screen Identifies Host Factors Essential for Influenza Virus Replication. *Cell Rep*, 23(2), 596-607.

Hanahan, D., Jessee, J. & Bloom, F. R. (1991) Plasmid transformation of Escherichia coli and other bacteria. *Methods Enzymol*, 204, 63-113.

Hancock, A. S., Stairiker, C. J., Boesteanu, A. C., Monzón-Casanova, E., Lukasiak, S., Mueller, Y. M., Stubbs, A. P., García-Sastre, A., Turner, M. & Katsikis, P. D. (2018) Transcriptome Analysis of Infected and Bystander Type 2 Alveolar Epithelial Cells during Influenza A Virus Infection Reveals In Vivo Wnt Pathway Downregulation. *J Virol*, 92(21), e01325-18.

Harris, A., Cardone, G., Winkler, D. C., Heymann, J. B., Brecher, M., White, J. M. & Steven, A. C. (2006) Influenza virus pleiomorphy characterized by cryoelectron tomography. *Proc Natl Acad Sci U S A*, 103(50), 19123-7.

Harris, A., Forouhar, F., Qiu, S., Sha, B. & Luo, M. (2001) The crystal structure of the influenza matrix protein M1 at neutral pH: M1-M1 protein interfaces can rotate in the oligomeric structures of M1. *Virology*, 289(1), 34-44.

Hartmann, A. M., Nayler, O., Schwaiger, F. W., Obermeier, A. & Stamm, S. (1999) The interaction and colocalization of Sam68 with the splicing-associated factor YT521-B in nuclear dots is regulated by the Src family kinase p59(fyn). *Mol Biol Cell*, 10(11), 3909-26.

Hartshorn, K. L., Webby, R., White, M. R., Tecle, T., Pan, C., Boucher, S., Moreland, R. J., Crouch, E. C. & Scheule, R. K. (2008) Role of viral hemagglutinin glycosylation in anti-influenza activities of recombinant surfactant protein D. *Respir Res*, 9(1), 65.

Hay, A. J., Skehel, J. J. & McCauley, J. (1982) Characterization of influenza virus RNA complete transcripts. *Virology*, 116(2), 517-22.

Hay, A. J., Wolstenholme, A. J., Skehel, J. J. & Smith, M. H. (1985) The molecular basis of the specific anti-influenza action of amantadine. *Embo j*, 4(11), 3021-4.

Hayashi, F., Means, T. K. & Luster, A. D. (2003) Toll-like receptors stimulate human neutrophil function. *Blood*, 102(7), 2660-9.

Hayden, F. G., Sugaya, N., Hirotsu, N., Lee, N., de Jong, M. D., Hurt, A. C., Ishida, T., Sekino, H., Yamada, K., Portsmouth, S., Kawaguchi, K., Shishido, T., Arai, M., Tsuchiya, K., Uehara, T. & Watanabe, A. (2018) Baloxavir Marboxil for Uncomplicated Influenza in Adults and Adolescents. *N Engl J Med*, 379(10), 913-23.

Hayman, T. J., Hsu, A. C., Kolesnik, T. B., Dagley, L. F., Willemsen, J., Tate, M. D., Baker, P. J., Kershaw, N. J., Kedzierski, L., Webb, A. I., Wark, P. A., Kedzierska, K., Masters, S. L., Belz, G. T., Binder, M., Hansbro, P. M., Nicola, N. A. & Nicholson, S.

E. (2019) RIPLET, and not TRIM25, is required for endogenous RIG-I-dependent antiviral responses. *Immunol Cell Biol*, 97(9), 840-52.

He, W., Zhang, W., Yan, H., Xu, H., Xie, Y., Wu, Q., Wang, C. & Dong, G. (2021) Distribution and evolution of H1N1 influenza A viruses with adamantanes-resistant mutations worldwide from 1918 to 2019. *J Med Virol*, 93(6), 3473-83.

Heil, F., Hemmi, H., Hochrein, H., Ampenberger, F., Kirschning, C., Akira, S., Lipford, G., Wagner, H. & Bauer, S. (2004) Species-specific recognition of single-stranded RNA via toll-like receptor 7 and 8. *Science*, 303(5663), 1526-9.

Heilman, K. L., Leach, R. A. & Tuck, M. T. (1996) Internal 6-methyladenine residues increase the in vitro translation efficiency of dihydrofolate reductase messenger RNA. *Int J Biochem Cell Biol*, 28(7), 823-9.

Heim, A., Grimm, C., Müller, U., Häußler, S., Mackeen, M. M., Merl, J., Hauck, S. M., Kessler, B. M., Schofield, C. J., Wolf, A. & Böttger, A. (2014) Jumonji domain containing protein 6 (Jmjd6) modulates splicing and specifically interacts with arginine-serine-rich (RS) domains of SR- and SR-like proteins. *Nucleic Acids Res*, 42(12), 7833-50.

Hercyk, N., Horikami, S. M. & Moyer, S. A. (1988) The vesicular stomatitis virus L protein possesses the mRNA methyltransferase activities. *Virology*, 163(1), 222-5.

Herz, C., Stavnezer, E., Krug, R. & Gurney, T., Jr. (1981) Influenza virus, an RNA virus, synthesizes its messenger RNA in the nucleus of infected cells. *Cell*, 26(3 Pt 1), 391-400.

Hilsch, M., Goldenbogen, B., Sieben, C., Höfer, C. T., Rabe, J. P., Klipp, E., Herrmann, A. & Chiantia, S. (2014) Influenza A matrix protein M1 multimerizes upon binding to lipid membranes. *Biophys J*, 107(4), 912-23.

Ho, A. W., Prabhu, N., Betts, R. J., Ge, M. Q., Dai, X., Hutchinson, P. E., Lew, F. C., Wong, K. L., Hanson, B. J., Macary, P. A. & Kemeny, D. M. (2011) Lung CD103+ dendritic cells efficiently transport influenza virus to the lymph node and load viral antigen onto MHC class I for presentation to CD8 T cells. *J Immunol*, 187(11), 6011-21.

Ho, C. K., Sriskanda, V., McCracken, S., Bentley, D., Schwer, B. & Shuman, S. (1998) The guanylyltransferase domain of mammalian mRNA capping enzyme binds to the phosphorylated carboxyl-terminal domain of RNA polymerase II. *J Biol Chem*, 273(16), 9577-85.

Ho, J. S. Y., Zhu, Z. & Marazzi, I. (2021) Unconventional viral gene expression mechanisms as therapeutic targets. *Nature*, 593(7859), 362-71.

Hong, X., Zang, J., White, J., Wang, C., Pan, C. H., Zhao, R., Murphy, R. C., Dai, S., Henson, P., Kappler, J. W., Hagman, J. & Zhang, G. (2010) Interaction of JMJD6 with single-stranded RNA. *Proc Natl Acad Sci U S A*, 107(33), 14568-72.

Hornung, V., Ellegast, J., Kim, S., Brzózka, K., Jung, A., Kato, H., Poeck, H., Akira, S., Conzelmann, K. K., Schlee, M., Endres, S. & Hartmann, G. (2006) 5'-Triphosphate RNA is the ligand for RIG-I. *Science*, 314(5801), 994-7.

Hou, F., Sun, L., Zheng, H., Skaug, B., Jiang, Q. X. & Chen, Z. J. (2011) MAVS forms functional prion-like aggregates to activate and propagate antiviral innate immune response. *Cell*, 146(3), 448-61.

Hsu, M. T., Parvin, J. D., Gupta, S., Krystal, M. & Palese, P. (1987) Genomic RNAs of influenza viruses are held in a circular conformation in virions and in infected cells by a terminal panhandle. *Proc Natl Acad Sci U S A*, 84(22), 8140-4.

Huang, H., Weng, H., Sun, W., Qin, X., Shi, H., Wu, H., Zhao, B. S., Mesquita, A., Liu, C., Yuan, C. L., Hu, Y. C., Hüttelmaier, S., Skibbe, J. R., Su, R., Deng, X., Dong, L., Sun, M., Li, C., Nachtergaele, S., Wang, Y., Hu, C., Ferchen, K., Greis, K. D., Jiang, X., Wei, M., Qu, L., Guan, J. L., He, C., Yang, J. & Chen, J. (2018) Recognition of RNA N(6)-methyladenosine by IGF2BP proteins enhances mRNA stability and translation. *Nat Cell Biol*, 20(3), 285-95.

Huang, I. C., Bailey, C. C., Weyer, J. L., Radoshitzky, S. R., Becker, M. M., Chiang, J. J., Brass, A. L., Ahmed, A. A., Chi, X., Dong, L., Longobardi, L. E., Boltz, D., Kuhn, J. H., Elledge, S. J., Bavari, S., Denison, M. R., Choe, H. & Farzan, M. (2011) Distinct patterns of IFITM-mediated restriction of filoviruses, SARS coronavirus, and influenza A virus. *PLoS Pathog*, 7(1), e1001258.

Huang, S., Chen, J., Chen, Q., Wang, H., Yao, Y., Chen, J. & Chen, Z. (2013) A second CRM1-dependent nuclear export signal in the influenza A virus NS2 protein contributes to the nuclear export of viral ribonucleoproteins. *J Virol*, 87(2), 767-78.

Huet, S., Avilov, S. V., Ferbitz, L., Daigle, N., Cusack, S. & Ellenberg, J. (2010) Nuclear import and assembly of influenza A virus RNA polymerase studied in live cells by fluorescence cross-correlation spectroscopy. *J Virol*, 84(3), 1254-64.

Hughey, P. G., Compans, R. W., Zebedee, S. L. & Lamb, R. A. (1992) Expression of the influenza A virus M2 protein is restricted to apical surfaces of polarized epithelial cells. *J Virol*, 66(9), 5542-52.

Hussain, M., Galvin, H. D., Haw, T. Y., Nutsford, A. N. & Husain, M. (2017) Drug resistance in influenza A virus: the epidemiology and management. *Infect Drug Resist*, 10, 121-34.

Hutchinson, E. C., Charles, P. D., Hester, S. S., Thomas, B., Trudgian, D., Martínez-Alonso, M. & Fodor, E. (2014) Conserved and host-specific features of influenza virion architecture. *Nat Commun*, 5, 4816.

Hutchinson, E. C., Orr, O. E., Man Liu, S., Engelhardt, O. G. & Fodor, E. (2011) Characterization of the interaction between the influenza A virus polymerase subunit PB1 and the host nuclear import factor Ran-binding protein 5. *J Gen Virol*, 92(Pt 8), 1859-69.

Hüttelmaier, S., Zenklusen, D., Lederer, M., Dictenberg, J., Lorenz, M., Meng, X., Bassell, G. J., Condeelis, J. & Singer, R. H. (2005) Spatial regulation of beta-actin translation by Src-dependent phosphorylation of ZBP1. *Nature*, 438(7067), 512-5.

Imai, Y., Kuba, K., Neely, G. G., Yaghubian-Malhami, R., Perkmann, T., van Loo, G., Ermolaeva, M., Veldhuizen, R., Leung, Y. H., Wang, H., Liu, H., Sun, Y., Pasparakis, M., Kopf, M., Mech, C., Bavari, S., Peiris, J. S., Slutsky, A. S., Akira, S., Hultqvist, M.,

Holmdahl, R., Nicholls, J., Jiang, C., Binder, C. J. & Penninger, J. M. (2008) Identification of oxidative stress and Toll-like receptor 4 signaling as a key pathway of acute lung injury. *Cell*, 133(2), 235-49.

Inesta-Vaquera, F., Chaugule, V. K., Galloway, A., Chandler, L., Rojas-Fernandez, A., Weidlich, S., Peggie, M. & Cowling, V. H. (2018) DHX15 regulates CMTR1-dependent gene expression and cell proliferation. *Life Sci Alliance*, 1(3), e201800092.

InvivoGen (2011) *Human Type I IFN Reporter Cells* Available online: https://www.invivogen.com/hek-blue-ifn-ab#details [Accessed 2022].

Ioannidis, I., Ye, F., McNally, B., Willette, M. & Flaño, E. (2013) Toll-like receptor expression and induction of type I and type III interferons in primary airway epithelial cells. *J Virol*, 87(6), 3261-70.

Isaacs, A. & Lindenmann, J. (1957) Virus interferance. I. The interferon. *Proc R Soc Lond B*, 147(927), 258-67.

Isaacs, A., Lindenmann, J. & Valentine, R. C. (1957) Virus interference. II. Some properties of interferon. *Proc R Soc Lond B*, 147(927), 268-73.

Iwasaki, A. & Pillai, P. S. (2014) Innate immunity to influenza virus infection. *Nat Rev Immunol*, 14(5), 315-28.

Iwatsuki-Horimoto, K., Horimoto, T., Fujii, Y. & Kawaoka, Y. (2004) Generation of influenza A virus NS2 (NEP) mutants with an altered nuclear export signal sequence. *J Virol*, 78(18), 10149-55.

Iwatsuki-Horimoto, K., Horimoto, T., Noda, T., Kiso, M., Maeda, J., Watanabe, S., Muramoto, Y., Fujii, K. & Kawaoka, Y. (2006) The cytoplasmic tail of the influenza A virus M2 protein plays a role in viral assembly. *J Virol*, 80(11), 5233-40.

Jagger, B. W., Wise, H. M., Kash, J. C., Walters, K. A., Wills, N. M., Xiao, Y. L., Dunfee, R. L., Schwartzman, L. M., Ozinsky, A., Bell, G. L., Dalton, R. M., Lo, A., Efstathiou, S., Atkins, J. F., Firth, A. E., Taubenberger, J. K. & Digard, P. (2012) An overlapping protein-coding region in influenza A virus segment 3 modulates the host response. *Science*, 337(6091), 199-204.

Jelinek, I., Leonard, J. N., Price, G. E., Brown, K. N., Meyer-Manlapat, A., Goldsmith, P. K., Wang, Y., Venzon, D., Epstein, S. L. & Segal, D. M. (2011) TLR3-specific double-stranded RNA oligonucleotide adjuvants induce dendritic cell cross-presentation, CTL responses, and antiviral protection. *J Immunol*, 186(4), 2422-9.

Ji, G., Xiao, X., Huang, M. & Wu, Q. (2022) Jmjd6 regulates ES cell homeostasis and enhances reprogramming efficiency. *Heliyon*, 8(3), e09105.

Ji, Z. X., Wang, X. Q. & Liu, X. F. (2021) NS1: A Key Protein in the "Game" Between Influenza A Virus and Host in Innate Immunity. *Front Cell Infect Microbiol*, 11, 670177.

Jia, G., Fu, Y., Zhao, X., Dai, Q., Zheng, G., Yang, Y., Yi, C., Lindahl, T., Pan, T., Yang, Y. G. & He, C. (2011) N6-methyladenosine in nuclear RNA is a major substrate of the obesity-associated FTO. *Nat Chem Biol*, 7(12), 885-7.

Jiang, L., Li, Y., He, Y., Wei, D., Yan, L. & Wen, H. (2021) Knockdown of m6A Reader IGF2BP3 Inhibited Hypoxia-Induced Cell Migration and Angiogenesis by Regulating Hypoxia Inducible Factor-1α in Stomach Cancer. *Front Oncol*, 11, 711207.

Jorba, N., Coloma, R. & Ortín, J. (2009) Genetic trans-complementation establishes a new model for influenza virus RNA transcription and replication. *PLoS Pathog*, 5(5), e1000462.

Josset, L., Textoris, J., Loriod, B., Ferraris, O., Moules, V., Lina, B., N'Guyen, C., Diaz, J. J. & Rosa-Calatrava, M. (2010) Gene expression signature-based screening identifies new broadly effective influenza a antivirals. *PLoS One*, 5(10).

Jung, H. E. & Lee, H. K. (2020) Host Protective Immune Responses against Influenza A Virus Infection. *Viruses*, 12(5).

Jureka, A. S., Kleinpeter, A. B., Cornilescu, G., Cornilescu, C. C. & Petit, C. M. (2015) Structural Basis for a Novel Interaction between the NS1 Protein Derived from the 1918 Influenza Virus and RIG-I. *Structure*, 23(11), 2001-10.

Kaiser, L., Fritz, R. S., Straus, S. E., Gubareva, L. & Hayden, F. G. (2001) Symptom pathogenesis during acute influenza: interleukin-6 and other cytokine responses. *J Med Virol*, 64(3), 262-8.

Kalil, A. C. & Thomas, P. G. (2019) Influenza virus-related critical illness: pathophysiology and epidemiology. *Crit Care*, 23(1), 258.

Kandasamy, M., Suryawanshi, A., Tundup, S., Perez, J. T., Schmolke, M., Manicassamy, S. & Manicassamy, B. (2016) RIG-I Signaling Is Critical for Efficient Polyfunctional T Cell Responses during Influenza Virus Infection. *PLoS Pathog*, 12(7), e1005754.

Kane, S. E. & Beemon, K. (1985) Precise localization of m6A in Rous sarcoma virus RNA reveals clustering of methylation sites: implications for RNA processing. *Mol Cell Biol*, 5(9), 2298-306.

Kang, D. C., Gopalkrishnan, R. V., Wu, Q., Jankowsky, E., Pyle, A. M. & Fisher, P. B. (2002) mda-5: An interferon-inducible putative RNA helicase with double-stranded RNA-dependent ATPase activity and melanoma growth-suppressive properties. *Proc Natl Acad Sci U S A*, 99(2), 637-42.

Karikó, K., Muramatsu, H., Welsh, F. A., Ludwig, J., Kato, H., Akira, S. & Weissman, D. (2008) Incorporation of pseudouridine into mRNA yields superior nonimmunogenic vector with increased translational capacity and biological stability. *Mol Ther*, 16(11), 1833-40.

Karlas, A., Machuy, N., Shin, Y., Pleissner, K. P., Artarini, A., Heuer, D., Becker, D., Khalil, H., Ogilvie, L. A., Hess, S., Mäurer, A. P., Müller, E., Wolff, T., Rudel, T. & Meyer, T. F. (2010) Genome-wide RNAi screen identifies human host factors crucial for influenza virus replication. *Nature*, 463(7282), 818-22.

Karyopharm Therapeutics Trial of Safety and Tolerability of Oral Verdinexor (KPT-335) in Healthy Adults. https://ClinicalTrials.gov/show/NCT02431364.

Karyopharm Therapeutics (2022) *Verdinexor* Available online: https://www.karyopharm.com/pipeline/oral-verdinexor/ [Accessed 2022].

Kasowitz, S. D., Ma, J., Anderson, S. J., Leu, N. A., Xu, Y., Gregory, B. D., Schultz, R. M. & Wang, P. J. (2018) Nuclear m6A reader YTHDC1 regulates alternative polyadenylation and splicing during mouse oocyte development. *PLoS Genet*, 14(5), e1007412.

Katze, M. G., DeCorato, D. & Krug, R. M. (1986) Cellular mRNA translation is blocked at both initiation and elongation after infection by influenza virus or adenovirus. *J Virol*, 60(3), 1027-39.

Kennedy, E. M., Bogerd, H. P., Kornepati, A. V., Kang, D., Ghoshal, D., Marshall, J. B., Poling, B. C., Tsai, K., Gokhale, N. S., Horner, S. M. & Cullen, B. R. (2016) Posttranscriptional m(6)A Editing of HIV-1 mRNAs Enhances Viral Gene Expression. *Cell Host Microbe*, 19(5), 675-85.

Khurana, E., Devane, R. H., Dal Peraro, M. & Klein, M. L. (2011) Computational study of drug binding to the membrane-bound tetrameric M2 peptide bundle from influenza A virus. *Biochim Biophys Acta*, 1808(2), 530-7.

Kilbourne, E. D. & Murphy, J. S. (1960) Genetic studies of influenza viruses. I. Viral morphology and growth capacity as exchangeable genetic traits. Rapid in ovo adaptation of early passage Asian strain isolates by combination with PR8. *J Exp Med*, 111(3), 387-406.

Killingley, B. & Nguyen-Van-Tam, J. (2013) Routes of influenza transmission. *Influenza Other Respir Viruses*, 7 Suppl 2(Suppl 2), 42-51.

Kim, J. H., Bryant, H., Fiedler, E., Cao, T. & Rayner, J. O. (2022) Real-time tracking of bioluminescent influenza A virus infection in mice. *Sci Rep*, 12(1), 3152.

Kolakofsky, D., Le Mercier, P., Nishio, M., Blackledge, M., Crépin, T. & Ruigrok, R. W. H. (2021) Sendai Virus and a Unified Model of Mononegavirus RNA Synthesis. *Viruses*, 13(12), 2466.

Konarska, M. M., Padgett, R. A. & Sharp, P. A. (1984) Recognition of cap structure in splicing in vitro of mRNA precursors. *Cell*, 38(3), 731-6.

Koutsakos, M., Nguyen, T. H., Barclay, W. S. & Kedzierska, K. (2016) Knowns and unknowns of influenza B viruses. *Future Microbiol*, 11(1), 119-35.

Kowalinski, E., Lunardi, T., McCarthy, A. A., Louber, J., Brunel, J., Grigorov, B., Gerlier, D. & Cusack, S. (2011) Structural basis for the activation of innate immune pattern-recognition receptor RIG-I by viral RNA. *Cell*, 147(2), 423-35.

Krammer, F. (2019) The human antibody response to influenza A virus infection and vaccination. *Nat Rev Immunol*, 19(6), 383-97.

Krammer, F., Smith, G. J. D., Fouchier, R. A. M., Peiris, M., Kedzierska, K., Doherty, P. C., Palese, P., Shaw, M. L., Treanor, J., Webster, R. G. & García-Sastre, A. (2018) Influenza. *Nat Rev Dis Primers*, 4(1), 3.

Kriplani, N., Clohisey, S., Fonseca, S., Fletcher, S., Lee, H.-M., Ashworth, J., Kurian, D., Lycett, S., Tait-Burkard, C., Baillie, J. K., Woolhouse, M. E. J., Carding, S. R., Stewart, J. P. & Digard, P. (2021) Secreted SARS-CoV-2 ORF8 modulates the cytokine expression profile of human macrophages. *bioRxiv*, 2021.08.13.456266.

Krug, R. M., Bouloy, M. & Plotch, S. J. (1980a) RNA primers and the role of host nuclear RNA polymerase II in influenza viral RNA transcription. *Philos Trans R Soc Lond B Biol Sci*, 288(1029), 359-70.

Krug, R. M., Broni, B. A. & Bouloy, M. (1979) Are the 5' ends of influenza viral mRNAs synthesized in vivo donated by host mRNAs? *Cell*, 18(2), 329-34.

Krug, R. M., Broni, B. A., LaFiandra, A. J., Morgan, M. A. & Shatkin, A. J. (1980b) Priming and inhibitory activities of RNAs for the influenza viral transcriptase do not require base pairing with the virion template RNA. *Proc Natl Acad Sci U S A*, 77(10), 5874-8.

Krug, R. M., Morgan, M. A. & Shatkin, A. J. (1976) Influenza viral mRNA contains internal N6-methyladenosine and 5'-terminal 7-methylguanosine in cap structures. *J Virol*, 20(1), 45-53.

Krug, R. M., Shaw, M., Broni, B., Shapiro, G. & Haller, O. (1985) Inhibition of influenza viral mRNA synthesis in cells expressing the interferon-induced Mx gene product. *J Virol*, 56(1), 201-6.

Kumar, P., Sweeney, T. R., Skabkin, M. A., Skabkina, O. V., Hellen, C. U. & Pestova, T. V. (2014) Inhibition of translation by IFIT family members is determined by their ability to interact selectively with the 5'-terminal regions of cap0-, cap1- and 5'ppp- mRNAs. *Nucleic Acids Res*, 42(5), 3228-45.

Kumar, R. & Nanduri, B. (2010) HPIDB--a unified resource for host-pathogen interactions. *BMC Bioinformatics*, 11 Suppl 6(Suppl 6), S16.

Kumari, R., Guo, Z., Kumar, A., Wiens, M., Gangappa, S., Katz, J. M., Cox, N. J., Lal, R. B., Sarkar, D., Fisher, P. B., García-Sastre, A., Fujita, T., Kumar, V., Sambhara, S., Ranjan, P. & Lal, S. K. (2020) Influenza virus NS1- C/EBPβ gene regulatory complex inhibits RIG-I transcription. *Antiviral Res*, 176, 104747.

Kunisaki, Y., Masuko, S., Noda, M., Inayoshi, A., Sanui, T., Harada, M., Sasazuki, T. & Fukui, Y. (2004) Defective fetal liver erythropoiesis and T lymphopoiesis in mice lacking the phosphatidylserine receptor. *Blood*, 103(9), 3362-4.

Kuo, R. L., Li, L. H., Lin, S. J., Li, Z. H., Chen, G. W., Chang, C. K., Wang, Y. R., Tam, E. H., Gong, Y. N., Krug, R. M. & Shih, S. R. (2016) Role of N Terminus-Truncated NS1 Proteins of Influenza A Virus in Inhibiting IRF3 Activation. *J Virol*, 90(9), 4696-705.

Kuriakose, T., Man, S. M., Malireddi, R. K., Karki, R., Kesavardhana, S., Place, D. E., Neale, G., Vogel, P. & Kanneganti, T. D. (2016) ZBP1/DAI is an innate sensor of influenza virus triggering the NLRP3 inflammasome and programmed cell death pathways. *Sci Immunol*, 1(2), aag2045.

Kutay, U., Bischoff, F. R., Kostka, S., Kraft, R. & Görlich, D. (1997) Export of importin alpha from the nucleus is mediated by a specific nuclear transport factor. *Cell*, 90(6), 1061-71.

Kwok, C. T. J. (2018) *JMJD6 dioxygenase regulates macrophage host responses and is a proviral host factor for vaccinia and influenza A virus growth*. Ph.D. Thesis. University of Edinburgh. Available online: http://hdl.handle.net/1842/31551 [Accessed].

Kwok, J., O'Shea, M., Hume, D. A. & Lengeling, A. (2017) Jmjd6, a JmjC Dioxygenase with Many Interaction Partners and Pleiotropic Functions. *Front Genet*, 8, 32.

La Gruta, N. L. & Turner, S. J. (2014) T cell mediated immunity to influenza: mechanisms of viral control. *Trends Immunol*, 35(8), 396-402.

Lai, J. C., Chan, W. W., Kien, F., Nicholls, J. M., Peiris, J. S. & Garcia, J. M. (2010) Formation of virus-like particles from human cell lines exclusively expressing influenza neuraminidase. *J Gen Virol*, 91(Pt 9), 2322-30.

Lakadamyali, M., Rust, M. J. & Zhuang, X. (2006) Ligands for clathrin-mediated endocytosis are differentially sorted into distinct populations of early endosomes. *Cell*, 124(5), 997-1009.

Lakdawala, S. S., Lamirande, E. W., Suguitan, A. L., Jr., Wang, W., Santos, C. P., Vogel, L., Matsuoka, Y., Lindsley, W. G., Jin, H. & Subbarao, K. (2011) Eurasian-origin gene segments contribute to the transmissibility, aerosol release, and morphology of the 2009 pandemic H1N1 influenza virus. *PLoS Pathog*, 7(12), e1002443.

Lakdawala, S. S., Wu, Y., Wawrzusin, P., Kabat, J., Broadbent, A. J., Lamirande, E. W., Fodor, E., Altan-Bonnet, N., Shroff, H. & Subbarao, K. (2014) Influenza a virus assembly intermediates fuse in the cytoplasm. *PLoS Pathog*, 10(3), e1003971.

Lampejo, T. (2020) Influenza and antiviral resistance: an overview. *Eur J Clin Microbiol Infect Dis*, 39(7), 1201-8.

Latham, T. & Galarza, J. M. (2001) Formation of wild-type and chimeric influenza virus-like particles following simultaneous expression of only four structural proteins. *J Virol*, 75(13), 6154-65.

Lawrence, P., Conderino, J. S. & Rieder, E. (2014) Redistribution of demethylated RNA helicase A during foot-and-mouth disease virus infection: role of Jumonji C-domain containing protein 6 in RHA demethylation. *Virology*, 452-453, 1-11.

Lawrence, P. & Rieder, E. (2009) Identification of RNA helicase A as a new host factor in the replication cycle of foot-and-mouth disease virus. *J Virol*, 83(21), 11356-66.

Lawson, H., Sepulveda, C., van de Lagemaat, L. N., Durko, J., Barile, M., Tavosanis, A., Georges, E., Shmakova, A., Timms, P., Carter, R. N., Allen, L., Campos, J., Vukovic, M., Guitart, A. V., Giles, P., O'Shea, M., Vernimmen, D., Morton, N. M., Rodrigues, N. P., Göttgens, B., Schofield, C. J., Lengeling, A., O'Carroll, D. & Kranc, K. R. (2021) JMJD6 promotes self-renewal and regenerative capacity of hematopoietic stem cells. *Blood Adv*, 5(3), 889-99.

Le Goffic, R., Balloy, V., Lagranderie, M., Alexopoulou, L., Escriou, N., Flavell, R., Chignard, M. & Si-Tahar, M. (2006) Detrimental contribution of the Toll-like receptor (TLR)3 to influenza A virus-induced acute pneumonia. *PLoS Pathog*, 2(6), e53.

Le Goffic, R., Pothlichet, J., Vitour, D., Fujita, T., Meurs, E., Chignard, M. & Si-Tahar, M. (2007) Cutting Edge: Influenza A virus activates TLR3-dependent inflammatory and RIG-I-dependent antiviral responses in human lung epithelial cells. *J Immunol*, 178(6), 3368-72.

Le, H. T., Sorrell, A. M. & Siddle, K. (2012) Two isoforms of the mRNA binding protein IGF2BP2 are generated by alternative translational initiation. *PLoS One*, 7(3), e33140.

Lee, S. M., Kok, K. H., Jaume, M., Cheung, T. K., Yip, T. F., Lai, J. C., Guan, Y., Webster, R. G., Jin, D. Y. & Peiris, J. S. (2014) Toll-like receptor 10 is involved in induction of innate immune responses to influenza virus infection. *Proc Natl Acad Sci U S A*, 111(10), 3793-8.

Lee, Y. L., Kung, F. C., Lin, C. H. & Huang, Y. S. (2020) CMTR1-Catalyzed 2'-O-Ribose Methylation Controls Neuronal Development by Regulating Camk2α Expression Independent of RIG-I Signaling. *Cell Rep*, 33(3), 108269.

Leser, G. P. & Lamb, R. A. (2005) Influenza virus assembly and budding in raft-derived microdomains: a quantitative analysis of the surface distribution of HA, NA and M2 proteins. *Virology*, 342(2), 215-27.

LeVine, A. M., Whitsett, J. A., Hartshorn, K. L., Crouch, E. C. & Korfhagen, T. R. (2001) Surfactant protein D enhances clearance of influenza A virus from the lung in vivo. *J Immunol*, 167(10), 5868-73.

Li, B., Clohisey, S. M., Chia, B. S., Wang, B., Cui, A., Eisenhaure, T., Schweitzer, L. D., Hoover, P., Parkinson, N. J., Nachshon, A., Smith, N., Regan, T., Farr, D., Gutmann, M. U., Bukhari, S. I., Law, A., Sangesland, M., Gat-Viks, I., Digard, P., Vasudevan, S., Lingwood, D., Dockrell, D. H., Doench, J. G., Baillie, J. K. & Hacohen, N. (2020a) Genome-wide CRISPR screen identifies host dependency factors for influenza A virus infection. *Nat Commun*, 11(1), 164.

Li, T., Li, Z., Deans, E. E., Mittler, E., Liu, M., Chandran, K. & Ivanovic, T. (2021) The shape of pleomorphic virions determines resistance to cell-entry pressure. *Nat Microbiol*, 6(5), 617-29.

Li, W., Wang, H. & Zheng, S. J. (2022a) Roles of RNA Sensors in Host Innate Response to Influenza Virus and Coronavirus Infections. *Int J Mol Sci*, 23(15).

Li, Y., Bedi, R. K., Moroz-Omori, E. V. & Caflisch, A. (2020b) Structural and Dynamic Insights into Redundant Function of YTHDF Proteins. *J Chem Inf Model*, 60(12), 5932-5.

Li, Y. J., Xu, Q. W., Xu, C. H. & Li, W. M. (2022b) MSC Promotes the Secretion of Exosomal miR-34a-5p and Improve Intestinal Barrier Function Through METTL3-Mediated Pre-miR-34A m(6)A Modification. *Mol Neurobiol*, 59(8), 5222-35.

Liang, S., Silva, J. C., Suska, O., Lukoszek, R., Almohammed, R. & Cowling, V. H. (2022) CMTR1 is recruited to transcription start sites and promotes ribosomal protein and histone gene expression in embryonic stem cells. *Nucleic Acids Res*, 50(5), 2905-22.

Liao, B., Hu, Y., Herrick, D. J. & Brewer, G. (2005) The RNA-binding protein IMP-3 is a translational activator of insulin-like growth factor II leader-3 mRNA during proliferation of human K562 leukemia cells. *J Biol Chem*, 280(18), 18517-24.

Lichinchi, G., Gao, S., Saletore, Y., Gonzalez, G. M., Bansal, V., Wang, Y., Mason, C. E. & Rana, T. M. (2016) Dynamics of the human and viral m(6)A RNA methylomes during HIV-1 infection of T cells. *Nat Microbiol*, 1(4), 16011.

Limburg, H., Harbig, A., Bestle, D., Stein, D. A., Moulton, H. M., Jaeger, J., Janga, H., Hardes, K., Koepke, J., Schulte, L., Koczulla, A. R., Schmeck, B., Klenk, H. D. & Böttcher-Friebertshäuser, E. (2019) TMPRSS2 Is the Major Activating Protease of Influenza A Virus in Primary Human Airway Cells and Influenza B Virus in Human Type II Pneumocytes. *J Virol*, 93(21), e00649-19.

Linder, B., Grozhik, A. V., Olarerin-George, A. O., Meydan, C., Mason, C. E. & Jaffrey, S. R. (2015) Single-nucleotide-resolution mapping of m6A and m6Am throughout the transcriptome. *Nat Methods*, 12(8), 767-72.

Liniger, M., Summerfield, A., Zimmer, G., McCullough, K. C. & Ruggli, N. (2012) Chicken cells sense influenza A virus infection through MDA5 and CARDIF signaling involving LGP2. *J Virol*, 86(2), 705-17.

Liu, B., Zhang, M., Chu, H., Zhang, H., Wu, H., Song, G., Wang, P., Zhao, K., Hou, J., Wang, X., Zhang, L. & Gao, C. (2017a) The ubiquitin E3 ligase TRIM31 promotes aggregation and activation of the signaling adaptor MAVS through Lys63-linked polyubiquitination. *Nat Immunol*, 18(2), 214-24.

Liu, G., Lu, Y., Thulasi Raman, S. N., Xu, F., Wu, Q., Li, Z., Brownlie, R., Liu, Q. & Zhou, Y. (2018) Nuclear-resident RIG-I senses viral replication inducing antiviral immunity. *Nat Commun*, 9(1), 3199.

Liu, G., Park, H. S., Pyo, H. M., Liu, Q. & Zhou, Y. (2015a) Influenza A Virus Panhandle Structure Is Directly Involved in RIG-I Activation and Interferon Induction. *J Virol*, 89(11), 6067-79.

Liu, J., Xu, Y. P., Li, K., Ye, Q., Zhou, H. Y., Sun, H., Li, X., Yu, L., Deng, Y. Q., Li, R. T., Cheng, M. L., He, B., Zhou, J., Li, X. F., Wu, A., Yi, C. & Qin, C. F. (2021) The m(6)A methylome of SARS-CoV-2 in host cells. *Cell Res*, 31(4), 404-14.

Liu, J., Yue, Y., Han, D., Wang, X., Fu, Y., Zhang, L., Jia, G., Yu, M., Lu, Z., Deng, X., Dai, Q., Chen, W. & He, C. (2014) A METTL3-METTL14 complex mediates mammalian nuclear RNA N6-adenosine methylation. *Nat Chem Biol*, 10(2), 93-5.

Liu, N., Dai, Q., Zheng, G., He, C., Parisien, M. & Pan, T. (2015b) N(6)-methyladenosine-dependent RNA structural switches regulate RNA-protein interactions. *Nature*, 518(7540), 560-4.

Liu, N., Zhou, K. I., Parisien, M., Dai, Q., Diatchenko, L. & Pan, T. (2017b) N6-methyladenosine alters RNA structure to regulate binding of a low-complexity protein. *Nucleic Acids Res*, 45(10), 6051-63.

Liu, W., Ma, Q., Wong, K., Li, W., Ohgi, K., Zhang, J., Aggarwal, A. & Rosenfeld, M. G. (2013) Brd4 and JMJD6-associated anti-pause enhancers in regulation of transcriptional pause release. *Cell*, 155(7), 1581-95.

Liu, Y., Long, Y. H., Wang, S. Q., Zhang, Y. Y., Li, Y. F., Mi, J. S., Yu, C. H., Li, D. Y., Zhang, J. H. & Zhang, X. J. (2019) JMJD6 regulates histone H2A.X phosphorylation and promotes autophagy in triple-negative breast cancer cells via a novel tyrosine kinase activity. *Oncogene*, 38(7), 980-97.

Ljunggren, H. G. & Kärre, K. (1990) In search of the 'missing self': MHC molecules and NK cell recognition. *Immunol Today*, 11(7), 237-44.

Londrigan, S. L., Tate, M. D., Brooks, A. G. & Reading, P. C. (2012) Cell-surface receptors on macrophages and dendritic cells for attachment and entry of influenza virus. *J Leukoc Biol*, 92(1), 97-106.

Long, J. S., Giotis, E. S., Moncorgé, O., Frise, R., Mistry, B., James, J., Morisson, M., Iqbal, M., Vignal, A., Skinner, M. A. & Barclay, W. S. (2016) Species difference in ANP32A underlies influenza A virus polymerase host restriction. *Nature*, 529(7584), 101-4.

Loo, Y. M., Fornek, J., Crochet, N., Bajwa, G., Perwitasari, O., Martinez-Sobrido, L., Akira, S., Gill, M. A., García-Sastre, A., Katze, M. G. & Gale, M., Jr. (2008) Distinct RIG-I and MDA5 signaling by RNA viruses in innate immunity. *J Virol*, 82(1), 335-45.

Lu, C., Xu, H., Ranjith-Kumar, C. T., Brooks, M. T., Hou, T. Y., Hu, F., Herr, A. B., Strong, R. K., Kao, C. C. & Li, P. (2010) The structural basis of 5' triphosphate double-stranded RNA recognition by RIG-I C-terminal domain. *Structure*, 18(8), 1032-43.

Lukarska, M., Fournier, G., Pflug, A., Resa-Infante, P., Reich, S., Naffakh, N. & Cusack, S. (2017) Structural basis of an essential interaction between influenza polymerase and Pol II CTD. *Nature*, 541(7635), 117-21.

Lutz, A., Dyall, J., Olivo, P. D. & Pekosz, A. (2005) Virus-inducible reporter genes as a tool for detecting and quantifying influenza A virus replication. *J Virol Methods*, 126(1-2), 13-20.

Macias, A. E., McElhaney, J. E., Chaves, S. S., Nealon, J., Nunes, M. C., Samson, S. I., Seet, B. T., Weinke, T. & Yu, H. (2021) The disease burden of influenza beyond respiratory illness. *Vaccine*, 39 Suppl 1, A6-A14.

Maeda, T., Kawasaki, K. & Ohnishi, S. (1981) Interaction of influenza virus hemagglutinin with target membrane lipids is a key step in virus-induced hemolysis and fusion at pH 5.2. *Proc Natl Acad Sci U S A*, 78(7), 4133-7.

Magor, K. E., Miranzo Navarro, D., Barber, M. R., Petkau, K., Fleming-Canepa, X., Blyth, G. A. & Blaine, A. H. (2013) Defense genes missing from the flight division. *Dev Comp Immunol*, 41(3), 377-88.

Mahapatra, L., Andruska, N., Mao, C., Le, J. & Shapiro, D. J. (2017) A Novel IMP1 Inhibitor, BTYNB, Targets c-Myc and Inhibits Melanoma and Ovarian Cancer Cell Proliferation. *Transl Oncol*, 10(5), 818-27.

Malathi, K., Dong, B., Gale, M., Jr. & Silverman, R. H. (2007) Small self-RNA generated by RNase L amplifies antiviral innate immunity. *Nature*, 448(7155), 816-9.

Malik, G. & Zhou, Y. (2020) Innate Immune Sensing of Influenza A Virus. *Viruses*, 12(7), 755.

Mandelboim, O., Lieberman, N., Lev, M., Paul, L., Arnon, T. I., Bushkin, Y., Davis, D. M., Strominger, J. L., Yewdell, J. W. & Porgador, A. (2001) Recognition of haemagglutinins on virus-infected cells by NKp46 activates lysis by human NK cells. *Nature*, 409(6823), 1055-60.

Mantri, M., Krojer, T., Bagg, E. A., Webby, C. A., Butler, D. S., Kochan, G., Kavanagh, K. L., Oppermann, U., McDonough, M. A. & Schofield, C. J. (2010) Crystal Structure of the 2-Oxoglutarate- and Fe(II)-Dependent Lysyl Hydroxylase JMJD6. *J Mol Biol*, 401(2), 211-22.

Martin, K. & Helenius, A. (1991a) Nuclear transport of influenza virus ribonucleoproteins: the viral matrix protein (M1) promotes export and inhibits import. *Cell*, 67(1), 117-30.

Martin, K. & Helenius, A. (1991b) Transport of incoming influenza virus nucleocapsids into the nucleus. *J Virol*, 65(1), 232-44.

Matikainen, S., Sirén, J., Tissari, J., Veckman, V., Pirhonen, J., Severa, M., Sun, Q., Lin, R., Meri, S., Uzé, G., Hiscott, J. & Julkunen, I. (2006) Tumor necrosis factor alpha enhances influenza A virus-induced expression of antiviral cytokines by activating RIG-I gene expression. *J Virol*, 80(7), 3515-22.

Matrosovich, M., Tuzikov, A., Bovin, N., Gambaryan, A., Klimov, A., Castrucci, M. R., Donatelli, I. & Kawaoka, Y. (2000) Early alterations of the receptor-binding properties of H1, H2, and H3 avian influenza virus hemagglutinins after their introduction into mammals. *J Virol*, 74(18), 8502-12.

Matsuzaki, Y., Mizuta, K., Aoki, Y., Suto, A., Abiko, C., Sanjoh, K., Sugawara, K., Takashita, E., Itagaki, T., Katsushima, Y., Ujike, M., Obuchi, M., Odagiri, T. & Tashiro, M. (2010) A two-year survey of the oseltamivir-resistant influenza A(H1N1) virus in Yamagata, Japan and the clinical effectiveness of oseltamivir and zanamivir. *Virol J*, 7, 53.

McAuley, J. L., Corcilius, L., Tan, H. X., Payne, R. J., McGuckin, M. A. & Brown, L. E. (2017) The cell surface mucin MUC1 limits the severity of influenza A virus infection. *Mucosal Immunol*, 10(6), 1581-93.

McCown, M. F. & Pekosz, A. (2005) The influenza A virus M2 cytoplasmic tail is required for infectious virus production and efficient genome packaging. *J Virol*, 79(6), 3595-605.

McGeoch, D., Fellner, P. & Newton, C. (1976) Influenza virus genome consists of eight distinct RNA species. *Proc Natl Acad Sci U S A*, 73(9), 3045-9.

Meyer, K. D., Patil, D. P., Zhou, J., Zinoviev, A., Skabkin, M. A., Elemento, O., Pestova, T. V., Qian, S. B. & Jaffrey, S. R. (2015) 5' UTR m(6)A Promotes Cap-Independent Translation. *Cell*, 163(4), 999-1010.

Mibayashi, M., Martínez-Sobrido, L., Loo, Y. M., Cárdenas, W. B., Gale, M., Jr. & García-Sastre, A. (2007) Inhibition of retinoic acid-inducible gene I-mediated induction of beta interferon by the NS1 protein of influenza A virus. *J Virol*, 81(2), 514-24.

Mifsud, E. J., Kuba, M. & Barr, I. G. (2021) Innate Immune Responses to Influenza Virus Infections in the Upper Respiratory Tract. *Viruses*, 13(10), 2090.

Min, J. Y. & Krug, R. M. (2006) The primary function of RNA binding by the influenza A virus NS1 protein in infected cells: Inhibiting the 2'-5' oligo (A) synthetase/RNase L pathway. *Proc Natl Acad Sci U S A*, 103(18), 7100-5.

Miotti, S., Gulino, A., Ferri, R., Parenza, M., Chronowska, A., Lecis, D., Sangaletti, S., Tagliabue, E., Tripodo, C. & Colombo, M. P. (2017) Antibody-mediated blockade of JMJD6 interaction with collagen I exerts antifibrotic and antimetastatic activities. *Faseb j*, 31(12), 5356-70.

Momose, F., Kikuchi, Y., Komase, K. & Morikawa, Y. (2007) Visualization of microtubule-mediated transport of influenza viral progeny ribonucleoprotein. *Microbes Infect*, 9(12-13), 1422-33.

Momose, F., Sekimoto, T., Ohkura, T., Jo, S., Kawaguchi, A., Nagata, K. & Morikawa, Y. (2011) Apical transport of influenza A virus ribonucleoprotein requires Rab11-positive recycling endosome. *PLoS One*, 6(6), e21123.

Moscona, A. (2005) Neuraminidase inhibitors for influenza. *N Engl J Med*, 353(13), 1363-73.

Moscona, A. (2009) Global transmission of oseltamivir-resistant influenza. *N Engl J Med*, 360(10), 953-6.

Mosley, V. M. & Wyckoff, R. W. (1946) Electron micrography of the virus of influenza. *Nature*, 157, 263.

Moss, B., Gershowitz, A., Stringer, J. R., Holland, L. E. & Wagner, E. K. (1977) 5'-Terminal and internal methylated nucleosides in herpes simplex virus type 1 mRNA. *J Virol*, 23(2), 234-9.

Mowen, K. A., Tang, J., Zhu, W., Schurter, B. T., Shuai, K., Herschman, H. R. & David, M. (2001) Arginine methylation of STAT1 modulates IFNalpha/beta-induced transcription. *Cell*, 104(5), 731-41.

Müller, S., Bley, N., Busch, B., Glaß, M., Lederer, M., Misiak, C., Fuchs, T., Wedler, A., Haase, J., Bertoldo, J. B., Michl, P. & Hüttelmaier, S. (2020) The oncofetal RNA-binding protein IGF2BP1 is a druggable, post-transcriptional super-enhancer of E2F-driven gene expression in cancer. *Nucleic Acids Res*, 48(15), 8576-90.

Muramoto, Y., Noda, T., Kawakami, E., Akkina, R. & Kawaoka, Y. (2013) Identification of novel influenza A virus proteins translated from PA mRNA. *J Virol*, 87(5), 2455-62.

Muthukrishnan, S., Morgan, M., Banerjee, A. K. & Shatkin, A. J. (1976) Influence of 5'-terminal m7G and 2'--O-methylated residues on messenger ribonucleic acid binding to ribosomes. *Biochemistry*, 15(26), 5761-8.

Muthukrishnan, S., Moss, B., Cooper, J. A. & Maxwell, E. S. (1978) Influence of 5'-terminal cap structure on the initiation of translation of vaccinia virus mRNA. *J Biol Chem*, 253(5), 1710-5.

Narayan, P., Ayers, D. F., Rottman, F. M., Maroney, P. A. & Nilsen, T. W. (1987) Unequal distribution of N6-methyladenosine in influenza virus mRNAs. *Mol Cell Biol*, 7(4), 1572-5.

Nayak, D. P., Balogun, R. A., Yamada, H., Zhou, Z. H. & Barman, S. (2009) Influenza virus morphogenesis and budding. *Virus Res*, 143(2), 147-61.

Neumann, G., Hughes, M. T. & Kawaoka, Y. (2000) Influenza A virus NS2 protein mediates vRNP nuclear export through NES-independent interaction with hCRM1. *Embo j*, 19(24), 6751-8.

Nielsen, J., Christiansen, J., Lykke-Andersen, J., Johnsen, A. H., Wewer, U. M. & Nielsen, F. C. (1999) A family of insulin-like growth factor II mRNA-binding proteins represses translation in late development. *Mol Cell Biol*, 19(2), 1262-70.

Nielsen, J., Kristensen, M. A., Willemoës, M., Nielsen, F. C. & Christiansen, J. (2004) Sequential dimerization of human zipcode-binding protein IMP1 on RNA: a cooperative mechanism providing RNP stability. *Nucleic Acids Res*, 32(14), 4368-76.

Noda, T., Murakami, S., Nakatsu, S., Imai, H., Muramoto, Y., Shindo, K., Sagara, H. & Kawaoka, Y. (2018) Importance of the 1+7 configuration of ribonucleoprotein complexes for influenza A virus genome packaging. *Nat Commun*, 9(1), 54.

Nogusa, S., Thapa, R. J., Dillon, C. P., Liedmann, S., Oguin, T. H., 3rd, Ingram, J. P., Rodriguez, D. A., Kosoff, R., Sharma, S., Sturm, O., Verbist, K., Gough, P. J., Bertin, J., Hartmann, B. M., Sealfon, S. C., Kaiser, W. J., Mocarski, E. S., López, C. B., Thomas, P. G., Oberst, A., Green, D. R. & Balachandran, S. (2016) RIPK3 Activates Parallel Pathways of MLKL-Driven Necroptosis and FADD-Mediated Apoptosis to Protect against Influenza A Virus. *Cell Host Microbe*, 20(1), 13-24.

Noshi, T., Kitano, M., Taniguchi, K., Yamamoto, A., Omoto, S., Baba, K., Hashimoto, T., Ishida, K., Kushima, Y., Hattori, K., Kawai, M., Yoshida, R., Kobayashi, M., Yoshinaga, T., Sato, A., Okamatsu, M., Sakoda, Y., Kida, H., Shishido, T. & Naito, A. (2018) In vitro characterization of baloxavir acid, a first-in-class cap-dependent endonuclease inhibitor of the influenza virus polymerase PA subunit. *Antiviral Res*, 160, 109-17.

Noton, S. L., Medcalf, E., Fisher, D., Mullin, A. E., Elton, D. & Digard, P. (2007) Identification of the domains of the influenza A virus M1 matrix protein required for NP binding, oligomerization and incorporation into virions. *J Gen Virol*, 88(Pt 8), 2280-2290.

Nypaver, C., Dehlinger, C. & Carter, C. (2021) Influenza and Influenza Vaccine: A Review. *J Midwifery Womens Health*, 66(1), 45-53.

O'Neill, R. E., Jaskunas, R., Blobel, G., Palese, P. & Moroianu, J. (1995) Nuclear import of influenza virus RNA can be mediated by viral nucleoprotein and transport factors required for protein import. *J Biol Chem*, 270(39), 22701-4.

O'Neill, R. E., Talon, J. & Palese, P. (1998) The influenza virus NEP (NS2 protein) mediates the nuclear export of viral ribonucleoproteins. *Embo j*, 17(1), 288-96.

Oh, S. W., Onomoto, K., Wakimoto, M., Onoguchi, K., Ishidate, F., Fujiwara, T., Yoneyama, M., Kato, H. & Fujita, T. (2016) Leader-Containing Uncapped Viral Transcript Activates RIG-I in Antiviral Stress Granules. *PLoS Pathog*, 12(2), e1005444.

Ohara, O., Nagase, T., Ishikawa, K., Nakajima, D., Ohira, M., Seki, N. & Nomura, N. (1997) Construction and characterization of human brain cDNA libraries suitable for analysis of cDNA clones encoding relatively large proteins. *DNA Res*, 4(1), 53-9.

Ohno, M., Sakamoto, H. & Shimura, Y. (1987) Preferential excision of the 5' proximal intron from mRNA precursors with two introns as mediated by the cap structure. *Proc Natl Acad Sci U S A*, 84(15), 5187-91.

Ohuchi, M., Ohuchi, R., Feldmann, A. & Klenk, H. D. (1997) Regulation of receptor binding affinity of influenza virus hemagglutinin by its carbohydrate moiety. *J Virol*, 71(11), 8377-84.

Olschewski, S., Cusack, S. & Rosenthal, M. (2020) The Cap-Snatching Mechanism of Bunyaviruses. *Trends Microbiol*, 28(4), 293-303.

Onoguchi, K., Yoneyama, M., Takemura, A., Akira, S., Taniguchi, T., Namiki, H. & Fujita, T. (2007) Viral infections activate types I and III interferon genes through a common mechanism. *J Biol Chem*, 282(10), 7576-81.

Opitz, B., Rejaibi, A., Dauber, B., Eckhard, J., Vinzing, M., Schmeck, B., Hippenstiel, S., Suttorp, N. & Wolff, T. (2007) IFNbeta induction by influenza A virus is mediated by RIG-I which is regulated by the viral NS1 protein. *Cell Microbiol*, 9(4), 930-8.

Ortega, J., Martín-Benito, J., Zürcher, T., Valpuesta, J. M., Carrascosa, J. L. & Ortín, J. (2000) Ultrastructural and functional analyses of recombinant influenza virus ribonucleoproteins suggest dimerization of nucleoprotein during virus amplification. *J Virol*, 74(1), 156-63.

Oshiumi, H., Miyashita, M., Matsumoto, M. & Seya, T. (2013) A distinct role of Riplet-mediated K63-Linked polyubiquitination of the RIG-I repressor domain in human antiviral innate immune responses. *PLoS Pathog*, 9(8), e1003533.

Pabis, M., Neufeld, N., Steiner, M. C., Bojic, T., Shav-Tal, Y. & Neugebauer, K. M. (2013) The nuclear cap-binding complex interacts with the U4/U6·U5 tri-snRNP and promotes spliceosome assembly in mammalian cells. *Rna*, 19(8), 1054-63.

Palese, P. & Schulman, J. L. (1976) Mapping of the influenza virus genome: identification of the hemagglutinin and the neuraminidase genes. *Proc Natl Acad Sci U S A*, 73(6), 2142-6.

Palese, P., Tobita, K., Ueda, M. & Compans, R. W. (1974) Characterization of temperature sensitive influenza virus mutants defective in neuraminidase. *Virology*, 61(2), 397-410.

Parvin, R., Shehata, A. A., Heenemann, K., Gac, M., Rueckner, A., Halami, M. Y. & Vahlenkamp, T. W. (2015) Differential replication properties among H9N2 avian influenza viruses of Eurasian origin. *Vet Res*, 46(1), 75.

Patel, J. R., Jain, A., Chou, Y. Y., Baum, A., Ha, T. & García-Sastre, A. (2013) ATPase-driven oligomerization of RIG-I on RNA allows optimal activation of type-I interferon. *EMBO Rep*, 14(9), 780-7.

Pavlovic, J., Haller, O. & Staeheli, P. (1992) Human and mouse Mx proteins inhibit different steps of the influenza virus multiplication cycle. *J Virol*, 66(4), 2564-9.

Peisley, A., Wu, B., Xu, H., Chen, Z. J. & Hur, S. (2014) Structural basis for ubiquitin-mediated antiviral signal activation by RIG-I. *Nature*, 509(7498), 110-4.

Pendleton, K. E., Chen, B., Liu, K., Hunter, O. V., Xie, Y., Tu, B. P. & Conrad, N. K. (2017) The U6 snRNA m(6)A Methyltransferase METTL16 Regulates SAM Synthetase Intron Retention. *Cell*, 169(5), 824-35.e14.

Perwitasari, O., Johnson, S., Yan, X., Howerth, E., Shacham, S., Landesman, Y., Baloglu, E., McCauley, D., Tamir, S., Tompkins, S. M. & Tripp, R. A. (2014) Verdinexor, a novel selective inhibitor of nuclear export, reduces influenza a virus replication in vitro and in vivo. *J Virol*, 88(17), 10228-43.

Perwitasari, O., Johnson, S., Yan, X., Register, E., Crabtree, J., Gabbard, J., Howerth, E., Shacham, S., Carlson, R., Tamir, S. & Tripp, R. A. (2016) Antiviral Efficacy of Verdinexor In Vivo in Two Animal Models of Influenza A Virus Infection. *PLoS One*, 11(11), e0167221.

Pestka, S., Krause, C. D. & Walter, M. R. (2004) Interferons, interferon-like cytokines, and their receptors. *Immunol Rev*, 202, 8-32.

Petrich, A., Dunsing, V., Bobone, S. & Chiantia, S. (2021) Influenza A M2 recruits M1 to the plasma membrane: A fluorescence fluctuation microscopy study. *Biophys J*, 120(24), 5478-90.

Pham, H. T., Park, M. Y., Kim, K. K., Kim, Y. G. & Ahn, J. H. (2006) Intracellular localization of human ZBP1: Differential regulation by the Z-DNA binding domain, Zalpha, in splice variants. *Biochem Biophys Res Commun*, 348(1), 145-52.

Pichlmair, A., Kandasamy, K., Alvisi, G., Mulhern, O., Sacco, R., Habjan, M., Binder, M., Stefanovic, A., Eberle, C. A., Goncalves, A., Bürckstümmer, T., Müller, A. C., Fauster, A., Holze, C., Lindsten, K., Goodbourn, S., Kochs, G., Weber, F., Bartenschlager, R., Bowie, A. G., Bennett, K. L., Colinge, J. & Superti-Furga, G. (2012) Viral immune modulators perturb the human molecular network by common and unique strategies. *Nature*, 487(7408), 486-90.

Pichlmair, A., Schulz, O., Tan, C. P., Näslund, T. I., Liljeström, P., Weber, F. & Reis e Sousa, C. (2006) RIG-I-mediated antiviral responses to single-stranded RNA bearing 5'-phosphates. *Science*, 314(5801), 997-1001.

Pinto, L. H., Holsinger, L. J. & Lamb, R. A. (1992) Influenza virus M2 protein has ion channel activity. *Cell*, 69(3), 517-28.

Pinto, R. M., Lycett, S., Gaunt, E. & Digard, P. (2021) Accessory Gene Products of Influenza A Virus. *Cold Spring Harb Perspect Med*, 11(12), a038380.

Pirbaluty, A. M., Mehrban, H., Kadkhodaei, S., Ravash, R., Oryan, A., Ghaderi-Zefrehei, M. & Smith, J. (2022) Network Meta-Analysis of Chicken Microarray Data following Avian Influenza Challenge-A Comparison of Highly and Lowly Pathogenic Strains. *Genes (Basel)*, 13(3), 435.

Pizzorno, A., Terrier, O., Nicolas de Lamballerie, C., Julien, T., Padey, B., Traversier, A., Roche, M., Hamelin, M. E., Rhéaume, C., Croze, S., Escuret, V., Poissy, J., Lina, B., Legras-Lachuer, C., Textoris, J., Boivin, G. & Rosa-Calatrava, M. (2019) Repurposing of Drugs as Novel Influenza Inhibitors From Clinical Gene Expression Infection Signatures. *Front Immunol*, 10, 60.

Plotch, S. J., Bouloy, M., Ulmanen, I. & Krug, R. M. (1981) A unique cap(m7GpppXm)-dependent influenza virion endonuclease cleaves capped RNAs to generate the primers that initiate viral RNA transcription. *Cell*, 23(3), 847-58.

Pohl, M. O., Lanz, C. & Stertz, S. (2016) Late stages of the influenza A virus replication cycle-a tight interplay between virus and host. *J Gen Virol*, 97(9), 2058-72.

Poon, L. L., Pritlove, D. C., Fodor, E. & Brownlee, G. G. (1999) Direct evidence that the poly(A) tail of influenza A virus mRNA is synthesized by reiterative copying of a U track in the virion RNA template. *J Virol*, 73(4), 3473-6.

Poulard, C., Rambaud, J., Hussein, N., Corbo, L. & Le Romancer, M. (2014) JMJD6 regulates ERα methylation on arginine. *PLoS One*, 9(2), e87982.

Proteintech (2020) *How do I know if the antibody will cross-react?* Available online: https://www.ptglab.com/news/blog/how-do-i-know-if-the-antibody-will-cross-react/ [Accessed 2022].

Raguz, N., Heim, A., Engal, E., Wesche, J., Merl-Pham, J., Hauck, S. M., Erkelenz, S., Schaal, H., Bensaude, O., Wolf, A., Salton, M. & Böttger, A. (2020) JMJD6 Regulates Splicing of Its Own Gene Resulting in Alternatively Spliced Isoforms with Different Nuclear Targets. *Int J Mol Sci*, 21(18), 6618.

Rahim, M. N., Klewes, L., Zahedi-Amiri, A., Mai, S. & Coombs, K. M. (2018) Global Interactomics Connect Nuclear Mitotic Apparatus Protein NUMA1 to Influenza Virus Maturation. *Viruses*, 10(12), 731.

Rajsbaum, R., Albrecht, R. A., Wang, M. K., Maharaj, N. P., Versteeg, G. A., Nistal-Villán, E., García-Sastre, A. & Gack, M. U. (2012) Species-specific inhibition of RIG-I ubiquitination and IFN induction by the influenza A virus NS1 protein. *PLoS Pathog*, 8(11), e1003059.

Randall, R. E. & Goodbourn, S. (2008) Interferons and viruses: an interplay between induction, signalling, antiviral responses and virus countermeasures. *J Gen Virol*, 89(Pt 1), 1-47.

Read, E. K. & Digard, P. (2010) Individual influenza A virus mRNAs show differential dependence on cellular NXF1/TAP for their nuclear export. *J Gen Virol*, 91(Pt 5), 1290-301.

Reeves, R. & Nissen, M. S. (1990) The A.T-DNA-binding domain of mammalian high mobility group I chromosomal proteins. A novel peptide motif for recognizing DNA structure. *J Biol Chem*, 265(15), 8573-82.

Rehwinkel, J., Tan, C. P., Goubau, D., Schulz, O., Pichlmair, A., Bier, K., Robb, N., Vreede, F., Barclay, W., Fodor, E. & Reis e Sousa, C. (2010) RIG-I detects viral genomic RNA during negative-strand RNA virus infection. *Cell*, 140(3), 397-408.

Reich, S., Guilligay, D., Pflug, A., Malet, H., Berger, I., Crépin, T., Hart, D., Lunardi, T., Nanao, M., Ruigrok, R. W. & Cusack, S. (2014) Structural insight into cap-snatching and RNA synthesis by influenza polymerase. *Nature*, 516(7531), 361-6.

Richardson, J. C. & Akkina, R. K. (1991) NS2 protein of influenza virus is found in purified virus and phosphorylated in infected cells. *Arch Virol*, 116(1-4), 69-80.

Roberts, N. J., Jr. (2020) Diverse and Unexpected Roles of Human Monocytes/Macrophages in the Immune Response to Influenza Virus. *Viruses*, 12(4), 379.

Roberts, P. C., Lamb, R. A. & Compans, R. W. (1998) The M1 and M2 proteins of influenza A virus are important determinants in filamentous particle formation. *Virology*, 240(1), 127-37.

Robertson, J. S., Schubert, M. & Lazzarini, R. A. (1981) Polyadenylation sites for influenza virus mRNA. *J Virol*, 38(1), 157-63.

Rodgers, B. C. & Mims, C. A. (1982) Influenza virus replication in human alveolar macrophages. *J Med Virol*, 9(3), 177-84.

Rosenthal, M., Gogrefe, N., Vogel, D., Reguera, J., Rauschenberger, B., Cusack, S., Günther, S. & Reindl, S. (2017) Structural insights into reptarenavirus cap-snatching machinery. *PLoS Pathog*, 13(5), e1006400.

Rossman, J. S., Jing, X., Leser, G. P. & Lamb, R. A. (2010) Influenza virus M2 protein mediates ESCRT-independent membrane scission. *Cell*, 142(6), 902-13.

Rossman, J. S. & Lamb, R. A. (2011) Influenza virus assembly and budding. *Virology*, 411(2), 229-36.

Ruigrok, R. W. & Baudin, F. (1995) Structure of influenza virus ribonucleoprotein particles. II. Purified RNA-free influenza virus ribonucleoprotein forms structures that are indistinguishable from the intact influenza virus ribonucleoprotein particles. *J Gen Virol*, 76 (Pt 4), 1009-14.

Saito, R., Sato, I., Suzuki, Y., Baranovich, T., Matsuda, R., Ishitani, N., Dapat, C., Dapat, I. C., Zaraket, H., Oguma, T. & Suzuki, H. (2010) Reduced effectiveness of oseltamivir in children infected with oseltamivir-resistant influenza A (H1N1) viruses with His275Tyr mutation. *Pediatr Infect Dis J*, 29(10), 898-904.

Sato, M., Tanaka, N., Hata, N., Oda, E. & Taniguchi, T. (1998) Involvement of the IRF family transcription factor IRF-3 in virus-induced activation of the IFN-beta gene. *FEBS Lett*, 425(1), 112-6.

Schafer, S. L., Lin, R., Moore, P. A., Hiscott, J. & Pitha, P. M. (1998) Regulation of type I interferon gene expression by interferon regulatory factor-3. *J Biol Chem*, 273(5), 2714-20.

Scheiffele, P., Roth, M. G. & Simons, K. (1997) Interaction of influenza virus haemagglutinin with sphingolipid-cholesterol membrane domains via its transmembrane domain. *Embo j*, 16(18), 5501-8.

Schmidt, A., Schwerd, T., Hamm, W., Hellmuth, J. C., Cui, S., Wenzel, M., Hoffmann, F. S., Michallet, M. C., Besch, R., Hopfner, K. P., Endres, S. & Rothenfusser, S. (2009) 5'-triphosphate RNA requires base-paired structures to activate antiviral signaling via RIG-I. *Proc Natl Acad Sci U S A*, 106(29), 12067-72.

Schmidt, N. W., Mishra, A., Wang, J., DeGrado, W. F. & Wong, G. C. (2013) Influenza virus A M2 protein generates negative Gaussian membrane curvature necessary for budding and scission. *J Am Chem Soc*, 135(37), 13710-9.

Schnell, J. R. & Chou, J. J. (2008) Structure and mechanism of the M2 proton channel of influenza A virus. *Nature*, 451(7178), 591-5.

Scholtissek, C. & Becht, H. (1971) Binding of ribonucleic acids to the RNP-antigen protein of influenza viruses. *J Gen Virol*, 10(1), 11-6.

Schuberth-Wagner, C., Ludwig, J., Bruder, A. K., Herzner, A. M., Zillinger, T., Goldeck, M., Schmidt, T., Schmid-Burgk, J. L., Kerber, R., Wolter, S., Stümpel, J. P., Roth, A., Bartok, E., Drosten, C., Coch, C., Hornung, V., Barchet, W., Kümmerer, B. M., Hartmann, G. & Schlee, M. (2015) A Conserved Histidine in the RNA Sensor RIG-I Controls Immune Tolerance to N1-2'O-Methylated Self RNA. *Immunity*, 43(1), 41-51.

Schulze, I. T. (1970) The structure of influenza virus. I. The polypeptides of the virion. *Virology*, 42(4), 890-904.

Sederdahl, B. K. & Williams, J. V. (2020) Epidemiology and Clinical Characteristics of Influenza C Virus. *Viruses*, 12(1), 89.

Seladi-Schulman, J., Steel, J. & Lowen, A. C. (2013) Spherical influenza viruses have a fitness advantage in embryonated eggs, while filament-producing strains are selected in vivo. *J Virol*, 87(24), 13343-53.

Selman, M., Dankar, S. K., Forbes, N. E., Jia, J. J. & Brown, E. G. (2012) Adaptive mutation in influenza A virus non-structural gene is linked to host switching and induces a novel protein by alternative splicing. *Emerg Microbes Infect*, 1(11), e42.

Seth, R. B., Sun, L., Ea, C. K. & Chen, Z. J. (2005) Identification and characterization of MAVS, a mitochondrial antiviral signaling protein that activates NF-kappaB and IRF 3. *Cell*, 122(5), 669-82.

Sha, B. & Luo, M. (1997) Structure of a bifunctional membrane-RNA binding protein, influenza virus matrix protein M1. *Nat Struct Biol*, 4(3), 239-44.

Shafer, B., Chu, C. & Shatkin, A. J. (2005) Human mRNA cap methyltransferase: alternative nuclear localization signal motifs ensure nuclear localization required for viability. *Mol Cell Biol*, 25(7), 2644-9.

Shatkin, A. J. (1976) Capping of eucaryotic mRNAs. *Cell*, 9(4 pt 2), 645-53.

Shaw, M. L., Stone, K. L., Colangelo, C. M., Gulcicek, E. E. & Palese, P. (2008) Cellular proteins in influenza virus particles. *PLoS Pathog*, 4(6), e1000085.

Sheppard, D. (1994) Dominant negative mutants: tools for the study of protein function in vitro and in vivo. *Am J Respir Cell Mol Biol*, 11(1), 1-6.

Shimizu, T., Takizawa, N., Watanabe, K., Nagata, K. & Kobayashi, N. (2011) Crucial role of the influenza virus NS2 (NEP) C-terminal domain in M1 binding and nuclear export of vRNP. *FEBS Lett*, 585(1), 41-6.

Shinya, K., Ebina, M., Yamada, S., Ono, M., Kasai, N. & Kawaoka, Y. (2006) Avian flu: influenza virus receptors in the human airway. *Nature*, 440(7083), 435-6.

Shinya, K., Hatta, M., Yamada, S., Takada, A., Watanabe, S., Halfmann, P., Horimoto, T., Neumann, G., Kim, J. H., Lim, W., Guan, Y., Peiris, M., Kiso, M., Suzuki, T., Suzuki, Y. & Kawaoka, Y. (2005) Characterization of a human H5N1 influenza A virus isolated in 2003. *J Virol*, 79(15), 9926-32.

Sikorski, P. J., Warminski, M., Kubacka, D., Ratajczak, T., Nowis, D., Kowalska, J. & Jemielity, J. (2020) The identity and methylation status of the first transcribed nucleotide in eukaryotic mRNA 5' cap modulates protein expression in living cells. *Nucleic Acids Res*, 48(4), 1607-26.

Silverman, R. H. (2007) Viral encounters with 2',5'-oligoadenylate synthetase and RNase L during the interferon antiviral response. *J Virol*, 81(23), 12720-9.

Śledź, P. & Jinek, M. (2016) Structural insights into the molecular mechanism of the m(6)A writer complex. *Elife*, 5, e18434.

Smietanski, M., Werner, M., Purta, E., Kaminska, K. H., Stepinski, J., Darzynkiewicz, E., Nowotny, M. & Bujnicki, J. M. (2014) Structural analysis of human 2'-O-ribose methyltransferases involved in mRNA cap structure formation. *Nat Commun*, 5, 3004.

Smith, G. L., Talbot-Cooper, C. & Lu, Y. (2018) How Does Vaccinia Virus Interfere With Interferon? *Adv Virus Res*, 100, 355-78.

Smith, W. A., Schurter, B. T., Wong-Staal, F. & David, M. (2004) Arginine methylation of RNA helicase a determines its subcellular localization. *J Biol Chem*, 279(22), 22795-8.

Speshock, J. L., Doyon-Reale, N., Rabah, R., Neely, M. N. & Roberts, P. C. (2007) Filamentous influenza A virus infection predisposes mice to fatal septicemia following superinfection with Streptococcus pneumoniae serotype 3. *Infect Immun*, 75(6), 3102-11.

Stouffer, A. L., Acharya, R., Salom, D., Levine, A. S., Di Costanzo, L., Soto, C. S., Tereshko, V., Nanda, V., Stayrook, S. & DeGrado, W. F. (2008) Structural basis for the function and inhibition of an influenza virus proton channel. *Nature*, 451(7178), 596-9.

Su, A. I., Pezacki, J. P., Wodicka, L., Brideau, A. D., Supekova, L., Thimme, R., Wieland, S., Bukh, J., Purcell, R. H., Schultz, P. G. & Chisari, F. V. (2002) Genomic analysis of the host response to hepatitis C virus infection. *Proc Natl Acad Sci U S A*, 99(24), 15669-74.

Su, W. C., Chen, Y. C., Tseng, C. H., Hsu, P. W., Tung, K. F., Jeng, K. S. & Lai, M. M. (2013) Pooled RNAi screen identifies ubiquitin ligase Itch as crucial for influenza A virus release from the endosome during virus entry. *Proc Natl Acad Sci U S A*, 110(43), 17516-21.

Sun, E., He, J. & Zhuang, X. (2013) Dissecting the role of COPI complexes in influenza virus infection. *J Virol*, 87(5), 2673-85.

Sun, L., Fazal, F. M., Li, P., Broughton, J. P., Lee, B., Tang, L., Huang, W., Kool, E. T., Chang, H. Y. & Zhang, Q. C. (2019) RNA structure maps across mammalian cellular compartments. *Nat Struct Mol Biol*, 26(4), 322-330.

Takaoka, A., Wang, Z., Choi, M. K., Yanai, H., Negishi, H., Ban, T., Lu, Y., Miyagishi, M., Kodama, T., Honda, K., Ohba, Y. & Taniguchi, T. (2007) DAI (DLM-1/ZBP1) is a cytosolic DNA sensor and an activator of innate immune response. *Nature*, 448(7152), 501-5.

Takashita, E., Kawakami, C., Morita, H., Ogawa, R., Fujisaki, S., Shirakura, M., Miura, H., Nakamura, K., Kishida, N., Kuwahara, T., Mitamura, K., Abe, T., Ichikawa, M., Yamazaki, M., Watanabe, S., Odagiri, T. & On Behalf Of The Influenza Virus Surveillance Group Of, J. (2019a) Detection of influenza A(H3N2) viruses exhibiting reduced susceptibility to the novel cap-dependent endonuclease inhibitor baloxavir in Japan, December 2018. *Euro Surveill*, 24(3), 1800698.

Takashita, E., Kawakami, C., Ogawa, R., Morita, H., Fujisaki, S., Shirakura, M., Miura, H., Nakamura, K., Kishida, N., Kuwahara, T., Ota, A., Togashi, H., Saito, A., Mitamura, K., Abe, T., Ichikawa, M., Yamazaki, M., Watanabe, S. & Odagiri, T. (2019b) Influenza A(H3N2) virus exhibiting reduced susceptibility to baloxavir due to a polymerase acidic subunit I38T substitution detected from a hospitalised child without prior baloxavir treatment, Japan, January 2019. *Euro Surveill*, 24(12), 1900170.

Takashita, E., Morita, H., Ogawa, R., Nakamura, K., Fujisaki, S., Shirakura, M., Kuwahara, T., Kishida, N., Watanabe, S. & Odagiri, T. (2018) Susceptibility of Influenza Viruses to the Novel Cap-Dependent Endonuclease Inhibitor Baloxavir Marboxil. *Front Microbiol*, 9, 3026.

Takizawa, N., Momose, F., Morikawa, Y. & Nomoto, A. (2016) Influenza A Virus Hemagglutinin is Required for the Assembly of Viral Components Including Bundled vRNPs at the Lipid Raft. *Viruses*, 8(9), 249.

Tarendeau, F., Boudet, J., Guilligay, D., Mas, P. J., Bougault, C. M., Boulo, S., Baudin, F., Ruigrok, R. W., Daigle, N., Ellenberg, J., Cusack, S., Simorre, J. P. & Hart, D. J.

(2007) Structure and nuclear import function of the C-terminal domain of influenza virus polymerase PB2 subunit. *Nat Struct Mol Biol*, 14(3), 229-33.

Te Velthuis, A. J. W., Long, J. C., Bauer, D. L. V., Fan, R. L. Y., Yen, H. L., Sharps, J., Siegers, J. Y., Killip, M. J., French, H., Oliva-Martín, M. J., Randall, R. E., de Wit, E., van Riel, D., Poon, L. L. M. & Fodor, E. (2018) Mini viral RNAs act as innate immune agonists during influenza virus infection. *Nat Microbiol*, 3(11), 1234-42.

Thapa, R. J., Ingram, J. P., Ragan, K. B., Nogusa, S., Boyd, D. F., Benitez, A. A., Sridharan, H., Kosoff, R., Shubina, M., Landsteiner, V. J., Andrake, M., Vogel, P., Sigal, L. J., tenOever, B. R., Thomas, P. G., Upton, J. W. & Balachandran, S. (2016) DAI Senses Influenza A Virus Genomic RNA and Activates RIPK3-Dependent Cell Death. *Cell Host Microbe*, 20(5), 674-81.

Tibrewal, N., Liu, T., Li, H. & Birge, R. B. (2007) Characterization of the biochemical and biophysical properties of the phosphatidylserine receptor (PS-R) gene product. *Mol Cell Biochem*, 304(1-2), 119-25.

Tikhanovich, I., Kuravi, S., Artigues, A., Villar, M. T., Dorko, K., Nawabi, A., Roberts, B. & Weinman, S. A. (2015) Dynamic Arginine Methylation of Tumor Necrosis Factor (TNF) Receptor-associated Factor 6 Regulates Toll-like Receptor Signaling. *J Biol Chem*, 290(36), 22236-49.

To, K. K. W., Zhou, J., Song, Y. Q., Hung, I. F. N., Ip, W. C. T., Cheng, Z. S., Chan, A. S. F., Kao, R. Y. T., Wu, A. K. L., Chau, S., Luk, W. K., Ip, M. S. M., Chan, K. H. & Yuen, K. Y. (2014) Surfactant protein B gene polymorphism is associated with severe influenza. *Chest*, 145(6), 1237-43.

Toczydlowska-Socha, D., Zielinska, M. M., Kurkowska, M., Astha, Almeida, C. F., Stefaniak, F., Purta, E. & Bujnicki, J. M. (2018) Human RNA cap1 methyltransferase CMTr1 cooperates with RNA helicase DHX15 to modify RNAs with highly structured 5' termini. *Philos Trans R Soc Lond B Biol Sci*, 373(1762), 20180161.

Tong, S., Zhu, X., Li, Y., Shi, M., Zhang, J., Bourgeois, M., Yang, H., Chen, X., Recuenco, S., Gomez, J., Chen, L. M., Johnson, A., Tao, Y., Dreyfus, C., Yu, W., McBride, R., Carney, P. J., Gilbert, A. T., Chang, J., Guo, Z., Davis, C. T., Paulson, J. C., Stevens, J., Rupprecht, C. E., Holmes, E. C., Wilson, I. A. & Donis, R. O. (2013) New world bats harbor diverse influenza A viruses. *PLoS Pathog*, 9(10), e1003657.

Topham, D. J., Tripp, R. A. & Doherty, P. C. (1997) CD8+ T cells clear influenza virus by perforin or Fas-dependent processes. *J Immunol*, 159(11), 5197-200.

Tran, A. T., Rahim, M. N., Ranadheera, C., Kroeker, A., Cortens, J. P., Opanubi, K. J., Wilkins, J. A. & Coombs, K. M. (2013) Knockdown of specific host factors protects against influenza virus-induced cell death. *Cell Death Dis*, 4(8), e769.

Tripathi, S., Pohl, M. O., Zhou, Y., Rodriguez-Frandsen, A., Wang, G., Stein, D. A., Moulton, H. M., DeJesus, P., Che, J., Mulder, L. C., Yángüez, E., Andenmatten, D., Pache, L., Manicassamy, B., Albrecht, R. A., Gonzalez, M. G., Nguyen, Q., Brass, A., Elledge, S., White, M., Shapira, S., Hacohen, N., Karlas, A., Meyer, T. F., Shales, M., Gatorano, A., Johnson, J. R., Jang, G., Johnson, T., Verschueren, E., Sanders, D., Krogan, N., Shaw, M., König, R., Stertz, S., García-Sastre, A. & Chanda, S. K. (2015)

Meta- and Orthogonal Integration of Influenza "OMICs" Data Defines a Role for UBR4 in Virus Budding. *Cell Host Microbe*, 18(6), 723-35.

Tsai, S. Y., Segovia, J. A., Chang, T. H., Morris, I. R., Berton, M. T., Tessier, P. A., Tardif, M. R., Cesaro, A. & Bose, S. (2014) DAMP molecule S100A9 acts as a molecular pattern to enhance inflammation during influenza A virus infection: role of DDX21-TRIF-TLR4-MyD88 pathway. *PLoS Pathog*, 10(1), e1003848.

Tsai, W. C., Reineke, L. C., Jain, A., Jung, S. Y. & Lloyd, R. E. (2017) Histone arginine demethylase JMJD6 is linked to stress granule assembly through demethylation of the stress granule-nucleating protein G3BP1. *J Biol Chem*, 292(46), 18886-96.

Tumpey, T. M., García-Sastre, A., Taubenberger, J. K., Palese, P., Swayne, D. E., Pantin-Jackwood, M. J., Schultz-Cherry, S., Solórzano, A., Van Rooijen, N., Katz, J. M. & Basler, C. F. (2005) Pathogenicity of influenza viruses with genes from the 1918 pandemic virus: functional roles of alveolar macrophages and neutrophils in limiting virus replication and mortality in mice. *J Virol*, 79(23), 14933-44.

Turan, K., Mibayashi, M., Sugiyama, K., Saito, S., Numajiri, A. & Nagata, K. (2004) Nuclear MxA proteins form a complex with influenza virus NP and inhibit the transcription of the engineered influenza virus genome. *Nucleic Acids Res*, 32(2), 643-52.

Turnbull, M. L., Wise, H. M., Nicol, M. Q., Smith, N., Dunfee, R. L., Beard, P. M., Jagger, B. W., Ligertwood, Y., Hardisty, G. R., Xiao, H., Benton, D. J., Coburn, A. M., Paulo, J. A., Gygi, S. P., McCauley, J. W., Taubenberger, J. K., Lycett, S. J., Weekes, M. P., Dutia, B. M. & Digard, P. (2016) Role of the B Allele of Influenza A Virus Segment 8 in Setting Mammalian Host Range and Pathogenicity. *J Virol*, 90(20), 9263-84.

Tuvim, M. J., Gilbert, B. E., Dickey, B. F. & Evans, S. E. (2012) Synergistic TLR2/6 and TLR9 activation protects mice against lethal influenza pneumonia. *PLoS One*, 7(1), e30596.

Uehara, T., Hayden, F. G., Kawaguchi, K., Omoto, S., Hurt, A. C., De Jong, M. D., Hirotsu, N., Sugaya, N., Lee, N., Baba, K., Shishido, T., Tsuchiya, K., Portsmouth, S. & Kida, H. (2020) Treatment-Emergent Influenza Variant Viruses With Reduced Baloxavir Susceptibility: Impact on Clinical and Virologic Outcomes in Uncomplicated Influenza. *J Infect Dis*, 221(3), 346-55.

UK Health Security Agency (2021) *Guidance on use of antiviral agents for the treatment and prophylaxis of seasonal influenza.* Available online: https://www.gov.uk/government/publications/influenza-treatment-and-prophylaxis-using-anti-viral-agents [Accessed 2022].

UK Health Security Agency (2022) *National flu and COVID-19 surveillance reports: 2021 to 2022 season* Available online: https://www.gov.uk/government/statistics/national-flu-and-covid-19-surveillance-reports-2021-to-2022-season [Accessed 2022].

Ulmanen, I., Broni, B. A. & Krug, R. M. (1981) Role of two of the influenza virus core P proteins in recognizing cap 1 structures (m7GpppNm) on RNAs and in initiating viral RNA transcription. *Proc Natl Acad Sci U S A*, 78(12), 7355-9.

Unoki, M., Masuda, A., Dohmae, N., Arita, K., Yoshimatsu, M., Iwai, Y., Fukui, Y., Ueda, K., Hamamoto, R., Shirakawa, M., Sasaki, H. & Nakamura, Y. (2013) Lysyl 5-hydroxylation, a novel histone modification, by Jumonji domain containing 6 (JMJD6). *J Biol Chem*, 288(9), 6053-62.

Upton, J. W., Kaiser, W. J. & Mocarski, E. S. (2012) DAI/ZBP1/DLM-1 complexes with RIP3 to mediate virus-induced programmed necrosis that is targeted by murine cytomegalovirus vIRA. *Cell Host Microbe*, 11(3), 290-7.

van de Sandt, C. E., Kreijtz, J. H. & Rimmelzwaan, G. F. (2012) Evasion of influenza A viruses from innate and adaptive immune responses. *Viruses*, 4(9), 1438-76.

Vangimalla, S. S., Ganesan, M., Kharbanda, K. K. & Osna, N. A. (2017) Bifunctional Enzyme JMJD6 Contributes to Multiple Disease Pathogenesis: New Twist on the Old Story. *Biomolecules*, 7(2), 41.

Varga, Z. T., Ramos, I., Hai, R., Schmolke, M., García-Sastre, A., Fernandez-Sesma, A. & Palese, P. (2011) The influenza virus protein PB1-F2 inhibits the induction of type I interferon at the level of the MAVS adaptor protein. *PLoS Pathog*, 7(6), e1002067.

Vasin, A. V., Temkina, O. A., Egorov, V. V., Klotchenko, S. A., Plotnikova, M. A. & Kiselev, O. I. (2014) Molecular mechanisms enhancing the proteome of influenza A viruses: an overview of recently discovered proteins. *Virus Res*, 185, 53-63.

Veler, H., Fan, H., Keown, J. R., Sharps, J., Fournier, M., Grimes, J. M. & Fodor, E. (2022) The C-Terminal Domains of the PB2 Subunit of the Influenza A Virus RNA Polymerase Directly Interact with Cellular GTPase Rab11a. *J Virol*, 96(5), e0197921.

Vijayakrishnan, S., Loney, C., Jackson, D., Suphamungmee, W., Rixon, F. J. & Bhella, D. (2013) Cryotomography of budding influenza A virus reveals filaments with diverse morphologies that mostly do not bear a genome at their distal end. *PLoS Pathog*, 9(6), e1003413.

Vreede, F. T., Jung, T. E. & Brownlee, G. G. (2004) Model suggesting that replication of influenza virus is regulated by stabilization of replicative intermediates. *J Virol*, 78(17), 9568-72.

Wang, J., Yuan, X. & Ding, N. (2021) IGF2BP2 knockdown inhibits LPS-induced pyroptosis in BEAS-2B cells by targeting caspase 4, a crucial molecule of the non-canonical pyroptosis pathway. *Exp Ther Med*, 21(6), 593.

Wang, J. P., Bowen, G. N., Padden, C., Cerny, A., Finberg, R. W., Newburger, P. E. & Kurt-Jones, E. A. (2008a) Toll-like receptor-mediated activation of neutrophils by influenza A virus. *Blood*, 112(5), 2028-34.

Wang, J. P., Liu, P., Latz, E., Golenbock, D. T., Finberg, R. W. & Libraty, D. H. (2006) Flavivirus activation of plasmacytoid dendritic cells delineates key elements of TLR7 signaling beyond endosomal recognition. *J Immunol*, 177(10), 7114-21.

Wang, P., Doxtader, K. A. & Nam, Y. (2016) Structural Basis for Cooperative Function of Mettl3 and Mettl14 Methyltransferases. *Mol Cell*, 63(2), 306-17.

Wang, P., Palese, P. & O'Neill, R. E. (1997) The NPI-1/NPI-3 (karyopherin alpha) binding site on the influenza a virus nucleoprotein NP is a nonconventional nuclear localization signal. *J Virol*, 71(3), 1850-6.

Wang, W., Cui, Z. Q., Han, H., Zhang, Z. P., Wei, H. P., Zhou, Y. F., Chen, Z. & Zhang, X. E. (2008b) Imaging and characterizing influenza A virus mRNA transport in living cells. *Nucleic Acids Res*, 36(15), 4913-28.

Wang, X., Lu, Z., Gomez, A., Hon, G. C., Yue, Y., Han, D., Fu, Y., Parisien, M., Dai, Q., Jia, G., Ren, B., Pan, T. & He, C. (2014a) N6-methyladenosine-dependent regulation of messenger RNA stability. *Nature*, 505(7481), 117-20.

Wang, X., Zhao, B. S., Roundtree, I. A., Lu, Z., Han, D., Ma, H., Weng, X., Chen, K., Shi, H. & He, C. (2015) N(6)-methyladenosine Modulates Messenger RNA Translation Efficiency. *Cell*, 161(6), 1388-99.

Wang, Y., Li, Y., Toth, J. I., Petroski, M. D., Zhang, Z. & Zhao, J. C. (2014b) N6-methyladenosine modification destabilizes developmental regulators in embryonic stem cells. *Nat Cell Biol*, 16(2), 191-8.

Wang, Y., Ludwig, J., Schuberth, C., Goldeck, M., Schlee, M., Li, H., Juranek, S., Sheng, G., Micura, R., Tuschl, T., Hartmann, G. & Patel, D. J. (2010) Structural and functional insights into 5'-ppp RNA pattern recognition by the innate immune receptor RIG-I. *Nat Struct Mol Biol*, 17(7), 781-7.

Watanabe, T. & Kawaoka, Y. (2015) Influenza virus-host interactomes as a basis for antiviral drug development. *Curr Opin Virol*, 14, 71-8.

Webby, C. J., Wolf, A., Gromak, N., Dreger, M., Kramer, H., Kessler, B., Nielsen, M. L., Schmitz, C., Butler, D. S., Yates, J. R., 3rd, Delahunty, C. M., Hahn, P., Lengeling, A., Mann, M., Proudfoot, N. J., Schofield, C. J. & Böttger, A. (2009) Jmjd6 catalyses lysyl-hydroxylation of U2AF65, a protein associated with RNA splicing. *Science*, 325(5936), 90-3.

Webster, R. G. & Pereira, H. G. (1968) A common surface antigen in influenza viruses from human and avian sources. *J Gen Virol*, 3(2), 201-8.

Wei, C. M., Gershowitz, A. & Moss, B. (1975) Methylated nucleotides block 5' terminus of HeLa cell messenger RNA. *Cell*, 4(4), 379-86.

Wei, L., Cui, J., Song, Y., Zhang, S., Han, F., Yuan, R., Gong, L., Jiao, P. & Liao, M. (2014) Duck MDA5 functions in innate immunity against H5N1 highly pathogenic avian influenza virus infections. *Vet Res*, 45(1), 66.

Weis, W., Brown, J. H., Cusack, S., Paulson, J. C., Skehel, J. J. & Wiley, D. C. (1988) Structure of the influenza virus haemagglutinin complexed with its receptor, sialic acid. *Nature*, 333(6172), 426-31.

White, J., Kartenbeck, J. & Helenius, A. (1982) Membrane fusion activity of influenza virus. *Embo j*, 1(2), 217-22.

Whitsett, J. A. & Alenghat, T. (2015) Respiratory epithelial cells orchestrate pulmonary innate immunity. *Nat Immunol*, 16(1), 27-35.

Wilkinson, T. M., Li, C. K., Chui, C. S., Huang, A. K., Perkins, M., Liebner, J. C., Lambkin-Williams, R., Gilbert, A., Oxford, J., Nicholas, B., Staples, K. J., Dong, T., Douek, D. C., McMichael, A. J. & Xu, X. N. (2012) Preexisting influenza-specific CD4+ T cells correlate with disease protection against influenza challenge in humans. *Nat Med*, 18(2), 274-80.

Williams, G. D., Gokhale, N. S., Snider, D. L. & Horner, S. M. (2020) The mRNA Cap 2'-O-Methyltransferase CMTR1 Regulates the Expression of Certain Interferon-Stimulated Genes. *mSphere*, 5(3), e00202-20.

Wise, H. M., Foeglein, A., Sun, J., Dalton, R. M., Patel, S., Howard, W., Anderson, E. C., Barclay, W. S. & Digard, P. (2009) A complicated message: Identification of a novel PB1-related protein translated from influenza A virus segment 2 mRNA. *J Virol*, 83(16), 8021-31.

Wise, H. M., Gaunt, E., Ping, J., Holzer, B., Jasim, S., Lycett, S. J., Murphy, L., Livesey, A., Brown, R., Smith, N., Morgan, S., Clark, B., Kudryavtseva, K., Beard, P. M., Nguyen-Van-Tam, J., Salguero, F. J., Tchilian, E., Dutia, B. M., Brown, E. G. & Digard, P. (2019) An alternative AUG codon that produces an N-terminally extended form of the influenza A virus NP is a virulence factor for a swine-derived virus. *bioRxiv*, 738427.

Wise, H. M., Hutchinson, E. C., Jagger, B. W., Stuart, A. D., Kang, Z. H., Robb, N., Schwartzman, L. M., Kash, J. C., Fodor, E., Firth, A. E., Gog, J. R., Taubenberger, J. K. & Digard, P. (2012) Identification of a novel splice variant form of the influenza A virus M2 ion channel with an antigenically distinct ectodomain. *PLoS Pathog*, 8(11), e1002998.

Wisskirchen, C., Ludersdorfer, T. H., Müller, D. A., Moritz, E. & Pavlovic, J. (2011) The cellular RNA helicase UAP56 is required for prevention of double-stranded RNA formation during influenza A virus infection. *J Virol*, 85(17), 8646-55.

Wolf, A., Mantri, M., Heim, A., Muller, U., Fichter, E., Mackeen, M. M., Schermelleh, L., Dadie, G., Leonhardt, H., Venien-Bryan, C., Kessler, B. M., Schofield, C. J. & Bottger, A. (2013) The polyserine domain of the lysyl-5 hydroxylase Jmjd6 mediates subnuclear localization. *Biochem J*, 453(3), 357-70.

Wong, J. P., Christopher, M. E., Viswanathan, S., Karpoff, N., Dai, X., Das, D., Sun, L. Q., Wang, M. & Salazar, A. M. (2009) Activation of toll-like receptor signaling pathway for protection against influenza virus infection. *Vaccine*, 27(25-26), 3481-3.

Woodfin, B. M. & Kazim, A. L. (1993) Interaction of the amino-terminus of an influenza virus protein with mitochondria. *Arch Biochem Biophys*, 306(2), 427-30.

World Health Organization (2018) *Influenza (Seasonal)* Available online: https://www.who.int/news-room/fact-sheets/detail/influenza-(seasonal) [Accessed 2021].

Woyciniuk, P., Linder, M. & Scholtissek, C. (1995) The methyltransferase inhibitor Neplanocin A interferes with influenza virus replication by a mechanism different from that of 3-deazaadenosine. *Virus Res*, 35(1), 91-9.

Wu, B., Su, S., Patil, D. P., Liu, H., Gan, J., Jaffrey, S. R. & Ma, J. (2018) Molecular basis for the specific and multivariant recognitions of RNA substrates by human hnRNP A2/B1. *Nat Commun*, 9(1), 420.

Wu, W. & Metcalf, J. P. (2020) The Role of Type I IFNs in Influenza: Antiviral Superheroes or Immunopathogenic Villains? *J Innate Immun*, 12(6), 437-47.

Xiao, H., Killip, M. J., Staeheli, P., Randall, R. E. & Jackson, D. (2013) The human interferon-induced MxA protein inhibits early stages of influenza A virus infection by retaining the incoming viral genome in the cytoplasm. *J Virol*, 87(23), 13053-8.

Xu, C., Liu, K., Ahmed, H., Loppnau, P., Schapira, M. & Min, J. (2015) Structural Basis for the Discriminative Recognition of N6-Methyladenosine RNA by the Human YT521-B Homology Domain Family of Proteins. *J Biol Chem*, 290(41), 24902-13.

Xu, C., Wang, X., Liu, K., Roundtree, I. A., Tempel, W., Li, Y., Lu, Z., He, C. & Min, J. (2014) Structural basis for selective binding of m6A RNA by the YTHDC1 YTH domain. *Nat Chem Biol*, 10(11), 927-9.

Xueqing, H., Jun, Z., Yueqiang, J., Xin, L., Liya, H., Yuanyuan, F., Yuting, Z., Hao, Z., Hua, W., Jian, L. & Tiejun, Y. (2020) IGF2BP3 May Contributes to Lung Tumorigenesis by Regulating the Alternative Splicing of PKM. *Front Bioeng Biotechnol*, 8, 679.

Yamada, S., Suzuki, Y., Suzuki, T., Le, M. Q., Nidom, C. A., Sakai-Tagawa, Y., Muramoto, Y., Ito, M., Kiso, M., Horimoto, T., Shinya, K., Sawada, T., Kiso, M., Usui, T., Murata, T., Lin, Y., Hay, A., Haire, L. F., Stevens, D. J., Russell, R. J., Gamblin, S. J., Skehel, J. J. & Kawaoka, Y. (2006) Haemagglutinin mutations responsible for the binding of H5N1 influenza A viruses to human-type receptors. *Nature*, 444(7117), 378-82.

Yamamoto, M., Sato, S., Hemmi, H., Hoshino, K., Kaisho, T., Sanjo, H., Takeuchi, O., Sugiyama, M., Okabe, M., Takeda, K. & Akira, S. (2003) Role of adaptor TRIF in the MyD88-independent toll-like receptor signaling pathway. *Science*, 301(5633), 640-3.

Yamanaka, K., Ishihama, A. & Nagata, K. (1990) Reconstitution of influenza virus RNA-nucleoprotein complexes structurally resembling native viral ribonucleoprotein cores. *J Biol Chem*, 265(19), 11151-5.

Yamayoshi, S., Watanabe, M., Goto, H. & Kawaoka, Y. (2016) Identification of a Novel Viral Protein Expressed from the PB2 Segment of Influenza A Virus. *J Virol*, 90(1), 444-56.

Yan, J., Li, Q., Mao, A. P., Hu, M. M. & Shu, H. B. (2014) TRIM4 modulates type I interferon induction and cellular antiviral response by targeting RIG-I for K63-linked ubiquitination. *J Mol Cell Biol*, 6(2), 154-63.

Yanagihara, T., Sanematsu, F., Sato, T., Uruno, T., Duan, X., Tomino, T., Harada, Y., Watanabe, M., Wang, Y., Tanaka, Y., Nakanishi, Y., Suyama, M. & Yoshinori, F. (2015) Intronic regulation of Aire expression by Jmjd6 for self-tolerance induction in the thymus. *Nat Commun*, 6, 8820.

Yang, J., Chen, S., Yang, Y., Ma, X., Shao, B., Yang, S., Wei, Y. & Wei, X. (2020) Jumonji domain-containing protein 6 protein and its role in cancer. *Cell Prolif*, 53(2), e12747.

Yasuda, J., Nakada, S., Kato, A., Toyoda, T. & Ishihama, A. (1993) Molecular assembly of influenza virus: association of the NS2 protein with virion matrix. *Virology*, 196(1), 249-55.

Yoneyama, M., Kikuchi, M., Matsumoto, K., Imaizumi, T., Miyagishi, M., Taira, K., Foy, E., Loo, Y. M., Gale, M., Jr., Akira, S., Yonehara, S., Kato, A. & Fujita, T. (2005) Shared and unique functions of the DExD/H-box helicases RIG-I, MDA5, and LGP2 in antiviral innate immunity. *J Immunol*, 175(5), 2851-8.

Yoneyama, M., Kikuchi, M., Natsukawa, T., Shinobu, N., Imaizumi, T., Miyagishi, M., Taira, K., Akira, S. & Fujita, T. (2004) The RNA helicase RIG-I has an essential function in double-stranded RNA-induced innate antiviral responses. *Nat Immunol*, 5(7), 730-7.

York, A. & Fodor, E. (2013) Biogenesis, assembly, and export of viral messenger ribonucleoproteins in the influenza A virus infected cell. *RNA Biol*, 10(8), 1274-82.

York, A., Hengrung, N., Vreede, F. T., Huiskonen, J. T. & Fodor, E. (2013) Isolation and characterization of the positive-sense replicative intermediate of a negative-strand RNA virus. *Proc Natl Acad Sci U S A*, 110(45), E4238-45.

Yoshimura, A. & Ohnishi, S. (1984) Uncoating of influenza virus in endosomes. *J Virol*, 51(2), 497-504.

Yuan, P., Bartlam, M., Lou, Z., Chen, S., Zhou, J., He, X., Lv, Z., Ge, R., Li, X., Deng, T., Fodor, E., Rao, Z. & Liu, Y. (2009) Crystal structure of an avian influenza polymerase PA(N) reveals an endonuclease active site. *Nature*, 458(7240), 909-13.

Zelus, B. D., Giebelhaus, D. H., Eib, D. W., Kenner, K. A. & Moon, R. T. (1989) Expression of the poly(A)-binding protein during development of Xenopus laevis. *Mol Cell Biol*, 9(6), 2756-60.

Zhang, J., Leser, G. P., Pekosz, A. & Lamb, R. A. (2000) The cytoplasmic tails of the influenza virus spike glycoproteins are required for normal genome packaging. *Virology*, 269(2), 325-34.

Zhang, T., Yin, C., Boyd, D. F., Quarato, G., Ingram, J. P., Shubina, M., Ragan, K. B., Ishizuka, T., Crawford, J. C., Tummers, B., Rodriguez, D. A., Xue, J., Peri, S., Kaiser, W. J., López, C. B., Xu, Y., Upton, J. W., Thomas, P. G., Green, D. R. & Balachandran, S. (2020) Influenza Virus Z-RNAs Induce ZBP1-Mediated Necroptosis. *Cell*, 180(6), 1115-1129.e13.

Zhang, W., Wang, Q., Yang, F., Zhu, Z., Duan, Y., Yang, Y., Cao, W., Zhang, K., Ma, J., Liu, X. & Zheng, H. (2021) JMJD6 negatively regulates cytosolic RNA induced antiviral signaling by recruiting RNF5 to promote activated IRF3 K48 ubiquitination. *PLoS Pathog*, 17(3), e1009366.

Zhao, F., Wu, L., Wang, Q., Zhao, X., Chen, T., Yin, C., Yan, L. & Yang, X. (2022) Insulin-like growth factor 2 mRNA-binding protein 2-regulated alternative splicing of

nuclear factor 1 C-type causes excessive granulosa cell proliferation in polycystic ovary syndrome. *Cell Prolif*, 55(4), e13216.

Zhao, W., Lu, D., Liu, L., Cai, J., Zhou, Y., Yang, Y., Zhang, Y. & Zhang, J. (2017) Insulin-like growth factor 2 mRNA binding protein 3 (IGF2BP3) promotes lung tumorigenesis via attenuating p53 stability. *Oncotarget*, 8(55), 93672-87.

Zheng, G., Dahl, J. A., Niu, Y., Fedorcsak, P., Huang, C. M., Li, C. J., Vågbø, C. B., Shi, Y., Wang, W. L., Song, S. H., Lu, Z., Bosmans, R. P., Dai, Q., Hao, Y. J., Yang, X., Zhao, W. M., Tong, W. M., Wang, X. J., Bogdan, F., Furu, K., Fu, Y., Jia, G., Zhao, X., Liu, J., Krokan, H. E., Klungland, A., Yang, Y. G. & He, C. (2013) ALKBH5 is a mammalian RNA demethylase that impacts RNA metabolism and mouse fertility. *Mol Cell*, 49(1), 18-29.

Zhou, A., Dong, X., Liu, M. & Tang, B. (2021) Comprehensive Transcriptomic Analysis Identifies Novel Antiviral Factors Against Influenza A Virus Infection. *Front Immunol*, 12, 632798.

Zhou, Y., Huang, T., Siu, H. L., Wong, C. C., Dong, Y., Wu, F., Zhang, B., Wu, W. K., Cheng, A. S., Yu, J., To, K. F. & Kang, W. (2017) IGF2BP3 functions as a potential oncogene and is a crucial target of miR-34a in gastric carcinogenesis. *Mol Cancer*, 16(1), 77.

Zhu, T., Roundtree, I. A., Wang, P., Wang, X., Wang, L., Sun, C., Tian, Y., Li, J., He, C. & Xu, Y. (2014) Crystal structure of the YTH domain of YTHDF2 reveals mechanism for recognition of N6-methyladenosine. *Cell Res*, 24(12), 1493-6.

Zimmermann, P., Mänz, B., Haller, O., Schwemmle, M. & Kochs, G. (2011) The viral nucleoprotein determines Mx sensitivity of influenza A viruses. *J Virol*, 85(16), 8133-40.

Züst, R., Cervantes-Barragan, L., Habjan, M., Maier, R., Neuman, B. W., Ziebuhr, J., Szretter, K. J., Baker, S. C., Barchet, W., Diamond, M. S., Siddell, S. G., Ludewig, B. & Thiel, V. (2011) Ribose 2'-O-methylation provides a molecular signature for the distinction of self and non-self mRNA dependent on the RNA sensor Mda5. *Nat Immunol*, 12(2), 137-43.